Quantum Information & Open-System Dynamics:

Periodic Driving Within and Complete Positivity Beyond The Markovian Limit

Von der Fakultät für Mathematik, Informatik und Naturwissenschaften
der RWTH Aachen University zur Erlangung des akademischen Grades
eines Doktors der Naturwissenschaften genehmigte Dissertation

vorgelegt von

Viktor Reimer, M. Sc.

aus Dshetysaj (Kasachstan)

Berichter: apl.-Prof. Dr. rer. nat. Maarten Rolf Wegewijs
Univ.-Prof. Dr. phil. Herbert Schoeller

Tag der mündlichen Prüfung: 19. Juli 2019

It will be difficult.
But the difficulty really is psychological
and exists in the perpetual torment that results from your saying to yourself,

'But how can it be like that?'

which is a reflection of uncontrolled but utterly vain desire
to see it in terms of something familiar.

—Richard P. Feynman—

Summary

In this thesis, the dynamics of generic open quantum systems is studied at the interface of quantum information and statistical field theory. Taking advantage of their synergies, we put the dynamical correlations that such systems develop with their *effective* environment on center stage: The key step to access the latter is a reformulation of the open system's dynamics as derived from nontrivial microscopic models in terms of Kraus operator-sums. This decomposition into physical processes conditional on measurements performed on the effective environment enables progress on three interrelated questions.

How do quantum (non-)Markovian systems affect their environment?

The common notion of a Markovian process entails an environment that loosely speaking retains no 'memory' of its previous interactions with the system. More precisely, the dynamics is insensitive to a division at intermediate times at which the environment is reinitialized. We provide some new physical intuition for different divisibility criteria by explicitly determining the dynamics of the effective environment for a tunnel-coupled resonant level without interactions. From the time-dependence of transport currents and observable measures of information exchange between the system and its environment, we find that the *details* of the reinitialization matter even in this simple model. Obtaining this complete picture of the open system's dynamics not only requires an exact treatment of the problem, but also a combination of various approaches –including the Kraus operator-sum.

How does periodic driving of the environment modify Markovian systems?

For any but the simplest models, a detailed analysis such as the above is out of reach due to the necessity of employing approximations. The paradigmatic *Born-Markov approximation* is the prime example that manages to maintain a consistent yet intuitive operational understanding of the dynamics even in the presence of fast time-periodic driving. We illustrate for quantum optical systems how such time-periodic driving influences the dynamical system-environment correlations and leads to *driven-dissipative phase transitions* which reflect a memory-effect within this originally Markovian setup. A hallmark feature of this transition is the temporary suppression of effective dissipation rates that gives rise to long-lived metastable states and interesting time-periodic steady states. We develop a new formalism for efficiently computing these periodic steady states without the need to integrate over the full transient approach.

How can approximations beyond the Markovian limit be formulated?

Beyond these Markovian approximations, little is known regarding the preservation of even the most fundamental properties of a reduced system state, namely its positivity and trace-normalization. Here, we focus on the stronger notion of *completely positive* dynamics and reorganize the real-time diagrammatic series into an operational framework of a Kraus operator-sum in which each term makes this property explicit and has a transparent physical meaning. Based on these principles, we establish for the first time the fundamental structure of the Nakajima-Zwanzig memory-kernel that guarantees the solution of a time-nonlocal quantum master equation to be completely positive. This is a crucial step towards non-Markovian approximation schemes that do not violate fundamental dynamical properties.

Zusammenfassung

In dieser Arbeit wird die Dynamik generischer offener Quantensysteme an der Schnittstelle zwischen der Quanteninformations- und statistischen Feldtheorie untersucht. Unter Ausnutzung von Synergien stellen wir die dynamischen Korrelationen, die solche Systeme mit ihren *effektiven* Umgebungen entwickeln, in den Mittelpunkt: Der wesentliche Schritt für den Zugang zu Letzteren ist die Reformulierung der Dynamik eines offenen Systems, hergeleitet aus nicht-trivialen mikroskopischen Modellen, im Sinne von Kraus Operator-Summen. Diese Zerlegung in physikalische Prozesse, die von Messungen der effektiven Umgebung abhängig sind, ermöglicht Fortschritte in drei zusammenhängenden Fragestellungen.

Wie beeinflussen (nicht-)Markov'sche Quantensysteme ihre Umgebung?

Die übliche Vorstellung eines Markov'schen Prozesses beinhaltet eine Umgebung, die kein Gedächtnis über ihre vorherigen Interaktionen mit dem System hat. Genauer gesagt ist die Dynamik unempfindlich gegenüber einer Aufteilung zu Zwischenzeiten, an denen die Umgebung neu initialisiert wird. Wir entwickeln einige neue physikalische Intuition verschiedener Aufteilungskriterien, indem wir explizit die Dynamik der effektiven Umgebung eines tunnelgekoppelten Resonant-Levels ohne Wechselwirkungen bestimmen. Aus der Zeitabhängigkeit von Transportströmen und messbaren Größen für den Informationsaustausch zwischen System und Umgebung schließen wir, dass die *Details* der Neuinitialisierung selbst in diesem einfachen Modell von Bedeutung sind. Dieses vollständige Bild der Dynamik des offenen Quantensystems erfordert nicht nur eine exakte Behandlung des Problems, sondern auch die Kombination verschiedener Herangehensweisen –die Kraus Operator-Summe eingeschlossen.

Wie modifiziert periodische Modulation der Umgebung Markov'sche Systeme?

Eine detaillierte Analyse wie die obige ist aufgrund der Notwendigkeit von Näherungen für alle Modelle außer den einfachsten nicht möglich. Die paradigmatische *Born-Markov-Approximation* ist das Musterbeispiel einer Näherung, welche es schafft ein konsistentes und dennoch intuitives operatives Verständnis der Dynamik sogar in Anwesenheit schneller periodischer Modulation zu erhalten. Wir illustrieren für quantenoptische Systeme, wie solch eine periodische Modulation die dynamischen Korrelationen zwischen System und Umgebung beeinflusst und zu *getrieben-dissipativen Phasenübergängen* führt, die ein Gedächtnis in diesem eigentlich Markov'schen Szenario widerspiegeln. Ein charakteristisches Merkmal dieser Phasenübergänge ist die temporäre Unterdrückung effektiver Dissipationsraten, was zu langlebigen metastabilen und interessanten periodisch-stationären Zuständen führt. Wir entwickeln einen neuen Formalismus, der es erlaubt letztere Zustände numerisch effizient zu berechnen, ohne über die volle transiente Zeitentwicklung zu integrieren.

Wie können Näherungen jenseits des Markov'schen Limits formuliert werden?

Jenseits dieser Markov'schen Näherungen ist wenig über die Erhaltung selbst der fundamentalsten Eigenschaften eines reduzierten Systemzustands bekannt, nämlich seiner Positivität und Spurnormalisierung. Hier konzentrieren wir uns auf den stärkeren Begriff der *vollständig-positiven* Dynamik und reorganisieren die Echtzeit-Diagrammreihe zu einer Kraus Operator-Summe, in der jeder Term diese Eigenschaft explizit werden lässt und eine transparente physikalische Bedeutung hat. Darauf basierend etablieren wir zum ersten Mal die fundamen-

tale Struktur des Nakajima-Zwanzig Kernels, welche die vollständige Positivität der Lösung einer nicht-zeitlokalen Quantenmastergleichung garantiert. Dies ist ein entscheidender Schritt hin zu nicht-Markov'schen Näherungsverfahren, die diese fundamentalen dynamischen Eigenschaften nicht verletzen.

Table of contents

1 Introduction

It from bit symbolizes the idea that every item of the physical world has at bottom –at a very deep bottom, in most instances– an immaterial source and explanation; that what we call reality arises in the last analysis from the posing of yes-no questions and the registering of equipment-evoked responses; in short, that all things physical are information-theoretic in origin and this is a participatory universe.

—John A. Wheeler [1]

This thesis discusses the dynamics of open quantum systems from two complementary perspectives: quantum information theory and statistical physics. It first and foremost aims at connecting the quite distinct formalisms that have developed in both communities in order to further stimulate an exchange of ideas and techniques. The emergence of quantum information theory over the past two decades prompted an increasing appreciation of the 'It-from-bit' idea put forward by Wheeler [1] and the memorable phrase by Landauer [2] that 'information is physical'. Both recognized the special, overarching role of information that goes way beyond the thermodynamic and mathematical considerations that led to the development of classical information theory in the midst of the 20th century. Throughout this thesis, we will adopt well-established concepts of quantum information theory as a guiding principle for the analysis of correlations and their dynamics in open many-body systems. A particular focus is put on the physical role of information for the properties of complete positivity and Markovianity as introduced below. Interested readers from both quantum information and statistical physics communities should be able to equally benefit from the presented results: the former by deepening the understanding of sophisticated non-equilibrium many-body methods and their connection to well-established quantum-information theorems; the latter by further appreciating the benefits of these theorems in a formulation that interfaces existing methods and allows to improve them or devise new ones through a clear operational understanding of the dynamics.

Open systems have historically been investigated in the context of thermodynamics and statistical physics where a microscopic treatment in terms of canonical or grand-canonical ensembles is inherent to describing a system's exchange of energy and particles with its environment. Already the early works by Boltzmann and Gibbs around 1865 on these subjects formalized Clausius' thermodynamic concept of entropy [3] as a statistical measure for an observer's ignorance about the micro state of the system given its statistical macro state. It was further extended with the formulation of quantum theory by von Neumann [4] but it wasn't until the consideration of classical information theory on a more abstract level by Shannon [5] that established entropy as a fundamental measure of information. With his work the paradigm has shifted from the *microscopic details* of thermodynamic processes of open systems to questions focusing on the *feasibility* of processes formulated as communication protocols. Consequently, many powerful theorems on reliable communication and manipulation of information under the influence of a noisy environment have been formulated and prompted increased efforts towards the physical implementation of such protocols, eventually enabling the computer and information age we are living in.

These advances have not been restricted to classical information theory but have led to the emergence of quantum information theory as an independent field of research concerned with the feasibility and realization of quantum computation and communication. Quantum

computers are surmised to be far more powerful than their classical counterparts because the fundamental information carrier is a quantum superposition, a so called qubit, of the classical binary states represented by values 0 or 1 that can be coherently manipulated and controlled. Indeed, the age of quantum computation has already begun with physical realizations commercially available and major corporations heavily investing into research. This research is still exploring various implementations of quantum computation on a fundamental level, including different physical platforms based on trapped atoms [6], superconducting circuits [7, 8] or mesoscopic quantum-dot devices [9, 10], as well as different computing paradigms such as quantum annealing [11] or quantum walks [12]. However, also engineering issues become increasingly important in the strive to scale to more powerful quantum computers that are capable of solving complex problems encountered not only in physics but across many other disciplines, see Ref. [13] for a discussion.

The way towards these implementations of quantum computation has been paved by the appreciation of *entanglement* in quantum error-correction schemes to mitigate the noisy influence of the environment on an open quantum system: Shor [14] and Steane [15] independently showed that this can be dynamically corrected for by encoding multiple *entangled* physical qubits into a robust logical qubit such that a set of projective measurements and subsequent local operations conditional on the measurement outcomes can 'undo' the effect of the environment. This is different from classical bits for which mere redundancy, i.e., having multiple copies of the same bit of information, can already effectively mitigate the noise introduced by the environment[1]. One can think of these quantum error-correction schemes as procedures that effectively monitor the undesired system-environment correlations as to be able to correct for their influence without revealing and thereby destroying the quantum information of interest. These quantum computation and communication-inspired ideas thus provide a new view on correlations and entanglement in physical open many-body systems.

Indeed, the remarkable theoretical insights about information and entanglement started to feed back into the statistical physics community, see for example Ref. [17] for a review of its impact in quantum thermodynamics. Perhaps one of the most remarkable insights about correlations and entanglement in many-body systems is related to the area law [18]: Under fairly general physical assumptions, the entanglement across any bipartition of a system only scales with the surface area of the partition instead of the volume. Consequently, the many-body state of numerous systems is restricted to an exponentially small subspace of the vast Hilbert space which allows for an efficient parametrization in terms of so called tensor network states, such as matrix product states (MPS), projected entangled pair states (PEPS) and multi-scale entanglement renormalization ansatz (MERA) states, see Ref. [19] for a recent review. Modern numerical techniques like the density matrix renormalization group (DMRG) explicitly make use of this structure to simulate ever larger system sizes or to reach time-scales of the transient dynamics that are otherwise not achievable. Despite recent efforts to generalize the discrete nature of tensor networks to the continuous case [20], such methods have so far proven most useful for low-dimensional lattice problems and reaching the thermodynamic limit is in general difficult.

In this thesis, we will instead be interested in transport-impurity models where a small, local system exchanges particles with its continuous environment comprised of one or more large reservoirs each in a thermodynamic equilibrium state. In this continuous setup, the

[1]The reason that this is not possible in the case of qubits is not the no-cloning theorem [16] which holds for any (quantum or classical) dynamical stochastic mapping from an in- to an output, but primarily their inherent continuous superposition of binary states.

environment is effectively modeled in terms of its thermodynamic parameters (temperature and chemical potential) and spectral properties (possibly energy-dependent coupling parameters), in contrast to lattice models where the full microscopic details of the environment are taken into account. The rationale behind this is to arrive at an *effective* description of the local impurity system in terms of quantum master equations (QME) for the reduced quantum state that incorporates many details of its surroundings while emphasizing the role of the system-environment *coupling*. For these impurity models, much less is known about the general structure of entanglement and correlations particularly between system and environment. The key difference to quantum information theory is that the noisy influence of the environment on the open system's continuous evolution is explicitly parametrized by *time* instead of considering discrete step-wise *processes*. The *transient dynamics* of system-environment models has continued to attract interest and proven to be a formidable theoretical challenge that is relevant not only in the context of quantum computation, e.g., using mesoscopic quantum dot devices [21, 22], but also in molecular transport [23, 24], photosynthetic complexes [25–27] and driven-dissipative quantum-optical systems [28–30], to name but a few.

One of the main issues in the theoretical description of such systems is concerned with the nontrivial backaction of the environment onto the system. Due to a finite time-span of correlations with the environment the latter does not act as a mere source of decoherence and dissipation. These correlations provide a *memory* for previous interactions of the system with the environment and may significantly alter the system's dynamics depending on its past. Such *non-Markovian* dynamics is one of the central issues addressed within this thesis and we will especially focus on its *observable* implications from an information perspective much of which can be illustrated using a surprisingly simple impurity model. The issues surrounding non-Markovianity become more pressing when an *exact* treatment of the impurity model in terms of QMEs is no longer feasible. This is the case for all but the most simple problems. Consistent approximation schemes that capture non-Markovian effects are notoriously difficult to formulate for several reasons: Most master equation approaches, e.g. Bloch-Redfield [31], are based on a leading-order perturbative expansion in the system-environment coupling which work well in the Markovian regime when memory effects are negligible. However, including higher-order terms in the expansion or taking into account the finite memory-time of the environment may result in unphysical reduced density operators $\rho(t)$ that are not positive-semidefinite[2] in certain parameter regimes. More subtly, ill-defined cases may appear even when the reduced system state itself is physical but derives from an unphysical joint state. To resolve this issue, it turns out to be necessary to consider the stronger notion of *complete positivity* and combine the tools provided by the quantum information community with statistical physics methods as pioneered by van Wonderen and Suttorp [32–34]. A key contribution of this thesis is to explicitly show how the perturbation series expressed in Keldysh *real-time* diagrams can be systematically reorganized into a Kraus operator-sum that allows for a clear operational understanding of system-environment interaction *processes* conditional on measurements performed on the environment. When respecting this structure, the reduced density operator is guaranteed to be physical at all times. Moreover, we can gain information about the nontrivial dynamical footprint of the system-environment interaction left in the *environment*, even though it was integrated out.

Motivated by these fundamental considerations that seem to have so far been overlooked in field-theoretical treatments, the primary objective of this thesis is to develop the formalism and illustrate it in a simple case study. This will provide crucial guidance for addressing

[2] We will simply refer to this as positivity (of the eigenvalues) of the reduced density operator, $\rho \geq 0$.

more realistic models that are relevant to experimental realizations of open quantum systems. Importantly, although we had no opportunity to illustrate the impact of local interactions on the system in this work, the developed toolbox can fully account for them and applies to interacting problems without modification but at the expense of simplicity. To make further progress, one could think of combining the reorganized perturbation series with renormalization group (RG) methods [35–37] which take as a starting point the noninteracting limit. The significance of this work is thus first of all that it provides the statistical physics community with new starting points for consistently approximating open-system dynamics in full compliance with quantum information insights. However, our simple case studies already reveal interesting phenomena in non-Markovian dynamics that seem broadly applicable even in more complicated models. We therefore hope that the developed methods for continuous time-evolution and their applications will also be of interest to the quantum information community to continue the long tradition of synergies.

Such synergies have in fact already spawned many interesting ideas to implement quantum computation and communication in physical many-body systems. For instance, instead of dynamically correcting for the decoherence introduced by the environment via error-correction schemes, it has been recognized that dissipation can also be beneficial, e.g., in *assisting* the formation of topologically protected qubits [38]. Especially non-Markovian dynamics has been discussed as a resource for interesting and technologically useful phenomena in open quantum systems: For quantum metrology purposes, it has been shown that non-Markovianity can boost the precision limits of measurements [39]. It can also speed up or facilitate the formation of entangled *steady* states [40] which may be used for computation and communication purposes. These ideas rely on the formation of either long-lived metastable states in (almost) decoherence free subspaces [41], or bistable behavior where the true steady state of the system is not unique and can be controlled by external parameters [42, 43].

In hope of finding more exotic nonequilibrium steady states, this emerging field of reservoir engineering is nowadays often complemented with *Floquet engineering* where system parameters are periodically driven time. Motivation for such exotic steady states can already be found in the classical case: The most famous example is Kapitza's pendulum [44] which develops a stable steady state pointing opposite to the gravitational force upon periodic driving of the suspension point. The natural context of such driven-dissipative oscillator systems is quantum optics where the periodic high-frequency driving of an external laser together with the dissipation caused by the spontaneous emission of photons by an atom or an imperfect cavity have led to remarkable effects like electromagnetically induced transparency (EIT) of an opaque atom gas [45, 46]. Periodic modulation of system parameters has also been achieved in mesoscopic quantum-dot devices which have been demonstrated as on-demand single-electron [47, 48] and also two-electron emitters [49, 50]. The fidelities of qubits and their manipulation have been drastically enhanced by use of dynamical decoupling schemes [51] which employ time-dependent control pulses to compensate the decoherence or reduce gate operation times. Moreover, topological phases can be induced by periodic parameter-modulation in systems which otherwise show trivial behavior [52, 53]. All these efforts open up exciting possibilities for finding novel nonequilibrium states that are not even found in more complex static systems. These interesting possibilities can in particular be investigated in simpler Markovian situations where the well-behaved leading-order expansion of the time-evolution in the system-environment coupling is sufficient.

The above mentioned aspects of open quantum systems and their dynamics only represent a fraction of the vast literature available on this subject. The following sections therefore

provide a more detailed introduction into those issues most relevant to this thesis. We first clearly define the problem at hand and point out an apparent misconception in the definition of the dynamical map that seems to be the origin of a long-lasting debate about the necessity of requiring complete positivity. With the main assumptions and restrictions clarified, the dilemma involved in defining 'Markovian' dynamics is depicted and two prominent descriptions in terms of time-local and nonlocal QMEs in the Markovian and non-Markovian regime are reviewed. Afterwards, we discuss alternatives to QME approaches with a focus on recent advances in numerical methods that might also benefit from or connect to our results.

1.1 Are all dynamical maps completely positive?

Any rigorous investigation of open-system evolution should start with a precise clarification of the dynamical map. Interestingly, this issue keeps on requiring a reconsideration of established open-system concepts, see in particular Ref. [54] for a recent review. In general, the open nature of the system S of interest is considered to arise from a total closed system that is governed by a unitary evolution $U(t)$ of a system and its environment E. An *effective* description of the system alone in terms of its reduced density operator $\rho(t)$ is then obtained by discarding all information about the environment and amounts to tracing out the environment degrees of freedom. This is assumed to define the *dynamical map* $\Pi(t)$,

$$\rho(t) := \Pi(t)\rho(0) = \underset{\mathrm{E}}{\mathrm{Tr}}\, U(t)\rho^{\mathrm{SE}}(0)U(t)^\dagger, \tag{1.1}$$

which propagates *any* initial reduced system density operator $\rho(0) := \mathrm{Tr}_{\mathrm{E}}\,\rho^{\mathrm{SE}}(0)$ to that at an arbitrary later time $\rho(t)$. This step already involves a very subtle issue that we return to below. Assuming this for now, the dynamical map *must* as such preserve the statistical properties of any initial system state it acts on in the sense that the output's eigenvalues must represent the probability distribution of finding the system in one of the eigenstates of $\rho(t)$. For this to be the case, the eigenvalues must be non-negative, $\rho(t) \geq 0$, and sum up to unity, $\mathrm{Tr}_{\mathrm{S}}\,\rho(t) = 1$. We will refer to the corresponding properties of the dynamical map as positivity-preservation (PP) and trace-preservation (TP).

The property of *complete positivity* (CP) has a more subtle physical origin and its significance has long been debated. It is best illustrated with Pechukas' notion of a 'blind and dead' witness [55]: Consider a case where the system is initially *entangled* with external degrees of freedom P that neither interact with the system and environment (blind) nor evolve in time (dead). An example of this situation is encountered when sharing a pair of entangled photons between a local noisy laboratory SE and a satellite P orbiting earth as has recently been achieved within the QUESS collaboration for establishing secure long-range quantum communication channels [56], see Fig. 1.1. Clearly, within the scope of the laboratory there is no way of acknowledging the existence of these external degrees of freedom and the dynamical map describing the local dynamics should not depend on them because this would essentially require the whole universe to be taken into account. The notion of positivity-preservation is *not sufficient* to consistently treat such situations. This becomes apparent when monitoring the combined evolution of system and witness under the dynamical map $\Pi(t)$: Denoting with $\mathcal{I}$ the identity operation on the witness P, the operator $\rho^{\mathrm{SP}}(t) = [\Pi(t) \otimes \mathcal{I}]\rho^{\mathrm{SP}}(0)$ is positive and hence a valid density operator for all possible dimensions of P only if the dynamical map is *completely positive*. A prime example of a positive but not completely positive dynamical map is the transpose operation [57]. In this thesis, we will however also encounter cases where both properties coincide due to simplifying features of the model.

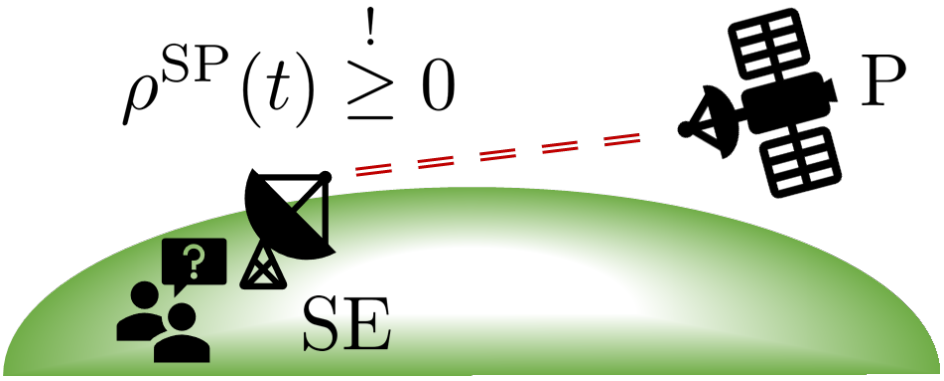

Figure 1.1: In the collaborative effort *Quantum Experiments at Space Scale* (QUESS) [56] a secure long-range quantum channel for quantum key distribution is established by sharing entangled photons (red) between ground stations (SE) located in Graz, Nanshan and Xinglong via the Micius satellite (P). Complete positivity of the dynamics not only ensures that *local* operations in noisy laboratories of the ground stations result in a physical reduced state $\rho(t) \geq 0$ of the system S, but that furthermore the *entanglement* with the satellite P is correctly accounted for, i.e., that also the state $\rho^{\mathrm{SP}}(t) = [\Pi(t) \otimes \mathcal{I}]\rho^{\mathrm{SP}}(0) \geq 0$ is physical.

The above intuitive argument for the *physical* necessity of the CP property has triggered a decade long debate famously initiated by Pechukas and Alicki [55, 58, 59]: How could it be that a blind and dead witness generically forces the dynamical map to be CP rather than PP? Pechukas argued that this was an 'artifact' of considering initially uncorrelated system-environment states $\rho^{\mathrm{SE}}(0) = \rho(0) \otimes \rho^{\mathrm{E}}$ for which it is straightforward to prove that the dynamical map is indeed CP. On the other hand, no rigorous proof exists for arbitrary *correlated* initial conditions of the total system-environment state and instances of the dynamical map being negative or not a map at all have been reported. Consequently, much effort was put into characterizing the classes of initial conditions that do lead to CP dynamical maps [60–62]. There, the lack of initial quantum correlations in form of a vanishing quantum discord was thought to be a necessary and sufficient condition for CP dynamical maps [63] but was soon after shown to be a mistake [60, 64] leaving a full characterization still unsolved. More recently, in Ref. [65], the notion of admissible unitary dynamics and initial conditions was introduced to rule out the unphysical cases, whereas Ref. [66] proposed an *operational* point of view that instead parametrizes the CP dynamics in terms of the preparation and measurement operations performed in experimental setups.

What quantum information theory makes particularly clear are the drastic consequences of non-CP dynamics and the importance of accounting for entanglement: The assumption of CP dynamical maps is for instance inherent to many proposals of quantum error correction schemes [67] but recent studies suggest that an extension to PP dynamical maps is still conceptually possible [68]. More critical is the connection of CP to the validity of *fundamental* bounds: The Holevo bound on the accessible information about a quantum state has been shown to be violated if the CP property is dropped [69]. Also, there is a one-to-one correspondence [70] between complete positivity and the validity of the quantum data-processing inequality [71], which prohibits the increase of a quantum state's information content by local post-processing. However, no experimental indication for a violation of these inequalities exists. All this highlights the importance of CP over PP dynamical maps and further motivates

the clear-cut introduction of this physical assumption that is intimately tied to the deep and difficult implications of entanglement. For instance, it should be noted that every PP map detects some entangled states of bipartite systems [72, 73]. A full mathematical characterization of such PP maps is equivalent to solving the bipartite entanglement problem [74] which is unknown as of now in contrast to the characterization of CP maps, see below. The study of non-CP maps is therefore by itself an interesting issue of ongoing research, see e.g. Ref. [75].

Recent work by Schmid *et al.* [54] pointed out a misconception in the definition of a dynamical map that clarifies much of the ongoing debate by showing that similar difficulties are not restricted to the quantum case but also arise in classical systems. The misconception is related to how variability of the initial state $\rho(0)$ is introduced such that the dynamical map $\Pi(t)$ is valid for *any* input: For an initially factorizing system-environment state variability is trivially obtained by tracing out the environment degrees of freedom from the total state, but it requires more careful treatment in the case of initial correlations. Schmid *et al.* argue that in order to properly define the dynamical map, one should separate the common cause due to the total initial state $\rho^{\mathrm{SE}}(0)$ from the *cause-effect* relation between the system's in- and output. The conventional description of open-system dynamics has failed to do so because it introduced variability of the input state by considering sets of system-environment states $\rho^{\mathrm{SE}}(0)$ with differing marginal states $\rho(0) = \mathrm{Tr}_{\mathrm{E}}\,\rho^{\mathrm{SE}}(0)$. Thereby, one has however also introduced variability in the *dynamics* itself. As a result, one obtains multiple *inference* maps as lookup-tables connecting the in- and output states, each governed by a different dynamics due to the common cause. Incorrectly combining these maps to a single *universal dynamical map* may then not even be possible or leads to the reported cases of non-CP and non-linear maps. It is interesting to note that this issue of inference and causation is also relevant to machine- and deep-learning algorithms [76, 77]: In order to create genuine artificial intelligence, such algorithms not only need to detect correlations in huge data sets but also infer their cause –a task for which a quantum advantage has been shown [78], see also Ref. [79] for a recent review of quantum machine learning.

All these recent insights further strengthened the *physical* importance and implications of completely positive open-system dynamics. In this work, we do not aim at further contributing to this ongoing debate but take a more practical stance and restrict ourselves to the case of initially factorizing states $\rho^{\mathrm{SE}}(0) = \rho(0) \otimes \rho^{\mathrm{E}}$ for which the dynamics is always CP. This in particular allows for the application of many powerful theorems on open system dynamics that rely on CP and not on PP maps. For example, Stinespring's dilation theorem [80] states that any CP-TP dynamical map on a system can be considered to arise from an *enlarged, effective* microscopic model of the type (1.1) where the initial state factorizes $\rho^{\mathrm{SE}}(0) \to \rho(0) \otimes |0\rangle\langle 0|$ into an effective *pure* environment. Such *purification* concepts are ubiquitous in quantum information theory and have also proven useful in statistical physics, for example in efficiently simulating finite temperature effects within the DMRG framework [81]. The credo of 'entering the church of purification' turns out to be equally crucial for developing a CP Keldysh real-time formalism as we do in this thesis. This formalism additionally benefits from the Kraus' operator-sum representation theorem developed by Sudarshan, Mathews, Rau [82] and Kraus [83], cf. Ref. [84]. This result fixes the *form* of a CP-TP dynamical map to be

$$\Pi(t)\rho(0) = \sum_e K^e(t)\rho(0)K^e(t)^\dagger, \tag{1.2}$$

where the so-called Kraus operators $K^e(t)$ obey the sum-rule $\sum_e K^e(t)^\dagger K^e(t) = \mathbb{1}$. It should be stressed again that in contrast to this, the general form of PP maps is unknown. This is a

crucial *practical* reason for working with CP maps besides the above-mentioned fundamental ones. A direct microscopic derivation of the explicit time-dependence of these Kraus operators has been a long-standing issue in open-system dynamics and we make progress on this by generalizing and unifying seemingly distinct recent approaches along these lines [32, 85].

1.2 How can quantum Markovianity be understood?

As pointed out above, the issue of non-Markovian dynamics arising from memory-effects and the backaction of the environment onto the system has increasingly picked up interest in the quantum information community, as indicated by the recent topical reviews on this matter [86–88]. On a fundamental level, the question arises how the classical notion of a stochastic Markov process may be consistently generalized to the quantum realm. In classical probability theory, the Markov condition for a time-dependent stochastic process for an observable $X(t)$ is characterized by the relation

$$p(x_i, t_i|x_{i-1}, t_{i-1}; \ldots; x_0, t_0) = p(x_i, t_i|x_{i-1}, t_{i-1}) \tag{1.3}$$

for the conditional probabilities $p(x_i, t_i|x_{i-1}, t_{i-1})$ of finding the value x_i at time t_i given that it had the value x_{i-1} at an earlier time t_{i-1}, see Fig. 1.2(a). A classical Markov process does not retain a memory of the full history of previous events but only depends on the two-point transition probabilities which form a semigroup due to the Chapman-Kolmogorov equation

$$p(x_i, t_i|x_j, t_j) = \sum_{x_k} p(x_i, t_i|x_k, t_k)\, p(x_k, t_k|x_j, t_j). \tag{1.4}$$

This feature significantly simplifies the mathematical structure of classical Markov processes and one would hope that an analogous description in the quantum realm is feasible.

How should however the conditional probabilities $p(x_i, t_i|x_{i-1}, t_{i-1}; \ldots; x_0, t_0)$ be understood in the non-commutative quantum theory? To obtain an event $\{x_i, t_i\}$, a measurement of the system is required which will in general disturb the subsequent statistics. A stochastic quantum process may furthermore depend on the details of the measurement operation itself. Physically, the definition of what 'memory' refers to in the quantum case is not as clear-cut as in the classical case. These issues render it unlikely that a quantum analogue to Eq. (1.3) exists. Therefore, efforts in defining quantum Markov processes have focused on instead extending the Chapman-Kolmogorov equation (1.4) in form of *divisibility* properties of the dynamical map $\Pi(t)$, see Fig. 1.2(b).

Two major mathematical distinctions of Markovianity have emerged from these considerations [87, 88]: The 'truly Markovian' semigroup-divisibility $\Pi(t) = \Pi(t - t')\Pi(t')$ is the oldest [89, 90] and arguably the most direct generalization of the Chapman-Kolmogorov equation to quantum dynamical maps. It entails the possibility of decomposing the evolution into a repeated action of the *same* map over different time-intervals. Such semigroup-divisible dynamics is highly restricted in its form and has a simple exponential solution that is conveniently represented in terms of QMEs with time-independent generators. This is in fact quite similar to the classical case but generalizes it by accounting for off-diagonal elements of the density operator. Only recently [91, 92], the more subtle notion of CP-divisibility $\Pi(t) = \Pi(t, t')\Pi(t')$ was identified where the divisor map $\Pi(t, t')$ is required to be CP-TP but may be *different* from $\Pi(t)$. This represents a rather loose generalization of the Chapman-Kolmogorov equation (1.4). Regarding CP-divisibility as a hallmark feature for generic 'quantum Markovian' processes is motivated by the fact that the divisor map $\Pi(t, t')$ may still be

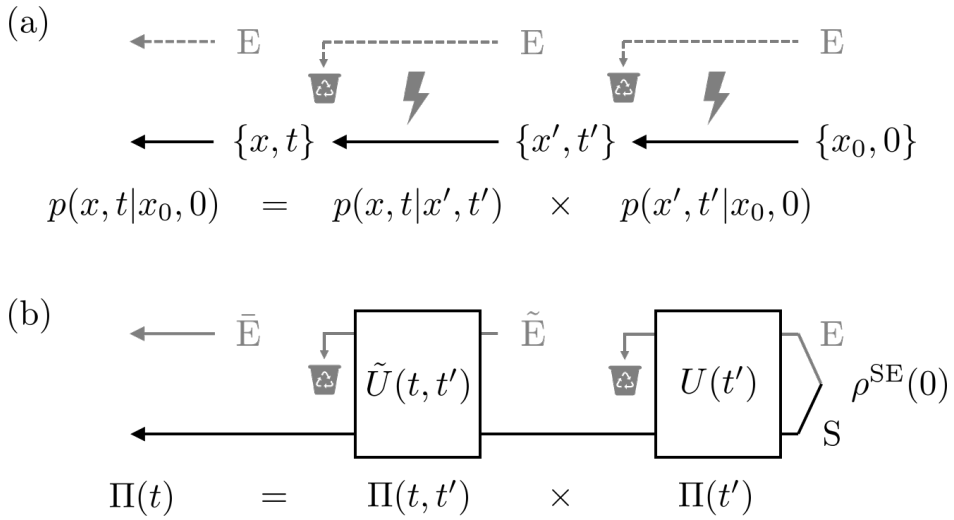

Figure 1.2: Markovian processes are commonly understood to retain no 'memory' of previous interactions of the system with its environment. (a) In the classical case, the notion of memory is well-defined: In a stochastic Markov process (from right to left), the dynamics between subsequent measurements $\{x_i, t_i\}$ of the system is fully characterized by the two-point conditional probabilities $p(x,t|x',t')$. These obey the Chapman-Kolmogorov equation (1.4) and arise from noise introduced by the environment E which is reinitialized (trash-can) to the *same* state after each measurement. (b) In the quantum case, memory is not as straightforwardly understood since measurements may disturb the subsequent dynamics. One may nevertheless interrupt the dynamics at intermediate times $\Pi(t) = \Pi(t,t')\Pi(t')$ by resetting the environment E *without* changing the reduced system's final state at time t. In the semigroup-divisible case $\Pi(t,t') = \Pi(t-t')$ and the environment is reset to the same state as in the classical case. However, resetting it to *different* states, or changing the subsequent evolution is also possible in the quantum case and referred to as CP-divisibility.

considered to arise from a microscopic albeit different physical model due to Stinespring's dilation theorem [80]. However, such dynamics does in general *not* admit a simple exponential solution but requires a nontrivial time-ordering because the corresponding QMEs have time-dependent generators. Correspondingly, CP-divisible dynamics is much more intricate to deal with than semigroup-divisible dynamics but in any case provides a helpful further characterization of interesting dynamics beyond a simple exponential behavior. Finally, it should be stressed that the dynamical map $\Pi(t)$ is, as long as it is invertible[3], *always* mathematically divisible if the CP requirement on the divisor $\Pi(t,t')$ is dropped. In that case, there exists no valid *physical* picture for the divisor since Stinespring's dilation theorem does not apply and we can refer to such dynamics as 'truly non-Markovian'.

There are numerous other distinctions of quantum Markovianity that instead focus on its *observable* impact on the dynamics and its useful implications for purposes in quantum metrology [39] and steady-state entanglement [40] mentioned earlier. One prominent distinction instead starts by defining 'memory' retained in the environment as motivated by the unproblematic classical Markov notion. Several quantitative measures of such memory in terms of an information flow from the environment back to the system have been proposed as an indicator of non-Markovianity. For instance, Breuer *et al.* [87] proposed the distin-

[3]Note that the inverse $\Pi(t)^{-1}$ cannot be a CP-TP dynamical map unless $\Pi(t)$ itself is unitary.

guishability of quantum states as a hallmark feature which should monotonously decrease during a Markovian process where the information flow is unidirectional from the system to the environment. A different approach is followed by Rivas *et al.* [93] who argue from the CP-divisibility criterion and instead propose the monotonicity of entropic quantities such as the entanglement entropy, quantum mutual information or quantum Fisher information as a decisive feature of Markovian dynamics. All these statistical measures have the advantage that they can be experimentally accessed as has recently been demonstrated in all-optical setups [94] and ion-trap experiments [95]. Yet, it is not always possible to reconcile the observable measures with the divisibility criteria and this has triggered a lively debate about the meaningfulness of the latter [96]. In this thesis, we further contribute to this discussion by exhaustively analyzing the observable impact of the divisibility criteria for a simple, exactly solvable impurity model. In line with previous studies, we find that a loss of the semigroup-divisibility has the most pronounced oberservable consequences. However, also the transition from CP-divisible dynamics to the 'truly' non-Markovian regime exhibits measurable features.

Understanding quantum Markovianity is also an issue from a practical point of view: For any but the simplest impurity models, a rigorous derivation of the dynamical map $\Pi(t)$ from Eq. (1.1) calls for approximate treatments of the time-evolution. In the open-system setup, these have typically been based on a perturbative expansion in the system-environment coupling to derive tractable QMEs from the von Neumann equation for the total system. The following sections review a few commonly used descriptions in terms of (approximate) QMEs and their relation to the divisibility criteria. With this we also identify the methodological roadblocks for consistently describing non-Markovian dynamics that we aim to overcome.

1.2.1 Divisibility in time-local QMEs

The above discussion of memory being the source of non-Markovian features in practice often goes hand in hand with the *Born-Markov approximation* [97] as the prime example leading to semigroup-divisible dynamics: It entails a leading order perturbation expansion in the system-environment coupling on the level of the QME (Born) and the notion that relevant time-scales of the environment are much faster than those of the system (Markov) such that it *instantaneously* recovers its equilibrium state after each elementary interaction with the system. The memory-timescale of the environment is thus effectively set to zero. Despite these rather strict requirements, the Born-Markov approximation works surprisingly well in a broad range of problems. This is especially true for many quantum optical systems due to a natural separation of time-scales but also for transport problems in quantum-dot devices where the system-environment coupling can be tuned into the weak-coupling regime. In parts of this thesis, we will also exploit the simplifications of the Born-Markov approximation for *driven-dissipative* quantum optical systems to investigate the influence of a periodic parameter-modulation on the emergence of metastable and nonequilibrium steady states.

The main reason for the popularity of the Born-Markov approximation is associated with the special *form* of the resulting time-local QME[4]

$$\begin{aligned}\tfrac{d}{dt}\rho(t) &= [-iL + \Sigma]\rho(t) \\ &= -i[H,\rho(t)] + \sum_i \gamma_i \left[J_i\rho(t)J_i^\dagger - \tfrac{1}{2}\{J_i^\dagger J_i, \rho(t)\}\right]\end{aligned} \tag{1.5}$$

that renders an analytic treatment particularly easy: Due to the time-independence of the

[4]Units of $\hbar = k_\mathrm{B} = |e| = 1$ are used throughout the thesis.

generator, the dynamical map is given by a simple exponential $\Pi(t) = e^{[-iL+\Sigma]t}$ thereby revealing its semigroup-divisibility. Here, the Liouvillian $L = [H, \bullet]$ represents the coherent evolution of the reduced system in terms of the commutator $[A, B] = AB - BA$ with an effective Hamiltonian H, whereas the dissipative influence of the environment is captured by the jump operators J_i appearing in the incoherent part $\Sigma = \sum_i \gamma_i [J_i \bullet J_i^\dagger - \frac{1}{2}\{J_i^\dagger J_i, \bullet\}]$. Crucially, it was shown by Gorini, Kossakowski and Sudarshan [89] as well as Lindblad [90] that a semigroup-divisible dynamical map is CP-TP if and only if it is governed by a QME of such a GKSL form named after its authors. In particular, the CP property is ensured by the requirement that the constant decay rates $\gamma_i \geq 0$ acting as probabilities for the occurrence of quantum jumps J_i are non-negative. The inclusion of the anti-commutator $\{A, B\} = AB + BA$ with the jump operators ensures the TP property. This powerful theoretical insight has led to its widespread use in particular in a phenomenological modeling of open-system dynamics where a rigorous microscopic description is often difficult.

The generalization of the time-local QME (1.5) to an explicitly time-dependent generator has also been important in the context of CP-divisible dynamical maps:

$$\begin{aligned} \tfrac{d}{dt}\rho(t) &= [-iL(t) + \Sigma(t)]\rho(t) \\ &= -i[H(t), \rho(t)] + \sum_i \gamma_i(t) \left[J_i(t)\rho(t)J_i(t)^\dagger - \tfrac{1}{2}\{J_i(t)^\dagger J_i(t), \rho(t)\} \right]. \end{aligned} \tag{1.6}$$

Without further assumptions, *any* dynamics must have a generator of this form just by the requirements of trace and hermiticity preservation. However, applying the original proof by Gorini, Kossakowski, Sudarshan and Lindblad, to the divisor $\Pi(t, t')$, one can additionally show that the corresponding dynamical map is CP-divisible if and only if the time-dependent decay rates $\gamma_i(t) \geq 0$ happen to be non-negative at all times [87, 98]. One should carefully note that temporarily negative decay rates indicate a breakdown of the CP-divisibility property but make no statement about CP. Clearly, such QMEs are less straightforward to solve due to the nontrivial time-ordering involved and in general do not give rise to an exponential solution. Also, in contrast to the semigroup-divisible case obtained from the Born-Markov approximation, little is known about how CP-divisible dynamical maps can be obtained in approximate treatments: So far, time-dependent GKSL generators have either been used on a phenomenological level or have been extracted from *exact* microscopic open-system models for which we provide another example in Ch. 3. There, we study the resonant level model with the aim of assessing in detail the observable impact of the divisibility properties. We also develop some understanding of how the divisibility properties manifest themselves in the details of the model and are affected by commonly made approximations. Furthermore, our exact results provide a means to benchmark more advanced approximation schemes while explicitly keeping track of the CP and divisibility properties.

1.2.2 Relation to time-nonlocal QMEs

When it comes to actually devising novel approximation schemes for the perturbation expansion in the system-environment coupling that are valid beyond the Born-Markov limit, commonly employed methods are often either derived from or equivalent to the Nakajima-Zwanzig formalism [99, 100]. These generically lead to time-*non*local QMEs:

$$\tfrac{d}{dt}\rho(t) = -i[H, \rho(t)] + \int_0^t dt' \Sigma(t, t')\rho(t'). \tag{1.7}$$

Only in the Born-Markov approximation this readily simplifies to the time-local QME (1.5). The strong-coupling regime where the Born approximation typically fails and non-Markovian effects incorporated in the time-nonlocal kernel $\Sigma(t,t')$ become important [101] is however ubiquitous in molecular quantum dots [24] and nowadays also experimentally accessible in on-chip quantum optical systems [102–104] as well as semiconductor nanostructures [105, 106]. In quantum dot devices, also the backaction of the measurement apparatus onto the system has been found to lead to effects that are not fully captured by GKSL master equations [107]. These systems require more sophisticated approximation schemes that start from Eq. (1.7) and systematically go beyond the semigroup-divisible limit, see, e.g., Refs. [108, 109].

Unfortunately, the Born-Markov approximation is one of the scarce examples that manages to preserve the fundamental CP-TP property of dynamical maps, in contrast to higher-order expansions in the system-environment coupling where, as we will show, especially the CP (and possibly even PP) property can be lost depending on the parameters. To the best of the author's knowledge the impact of higher-order approximations on the divisibility properties has not been systematically investigated so far. These concerns raise the following pressing questions:

- What is the explicit relation between time-nonlocal QMEs of the type (1.7) and time-local QMEs of the type (1.6)?
- How do the CP and CP-divisibility theorems for the latter translate into the properties of the *memory-kernel* $\Sigma(t,t')$ featuring in the former?
- Do existing approximations preserve these properties? If not, can one improve them or devise novel schemes to consistently account for CP and CP-divisibility?

The first question has been addressed in the context of the time-convolutionless (TCL) approach to QMEs [110–113]. While it is straightforward to see that for the two QMEs to be equivalent the relation $\Sigma(t) := \int_0^t dt' \Sigma(t,t')\Pi(t')\Pi^{-1}(t)$ must hold, the occurrence of the inverse dynamical map has led to a debate about the general validity of TCL descriptions, see, e.g., Ref. [114]. In this thesis, we further contribute to this discussion with an explicit comparison of both QMEs for an exactly solvable model that shows no inconsistencies between them for any of the model parameters. The primary concern of this thesis is however the second question: We present a reorganization of the time-nonlocal Keldysh real-time perturbation series [115] that reveals the CP structure of the memory-kernel $\Sigma(t,t')$ and explicitly fixes each order to result in a CP dynamical map. Importantly, these advances are only possible by combining methods from both the quantum information and statistical physics communities building upon earlier studies [32–34]. How these findings translate into TCL approaches and also the final question regarding actual approximation schemes is mostly left for future research but we will be able to provide concrete guidance for further investigations in this largely unexplored direction.

1.3 How can open-system dynamics be efficiently simulated?

The above considerations of QME approaches to open-system dynamics reflect the trade-off between analytical insights enabled by powerful mathematical theorems and the necessity to perform approximations to be able to treat microscopic models with continuous environments. Of course, these considerations can be complemented with efficient numerical techniques. Although this is beyond the scope of the present work, it is nevertheless instructive to give

an overview of recent numerical advances that might benefit from our results and vice versa. They can be classified according to two different paradigms.

Hierarchical approaches are closely related to the QME methods employed within this thesis. Direct numerical integration in particular of time-nonlocal QMEs but also of time-local ones with explicitly time-dependent generators scales unfavorably with the simulation time which makes it difficult to reach the steady state of many open systems. In order to alleviate this issue, it may thus be useful to decompose the QME into a coupled *hierarchy* of equations that can either be more efficiently solved exactly or truncated in a controlled manner. Interestingly, our reorganization of the perturbation series presented in Ch. 5 naturally generates a hierarchy of CP dynamical maps. Understanding its relation to existing numerical techniques constitutes an interesting follow-up to this work. Two numerical methods appear particularly relevant in this regard:

The exact hierarchical quantum master equation (HQME) approach first developed by Tanimura and Kubo [116] and later on refined, e.g. by Jin [117] and Härtle [118, 119], is based on a path-integral formulation in terms of the Feynman-Vernon influence functional. The tiers of this infinite hierarchy are obtained from an expansion of the environmental correlation functions into sets of exponential terms. This simplifies the evaluation of appearing time-derivatives in nested commutators of the density operator with the coupling Hamiltonian and enables a closed representation. Fast convergence of this nontrivial perturbative expansion is typically restricted to high temperatures of the environment where taking into account the first few tiers is already sufficient. The HQME approach is thus well-suited for simulating the long-time dynamics at relatively high temperatures and due to its blackbox formulation can be applied to quite complex systems [120].

A different approach is taken in the transfer tensor method (TTM) [121–123] which exploits the fact that the memory-kernel $\Sigma(t, t')$ may decay on rather short time-scales [124, 125]. It also acts as a blackbox method to efficiently simulate the long-time dynamics in terms of a hierarchy of transfer tensors that take the short-time information about the memory-kernel as an input. The latter can be inferred either from stochastic approaches which can efficiently simulate the short-time evolution, see below, or from experimental data using quantum process tomography [57, 126]. The limiting aspect of this technique is not the achievable time-scale but rather the memory time-scale of the environment which determines the number of transfer tensors required, see also Ref. [127] for a detailed analysis of its limitations.

Stochastic approaches form a complementary alternative to obtaining the dynamical map by evolving pure system states under stochastic processes modeled as sequences of projective measurements on the environment, so-called quantum jumps [128]. Such a measurement picture provides a clear physical intuition that can even be experimentally probed [129, 130]. This raises the question how the conditional processes introduced in Ch. 5 are related to such quantum jump ideas. Because *pure states* are evolved instead of density operators, issues concerning the CP property are not encountered and initial system-environment correlations do not complicate matters. However, due to the inherent stochastic sampling, these approaches are typically restricted to short-time dynamics. Again, we mention two particular concepts:

On a more phenomenological level, stochastic Schrödinger equations have long been considered in various representations, see Ref. [88] for an overview. The underlying principle is to consider the open system in terms of a closed system Schrödinger equation and complement it by jump operators that can stochastically add or remove excitations. Sampling over multiple trajectories under this stochastic influence then results in an estimate for the

true evolution of the open system which works particularly well at short times and connects back to QME descriptions. Stochastic Schrödinger equations can also be derived for impurity models beyond the Born-Markov approximation [131]. These non-Markovian versions however have their own distinct problems as they typically result in nonlinear equations that are difficult to integrate. Also, the occurrence of negative probabilities for quantum jumps hinders a physical understanding of the processes.

Applying quantum Monte Carlo (QMC) techniques to open-system *dynamics* has long suffered from what is known as the dynamical sign problem [132] due to the oscillatory behavior of the unitary evolution operator and the quantum interference of competing processes. The recently proposed 'inchworm' QMC method alleviates this issue by "iteratively reusing information from shorter time propagation to obtain results for longer times" [133]. It is based on a stochastic sampling of diagrammatic contributions to the real-time perturbation series and might therefore be interesting for the diagrammatic method presented in this thesis.

1.4 Outline of the main results

The structure of this thesis is designed as to address the main issues outlined in Sec. 1.2. We focus on introducing and comparing analytical methods to understand open quantum system dynamics and exploiting the information-theoretic perspective. We are particularly concerned with measurements on the environment and the information encoded in the correlations with the system. The methods are illustrated by rather simple models in order to highlight these specific aspects without loosing focus in technically complicated calculations. We hope to provide sufficient guidance for follow-up work that investigates more realistic interacting models to further connect with experiments.

We present a navigation through the main results of the thesis:

- **Ch. 2.** First, the open-system setup we have in mind throughout the thesis is clearly defined as to avoid the pitfalls mentioned in Sec. 1.1. The information-theoretic background that is central to the developed techniques is introduced and compared with the main concepts of statistical physics. In particular, we point out a complementarity in their approaches to open-system dynamics that is hard to avoid and connect it to a duality between complete positivity and trace preservation. This allows us to exploit the synergies of these different methods. More specialized concepts of statistical physics are instead deferred to the main chapters 3–5 each of which is intended to be a self-contained discussion highlighting the aspects outlined in this introduction. While this may repeat a few concepts, it adapts these to the needs of each chapter. We hope this provides a coherent overview of quantum information theory from an open-system perspective that is more relevant and accessible for the statistical physics community.

- **Ch. 3, published in Ref. [134].** The observable impact of the divisibility criteria is analyzed for a noninteracting resonant level coupled arbitrarily strongly to a fermionic reservoir at arbitrary temperature and chemical potential. In the wideband-limit, this model is exactly solvable and enables us to analytically keep track not only of the CP but also the divisibility properties of the dynamical map. The latter strongly depend on the model parameters such that all discussed types of divisibility can be probed. We find that a single approach is not sufficient to do so: A combination of several methods is required to fully explore the dynamical map. In this context, a Heisenberg equation of motion (EOM) approach is employed to obtain a time-local QME

description most suitable for the analysis of divisibility properties. A superfermion approach in Liouville space instead results in a time-nonlocal QME and allows for a detailed comparison with the time-local form. It also provides crucial guidance for formulating approximation schemes that are relevant beyond this model. We give an example of a nonperturbative Markovian approximation that is capable of preserving the CP-TP property while retaining the exact steady state. These approaches are then complemented with an explicit derivation of the canonical Kraus operator-sum in order to investigate the dynamics of entropic measures quantifying the nontrivial footprint the system leaves in its effective environment. Finally, the analysis of the spectral properties of the dynamical map and particularly its time-dependent fixed-points reveals an interesting reentrant behavior of observables *outside* the semigroup-divisible regime.

- **Ch. 4, published in Ref. [135].** A diametrically opposed approach is followed for studying the influence of a periodic parameter modulation on nonequilibrium metastable and steady states of more sophisticated quantum optical systems. Here we make use of the Born-Markov approximation which even in this case enables a reduction to QMEs with explicitly time-dependent GKSL generators. Reaching sufficiently long times to probe these states can be numerically demanding and we develop a method to efficiently evaluate them by integrating over a single period of the parameter modulation only. This method can in fact be generalized to generic time-local QMEs with periodic generators. Applying this method to three different systems – two- and three-level models as well as a driven Kerr nonlinear cavity – we propose periodic modulation protocols of parameters leading to a temporary suppression of effective dissipation rates, and study the arising nonadiabatic features in the response of these systems. For the paradigmatic Kerr nonlinearity model we find that the emergence of long-lived metastable states causes a nonadiabatic, hysteretic behavior in the system-occupation which can be linked to the gap-closure of the Liouvillian superoperator.

- **Ch. 5, published in Refs. [136, 137].** A novel Keldysh real-time diagrammatic approach is established that explicitly enforces the CP property of the dynamical map even beyond the Born-Markov limit. This is achieved by casting the reorganized perturbation series into the form of a Kraus operator-sum. It thereby brings together on the most general level the methods used in the quantum information theory and statistical physics communities. The explicit diagrammatic structure of the memory-kernel $\Sigma(t, t')$ in terms of CP building blocks is derived which forms a convenient starting point for devising new and comparing with existing diagrammatic approximations. Concerning CP-TP approximation schemes, we find that a rigorous, simultaneous preservation of both complete positivity and trace cannot be based on diagram selection alone but requires nontrivial additional steps [32–34].

- **Ch. 6** Finally, we present the take-away messages for both communities addressed in this thesis and conclude with a discussion of the impact for future research, while more in-depth summaries can be found at the end of each chapter [Secs. 3.8, 4.7 and 5.6].

2 Complementary views on open-system dynamics

In this chapter we first review two formulations of generic open quantum system dynamics based on a quantum-information and field-theory approach, respectively. Already here fundamental differences in their scopes become evident: The former in a sense provides a bird's-eye view arguing in an input-output scheme how entanglement between the system and its environment are unitarily transformed and how information is encoded in these correlations. Primary interest of this quantum-information perspective is thus the environment's global *effect* on the open system where continuous time plays no explicit role. The latter instead focuses on the details within this input-output scheme and inquires how the system-environment *coupling* microscopically generates the dynamics in infinitesimal time steps. The corresponding field-theoretical approaches are therefore concerned with the *cause* of the environment's effect on the open system. As we will see, this simple complementarity of approaches to open-system dynamics translates into deep formal and practical differences.

The setup we have in mind is that of a nonequilibrium impurity or transport model where an arbitrary finite quantum system S with a discrete spectrum is coupled to one or more noninteracting reservoirs with continuous spectra. Each of these reservoirs is in a different thermodynamic equilibrium state and together they constitute the environment E. The large dimensions of the reservoirs rule out a direct treatment of the total system that is assumed to be closed and therefore evolves unitarily. Instead, the environment degrees of freedom are 'traced out' to arrive at a simpler effective description of the reduced density operator for the local system of interest as given in Eq. (1.1) and repeated here for convenience:

$$\rho(t) = \Pi(t)\rho(0) = \operatorname*{Tr}_{\mathrm{E}} U(t)[\rho(0) \otimes \rho^{\mathrm{E}}(0)]U(t)^{\dagger}. \tag{2.1}$$

It is essentially this discarding of information about the environment that causes an 'irreversible' duality between the quantum information and statistical field-theory approaches as we point out below. In Eq. (2.1) the initial total state is assumed to factorize $\rho^{\mathrm{SE}}(0) = \rho(0) \otimes \rho^{\mathrm{E}}(0)$. As explained in Sec. 1.1, the dynamical map $\Pi(t)$ is in this case completely positive (CP) and trace-preserving (TP). Under these assumptions, we inquire about general physical characteristics of such an evolution: First from the bird's-eye view of quantum information theory focusing on useful information measures for the system *and* its environment. Then we take the complementary close-up view of statistical physics suitable for practically calculating the explicit time-dependence of these measures in transport models.

Publications and acknowledgments. Parts of this chapter (including the adapted figures) have been published in V. Reimer, and M. R. Wegewijs, SciPost Physics **7**, 012 (2019) [CC BY 4.0 License], see Ref. [137], and V. Reimer, M. R. Wegewijs, K. Nestmann, and M. Pletyukhov, The Journal of Chemical Physics **151**, 044101 (2019) [Copyright 2019 by the American Institute of Physics], see Ref. [134]. While the general concepts of purification and the effective environment are well-known in the quantum information community, the specific derivations presented here are better adapted to the discussions in this thesis as compared to standard textbook presentations [57, 71] which have no interest in mixed environments or continuous dynamics.

2.1 A bird's-eye view of open-system dynamics

We start with the quantum-information perspective and investigate how much can be learned about the dynamics *without* access to the 'internal' specifics of the joint unitary evolution $U(t)$ of the system and its environment. This is very much the setup of a quantum process tomography [57] for experimentally characterizing the dynamical map. Also there, the only accessible turning knobs are the initialization procedure and the measurement of the final system at time t.

2.1.1 Purification

As a first step, we consider how the initial states of both the system $\rho^{\mathrm{S}}(0)$ and its environment $\rho^{\mathrm{E}}(0)$ may be prepared in principle[1]. Clearly, pure states may be prepared by any local projective measurement on each subsystem that causes a collapse onto the (nondegenerate) eigenstate to the measured eigenvalue. But how can an *arbitrary* mixed state that not necessarily derives from a thermodynamic equilibrium be experimentally prepared?

An answer to this question is provided by the *purification* [57]: One can consider mixed states to arise as the marginal of a pure *entangled* state on an enlarged Hilbert space. Take as an example the pure but entangled two-qubit Bell state $|\psi^{\mathrm{SP_S}}\rangle = \frac{1}{\sqrt{2}}(|0^{\mathrm{S}}\rangle\otimes|0^{\mathrm{P_S}}\rangle+|1^{\mathrm{S}}\rangle\otimes|1^{\mathrm{P_S}}\rangle)$. From this, we can create a mixed state by performing a complete local measurement on the 'purifying' qubit labeled by $\mathrm{P_S}$. Discarding the measurement outcome right away, we effectively marginalize the Bell state $|\psi^{\mathrm{SP_S}}\rangle$ over $\mathrm{P_S}$ since we only know that the measured qubit will be in one of its eigenstates but not in which one. Correspondingly, the other qubit S has now been prepared in the unbiased mixed state $\rho^{\mathrm{S}} = \mathrm{Tr}_{\mathrm{P_S}}|\psi^{\mathrm{SP_S}}\rangle\langle\psi^{\mathrm{SP_S}}| = \frac{1}{2}(|0^{\mathrm{S}}\rangle\langle 0^{\mathrm{S}}| + |1^{\mathrm{S}}\rangle\langle 1^{\mathrm{S}}|)$. Thus, the measured and then discarded qubit $\mathrm{P_S}$ acts as an auxiliary *preparing* system for the remaining qubit S. In this sense, the purification encodes the information content of the randomness of a mixed state in entanglement with the preparing system. Note that the specific choice of a purification is irrelevant as long as it produces the same reduced state. The limit of a *pure* state $\rho^{\mathrm{S}}(0)$ is also included: The total state $|\psi^{\mathrm{SP_S}}\rangle = |\psi^{\mathrm{S}}\rangle\otimes|\psi^{\mathrm{P_S}}\rangle$ then trivially factorizes and discarding $\mathrm{P_S}$ does not affect S in any way. Importantly, it can be shown [71] that a preparing system of the same dimension $\dim \mathrm{P_S} = \dim \mathrm{S}$ as the system of interest is sufficient to purify any mixed state of S.

Applying this individually to both the system $\mathrm{S}' = \mathrm{S}\otimes\mathrm{P_S}$ as well as to its environment $\mathrm{E}' = \mathrm{E}\otimes\mathrm{P_E}$ leaves us with four subsystems. It is of interest to keep track of all of these during the evolution as they provide information about how correlations encoded by entanglement with the other subsystems are being transformed. This evolution is depicted in Fig. 2.1 as a quantum circuit with time running from right to left, i.e., in the same order of writing expressions. Notably, only the subsystems S and E participate in the unitary evolution while the preparing systems $\mathrm{P_S}$ and $\mathrm{P_E}$ do not evolve: They form the blind and dead witness [55] discussed in Sec. 1.1. The fact that the total system was initially purified into $|\psi^{\mathrm{S'E'}}(0)\rangle = |\psi^{\mathrm{S'}}(0)\rangle\otimes|\psi^{\mathrm{E'}}(0)\rangle$ is beneficial because this state *stays* pure under the unitary dynamics:

$$|\psi^{\mathrm{S'E'}}(t)\rangle = U(t)\otimes\mathbb{1}^{\mathrm{P_SP_E}}\ |\psi^{\mathrm{S'E'}}(0)\rangle\,. \tag{2.2}$$

The joint evolution of system and environment generates entanglement between S' and E' causing their initial factorization to break down. The key insight is illustrated in Fig. 2.1 and

[1] To clearly distinguish the introduced subsystems, it is useful to deviate from the standard notation used throughout the thesis and explicitly label the reduced density operator $\rho \to \rho^{\mathrm{S}}$ in this chapter.

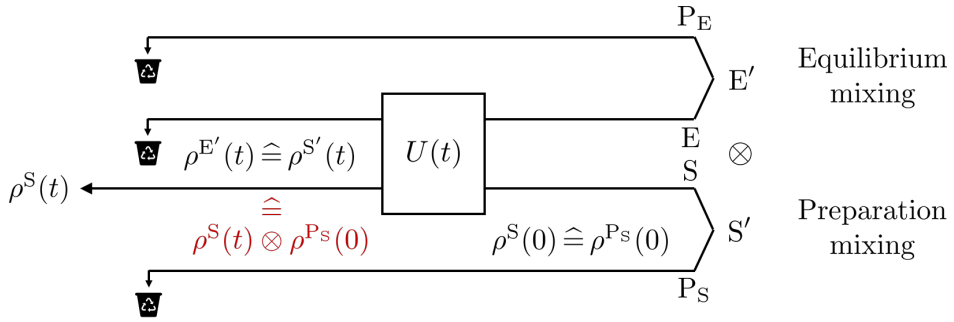

Figure 2.1: Dynamics $\rho^{\mathrm{S}}(t) = \mathrm{Tr}_{\mathrm{E}} U(t)[\rho^{\mathrm{S}}(0) \otimes \rho^{\mathrm{E}}(0)]U(t)^\dagger$ with *mixed* initial states for both system and environment. The extensions by the purifications $\mathrm{P_S}$ and $\mathrm{P_E}$ account for this mixing as initial entanglement of pure systems $\mathrm{S'}$ and $\mathrm{E'}$, respectively. The trashcan indicates the point in time where a system has become inaccessible (is traced out). An equality such as $\rho^{\mathrm{S}}(0) \mathrel{\widehat{=}} \rho^{\mathrm{P_S}}(0)$ indicates that the *spectra* of the reduced *density matrices* of two complementary subsystems are the same, while the operators act on different subsystem spaces S and P. The *red* product state only holds for a *pure* initial state $\rho^{\mathrm{S}}(0)$. Reprinted figure (adapted) with permission from J. Chem. Phys. **151**, 044101 (2019), see Ref. [134]. Copyright 2019 by the American Institute of Physics.

follows from the Schmidt decomposition theorem [57]: Because the joint state stays pure, the *spectra* of marginal states obtained by tracing out any pair of complementary subsystems are all equal. Each marginal spectrum contains the full nonlocal information about the entanglement across the corresponding bipartition and allows one to investigate not only properties of the system S but also the footprint it leaves in the other subsystems:

$$\rho^{\mathrm{S}}(t) = \operatorname*{Tr}_{\mathrm{E'P_S}} |\psi^{\mathrm{S'E'}}(t)\rangle \langle\psi^{\mathrm{S'E'}}(t)| \tag{2.3a}$$

$$\rho^{\mathrm{E'}}(t) = \operatorname*{Tr}_{\mathrm{SP_S}} |\psi^{\mathrm{S'E'}}(t)\rangle \langle\psi^{\mathrm{S'E'}}(t)| \tag{2.3b}$$

$$\rho^{\mathrm{S'}}(t) = \operatorname*{Tr}_{\mathrm{E'}} |\psi^{\mathrm{S'E'}}(t)\rangle \langle\psi^{\mathrm{S'E'}}(t)| \,. \tag{2.3c}$$

The above three subsystems are of particular interest for the following discussions.

2.1.2 Kraus operator-sum representation

The primary object of interest is the reduced system density operator (2.3a) obtained by tracing out all other subsystems. This tracing out can be done in a way that gives rise to a particularly useful representation of the open-system dynamics depicted in Fig. 2.2(a) without the preparation system $\mathrm{P_S}$ which is irrelevant to the following consideration: First, we purify the environment $\rho^{\mathrm{E'}}(0) = |0\rangle\langle 0|$ in terms of its initial eigenbasis $\rho^{\mathrm{E}}(0) := \sum_n \rho_n^{\mathrm{E}} |n\rangle\langle n|$ with

$$|0\rangle \equiv \sum_n \sqrt{\rho_n^{\mathrm{E}}}\, |n^{\mathrm{E}}\rangle \otimes |n^{\mathrm{P_E}}\rangle \,. \tag{2.4}$$

Next, the purified environment is completely absorbed into a mapping $W^{\mathrm{E'}} : \mathrm{S} \to \mathrm{S} \otimes \mathrm{E'}$ of the initial system state to a joint state of system *and* purified environment. Due to the unitarity

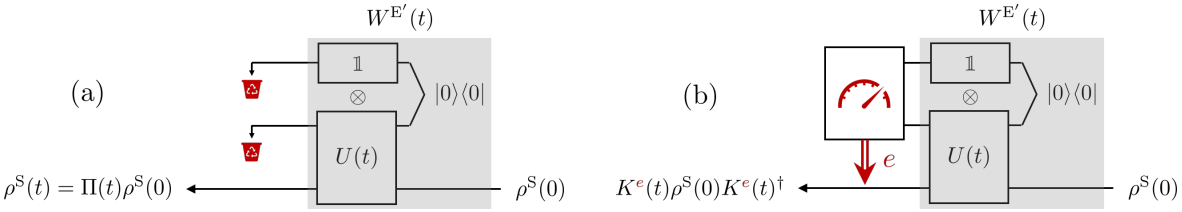

Figure 2.2: Quantum circuits corresponding to the operator sum (2.6) and its individual terms. (a) Reduced evolution: The evolved state is averaged over all *possible* outcomes e of measurements on the purified environment indicated by the trashcan. (b) Conditional evolution: Classical communication of a specific outcome e of a measurement results in a state update described by a single Kraus operator. Reprinted figure (adapted) under CC BY 4.0 License from SciPost Phys. **7**, 012 (2019), see Ref. [137].

of $U(t)$, the map defined by $W^{\mathrm{E}'}(t) := \big(U(t)\otimes\mathbb{1}^{\mathrm{P_E}}\big)\,|0\rangle$ is an isometric map[2] with the defining property $W^{\mathrm{E}'\dagger}W^{\mathrm{E}'} = \mathbb{1}^{\mathrm{S}}$. As a result, we have switched from the unitary evolution of the system and its environment to an *equivalent* isometric description of the open system,

$$\rho^{\mathrm{S}}(t) = \Pi(t)\rho^{\mathrm{S}}(0) = \operatorname*{Tr}_{\mathrm{E}'} W^{\mathrm{E}'}(t)\rho^{\mathrm{S}}(0)W^{\mathrm{E}'}(t)^\dagger, \tag{2.5}$$

where its *effective* environment is initialized into the pure state $|0\rangle$ as shown in Fig. 2.2(a).

The above re-expression of the dynamics is essentially a manifestation of Stinespring's dilation theorem [80]: Any completely positive and trace-preserving (CP-TP) map $\Pi(t)$ can be considered to arise from a joint unitary evolution with an initially uncorrelated *pure* environment that is eventually discarded. Note that representations with *mixed* environments –such as the one we started out with– may also exist, but only if certain additional conditions hold, see, e.g., the appendix '*Mixed-state measurement models and extreme operations*' in Ref. [139]. The CP-TP property becomes explicit when we expand the effective-environment trace featuring in Eq. (2.5) in terms of some orthonormal basis $\{|e\rangle\}$ for E' to arrive at the Kraus *operator-sum* representation of the form (1.2):

$$\Pi(t) = \sum_e K^e(t)\bullet K^e(t)^\dagger, \qquad K^e(t) = \langle e|\,W^{\mathrm{E}'}(t) = \langle e|\,U(t)\otimes\mathbb{1}^{\mathrm{P_E}}\,|0\rangle\,. \tag{2.6}$$

Here, the Kraus operators $K^e(t)$ act on the system only because of the final projection onto the effective-environment states $|e\rangle$. This projection also reveals a freedom in the operator-sum that is related to a rotation of the chosen measurement basis in the effective environment: Any two Kraus-operator sets are unitarily related [57, 140] as $K^e(t) = \sum_{e'}\tilde{K}^{e'}(t)\mathcal{U}_{e'e}(t)$ where $\mathcal{U}$ may be padded with additional zeros as to change the size of the Kraus operator-set. This becomes particularly important in Ch. 5 where an *infinitely* large set of Kraus operators $K^e(t)$ is derived for which it is difficult to find a unitary that can reduce the size of the set. That the quadratic form (2.6) ensures the complete positivity follows from again taking into account the preparation space: Any joint state $\rho^{\mathrm{SP_S}}(t)$ remains positive under the action of $(K^e(t)\bullet K^e(t)^\dagger)\otimes\mathcal{I}^{\mathrm{P_S}} = K^e(t)\otimes\mathbb{1}^{\mathrm{P_S}}\bullet K^e(t)^\dagger\otimes\mathbb{1}^{\mathrm{P_S}}$. The trace-preservation is instead enforced by the sum-rule $\sum_e K^e(t)^\dagger K^e(t) = \mathbb{1}^{\mathrm{S}}$ as easily verified from the isometry $W^{\mathrm{E}'}(t)$.

Besides the elegant mathematical framework that the Kraus operator-sum (2.6) provides,

[2] One can in general extend $W^{\mathrm{E}'}(t) \to \big(U(t)\otimes\mathbb{1}^{\mathrm{P_E}} + X(t)\big)\,|0\rangle$ to be unitary [57, 138]. However, the additional term obeys the property $X(t)\,|0\rangle = 0$ and thus drops out of all physical quantities.

the specific purification (2.4) establishes a useful *physical* intuition about the dynamics: The Kraus operator-sum (2.6) represents a decomposition of the unitary (isometric) evolution $W^{\mathrm{E}'}(t) = \sum_e K^e(t) \otimes |e\rangle\langle 0|$ into *physical* processes on the system that are *conditional* to a change of the *effective* environment. The initial purity of the effective environment is important as it allows for a clean 'count' of the entanglement generated by the coupling with the system. When a measurement on the effective environment does not find it in its original state, $|e\rangle \neq |0\rangle$, this directly probes the entanglement generated between the system S and the original environment E. Accordingly, the system evolution conditional on this outcome is $K^e(t)\rho^{\mathrm{S}}(0)K^e(t)^\dagger$ as shown in Fig. 2.2(b). We stress that the system-environment entanglement cannot be inferred from the *original* environment E due to its generally mixed nature (e.g. thermal noise) represented by entanglement with the preparing space $\mathrm{P_E}$. As in a quantum process tomography, the *initialization* into a pure state is important.

2.1.3 Information measures

This physical intuition of open-system dynamics being conditional on measurements on the effective environment highlights the importance of also keeping track of the state $\rho^{\mathrm{E}'}(t)$ obtained from Eq. (2.3b). Tracing out the *purified system* S' defines the so-called *complementary* quantum channel associated with $\Pi(t)$ which maps the initial system state to the final *environment* state. It plays a key role in the transmission of quantum information [71, 141] and measurement-information tradeoff [142]. The resulting effective-environment state

$$\rho^{\mathrm{E}'}(t) = \sum_{ee'} |e\rangle \left(\operatorname*{Tr}_{\mathrm{S}} K^e(t)\rho^{\mathrm{S}}(0)K^{e'}(t)^\dagger \right) \langle e'| \,, \tag{2.7}$$

can be represented by a matrix which features the *individual* Kraus operators –not just their sum– and the initial system state $\rho^{\mathrm{S}}(0)$. While the specific basis states $|e\rangle$ are generally unknown, the *spectrum* is independent of the choice of the particular purification, and therefore provides *intrinsic* information about the interaction of the system with *any* initially pure effective environment [57]. The same holds for the state $\rho^{\mathrm{S}'}(t)$ including the preparation $\mathrm{P_S}$ obtained from Eq. (2.3c) because it shares the same spectrum [cf. Sec. 2.1.1]. Knowledge of the density *matrices* for both system $\rho^{\mathrm{S}}(t)$ and effective environment $\rho^{\mathrm{E}'}(t)$ allows the computation of information measures based on the quantum entropy $S(x) := -\mathrm{Tr}\, x \log_2 x$ and enables a quantitative analysis of the information stored in the entanglement with the effective environment [84, 86, 143–145].

The *negative* conditional entropy of $\mathrm{S}' = \mathrm{S} \otimes \mathrm{P_S}$ given S *defines* the so-called *coherent information* [71, 146]. It can be computed using the entropy of the effective environment:

$$I_{\mathrm{c}}(t) := -[S(\rho^{\mathrm{S}'}(t)) - S(\rho^{\mathrm{S}}(t))] = S(\rho^{\mathrm{S}}(t)) - S(\rho^{\mathrm{E}'}(t)). \tag{2.8}$$

From its definition in (2.8) one can show [141, 147, 148] that S and $\mathrm{P_S}$ are entangled if $I_{\mathrm{c}}(t) > 0$, i.e., the positive coherent information quantifies how well the 'preparation-entanglement' between S and $\mathrm{P_S}$ is preserved during the time-evolution. As illustrated in Fig. 2.3, it is a measure for the competition between the time-evolution's *action*, which continuously converts the entanglement between S and $\mathrm{P_S}$ into entanglement with the effective environment E', and its *backaction* that entangles E' with the preparation $\mathrm{P_S}$ thereby affecting the system.

Action and backaction only differ when there is initial entanglement with the *preparing* system $\mathrm{P_S}$, i.e., when $\rho^{\mathrm{S}}(0)$ is mixed. For initially pure states $\rho^{\mathrm{S}}(0)$, there is no such entanglement and $I_{\mathrm{c}}(t) = 0$ for all $t \geq 0$ as illustrated in red in Fig. 2.1: In this case, the pu-

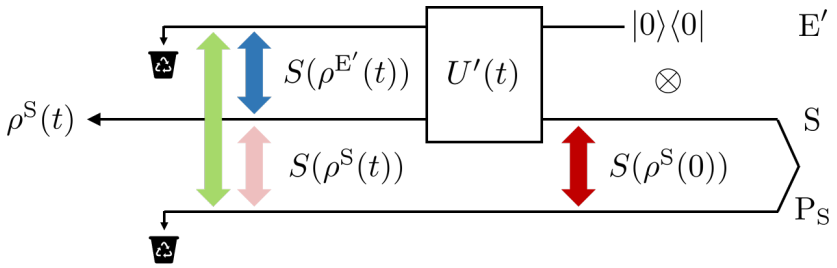

Figure 2.3: Equivalent representation of the dynamics indicating the effective environment E′ that is initially pure and uncorrelated ($\otimes$) with the system S, cf. Figs. 2.1 and 2.2(a). During the unitary joint evolution $U'(t) = U(t) \otimes \mathbb{1}^{\mathrm{P_S}}$, the entanglement of the system S with its initial preparation system $\mathrm{P_S}$ (red) is transformed into entanglement of E′ with both the system (blue) and the preparation (green) until it is fully consumed in the stationary limit, cf. Eq. (2.12). The coherent information $I_{\mathrm{c}}(t)$ [Eq. (2.8)] describes the competition between the first two through the difference of their entanglement entropies. A strictly zero (positive) mismatch $S(\rho(0)) - I_{\mathrm{c}}(t)$ is known [71, 146] to quantify the (in)ability to recover the state of the preparing system P by processing only the output $\rho(t)$. Reprinted figure (adapted) with permission from J. Chem. Phys. **151**, 044101 (2019), see Ref. [134]. Copyright 2019 by the American Institute of Physics.

rification $\rho^{\mathrm{S}'}(0) = \rho^{\mathrm{S}}(0) \otimes \rho^{\mathrm{P_S}}(0)$ is necessarily a tensor product of pure states (entanglement monogamy [57]), and stays a tensor product for all times $\rho^{\mathrm{S}'}(t) = \rho^{\mathrm{S}}(t) \otimes \rho^{\mathrm{P_S}}(0)$ because the extension $\mathrm{P_S}$ does not evolve in time [Eq. (2.2)]. Consequently, as $S(\rho^{\mathrm{P_S}}(t)) = S(\rho^{\mathrm{P_S}}(0)) = 0$, the entropy of S′ arises from the system itself and not its preparation, $S(\rho^{\mathrm{S}'}(t)) = S(\rho^{\mathrm{S}}(t))$ for $t \geq 0$, causing the coherent information I_{c} to vanish identically. Due to the second equality in Eq. (2.8), this in particular implies the equality of the spectra of E′ and S for all $t \geq 0$.

Another related information measure is the mismatch of the coherent information with the initial system entropy,

$$S(\rho^{\mathrm{S}}(0)) - I_{\mathrm{c}}(t) = S(\rho^{\mathrm{S}'}(t)) - [S(\rho^{\mathrm{S}}(t)) - S(\rho^{\mathrm{P_S}}(t)] \tag{2.9a}$$

$$= S(\rho^{\mathrm{E}'}(t)) - [S(\rho^{\mathrm{S}}(t)) - S(\rho^{\mathrm{S}}(0))], \tag{2.9b}$$

which describes the competition of entropy *productions* in the system and effective environment with $S(\rho^{\mathrm{E}'}(0)) = 0$, again exploiting the equivalence of spectra. The form (2.9a) follows from $\rho^{\mathrm{P_S}}(t) = \rho^{\mathrm{P_S}}(0)$ and shows that first, the mismatch is nonnegative by the Araki-Lieb [149] triangle inequality $|S(\rho^{\mathrm{A}}) - S(\rho^{\mathrm{B}})| \leq S(\rho^{\mathrm{AB}})$, and that second, it is less than twice the initial entropy by the subadditivity [57] upper bound, $S(\rho^{\mathrm{AB}}) \leq S(\rho^{\mathrm{A}}) + S(\rho^{\mathrm{B}})$:

$$0 \quad \leq \quad S(\rho^{\mathrm{S}}(0)) - I_{\mathrm{c}}(t) \quad \leq \quad 2S(\rho^{\mathrm{S}}(0)). \tag{2.10}$$

This implies that the entropy produced in the effective environment must always be larger than the entropy produced in the system if the latter is positive. It reaches the maximal value $2S(\rho^{\mathrm{S}}(0))$ in the stationary limit indicating that the entanglement between S and $\mathrm{P_S}$ has been fully broken in favor of entanglement between E and S, and separately $\mathrm{P_S}$, cf. Fig. 2.3.

The last statement generically follows for any evolution with a unique stationary state $\rho^{\mathrm{S}}(t \to \infty)$ that is independent of the initial state $\rho^{\mathrm{S}}(0)$ of the system: In the stationary limit the dynamical map $\Pi(\infty)$ is found to have the form of an *entanglement-breaking map* [71, 141]

which can be conveniently written in terms of a Kraus operator-sum determined by the spectrum of the stationary state $\rho^{\mathrm{S}}(\infty)$ alone:

$$\Pi(\infty) = \rho^{\mathrm{S}}(\infty) \operatorname*{Tr}_{\mathrm{S}} \bullet = \sum_{ij} K^{ij} \bullet K^{ij\dagger}, \qquad K^{ij} = \sqrt{\langle j| \rho^{\mathrm{S}}(\infty) |j\rangle}\ |j\rangle \langle i|\,. \tag{2.11}$$

Denoting with $|j\rangle$ and $|i\rangle$ the eigenbases of $\rho^{\mathrm{S}}(\infty)$ and $\rho^{\mathrm{S}}(0)$, respectively, we find from Eq. (2.7) that the stationary *effective environment* state is the tensor product

$$\langle ij| \rho^{\mathrm{E}'}(\infty) |i'j'\rangle = \langle i| \rho^{\mathrm{S}}(0) |i\rangle \langle j| \rho^{\mathrm{S}}(\infty) |j\rangle \delta_{ii'}\delta_{jj'} = \langle ij| \rho^{\mathrm{S}}(0) \otimes \rho^{\mathrm{S}}(\infty) |i'j'\rangle \tag{2.12}$$

of the *initial and stationary system* states. The subadditivity upper bound in Eq. (2.10) corresponds to $S(\rho^{\mathrm{E}'}(t)) \leq S(\rho^{\mathrm{S}}(t)) + S(\rho^{\mathrm{S}}(0))$, and we consequently see from Eq. (2.12) that this bound is reached in the stationary limit as $S(\rho^{\mathrm{E}'}(\infty)) = S(\rho^{\mathrm{S}}(0)) + S(\rho^{\mathrm{S}}(\infty))$. From a physical perspective, this indicates that in the stationary limit the preparation entanglement between S and $\mathrm{P_S}$ has been entirely broken and converted into entanglement between the system and its effective environment. A state tomography of the effective environment in principle allows one to extract the initial and final data of the system evolution. The initial state is not lost but can be found explicitly in the effective environment. Again, only the effective environment keeps a 'clean' count of the system's interaction with the outside world.

2.2 A close-up view of open-system dynamics

The deep insights from the bird's-eye view of quantum information theory highlight the importance of the *effective* environment and raise the question how to *practically* calculate it: An explicit calculation of its spectrum from Eq. (2.7) requires access to *individual* Kraus operators in the operator-sum (2.6) as a function of *time*. To achieve this, we now take the view of statistical physics and look into the details of the underlying unitary evolution $U(t)$ that enables an *infinitesimal* view on the dynamics in terms of quantum master equations.

In the typical quantum-information setup of finite-dimensional systems, directly working with $U(t)$ may be feasible but in the transport models with continuous spectra that we have in mind, field-theoretical methods must be employed to obtain the Kraus operators in practice. In this section, we review the foundations of methods based on a perturbative expansion of the unitary evolution in the system-environment coupling and the exploitation of Wick's theorem. In particular, the real-time diagrammatic technique [115] is introduced that will be adapted and modified in Ch. 5 to diagrammatically calculate Kraus operators within an approximate treatment *without* upsetting the CP property. This is crucial for the information measures introduced above to be well-defined as they all rely on complete positivity.

2.2.1 Normal-ordering

The main difficulties in the explicit calculation of the Kraus operator-sum (2.6) are related to evaluating the projection onto the effective-environment states $|e\rangle$, or equivalently evaluating the environment-trace in either Eq. (2.1) or (2.5). To prepare for the following discussions, we first explain how this is done in field-theoretical methods. The standard approach is to iteratively reduce strings of field operators $X_1 \ldots X_q$ that appear as a result of an expansion of the unitary $U(t) = T \exp(-i \int_0^t H^{\mathrm{tot}}(\tau) d\tau)$ into pair-contractions $\overbrace{X_1 X_2} \equiv \langle X_1 X_2 \rangle$. Here, the average $\langle \bullet \rangle = \mathrm{Tr_E} \bullet \rho^{\mathrm{E}}$ is considered to be evaluated with respect to the *initial* environment state ρ^{E} that is *mixed*. While we are mostly interested in grand-canonical equilibrium states

of *noninteracting* fermionic or bosonic environments, it should be noted that the following considerations can as well be generalized to interacting environments [150, 151].

The reduction into pair-contractions relative to the average $\langle\ \ \rangle$ involves a *normal-ordering* of field-operator strings $X_1 \dots X_q$ indicated by $:\ :$. Assuming a vanishing field average $\langle X_i \rangle = 0$, one recursively defines[3]

$$X_1 = :X_1: \tag{2.13a}$$

$$X_1 X_2 = :X_1 X_2: + \overbrace{X_1 X_2} \tag{2.13b}$$

$$X_1 X_2 X_3 = :X_1 X_2 X_3: + \overbrace{X_1 X_2} :X_3: + \overbrace{X_1 :X_2: X_3} + :X_1: \overbrace{X_2 X_3} \tag{2.13c}$$

and so on, and inductively verifies that the average of $:X_1 \dots X_q:$ is zero for each q. As a result, averaging over Eq. (2.13) reproduces the standard Wick's theorem that re-expresses any average as the sum over all possible products of pair-contractions only. Moreover, each *partial* average is zero, for example, $:\overbrace{X_1 X_2 X_3}: = 0$. For this to work in the case of fermions, the partial contractions must include a sign for disentangling the fields, $\overbrace{X_1 :X_2: X_3} \equiv -\overbrace{X_1 X_3}\ :X_2:$.

The sole purpose of normal-ordering is to reorganize the way contractions of $X_1 \dots X_q$ are performed: Operators within a normal-ordered sequence can only be contracted with operators from a different sequence. Thus, averages such as $\langle :X_1 \dots X_q: :Y_1 \dots Y_q: \rangle$ are evaluated by Wick's theorem in the usual way except that the normal-ordering restricts all pair contractions to be of the form $\langle X_i Y_j \rangle$. Importantly, such an average does *not* require the explicit calculation of the operators $:X_1 \dots X_q:$ and $:Y_1 \dots Y_q:$. In Ch. 5 and the accompanying App. E, this property of normal-ordering is used to decompose any operator A_m acting only on a definite set of environment modes $m = m_q \dots m_1$ into its environment-average plus all its *normal-ordered* partial contractions which account for all possible fluctuations:

$$A_m = \langle A_m \rangle + :\Big(A_m + \sum_{l \subset m} A_m^l \Big): \quad . \tag{2.14}$$

Here the shorthand notation $l \subset m$ denotes a subset of modes on which the remaining uncontracted fields in A_m^l act and we implicitly sum over all possible subsets excluding $l = 0$. This will turn out to be the key step to connect to the quantum-information approach.

2.2.2 Real-time diagrammatic series

Returning to the time-evolution problem, the Keldysh real-time diagrammatic approach [115] is based on formally expanding the unitary $U(t) = T \exp\big[-i \int_0^t d\tau V(\tau) \big]$ in the *system-environment coupling* V on both sides of Eq. (2.1) and then *explicitly* tracing out the environment degrees of freedom in terms of pair-contractions using Wick's theorem. To this end, it is useful to work in the interaction-picture $V(t) = U_0^\dagger(t) V U_0(t)$ with respect to the free, uncoupled evolution $U_0(t) = e^{-i(H+H^{\mathrm{E}})t}$ of the system and its environment that is only indicated by the explicit time-argument[4].

[3] For $\langle X_i \rangle \neq 0$ the construction must be extended by substituting $X_i \to X_i - \langle X_i \rangle \mathbb{1}$ together with $:\mathbb{1}: = 0$.

[4] Extension to an explicitly time-dependent Hamiltonian generating the unitary evolution is straightforwardly possible but requires a clear notational distinction of the interaction-picture time-argument.

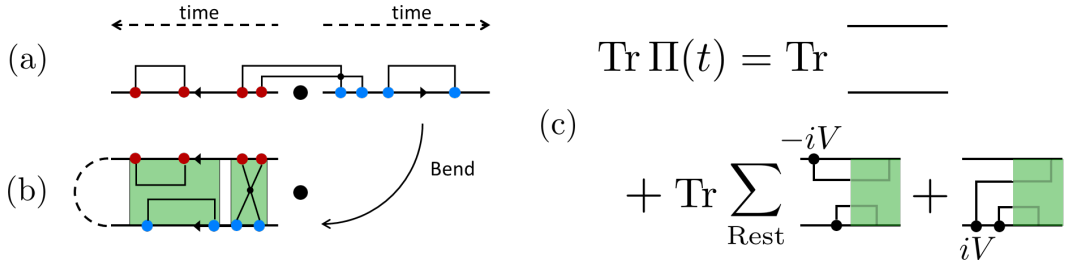

Figure 2.4: Two equivalent ways of drawing Keldysh real-time diagrams. (a) Nonstandard left-right form: time runs outward from the center. This is useful for later on identifying the operator-sum form of the real-time expansion in Ch. 5. (b) Standard forward-backward form, obtained by bending the right branch in (a) backward: Time runs from right to left to agree with the order of writing expressions. This form is advantageous for identifying the diagrammatically irreducible components (green) of the time-evolution that constitute the memory kernel $\Sigma(t,t')$ of the Dyson equation (2.16) that also features in the time-nonlocal quantum master equation. For fermions, the sign of the contribution of a diagram is given by $(-1)^{n_c}$ where n_c is the number of crossings of the environment contraction lines, which is the same for (a) and (b). We note that it is common to denote the adjoint $U(t)^\dagger = U(-t)$ the 'backward' evolution, imagining to traverse the contour first forward along the upper branch, then across the dashed connector 'backward' on the lower branch. Here, this is misleading: Time always runs in the forward direction, also on the lower contour. (c) The trace-preservation is easily checked from the diagrammatic contributions based on the cyclicity of the full trace, cf. Eq. (2.17). The trace over pairs of diagrams where the latest (leftmost) vertex is on the upper respectively lower branch vanishes identically, leaving only the free interaction-picture evolution which trivially preserves the trace. Reprinted figure (adapted) under CC BY 4.0 License from SciPost Phys. **7**, 012 (2019), see Ref. [137].

Each contribution to the Wick-averaged perturbation series for the dynamical map

$$\Pi(t) = \operatorname*{Tr}_{\mathrm{E}} \sum_n \int_{\tau_n \geq \ldots \geq \tau_1} [-iV(\tau_n)] \ldots [-iV(\tau_1)] \bullet \otimes \rho^{\mathrm{E}} \sum_{n'} \int_{\tau'_{n'} \geq \ldots \geq \tau'_1} [iV(\tau'_1)] \ldots [iV(\tau'_{n'})] \quad (2.15a)$$

$$= \sum_k \sum_{\text{diagrams}} \int_{t_k \geq \ldots \geq t_1} \operatorname*{Tr}_{\mathrm{E}} \ldots [-iV(t_i)] \ldots \bullet \otimes \rho^{\mathrm{E}} \ldots [iV(t_j)] \ldots . \quad (2.15b)$$

is represented by real-time *Keldysh diagrams* shown in Fig. 2.4: These keep track of whether a coupling term V represented by a vertex stems from the evolution $U(t)$ [left of ρ^{E} in (a), upper branch of the Keldysh time-contour in (b)] or from the adjoint evolution $U(t)^\dagger$ [right of ρ^{E}, lower branch of the contour]. As indicated in the caption, the two ways of drawing the same diagram have distinct advantages needed later on. Wick's theorem then expresses the environment trace as the sum of products of pair-contractions of environment field operators appearing in the *different* V's. These are drawn as connecting lines in Fig. 2.4 for the example of a bilinear coupling. In doing this, we assumed that the operator V has been normal-ordered[5] with respect to the initial environment state. Thus, any partial contraction of fields appearing in the same vertex V gives zero. Any nonzero environment average of the coupling

[5] Normal-ordering of the coupling V does not imply that the *unitary* U that it generates is normal-ordered: A sequence of normal-ordered V's contributing to U still allows for nonzero partial contractions.

is thereby absorbed into the definition $H+\langle V\rangle \to H$ of the system Hamiltonian. Explicit rules for translating diagrams to expressions are summarized in App. F.1 but the considerations of Ch. 5 do not require these details, the diagrammatic representations suffice. More model-specific diagrammatic rules [152–156] and their equivalent formulations in Liouville-space [35, 36, 157, 158] that we employ in Ch. 3 make this a very efficient technique for higher-order calculations [153–156, 159–163]. In particular, the change from separate time-ordering of $U(t)$ and $U(t)^\dagger$ in Eq. (2.15a) to a *two-branch time-ordered* integral in Eq. (2.15b) allows the transition to a Laplace frequency conjugate to the *physical time* in $\Pi(t)$. This is of practical use in calculations and crucial for formulating renormalization-group schemes [35, 164–167] where the Laplace frequency features as a flow parameter.

To make the connection to the time-nonlocal quantum master equation (1.7) one employs standard field-theoretical considerations to first infer the self-consistent Dyson equation from the resulting diagrammatic series:

$$\Pi(t) = \pi(t) + [\pi * \Sigma * \Pi](t) = \pi(t) + \int_0^t d\tau \int_0^\tau d\tau' \pi(t-\tau)\Sigma(\tau,\tau')\Pi(\tau'). \tag{2.16}$$

Here $[A*B](t) \equiv \int_0^t d\tau A(t,\tau)B(\tau,0)$ denotes a time-convolution that concatenates the action of two maps at a time τ to be integrated from an initial time $t=0$ to a final time t. In the Dyson equation, the coherent uncoupled evolution [$k=0$ in Eq. (2.15b)] is represented by the dynamical map $\pi(t,\tau) = \pi(t-\tau) = e^{-iH(t-t')} \bullet e^{iH(t-t')}$ where the environment is trivially traced out and which simplifies to the identity operation $\mathcal{I}$ in the interaction-picture. The self-energy or memory-kernel $\Sigma(t,t')$ is defined by the sum of two-branch-irreducible diagrams [152] and therefore incorporates the dissipative effect of the environment. For this distinction one needs to draw Keldysh real-time diagrams in the standard form shown in Fig. 2.4(b): Such a diagram is (ir)reducible when it can(not) be split up by a *vertical cut* without hitting a contraction line. The time-nonlocal QME (1.7) then follows from taking the time-derivative of the Dyson equation (2.16).

The self-consistent form of the Dyson equation or its infinitesimal QME version are useful because they allow one to explicitly scrutinize the trace-preservation of the open-system dynamics in terms of the diagrammatic contributions to the memory-kernel $\Sigma(t,t')$ generating it. This is illustrated in Fig. 2.4(c): When taking the system trace, pairs of irreducible diagrams with the latest (leftmost) vertex V appearing on opposite branches of the Keldysh contour exactly cancel with other terms in the series due to the cyclicity of the total trace:

$$\begin{aligned}\int dt_n \int dt'_{n'} \operatorname*{Tr}_{\mathrm{SE}} [-iV(t_n)] \bullet iV(t'_{n'}) = &- \int\limits_{t'_{n'}<t_n} dt_n dt'_{n'} \operatorname*{Tr}_{\mathrm{SE}} \bullet [iV(t'_{n'})][iV(t_n)] \\ &- \int\limits_{t'_{n'}>t_n} dt_n dt'_{n'} \operatorname*{Tr}_{\mathrm{SE}} [-iV(t'_{n'})][-iV(t_n)] \bullet .\end{aligned} \tag{2.17}$$

Here $\bullet$ denotes the initial state as well as all earlier vertices from the n-th and n'-th order terms of $U(t)$ and $U(t)^\dagger$, respectively. The resulting terms are already contained in different orders $(n\pm1, n'\mp1)$ of the double expansion in powers of V up to an opposite sign. Thus, all terms cancel pairwise except the zeroth order term $\pi(t)$ [first diagram in Fig. 2.4(c)] which guarantees that $\mathrm{Tr}_{\mathrm{S}}\,\Pi(t) = \mathrm{Tr}_{\mathrm{S}}$ holds order-by-order in the coupling-expansion.

Clearly, a summation of all diagrammatic contributions to the memory-kernel $\Sigma(t,t')$

virtually always requires an approximate treatment of the system-environment perturbation series. Even in the resonant level model discussed in Ch. 3, a summation based on the above real-time diagrammatics on the Keldysh contour is not apparent although possible [153]. An ingenious reformulation of the diagrammatic series in terms of so-called Liouville-space superfermions [36, 157] facilitates this by revealing a two-stage procedure that exactly sums up the series. A detailed review of this reformulation is presented in Sec. 3.4. What matters at this point are the implications for the CP property of the dynamical map when the perturbation series is naively truncated: Without a deeper understanding of the underlying structure, approximations based on omitting diagrammatic contributions to the series for the dynamical map $\Pi(t)$ or its time-nonlocal memory-kernel $\Sigma(t,t')$ are perilous as one might neglect contributions that are essential for the operator-sum structure (2.6) to guarantee a completely positive evolution. Reconciling the two quite distinct views presented above is crucial to make progress on this issue.

2.3 How to reconcile the complementary views?

Confronting the complementary views immediately raises the central question *how individual diagrams are related to terms in the Kraus operator-sum* (2.6). For instance, is it possible to develop an equivalent physical intuition in terms of a conditional evolution for the irreducible diagrams constituting the memory kernel $\Sigma(t,t')$? If so, the diagrammatic expressions should have some (possibly different) operator-sum representation and it would be desirable to have an explicit diagrammatic representation of the individual Kraus operators. This would enable one to track the CP property in each step of an approximation. However, the diagrammatic series as expressed above does not explicitly exhibit such a structure even though it is clear that the *full* series represents a CP-TP time-evolution and therefore *must* be related to an operator-sum. In Ch. 5 we present a reorganization of the Keldysh real-time diagrammatic series that addresses all these issues.

2.3.1 Complete positivity *versus* trace preservation

It is interesting that already at this point –before the detailed discussion of Ch. 5– there seems to be a fundamental *duality* in the CP and TP properties as represented by either the Kraus operator-sum (2.6) or the real-time diagrammatic series in form of the Dyson equation (2.16). This duality impedes an easy verification of *both* properties in either one of these representations and indicates that the relation we seek is not a matter of semantics or (re)definitions. Just as in the Kraus operator-sum (2.6) the complete positivity is preserved *process-by-process* via the quadratic form of each term reflecting a conditional evolution, the real-time diagrammatic series (2.16) allows one to scrutinize the trace preservation *order-by-order* in the system-environment coupling from the diagrammatic contributions to the memory-kernel $\Sigma(t,t')$. The respective other property is instead difficult to check in practice: In the operator-sum form, trace preservation is encoded in nonlinear relations $\sum_e K^e(t)^\dagger K^e(t)$ between *all* Kraus operators. Similarly, complete positivity can neither be inferred by inspecting just a few terms in the standard real-time diagrammatic series nor be guaranteed order-by-order in the system-environment coupling V, as will become clearer in Ch. 5. The duality fundamentally arises from discarding (tracing out) all information about the environment because the underlying unitary evolution $U(t)$ as well as the environment state ρ^{E} are then no longer explicitly available. *With* access to this discarded information, *both* properties are trivially checked to be consequences of the unitary evolution but it becomes difficult to do so after taking the trace. Each form of the dynamical map $\Pi(t)$ is tailored to highlight

only one of these properties, meanwhile obscuring the other [57, 97, 140, 168].

This duality between the CP and TP constraints has already been noted in Ref. [169] and can also be understood on a general level. While the discussion in Ch. 5 instead focuses on pin-pointing the *microscopic* origin of this duality in the individual Keldysh diagrammatic contributions, the general translation between both forms is provided by the well-known de Pillis-Jamiolkowski-Choi map [170–172]. It sets up a one-to-one correspondence between the *superoperator* $\Pi(t)$ and an *operator* on the doubled Hilbert space:

$$\mathrm{choi}[\Pi(t)] := \left(\Pi \otimes \mathcal{I}^{\mathrm{P_S}}\right) |\mathbb{1}^{\mathrm{SP_S}}\rangle \langle \mathbb{1}^{\mathrm{SP_S}}| \,. \tag{2.18}$$

This *Choi-operator* represents a special case of the purified system state (2.3c) introduced in Sec. 2.1.1 where the initially purified (unnormalized) state $|\mathbb{1}^{\mathrm{SP_S}}\rangle = \sum_k |k^{\mathrm{S}}\rangle \otimes |k^{\mathrm{P_S}}\rangle$ of the extended system $\mathrm{S} \otimes \mathrm{P_S}$ is *maximally* entangled. It can be shown [57] that testing the positivity of the Choi-operator is the 'worst-case' scenario regarding a violation of the CP property, i.e., it has a nonnegative spectrum $\mathrm{choi}[\Pi(t)] \geq 0$ if and only if the dynamical map is CP. Starting from the superoperator form (2.16) of $\Pi(t)$, we will now show how the correspondence $\Pi \leftrightarrow \mathrm{choi}[\Pi]$ simplifies the task of scrutinizing the CP property at the expense of obscuring the TP property.

Dyson form. First consider the diagrammatic perturbation series in the form of the self-consistent Dyson equation (2.16) and its formal solution $\Pi(t) = \pi(t) + \sum_{k=1}^{\infty}[(\pi * \Sigma*)^k \pi](t)$ written in terms of the trivially CP-TP uncoupled evolution $\pi(t)$ and the memory-kernel $\Sigma(t,t')$. Due to $\mathrm{Tr_S}\Sigma(t,t') = 0$ [cf. Eq. (2.17)], $\Pi(t)$ inherits the TP property from $\pi(t)$. However, the CP constraint is nontrivially passed on to $\Pi(t)$ because its Choi-operator $\mathrm{choi}[\Pi(t)] = \mathrm{choi}[\pi(t)] + \sum_{k=1}^{\infty} \mathrm{choi}\big[[(\pi * \Sigma*)^k \pi](t)\big]$ contains multiple terms, not all of which necessarily have a nonnegative spectrum as to ensure the complete positivity of $\Pi(t)$: Indeed, only $\mathrm{choi}[\pi(t)] \geq 0$ is known due to the complete positivity of $\pi(t)$ but it is unclear how the remaining terms conspire to result in $\mathrm{choi}[\Pi(t)] \geq 0$. Unraveling this structure is the main advance reported in Ch. 5.

Spectral form. The duality can similarly be illustrated by the spectral decomposition of the superoperator $\Pi(t)$. For this, we employ a convenient notation for Liouville-space superoperators $|A)(B|$ that are represented by $d^2 \times d^2$ matrices with $d = \dim \mathrm{S}$. Here, the action $(B|\bullet := \mathrm{Tr_S} B^\dagger \bullet$ on operators $|A) = A$ –represented as supervectors of dimension d^2– is defined in terms of the Hilbert-Schmidt scalar product $(B|A) = \mathrm{Tr_S} B^\dagger A$, by close analogy to operators and vectors in the usual Hilbert space. Since the dynamical map $\Pi(t)$ is a non-normal superoperator[6], it has distinct right eigenvectors $|m_k(t))$ (modes) and left eigenvectors $(a_k(t)|$ (amplitudes) to the same eigenvalue $\Pi_k(t)$. The TP property can be naturally considered as a left eigenvector equation $(a_1|\,\Pi(t) = 1 \cdot (a_1|$, where the dual right eigenvector $\Pi(t)\,|m_1) = |m_1)$ is a (generally time-dependent) *fixed-point* of the evolution that corresponds to the stationary state as $t \to \infty$. We will make explicit use of this in the discussion of the resonant level model in Ch. 3. Also here, the CP property is nontrivially encoded in *all* eigenvectors and eigenvalues.

Operator-sum form. The above situation is reversed when switching to the Choi-operator (2.18): Diagonalizing it and normalizing the eigenvectors to their nonnegative eigen-

[6] The dynamical map does not satisfy $\Pi(t)^\dagger \cdot \Pi(t) = \Pi(t) \cdot \Pi(t)^\dagger$ and can thus not be diagonalized by a *unitary* transformation but only by a similarity transformation.

values $\langle K^e|K^{e'}\rangle = \lambda_e \delta_{ee'}$ leads to an operator-sum,

$$\mathrm{choi}[\Pi(t)] = \sum_e |K^e(t)\rangle\rangle\langle\langle K^e(t)|\,, \tag{2.19}$$

where the *finite*[7] set of so-called canonical Kraus operators is identified by comparison of Eq. (2.18) with $|K^e(t)\rangle\rangle = (K^e(t)\otimes \mathbb{1}^{\mathrm{P_S}})\,|\mathbb{1}^{\mathrm{SP_S}}\rangle\rangle$. This also elucidates the label of the state $|0\rangle$ in Eq. (2.4): It corresponds to the index of the single initial Kraus operator $K^e(0) = \delta_{e,0}\mathbb{1}^{\mathrm{S}}$ which is the identity because of $\mathrm{choi}[\Pi(0)] = |\mathbb{1}^{\mathrm{SP_S}}\rangle\rangle\langle\langle\mathbb{1}^{\mathrm{SP_S}}|$, cf. Eq. (2.18). The CP property is now apparent on a term-by-term basis because the statistical mixing of individual pure states $|K^e(t)\rangle\rangle\langle\langle K^e(t)|$ always leads to a positive state $\mathrm{choi}[\Pi(t)] \geq 0$, see the discussion following Eq. (2.6). This step however mixes up both the eigenvectors *and* eigenvalues of $\Pi(t)$ even further such that the TP property can no longer be related to a *single* eigenvector of the diagonalized Choi-operator. One verifies that $\Pi(t)$ is a TP superoperator if and only if the partial trace of its Choi-operator over the subspace S yields the identity on the subspace $\mathrm{P_S}$:

$$\operatorname*{Tr}_{\mathrm{S}} \mathrm{choi}[\Pi(t)] = \mathbb{1}^{\mathrm{P_S}} \quad\Longleftrightarrow\quad \sum_e K^e(t)^\dagger K^e(t) = \mathbb{1}^{\mathrm{S}}. \tag{2.20}$$

Physically speaking, this requires that the Choi-operator has the maximally mixed state $\mathbb{1}^{\mathrm{P_S}}$ (up to normalization) as a marginal state, i.e., Eq. (2.20) constrains the *correlations* on the bipartite system. This is clearly a nontrivial property to enforce on the decomposition (2.19) into pure states and translates into the nonlinear relation between *all* Kraus operators shown on the right of Eq. (2.20) which must hold at all times.

2.3.2 Real-time diagrammatic series for Kraus operators

The duality demonstrated above makes clear that the views of quantum information and statistical field theory are complementary for deep *physical* reasons. Reconciling these views is thus not a task of semantics and definitions but relates to real problems, for example when considering approximations beyond the Born-Markov limit where the GKSL theorem cannot be applied to preserve the fundamental CP-TP property. Ideally, one would like to make use of the strength of each approach and switch back and forth between the operator-sum (2.6) and the Dyson or QME forms (2.16) whenever necessary.

This is exactly the strategy pursued in Ch. 5: There not only the *state* of the environment is purified as above in Sec. 2.1.1 but also[8] the unitary *evolution* $U(t)$. This will reveal an internal structure based on normal-ordering that allows for a reorganization of the Keldysh real-time diagrammatic series into groups of diagrams that describe evolution conditional on *partial* measurements of the open system's *effective* environment. As a result, a diagrammatic expansion of (the operators underlying) the Kraus operators in terms of the microscopic system-environment coupling is obtained which enables one to exploit field-theoretical methods in the setting of quantum information theory. It should be stressed from the start that the diagrammatic reorganization does not fully mitigate the CP-TP duality: From the 'vertex-flipping' rule (2.17), the trace preservation is easily inferred but we will see that this connects *all* groups of Keldysh diagrams that are related to *different* Kraus operators. This raises the question how consistent CP-TP approximation schemes based on these results may be

[7] The size of this set, $\mathrm{rank}\big[\mathrm{choi}[\Pi(t)]\big] \leq d^2 = \dim \mathrm{S}\otimes\mathrm{P_S}$, is minimal relative to any other unitarily related operator-sum, cf. the discussion following Eq. (2.6).

[8] Such purifications of the dynamics are known as dilations introduced by Stinespring [80].

formulated and we will address this challenging issue in detail in Ch. 5.

In conclusion, the formalism we will develop fills in a gap in the appreciation of purification ideas in open-system dynamics and clarifies the precise *operational* meaning of Keldysh real-time diagrams. This way the vague notions of (tunneling) 'processes' and 'consistent' approximations are made precise while remaining physically transparent –an important step for aligning our physical intuition about nonequilibrium systems with the complex tools necessary to describe them. It is remarkable that the technical advantages of purification and entanglement have been long recognized in many-body approaches such as DMRG [173–175] and tensor networks [176–178] but seem to have been hardly explored for statistical field-theoretical approaches to, e.g., nonequilibrium transport problems. Although our analysis focuses on the reduced density-operator method, it also relates to similar developments in nonequilibrium Green's functions [179] going back to quantum-field theory [180]. The only prior work we are aware of concerns two apparently distinct approaches that aim at *directly* obtaining a Kraus operator-sum from a projective, respectively perturbative approach to open-system dynamics: Ref. [85] put forward a projection technique for computing the square root $\sqrt{\rho(t)}$ of the state to guarantee CP of the dynamics for all t. Refs. [32–34] instead extended earlier work [181, 182] to *microscopically* derive the CP dynamics in an explicit Kraus operator-sum for bosonic reservoirs. While their concrete formulations seem quite distinct at first glance, we will show how the formalism developed in Ch. 5 in fact generalizes and encompasses both these works.

3 Quantum Markovianity: An exact case study

Before we turn to developing the real-time formalism in great generality, we first investigate the Markovianity issues raised in the introduction for an exactly solvable noninteracting fermionic model. As a case study featuring several types of divisible dynamics, we examine a tunable resonant level coupled arbitrarily strongly to a fermionic bath at arbitrary temperature in the wideband limit. To quantify the nonzero footprint left by the system in its effective environment, we determine the exact time-dependent state of the latter and related information measures such as entropy, exchange entropy and coherent information. In particular, the *observable* impact of divisibility on the time-dependence of the level occupation is investigated. We compare this with Markovian approximations to develop an understanding of how to go beyond the Markovian limit while maintaining complete positivity and trace.

Even for this simple model, overcoming the CP-TP duality requires several representations of the exact dynamical map (2.1) to be derived in Secs. 3.3–3.6 which are then compared in Sec. 3.7: In general, both the equations of motion [Sec. 3.3] and real-time approach [Sec. 3.4] prove to be advantageous for obtaining the exact dynamical map in a Liouville-space *superoperator form*. This form is suitable for studying the eigenmodes of $\Pi(t)$ as presented in Sec. 3.7 and elucidates the TP property even without explicitly diagonalizing $\Pi(t)$. On the other hand, the CP property is in general not directly related to the eigenspectrum of $\Pi(t)$ itself. Instead, it is associated to the spectrum of the *Choi-operator* that nontrivially mixes up both the eigenvectors *and* eigenvalues of $\Pi(t)$ such that the TP property can no longer be related to a *single* eigenvector of the Choi operator. As shown in the previous Ch. 2, diagonalization of the Choi-operator (2.18) leads to the dynamical map in the *operator-sum form* (2.6) in which the CP property is apparent from the quadratic form. Each term in the finite set of Kraus operators depends on the physical parameters of the model as well as on *time*. In contrast, the TP property has become complicated to check and now involves the nontrivial relation (2.20) because of the mixing of eigenvectors and eigenvalues involved with the Choi mapping pointed out above. More generally, the structure of the spectral decomposition of $\Pi(t)$ remains hidden in nonlinear relations of this type, even for our simple model, see Sec. 3.7 and App. A.3. Combining these forms unlocks a full characterization not only of the open system but also of its effective environment. Knowledge of the latter is crucial to not only calculate but also understand the physical implications of the information measures introduced in the previous chapter.

Publications and acknowledgments. Parts of this chapter and the associated appendices A–C (including the adapted figures) have been published in V. Reimer, M. R. Wegewijs, K. Nestmann, and M. Pletyukhov, The Journal of Chemical Physics **151**, 044101 (2019) [Copyright 2019 by the American Institute of Physics], see Ref. [134]. V. Reimer worked out the superfermion solution of the resonant level model, in particular its exponential representation, and acknowledges useful discussions with R. Saptsov in this regard. Motivated by discussions with S. Maniscalco, he also calculated the information measures to quantify the physical footprint left in the environment. The equivalent Heisenberg equations of motion were pointed out by M. Pletyukhov which highlighted the relation of time-local and nonlocal quantum master equations worked out in detail in collaboration with K. Nestmann. The fixed points of the dynamical map and its time-(non)local generator were noted by M. R. Wegewijs which revealed the reentrant behavior of system observables as a decisive feature of non-semigroup-divisible dynamics.

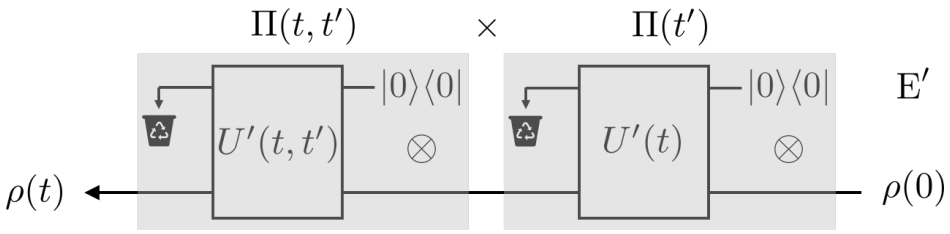

Figure 3.1: Interrupting the evolution by a complete measurement of the effective environment at an intermediate time t' and subsequently discarding the outcomes disrupts the system. If the evolution is CP-divisible, it is nevertheless possible to reach the uninterrupted final state $\rho(t)$ by unitary interaction with a new effective environment which is again discarded. The evolution cannot be the same as the original unless the evolution has the stronger property of being semigroup-divisible. Compare this with the classical Markovianity notion in Fig. 1.2(a). Reprinted figure (adapted) with permission from J. Chem. Phys. **151**, 044101 (2019), see Ref. [134]. Copyright 2019 by the American Institute of Physics.

3.1 Introduction

As pointed out in Sec. 1.2, the problem of extending the classical notion of Markovianity has received a lot of interest [87], in particular its relation to the divisibility,

$$\Pi(t) = \Pi(t,t')\,\Pi(t') \quad \text{for all } t \geq t' \geq 0. \tag{3.1}$$

Analogous to the classical case, one may define Markovianity as a factorization of the dynamics at *any* intermediate time $0 \leq t' \leq t$ into a repeated action $\Pi(t) = \Pi(t-t')\Pi(t')$ of the *same* CP-TP evolution over different time-intervals. This *semigroup* property implies that the dynamics is insensitive to a reinitialization of the effective environment at any time t', and the splitting is always physically meaningful because $\Pi(t-t')$ is CP-TP for all $t \geq t'$. Evolutions that fail to be a semigroup, may however *still* be considered Markovian in a weaker sense: A factorization $\Pi(t) = \Pi(t,t')\Pi(t')$ of the CP-TP map $\Pi(t)$ into two *different* evolutions at any time $0 \leq t' \leq t$ is still physically meaningful if we explicitly require the *divisor* $\Pi(t,t')$ to be CP-TP as well, cf. Fig. 1.2. This *CP-divisibility* [92, 98] then implies according to Kraus' theorem [Sec. 2.1.2] that the dynamics is also insensitive to a reinitialization of the effective environment, but now either to a different environment state or with a different unitary evolution $U'(t,t')$ which parametrically depends on the time t', see Fig. 3.1. If the divisor $\Pi(t,t')$ is not CP-TP, this argument breaks down and divisibility becomes meaningless: Whenever $\Pi(t)$ is invertible, it is also divisible without further constraining the divisor. We will explicitly illustrate this for our model [Eq. (3.17b)] whose dynamics fails to fulfill both the semigroup-divisibility and the CP-divisibility criterion in broad parameter regimes. In Sec. 3.7 we will see that whereas the loss of the semigroup-divisibility is clearly reflected in observables, the loss of CP-divisibility is more subtle to detect.

Despite the clear characterizations of CP-divisibility in terms of information measures [169], it is still under debate whether it can be considered a meaningful extension of Markovianity to the quantum case [96]. Here, we are chiefly interested in understanding the *physical* implications of the divisibility properties in a simple setting. In doing so one encounters the problem that these distinctions typically become pronounced for systems strongly coupled to continuous environments. As a result, rigorously investigating their measurable implications is often hindered by the practical necessity of making approximations in the

microscopic derivation of the dynamics, in particular for strongly interacting open systems with finite-temperature environments. Whereas weak-coupling approximations typically lead to semigroup dynamics $\Pi(t,t') = \Pi(t-t')$ governed by a time-independent GKSL [89, 90] quantum master equation (QME), microscopic derivations [183–185] may also give rise to more general *time-dependent* GKSL equations of the type (1.6):

$$\tfrac{d}{dt}\rho(t) = -i[H(t),\rho(t)] + \sum_i \gamma_i(t)\left[J_i(t)\rho(t)J_i(t)^\dagger - \tfrac{1}{2}\{J_i(t)^\dagger J_i(t),\rho(t)\}\right]. \tag{3.2}$$

In both cases, the divisibility properties can be easily assessed from the constituents of this QME: The coefficients $\gamma_i(t)$ of the jump operators $J_i(t)$ should be either nonnegative [92] for all times t (CP-divisibility), or both the nonnegative coefficients and the jump operators are time-independent [89, 90] (semigroup-divisibility). The exponential solution allows one to construct the Kraus operators in either case [186–188]. It should be stressed what a failure of these conditions implies: While a time-independent GKSL form with negative coefficients $\gamma_i < 0$ indicates a breakdown of the CP property, no general statement about CP can be made in the case of temporarily negative time-dependent coefficients $\gamma_i(t) < 0$. This situation is encountered even in our simple model. The dynamics may then *still* be CP (and it is) but to explicitly see this, one has to rely on model-specific forms which reveal this property [Sec. 3.4] or construct an operator-sum [Sec. 3.5] for $\Pi(t)$. Moreover, our explicit construction of the divisor $\Pi(t,t')$ allows to investigate what happens when CP-divisibility *fails*.

The recent generalizations [32, 85] mentioned at the end of Sec. 2.3.2 and also the real-time formalism to be presented in Ch. 5 apply beyond QMEs of the GKSL type (3.2), but it is unclear how they reflect divisibility properties. Therefore, exact solutions of microscopic models where these issues can be understood analytically are of interest. In search of solvable examples with interesting dynamics, much attention has been given to systems coupled to bosonic environments, such as the spin-boson and dissipative Jaynes-Cummings [33, 189–192] model. Here, we turn to fermionic models appearing in quantum transport problems, such as strongly coupled quantum dots. These offer rich non-equilibrium dynamics due to a variety of many-body effects [21, 23, 24, 193]. Somewhat surprisingly, a *single* fermionic mode coupled arbitrarily strongly to a noninteracting fermionic reservoir at arbitrary temperature already features several types of divisible dynamics in different parameter regimes. It therefore serves as an ideal playground to investigate the above mentioned questions. The full characterization of its divisibility properties calls for explicit construction of both the dynamical map $\Pi(t)$ as well as the divisor $\Pi(t,t')$ which seems not to have been discussed despite the known [194] exact solvability of the model. To achieve this, it turns out to be important to approach the exact solution from several angles in a consistent way. The overall goal of this chapter is to exhaustively investigate the impact of CP and divisibility on measurable properties of this exactly solvable model and illustrate how these are affected by approximations.

The chapter is organized as follows. We start in Sec. 3.2 by introducing the model and discussing the simplifying features that enable its exact solution. In Sec. 3.3 we first obtain the dynamical map $\Pi(t)$ using Heisenberg equations of motion [88, 195, 196] (EOM) for observables. Sec. 3.4 derives this result from the complementary perspective of state evolution using the real-time [35, 152, 158, 159] superfermion approach [36, 157, 197] revealing further properties and physical insights. In Sec. 3.5 we then construct the Kraus operator-sum from these solutions in order to compute information measures [Sec. 2.1.3] quantifying the system-environment backaction. In Sec. 3.6 the three representations are then used to construct two exact quantum master equations, one time-local (TCL) and one time-nonlocal (Nakajima-

Zwanzig) which are more suitable for discussing the impact of approximations. Finally, in Sec. 3.7 we construct the exact eigenvectors of the dynamical map $\Pi(t)$ as function of time and bring together the insights from all discussed approaches. We analyze the detailed time-development of the level occupation in dependence of the model parameters.

3.2 Resonant level model

The model that we consider describes a single, noninteracting fermionic mode (field operator d at energy ε) in tunneling contact with a continuous reservoir of fermions (field operator b_ω at energy ω), all without spin:

$$H^{\rm tot} = \varepsilon d^\dagger d + \int d\omega\, \omega\, b_\omega^\dagger b_\omega + \sqrt{\frac{\Gamma}{2\pi}} \int d\omega \big(d^\dagger b_\omega + b_\omega^\dagger d\big). \tag{3.3}$$

As often, the environment is coupled with an ω-independent tunneling rate $\Gamma > 0$ and constitutes a reservoir in thermal equilibrium at temperature T and chemical potential μ represented by the density operator $\rho^{\rm E} = \exp\big(-(H^{\rm R} - \mu N^{\rm R})/T\big)/Z$ in terms of $H^{\rm R}$, the second term in Eq. (3.3), and the particle-number operator $N^{\rm R} := \int d\omega\, b_\omega^\dagger b_\omega$. Concerning notation, it is convenient to label field operators with a particle/hole index $\eta = \pm$,

$$d_\eta = \begin{cases} d^\dagger & \eta = + \\ d & \eta = - \end{cases}, \qquad b_{\eta\omega} = \begin{cases} b_\omega^\dagger & \eta = + \\ b_\omega & \eta = - \end{cases}, \tag{3.4}$$

and denote $\bar\eta = -\eta$ such that $d_\eta^\dagger = d_{\bar\eta}$. Furthermore, we do not set $\mu = 0$ as this may later on lead to a confusion of ε with the level *detuning* $\epsilon := \varepsilon - \mu$, cf. Eq. (3.38).

The key observable of the model is the *transient* transport of fermions into the reservoir, i.e., the time-dependent level occupation $n = d^\dagger d$ or its parity $(-\mathbb{1})^n := e^{i\pi n} = \mathbb{1} - 2n$. Physically, we expect that a finite temperature $T < \infty$ leads to memory effects[1] since excitations created in the environment propagate on a finite time-scale T^{-1} before coupling back to the system. Explicitly following this fact in the derivations of the dynamical map $\Pi(t)$ is both instructive and technically advantageous, also for more complicated systems [36, 157, 197]. In particular, the infinite-temperature semigroup limit of the model plays a central role.

It is useful to briefly consider the translation of our model into spin language with $S^\pm = d_\pm$, $S^z = d^\dagger d - \mathbb{1}/2 = -(-\mathbb{1})^n/2$ and analogous definitions for the environment. In this picture one may identify the average parity $\langle(-\mathbb{1})^n\rangle$ and field $\langle d\rangle$ with the longitudinal and transverse components of the spin (Bloch vector) describing diagonal and off-diagonal density-matrix elements, respectively. In fermionic systems, the field amplitude $\langle d(t)\rangle$ vanishes at all times due to the fermion-parity superselection [200, 201] and we will make this assumption throughout. However, in the spin formulation it makes sense to consider $\langle d(t)\rangle \neq 0$ and we will comment on this. Considered as a spin-model, Eq. (3.3) is somewhat unconventional:

$$H^{\rm tot} = \varepsilon S^z + \int d\omega\, \omega\, s_\omega^z + \sqrt{\frac{\Gamma}{2\pi}} \int d\omega \big(S^+ s_\omega^- + s_\omega^+ S^-\big). \tag{3.5}$$

It corresponds to purely transverse exchange (spin-flip) interaction between a local spin in a magnetic field of strength ε and a reservoir of spins in magnetic fields of varying strength and

[1] Additional memory effects appear when lifting the assumption of infinite reservoir bandwidth (unrestricted ω integral) and ω-independent coupling Γ, see page 8 of Ref. [36] and also, e.g., Refs. [198, 199].

direction ω. In this language, the model can be compared with the spin-boson model [189] of a two-level system exchanging energy with a bosonic thermal bath. This model has been solved exactly in a rotating-wave-approximation (RWA) and at zero temperature of the bath leading to the semigroup Wigner-Weisskopf theory [202] but recent extensions included also finite-temperature effects going beyond the RWA [191, 192]. The same holds [190] for the more complicated setup of the dissipative Jaynes-Cummings model [203] where the two-level system exchanges energy with a radiation field via a single bosonic cavity mode. An exact treatment is quite complicated in both cases and often restricted to a description in terms of quantum master equations, see however the Kraus operator-sum treatment of Ref. [33].

3.3 Equation of motion approach

We start the discussion of the exact solution from the Heisenberg equations of motion (EOM) for a set of *observable* operators. This is familiar, e.g., from Green's function techniques [194, 204–207] or input-output formalisms in quantum optics [88, 195, 196, 208], and corresponds to computing the super-adjoint evolution $\Pi(t)^\dagger$ in contrast to the real-time approach discussed in Sec. 3.4 to directly obtain the system *state* evolution $\Pi(t)$ in superoperator form. Often, the approach is used in conjunction with various approximations and/or limits [135, 196, 209]. However, in this case we can follow it through exactly due to the wideband-limit [194].

Employing the Liouville-space supervector notation introduced in Sec. 2.3.1, the action of dynamical map (2.1) on the *system*-operator argument $\bullet$ can be expanded as

$$\begin{aligned}\Pi(t) = \sum_A |A)\,(A|\,\Pi(t)\bullet &= \sum_A A \operatorname*{Tr}_{\rm SE} A^\dagger U(t)(\bullet\otimes\rho^{\rm E})U(t)^\dagger \\ &= \sum_A A \operatorname*{Tr}_{\rm SE} U(t)^\dagger A^\dagger U(t)(\mathbb{1}^{\rm S}\otimes\rho^{\rm E})\bullet \\ &= \sum_A A \operatorname*{Tr}_{\rm S}\{\langle A(t)^\dagger\rangle^{\rm E}\bullet\} \end{aligned} \tag{3.6}$$

in terms of a complete orthogonal set $\mathcal{I} = \sum_A |A)\,(A|$ of system-operators $A = |A)$ normalized as $(A|A) = \mathrm{Tr}_{\rm S} A^\dagger A = 1$. Here, $\langle\circ\rangle^{\rm E} = \mathrm{Tr}_{\rm E}\circ(\mathbb{1}^{\rm S}\otimes\rho^{\rm E})$ denotes the environment average that reduces the *system-environment* Heisenberg-picture operators $A(t) \equiv U(t)^\dagger A U(t)$ to system-only operators. Their expectation values $\langle A(t)\rangle := \mathrm{Tr}_{\rm S}\langle A(t)\rangle^{\rm E}\rho(0)$ are obtained by additionally averaging with respect to the initial system state. Note that within this EOM approach, the CP-TP duality [Sec. 2.3.1] manifests itself in the nontrivial CP property reflected in the positivity of the Choi-operator (2.18) involving *all* 'Green's functions' $\langle A(t)^\dagger B\rangle$,

$$\mathrm{choi}[\Pi(t)] = (\Pi(t)\otimes\mathcal{I}^{\rm Ps})\,|\mathbb{1}^{\rm SPs}\rangle\,\langle\mathbb{1}^{\rm SPs}| = \sum_{AB}\langle A(t)^\dagger B\rangle\cdot A\otimes B^* \geq 0, \tag{3.7}$$

and the trivial TP property reflected in the evolution of the observable $\langle\mathbb{1}(t)\rangle^{\rm E} = \mathbb{1}$ for all $t \geq 0$ ensuring $(\mathbb{1}|\,\Pi(t) = (\mathbb{1}|$. The second equality in Eq. (3.7) follows from the identity $X\otimes\mathbb{1}\,|\mathbb{1}\rangle = \mathbb{1}\otimes X^T\,|\mathbb{1}\rangle$ for the action on a maximally entangled state $|\mathbb{1}\rangle = \sum_k |k\rangle\otimes|k\rangle$.

The calculation of the dynamical map $\Pi(t)$ thus boils down to taking partial averages $\langle A(t)\rangle^{\rm E}$ of Heisenberg-picture operators governed by the EOMs

$$\tfrac{d}{dt}A(t) = i[H^{\rm tot}(t), A(t)]. \tag{3.8}$$

Here, we choose the orthogonal system operator basis $\{d_+, d_-, \mathbb{1}, (-\mathbb{1})^n\}$ which simplifies matters in two ways: First, the dynamics $\langle \mathbb{1}(t)\rangle^{\mathrm{E}} = \mathbb{1}$ of the identity is trivial and second, the parity plays a crucial role in fermionic systems which becomes explicit in the superfermion method of Sec. 3.4. There, the fermion-parity superselection is exploited and allows an application even to interacting multi-level models [22, 197, 210, 211]. To close the equations of motion, it suffices to add the environment fields $b_{\eta\omega}$ which are conveniently chosen [157] to *anticommute* with system fields: $[d_{\eta'}, b_{\eta\omega}]_+ = 0$, see App. A.1.1 for a detailed derivation. Importantly, taking the partial averages *before* integrating these equations simplifies matters since by Wick's theorem terms containing an odd number of environment fields vanish, $\langle b_{\eta\omega}\rangle^{\mathrm{E}} = 0$, and pairs of environment fields correspond to Fermi-distribution functions

$$\langle b_{\eta'\omega'} b_{\eta\omega}\rangle^{\mathrm{E}} = \delta_{\eta',\bar{\eta}}\, \delta(\omega' - \omega) \left[\frac{1}{2} + \frac{\eta}{2} \tanh\left(\frac{\omega - \mu}{2T}\right)\right]. \tag{3.9}$$

The splitting into parts symmetric and anti-symmetric in ω is convenient because it corresponds to time-local and time-nonlocal contributions to the evolution, cf. Sec. 3.4.

3.3.1 Exact solution and divisibility

The environment-averaged system operators are governed [cf. App. A.1.1] by the EOMs

$$\frac{d}{dt}\langle d_\eta(t)\rangle^{\mathrm{E}} = i\eta \left(\varepsilon + i\eta \tfrac{1}{2}\Gamma\right) \langle d_\eta(t)\rangle^{\mathrm{E}} \tag{3.10a}$$

$$\frac{d}{dt}\langle (-\mathbb{1})^n(t)\rangle^{\mathrm{E}} = -\Gamma \langle (-\mathbb{1})^n(t)\rangle^{\mathrm{E}} + \Gamma h(t)\, \mathbb{1}. \tag{3.10b}$$

In Eq. (3.10b), the inhomogeneous term is determined by

$$h(t) := \int_0^t ds e^{-\frac{\Gamma}{2}s} \gamma(s), \tag{3.11}$$

which involves the Keldysh *correlation function*

$$\gamma(s) := \frac{1}{\pi} \int d\omega \cos\left[(\omega - \varepsilon)s\right] \tanh\left(\frac{\omega - \mu}{2T}\right) \tag{3.12a}$$

$$= 2T \frac{\sin\left[\epsilon s\right]}{\sinh\left[\pi T s\right]} \tag{3.12b}$$

depending on the relative time $s = t - t' > 0$ only, see App. B.1 for a derivation of the latter representation. It stems from the anti-symmetric part of the Fermi function (3.9) and accounts for the time-nonlocal effects due to propagation in the thermal environment at the energy of the resonant level. Thus, all temperature dependence is incorporated in this function and only the level *detuning* $\epsilon = \varepsilon - \mu$ with respect to the chemical potential enters.

Integrating the equations of motion (3.10) with initial values $\langle d_\eta(0)\rangle^{\mathrm{E}} = d_\eta$ and $\langle (-\mathbb{1})^n(0)\rangle^{\mathrm{E}} = (-\mathbb{1})^n$ gives

$$\langle d_\eta(t)\rangle^{\mathrm{E}} = e^{i\eta(\varepsilon + i\eta\frac{\Gamma}{2})t}\, d_\eta \tag{3.13a}$$

$$\langle (-\mathbb{1})^n(t)\rangle^{\mathrm{E}} = e^{-\Gamma t}(-\mathbb{1})^n + (1 - e^{-\Gamma t}) g(t) \mathbb{1}. \tag{3.13b}$$

The extraction of the conventional factor $(1 - e^{-\Gamma t})$ in Eq. (3.13b) is physically motivated,

since it isolates the dimensionless function

$$g(t) := \frac{\Gamma}{1-e^{-\Gamma t}} \int_0^t d\tau e^{-\Gamma(t-\tau)} h(\tau), \tag{3.14}$$

which reduces to the expectation value of the parity in the stationary limit:

$$\langle (-\mathbb{1})^n(\infty) \rangle = g(\infty). \tag{3.15}$$

The nontrivial time-dependence of the solution is thus fully determined by the functions (3.11) and (3.14) deriving from the Keldysh correlation function (3.12). In Fig. 3.2(a) and (b), we show how the oscillatory behavior of the correlation function is translated into both $h(t)$ and $g(t)$. The detuning sets the sign $\operatorname{sgn}\epsilon = \operatorname{sgn} h(t) = \operatorname{sgn} g(t)$ for all $t > 0$.

Substituting Eq. (3.13) into (3.6) and normalizing the operators gives the dynamical map in superoperator form:

$$\begin{aligned} \Pi(t) &= \sum_\eta d_\eta^\dagger \operatorname*{Tr}_{\mathrm{S}}\Big[e^{(i\eta\varepsilon - \frac{\Gamma}{2})t} d_\eta \bullet \Big] && \text{(3.16a)} \\ &\quad + \tfrac{1}{2}\mathbb{1} \operatorname*{Tr}_{\mathrm{S}}\Big[\bullet \Big] + \tfrac{1}{2}(-\mathbb{1})^n \operatorname*{Tr}_{\mathrm{S}}\Big[(1-e^{-\Gamma t}) g(t) \mathbb{1} \bullet + e^{-\Gamma t} (-\mathbb{1})^n \bullet \Big] \\ &= \sum_\eta e^{(i\eta\varepsilon - \frac{1}{2}\Gamma)t} \left| d_\eta^\dagger \right) \left(d_\eta^\dagger \right| && \text{(3.16b)} \\ &\quad + e^{-\Gamma t} \tfrac{1}{2} \left| (-\mathbb{1})^n \right) \Big[\left((-\mathbb{1})^n \right| - g(t) \left(\mathbb{1} \right| \Big] + \tfrac{1}{2} \Big[\left| \mathbb{1} \right) + g(t) \left| (-\mathbb{1})^n \right) \Big] \left(\mathbb{1} \right| . \end{aligned}$$

The TP property $\mathrm{Tr}_{\mathrm{S}}\Pi(t) = \mathrm{Tr}_{\mathrm{S}}$ is explicit through the second term in Eq. (3.16a) as all other terms produce traceless operators. Indeed, all further eigen-supervectors of the dynamics are easily derived from this form by simple reorganization of the terms into Eq. (3.16b). This spectral decomposition will be used in Sec. 3.7 to discuss the detailed time-dependence of observables. In contrast, the CP property is unclear from this representation and this motivates the complementary treatments in Secs. 3.4-3.5.

Postponing the issue of CP to Sec. 3.4, we may nevertheless inquire about the divisibility of the evolution into two factors as in Eq. (3.1). To this end, we integrate Eq. (3.10) from t' onward. The result for the divisor $\Pi(t,t')$ can be obtained from Eq. (3.16a) by replacing

$$(1-e^{-\Gamma t}) g(t) \to (1-e^{-\Gamma[t-t']}) g(t,t') \tag{3.17a}$$

and adjusting the time-interval to $[t,t']$ in all other terms. The function

$$g(t,t') := \frac{\Gamma}{1-e^{-\Gamma[t-t']}} \int_{t'}^t d\tau e^{-\Gamma(t-\tau)} h(\tau) \tag{3.17b}$$

interpolates between $g(t,0) = g(t)$ and $g(t,t) = h(t)$ and therefore shares many of their features, see Fig. 3.2(c). The evolution $\Pi(t)$ is thus *always* divisible and because the divisor $\Pi(t,t')$ has the same structure (3.16a) it is always a TP map. To distinguish meaningful types divisibility one has to investigate the properties of $g(t,t')$.

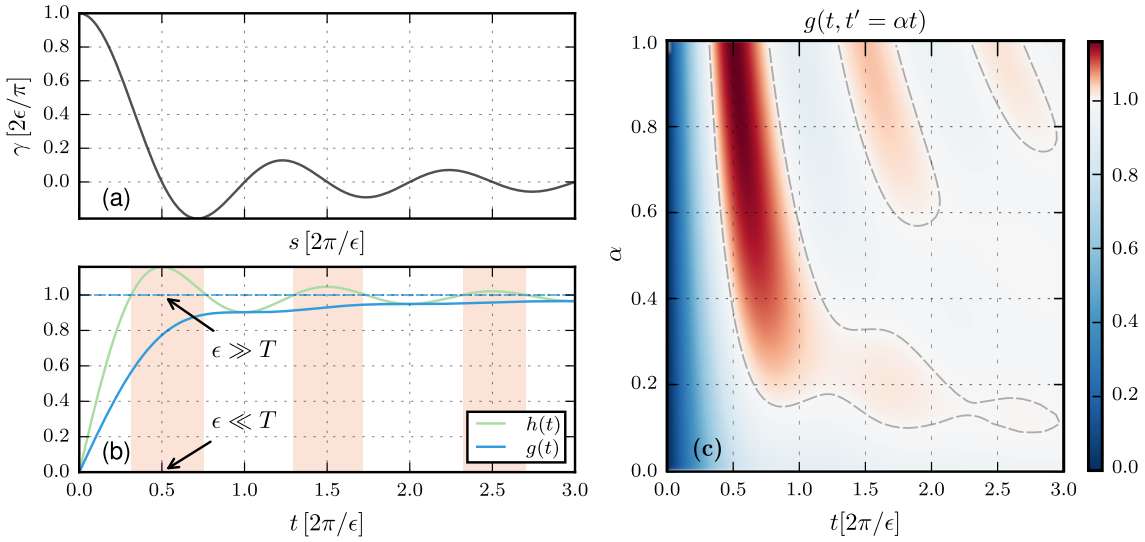

Figure 3.2: Time-dependent functions of the dynamics for $2\epsilon/\pi = 20\Gamma$ and $\pi T = 10^{-3}\cdot\Gamma/2$. (a) Reservoir correlation function $\gamma(s)$ [Eq. (3.12)] describing the time-nonlocal 'memory' effects. (b) The oscillatory behavior of $\gamma(s)$, while still present in the function $h(t)$ [Eq. (3.11), green] appearing in the *time-local* EOM (3.10), is smoothed out in the function $g(t)$ [Eq. (3.14), blue] which describes the cumulative nontrivial time-dependence of the EOM solution (3.13). In the semigroup limits of small [Eq. (3.18)] and large [Eq. (3.19)] detuning, both these functions instantly reduce to constant values of 0 and 1, respectively, as indicated by arrows. (c) Time-dependent function $g(t, t')$ [Eq. (3.17b)] determining the dynamics of the divisor $\Pi(t, t')$. As a function of the division ratio $\alpha = t'/t$, it interpolates between the functions $g(t)$ at $\alpha = 0$ and $h(t)$ at $\alpha = 1$. In contrast to $g(t)$, it may exceed the value of 1 indicated by the contour, cf. the discussion in Sec. 3.3.2. Reprinted figure (adapted) with permission from J. Chem. Phys. **151**, 044101 (2019), see Ref. [134]. Copyright 2019 by the American Institute of Physics.

3.3.2 Physical properties

The important functions $\gamma(s)$, $h(t)$, $g(t)$ and $g(t, t')$ incorporate the nontrivial time-dependence of the evolution and its divisor. Each function can in principle be expressed in terms of Digamma and Lerch functions reported before, see Ref. [157] and references therein. Their physical properties however rely on different representations which are derived in App. B and summarized below.

Semigroup-divisible limits. When the system is *thermally* close to resonance, $|\epsilon| \ll T$, the correlation function $\gamma(s)$ shows exponential decay with memory time T^{-1} and thus vanishes

$$\lim_{T/|\epsilon|\to\infty} \gamma(s) = \lim_{T/|\epsilon|\to\infty} h(t) = \lim_{T/|\epsilon|\to\infty} g(t) = 0 \tag{3.18}$$

in the infinite-temperature limit suppressing both $h(t)$ and $g(t)$ as a consequence. Far off resonance, $|\epsilon| \gg T$, the correlation function instead shows oscillating power-law decay with time-scale $|\epsilon|^{-1}$ and becomes time-local in the infinite-detuning limit

$$\lim_{|\epsilon|/T\to\infty} \gamma(t - t') = \bar{\delta}(t - t'), \tag{3.19a}$$

noting that the relevant δ-function is normalized on the real half-line $\int_0^t dt' \bar{\delta}(t-t') = 1$ since we solve an initial-value problem. In this limit, $h(t)$ and $g(t)$ still coincide,

$$\lim_{|\epsilon|/T\to\infty} h(t) = \lim_{|\epsilon|/T\to\infty} g(t) = \mathrm{sgn}(\epsilon)\,\theta(t), \tag{3.19b}$$

and reduce independently of T and Γ to a step function with $\theta(0) := 0$. Although both limits lack memory for different physical reasons, they share the semigroup property that $g(t)$ –but not the parity $\langle(-\mathbb{1})^n(t)\rangle$– is instantly stationary.

Generic behavior. In all other cases of finite temperatures or level detunings, the functions differ as shown in Fig. 3.2(b). The deviations are already pronounced at small times [App. B.4] as $h(t)$ starts out with double the slope:

$$h(t) \approx 2g(t) = \frac{2\epsilon}{\pi}\, t. \tag{3.20}$$

Whereas $h(t)$ is always nonmonotonic, the function $g(t)$ is nonmonotonic only for $\Gamma/2 > \pi T$, cf. App. B.3. This is due to the fact that the latter is obtained by an integration [Eq. (3.14)] which smoothens the oscillations of $h(t)$. However, both approach the same stationary limit

$$g(\infty) = h(\infty) = \frac{2}{\pi}\,\mathrm{Im}\,\psi\left(\frac{1}{2} + \frac{\frac{\Gamma}{2} + i\epsilon}{2\pi T}\right) \tag{3.21}$$

expressed in terms of the imaginary part of the Digamma function ψ, cf. Eq. (B.5a).

Physical bounds. The function $g(t)$ is bounded for any time and any set of parameters as

$$|g(t)| \leq 1. \tag{3.22}$$

That this condition holds for our model can be seen in two steps. First, the function never exceeds its asymptotic value $|g(t)| \leq |g(\infty)|$. This fact is not obvious and seems to rely on model-specific details [App. B.3]. Second, due to its relation (3.15) to the stationary expectation value of the parity, it is physically clear that $g(\infty)$ becomes maximal in the off-resonant semigroup limit $|\epsilon| \gg T$ where the stationary state is pure:

$$|g(\infty)| \leq \lim_{|\epsilon|/T\to\infty} |\langle(-\mathbb{1})^n(\infty)\rangle| = 1. \tag{3.23}$$

Divisibility. In contrast, $h(t)$ is not bounded by its asymptote: It may significantly overshoot it and more strongly $|h(t)| > 1$ for certain parameter regimes [App. B.2] as seen in Fig. 3.2(b). This behavior translates into the function $g(t,t')$. Specifically, the equivalence

$$|g(t,t')| \leq 1 \text{ for } t \geq t' \geq 0 \iff |h(t)| \leq 1 \text{ for } t \geq 0 \tag{3.24}$$

holds as one verifies as follows: Assuming first the left-hand side, this particularly includes $|g(t,t)| = |h(t)| \leq 1$ for all $t \geq 0$ by Eq. (3.17b). Conversely, the right-hand side implies in Eq. (3.17b) that $|g(t,t')| \leq 1$ for any $t \geq t' \geq 0$ as the integral is normalized to one. In contrast to $g(t)$, there is no physical reason why values $g(t,t') > 1$ should not occur and in Fig. 3.2(c) they indeed occur (red). The observable implications of the criterion

$$|g(t,t')| > 1 \iff |h(t)| > 1 \tag{3.25}$$

marked red in Fig. 3.2(b) are discussed in Sec. 3.7.

3.3.3 (Complete) positivity

A physical reason why the bound (3.22) *must necessarily* hold, may be sought in the preservation of the positivity (PP) of the state under evolution, i.e., the property $\Pi(t)\rho(0) \geq 0$ for every $\rho(0) \geq 0$. In the following we verify that the condition (3.22) is indeed equivalent to PP and furthermore comment on whether the CP property can be deduced from this or not.

For this, we consider *any* initial state irrespective of whether the fermion-parity superselection is obeyed and inquire the positivity of the reduced state

$$\rho(t) = \tfrac{1}{2}\Big[\mathbb{1} + \langle(-\mathbb{1})^n(t)\rangle\,(-\mathbb{1})^n\Big] + \sum_\eta \langle d_\eta(t)\rangle\, d_\eta, \tag{3.26}$$

explicitly taking into account the field $\langle d_\eta(t)\rangle$. Expressed in terms of the Bloch-vector magnitude $|b(t)|^2 := |\langle(-\mathbb{1})^n(t)\rangle|^2 + |2\langle d(t)\rangle|^2$, the PP property for this model requires that $|b(t)|^2 \leq 1$ for all $|b(0)|^2 \leq 1$. Eliminating $|2\langle d(0)\rangle|$ we can consider the parity and the Bloch-vector magnitude as independent variables up to the constraint $|\langle(-\mathbb{1})^n(0)\rangle| \leq |b(0)| \leq 1$. Inserting the expectation values $\langle A(t)\rangle := \mathrm{Tr_S}\langle A(t)\rangle^{\mathrm{E}}\rho(0)$ of the EOM solutions (3.13),

$$\langle d_\eta(t)\rangle = e^{(i\eta\varepsilon - \frac{\Gamma}{2})t}\,\langle d_\eta(0)\rangle \tag{3.27a}$$

$$\langle(-\mathbb{1})^n(t)\rangle = e^{-\Gamma t}\langle(-\mathbb{1})^n(0)\rangle + (1-e^{-\Gamma t})g(t), \tag{3.27b}$$

one can rewrite the explicit PP constraint as

$$0 \leq 1 - |b(t)|^2 = 1 + (1-e^{-\Gamma t})e^{-\Gamma t}\Big[\langle(-\mathbb{1})^n(0)\rangle - g(t)\Big]^2 - (1-e^{-\Gamma t})[g(t)]^2 - e^{-\Gamma t}|b(0)|^2. \tag{3.28}$$

We minimize over all states $\rho(0)$ by first setting $|b(0)| = 1$ in the last term and then varying $|\langle(-\mathbb{1})^n(0)\rangle| \leq 1$. In the case $|g(t)| \leq 1$, the minimum of the quadratic term in (3.28) is achievable for a physically allowed value $\langle(-\mathbb{1})^n(0)\rangle = g(t)$ and equals $(1-e^{-\Gamma t})[1-g(t)^2]$ which is positive if and only if $|g(t)| \leq 1$. Note that the minimum occurs for a mixed state with a nonzero $|\langle d(0)\rangle| = \sqrt{1-|g(t)|^2}/2$. In the other case $|g(t)| > 1$, the minimal achievable value of (3.28) occurs for $\langle(-\mathbb{1})^n(0)\rangle = \operatorname{sgn} g(t)$ (and $|\langle d(0)\rangle| = 0$) and equals $(1-e^{-\Gamma t})(1-|g(t)|)[1+e^{-\Gamma t}+(1-e^{-\Gamma t})|g(t)|] < 0$ which is always negative. Thus $\Pi(t)$ is PP if and only if $|g(t)| \leq 1$ as claimed above. This condition is also equivalent to the positivity of the probabilities for states obeying superselection, $|\langle d(0)\rangle| = 0$. In this case, the restriction on the eigenvalues of the state (3.26), $\Lambda_\eta = \frac{1}{2}[1+\eta\langle(-\mathbb{1})^n(t)\rangle] \leq 1$, requires $\max|\langle(-\mathbb{1})^n(t)\rangle| = e^{-\Gamma t} + (1-e^{-\Gamma t})|g(t)| \leq 1$ at time t which is equivalent to $|g(t)| \leq 1$. The maximal value of Eq. (3.27b) is achieved for an initially pure state with $\langle(-1)^n(0)\rangle = \operatorname{sgn} g(t)$.

Finally, we stress that for our model the PP condition is *incidentally* equivalent with the CP condition (3.22). Although CP implies PP, the converse does *not* hold in general since the PP restriction ignores the entanglement with the auxiliary system P required to prepare initial mixed system states, cf. Sec. 2.1. Also, CP is the more relevant condition because of its useful consequences which are *not* implied by PP. Verification of the stronger CP property is *not* possible from the EOM result (3.16) and requires either conversion to a Kraus operator-sum [Sec. 3.5] or –for our specific model– conversion to the exponential form obtained in the real-time approach [Sec. 3.4]. We stress that CP *cannot* be inferred

from by the spectral decomposition (3.16b), because the positivity of fixed points follows from $\Pi(t)$ being PP-TP, see the discussion Sec. 3.7. It also *cannot* be inferred from the time-local QME discussed in Sec. 3.6 for *any* set of model parameters: Even in the present model its form remains inconclusive in non-CP-divisible parameter regimes where $|h(t)| > 1$, but nevertheless $|g(t)| \leq 1$, see Eqs. (3.2) and (3.44).

3.4 Real-time superfermion approach

Although the EOM approach has a straightforward derivation and identifies the relevant time-dependent functions, the form (3.16) no longer reflects that the evolution (2.1) is actually CP. As pointed out above, it is a coincidence that in the present model both PP and CP *happen* to be equivalent to the bound (3.22), a property some other models also exhibit, see Refs. [108, 212]. Likewise, the bound (3.24) *happens* to be equivalent to CP-divisibility, but neither property is clear from the EOM approach itself. To further investigate this, we turn to a real-time approach equivalent to the one introduced in Sec. 2.2.2 that also facilitates the exact solution but naturally leads to a representation of the dynamics $\Pi(t)$ which avoids these issues. It focuses on the evolution of the state rather than observables.

3.4.1 Renormalized perturbation theory

A naive expansion of $U(t) = e^{-iH^{\mathrm{tot}}t}$ in Eq. (2.1) in the coupling $H^V = \sqrt{\Gamma/2\pi}\int d\omega \sum_\eta d_\eta b_{\bar{\eta}\omega}$ as in the Keldysh real-time approach [Sec. 2.2.2] does not lead to an obviously summable series for the state evolution $\Pi(t)$, even for quadratic fermionic models. Such a summable series can however be obtained when abandoning the Hamiltonian formulation and using an *intrinsically dissipative* reference for the expansion. This emerges naturally when using Liouville-space methods developed in Ref. [35] and can be formulated elegantly [157] in terms of fermionic superfields outlined below. This equivalent formulation importantly reveals the existence of *two* fundamental expansion 'parameters' in the wideband limit: the retarded reservoir correlation function capturing the time-local effects of the physical *infinite-temperature* limit, and the Keldysh correlation function $\gamma(s)$ [Eq. (3.12)] incorporating the time-nonlocal *finite*-temperature corrections. Exploiting this structure results in a renormalized perturbation theory that remarkably stops at finite order for quadratic models [157].

Superfermions. We collapse the two branches of the Keldysh-contour by directly expressing the time-evolution (2.1) as $\Pi(t) = \mathrm{Tr}_{\mathrm{E}}\{e^{-iL^{\mathrm{tot}}t}(\bullet \otimes \rho^{\mathrm{E}})\}$ in terms of the total Liouvillian superoperator $L^{\mathrm{tot}} := [H^{\mathrm{tot}}, \bullet]_-$. It acts on the fermionic Liouville-Fock space and allows for a 'second quantization' representation

$$L^{\mathrm{tot}} = \sum_\eta \eta\Big[\varepsilon G^+_\eta G^-_{\bar{\eta}} + \int d\omega \omega J^+_{\eta\omega} J^-_{\bar{\eta}\omega}\Big] + \sum_{\eta,q}\sqrt{\frac{\Gamma}{2\pi}}\int d\omega J^q_{\eta\omega} G^{\bar{q}}_{\bar{\eta}} \tag{3.29}$$

that is analogous to the Hilbert-Fock space but takes into account *mixed* states and superoperators [187, 213–217]. The fermionic creation ($q = +$) and annihilation ($q = -$) superfields

$$G^q_\eta = \tfrac{1}{\sqrt{2}}\big(d_\eta \bullet \mathbb{1} + q(-\mathbb{1})^n \bullet (-\mathbb{1})^n d_\eta\big) \tag{3.30a}$$

$$J^q_{\eta\omega} = \tfrac{1}{\sqrt{2}}\big(b_{\eta\omega} \bullet \mathbb{1} + q(-\mathbb{1})^{n^{\mathrm{R}}} \bullet (-\mathbb{1})^{n^{\mathrm{R}}} b_{\eta\omega}\big) \tag{3.30b}$$

for system and reservoir, respectively, obey the anti-commutation relations $[G^{q'}_{\eta'}, G^q_\eta]_+ =$

$\delta_{\eta',\bar{\eta}}\,\delta_{q',\bar{q}}$ and $[J^{q'}_{\eta'\omega'}, J^{q}_{\eta\omega}]_+ = \delta_{\eta',\bar{\eta}}\,\delta_{q',\bar{q}}\,\delta(\omega'-\omega)$. Contrary to the EOM approach, maximal simplicity is achieved with the convention [35, 157] of *commuting* system and environment fields, $[d_{\eta'}, b_{\eta\omega}]_- = 0$, which translates to $[G^{q'}_{\eta'}, J^{q}_{\eta\omega}]_- = 0$.

Through the parity-check in Eq. (3.30), both the fermionic superselection as well as the *Pauli principle* are incorporated [157]. The latter is expressed by the identity

$$[G^+_\eta]^2 = 0 \tag{3.31}$$

and indicates that the particle/hole index η [Eq. (3.4)] takes on the new formal role of a quantum number which cannot be 'doubly filled'. A second key feature of this method was overlooked in its previous applications: Bilinear products of superfields

$$\sum_\eta G^+_\eta G^-_{\bar{\eta}} = -\sum_\eta \mathcal{L}_\eta, \quad \sum_\eta \eta G^+_\eta G^+_{\bar{\eta}} = \sum_\eta \eta\mathcal{L}_\eta \tag{3.32a}$$

introduced by pair contractions correspond to superoperators of GKSL-form

$$\mathcal{L}_\eta := d_\eta \bullet d_{\bar{\eta}} - \tfrac{1}{2}\big[d_{\bar{\eta}} d_\eta, \bullet\big]_+. \tag{3.32b}$$

The Pauli principle (3.31) thereby implies the nonlinear relation $[\sum_\eta \eta\mathcal{L}_\eta]^2 = 0$ between these generators. For the reservoir, the parity-check reveals that only two (out of four) types of pair-contractions contribute:

$$\left\langle J^-_{\eta'\omega'} J^+_{\eta\omega} \right\rangle^{\mathrm{E}} = \delta_{\eta',\bar{\eta}}\delta(\omega'-\omega) \tag{3.33a}$$

$$\left\langle J^-_{\eta'\omega'} J^-_{\eta\omega} \right\rangle^{\mathrm{E}} = \eta\delta_{\eta',\bar{\eta}}\delta(\omega'-\omega)\tanh\left(\frac{\omega-\mu}{2T}\right). \tag{3.33b}$$

These respectively correspond to the symmetric and anti-symmetric part of the Fermi function (3.9). The algebraic structure thus *automatically* separates time-local (memoryless) contributions (3.33a) that remain at infinite temperature from the time-nonlocal (memory) contributions (3.33b) accounting for the finite-temperature corrections.

Renormalized perturbation theory. With these insights, we can identify two stages in the naive expansion of $\Pi(t)$ in powers of the coupling Liouvillian $L^V = \sum_{\eta,q}\sqrt{\Gamma/2\pi}\int d\omega J^q_{\eta\omega} G^{\bar{q}}_{\bar{\eta}}$, see App. A.2.1 for details. Using Wick's theorem, each term in the series is decomposed [35, 157, 158] into products of reservoir pair-contractions

$$\langle L^V(\tau) L^V(\tau')\rangle^{\mathrm{E}} = -\tfrac{\Gamma}{2}\sum_\eta \big[\bar{\delta}(\tau-\tau') - \eta\gamma(\tau-\tau')\big]\,\mathcal{L}_\eta, \tag{3.34}$$

where the time-dependence of $L^V(\tau) = e^{iL^0\tau} L^V e^{-iL^0\tau}$ again denotes the interaction-picture with respect to the free evolution $L^0 = \sum_\eta \eta[\varepsilon G^+_\eta G^-_{\bar{\eta}} + \int d\omega\omega J^+_{\eta\omega} J^-_{\bar{\eta}\omega}]$. As anticipated in the EOM approach, each pair-contraction has a time-local [$\bar{\delta}$, Eq. (3.19a)] and time-nonlocal contribution [γ, Eq. (3.12)]. Importantly, these contributions are now distinguished by their *algebraic* superoperator structure Eq. (3.32a): In contrast to the time-local term $\sum_\eta \mathcal{L}_\eta \sim G^+G^-$ combining creation *and* annihilation superfields, the time-nonlocal term $\sum_\eta \eta\mathcal{L}_\eta \sim G^+G^+$ *exclusively* features creation superfields such that any higher power vanishes by Eq. (3.31).

The perturbation series can thus be summed exactly in a two-stage procedure: First, the

time-local infinite-temperature contributions from Eq. (3.34) sum to the exponential

$$\Pi_\infty(t) = e^{-iLt+\frac{\Gamma}{2}t\sum_\eta \mathcal{L}_\eta} \tag{3.35}$$

due to the ensuing geometric series. For the second stage, this semigroup limit is used as the reference of a renormalized perturbation series featuring *only* creation superfields G^+ implying that it exactly terminates after a *single* correction due to Eq. (3.31):

$$\Pi(t) = \Pi_\infty(t) - \tfrac{1}{2}\left(1-e^{-\Gamma t}\right) g(t) \sum_\eta \eta\mathcal{L}_\eta \tag{3.36a}$$

$$= e^{-iLt+\frac{\Gamma}{2}t\sum_\eta[1-\eta g(t)]\mathcal{L}_\eta}. \tag{3.36b}$$

It is also the Pauli-exclusion principle that suggests to re-exponentiate the correction to obtain the elegant exponential form (3.36b). This can be done [App. A.2.1] using the Baker-Campbell-Hausdorff formula since the algebra of operators is closed. The appearance of the function $g(t)$ [Eq. (3.14)] already indicates that both expressions coincide with the EOM solution as one verifies using the supervector representation (A.9) of the GKSL generator.

3.4.2 Complete positivity and divisibility

The form (3.36b) reveals the CP and divisibility properties of the dynamical map $\Pi(t)$ without taking recourse to operator-sums [Sec. 3.5] or quantum master equations [Sec. 3.6].

Complete positivity. Its exponential form suggests to consider an auxiliary dynamics $\frac{d}{d\lambda}X(\lambda) = \Lambda X(\lambda)$ with $X(\lambda)|_{\lambda=0} = \mathcal{I}$: At a *fixed* time t, the physical map (3.36b) is equivalent to the formal solution $\Pi(t) = X(\lambda)|_{\lambda=1}$ of the auxiliary dynamics evaluated at the flow parameter $\lambda = 1$. This allows for the application of the GKSL theorem [89, 90] because the auxiliary generator given by $\Lambda = -iLt + \frac{\Gamma}{2}t\sum_\eta[1-\eta g(t)]\mathcal{L}_\eta$ has a λ-independent GKSL form[2]. Thus, $X(\lambda)$ is CP-TP if and only if the coefficients of the jump operators are positive, i.e., $|g(t)| \leq 1$, which clarifies that the bound (3.22) on the function $g(t)$ found in the EOM approach is actually the condition for CP which *must* hold for each t. The PP property thus happens to coincide with CP. We can extend this result to resolve the question of divisibility.

Divisibility. First, in the two semigroup limits where $g(t) = g(\infty)$ for $t > 0$ [Eqs. (3.18) and (3.19)], the time-linear exponent in Eq. (3.36b) indeed implies a Markovian semigroup $\Pi(t) = \Pi(t-t')\Pi(t')$. In all other cases, the dynamics is not a Markovian semigroup but we can explicitly construct the *divisor* $\Pi(t,t')$ to analyze the CP-divisibility condition. Analogous to the EOM approach, it is obtained by setting $g(t) \to g(t,t')$ and adjusting the time interval to $[t,t']$ in $\Pi(t)$ as given by Eq. (3.36b), see App. A.2.1 for the justification:

$$\Pi(t,t') = e^{-iL(t-t')+\frac{\Gamma}{2}t\sum_\eta[1-\eta g(t,t')]\mathcal{L}_\eta}. \tag{3.37}$$

Applying the same argument as in the discussion of the complete positivity of $\Pi(t)$ establishes that the divisor is CP-TP if and only if $|g(t,t')| \leq 1$ for all $t \geq t' \geq 0$, which we showed earlier [Eq. (3.24)] to be equivalent to the bound $|h(t)| \leq 1$. If this condition fails to hold [Eq. (3.25)] –as it does for a wide range of parameters in our model– the division of the evolution is no longer physically meaningful in the sense described in Sec. 3.1. The dynamics then exhibits 'truly' non-Markovian behavior which is neither semigroup- nor CP-divisible.

[2] One cannot apply the GKSL semigroup or CP-divisibility theorem (5.41) to the *physical* evolution because neither theorem is conclusive for many model parameters, see Sec. 3.6.

As a criterion, this is equivalent to Eq. (3.2) based on QMEs as we show in Sec. 3.6. However, the single function $g(t,t')$ completely characterizes the *explicit* divisor $\Pi(t,t')$ and its behavior is explored in Sec. 3.7.

3.5 Kraus operator-sum representation

From the exact solution $\Pi(t)$ in the form (3.16) or (3.36), we can construct the Kraus operator-sum. This also reveals the CP restriction $|g(t)| \leq 1$ just found in Sec. 3.4.2, but it furthermore gives access to the effective environment and information measures quantifying the system-environment interaction, see Sec. 2.1.3. The latter issue is clearly beyond the previously discussed methods. Our exact expressions for the Kraus operators provide a benchmark for approaches that aim at *directly* deriving them [32–34, 85, 137] in order to produce CP maps even under approximations. For instance, the $T \to \infty$ limit of the result reported below can also be obtained from the real-time formalism developed in Ch. 5 but in that framework it remains unclear how finite-temperature contributions can be summed up directly, cf. Sec. 5.5.

The Kraus operator-sum follows from diagonalizing the Choi-operator (2.19) which is explicitly carried out in App. A.3 to obtain a set of $d^2 = 4$ nonzero Kraus operators for generic parameters ε, μ, Γ and T:

$$\Pi(t) = \sum_{k=0,1} \sum_{\eta=\pm} K_\eta^k(t) \bullet K_\eta^k(t)^\dagger. \tag{3.38a}$$

Due to the block-diagonal structure of choi$[\Pi(t)]$, these four Kraus operators separate into two groups $k = \{0,1\}$ with $(-1)^k$ being their fermion parity.

For $k = 0$, we have

$$K_\eta^0(t) = \sqrt{\lambda_\eta^0(t)}\, \frac{\eta\sqrt{r(t)}^\eta dd^\dagger + \frac{1}{\sqrt{r(t)}^\eta} e^{-i\varepsilon t} d^\dagger d}{\sqrt{r(t) + \frac{1}{r(t)}}}, \tag{3.38b}$$

where both the Choi eigenvalues $\lambda_\eta^0(t)$ as well as the Choi eigenvectors determined by the single function $r(t)$ enter:

$$\lambda_\eta^0(t) = \tfrac{1}{2}(1 + e^{-\Gamma t}) + \eta\sqrt{e^{-\Gamma t} + [\tfrac{1}{2}(1 - e^{-\Gamma t})g(t)]^2} \tag{3.38c}$$

$$r(t) = e^{\frac{\Gamma}{2}t}\Big[\tfrac{1}{2}(1 - e^{-\Gamma t})g(t) + \sqrt{e^{-\Gamma t} + [\tfrac{1}{2}(1 - e^{-\Gamma t})g(t)]^2}\Big]. \tag{3.38d}$$

Note the separate dependence on the level position ε: It drops out only in the spectrum of $\rho(t)$ which depends on the level *detuning* $\epsilon = \varepsilon - \mu$ through $g(t)$ [Eq. (3.14)]. The operators $K_\eta^0(t)$ evolve the system conditional on no *net* fermion transfer having occurred with the η-index reflecting a nontrivial relative phase between an occupied and an unoccupied system. As pointed out in Sec. 2.1.3, only a single Kraus operator $K_\eta^0(0) = \delta_{\eta,+}\mathbb{1}$ proportional to the identity operator remains at the initial time.

For $k = 1$, the time-dependence of the Kraus operators enters only through $\lambda_\eta^1(t)$:

$$K_\eta^1(t) = \sqrt{\lambda_\eta^1(t)}\, d_\eta \tag{3.38e}$$

$$\lambda_\eta^1(t) = \tfrac{1}{2}(1 - e^{-\Gamma t})[1 - \eta g(t)]. \tag{3.38f}$$

These operators correspond to a conditional evolution in which a fermion has been effectively added to ($\eta = +$) or removed from ($\eta = -$) the system up to the finite time t. In accordance with this, both these Kraus operators initially vanish, $K^1_\eta(0) = 0$. Similarly, in the limit of large detuning ($|\epsilon| \gg T$) where $|g(t)| = |g(\infty)| = 1$ [Eq. (3.19)], tunneling into ($\epsilon > 0$) or out of ($\epsilon < 0$) the system becomes impossible for all times. This is reflected by the vanishing of two of the four Choi eigenvalues and their corresponding Kraus operators.

It is admittedly a disadvantage of the operator-sum (3.38) that represents the dynamics as an intricate competition between exponentially decaying terms depending only on Γ and the nontrivial evolution of $g(t)$ depending on all parameters Γ, T and ϵ. This is easier analyzed using the spectral decomposition of $\Pi(t)$ as obtained from the EOM in Sec. 3.7. Here, we merely note that the eigenvectors of $\Pi(t)$ are fully determined by sum-rules for the Kraus operators –similar to the TP condition (2.20)– given in App. A.3. Clearly, the CP property of the dynamical map $\Pi(t)$ is easily inferred from the Choi eigenvalues $\lambda^k_\eta(t) \geq 0$ and is equivalent to $|g(t)| \leq 1$ [Eq. (3.22)], independently confirming the result of Sec. 3.4.2.

System density matrix. The key advantage is that the Kraus operators give access to the spectra of both the system and effective environment state required for computing the information measures introduced in Sec. 2.1.3. In case of the system, the spectrum is however also easily expressed in terms of the parity evolution (3.27b) which due to the parity-superselection[3] fully determines the system state (3.26). Its eigenvalues,

$$\Lambda_\eta(t) = \tfrac{1}{2}\big[1 + \eta\langle(-\mathbb{1})^n(t)\rangle\big], \tag{3.39}$$

are positive due to the CP condition $|g(t)| \leq 1$ [cf. Sec. 3.3.3] and enter into the binary entropy $S(\rho(t)) = -\sum_\eta \Lambda_\eta(t)\log_2\Lambda_\eta(t)$ of the system.

Effective environment density matrix. The density matrix of the effective environment can be constructed from Eq. (2.7): $\rho^{\mathrm{E}'}(t)^{kk'}_{\eta\eta'} = \mathrm{Tr}_\mathrm{S} K^k_\eta(t)\rho(0)K^{k'}_{\eta'}(t)^\dagger$, see App. C.1. Due to parity-superselection [Sec. 3.2], the state decomposes into parity blocks and can therefore be considered as the mixed state of a *two-fermion*[4] effective environment E':

$$\rho^{\mathrm{E}'}(t) = \begin{bmatrix} \rho^{\mathrm{E}'}(t)^{00} & 0 \\ 0 & \rho^{\mathrm{E}'}(t)^{11} \end{bmatrix}. \tag{3.40}$$

These *blocks* are not independent: One finds that the effective environment factorizes for all times $t \geq 0$ into two *independent* fermion modes, $\rho^{\mathrm{E}'}(t) = \rho^{\mathrm{E}'+}(t) \otimes \rho^{\mathrm{E}'-}(t)$. The eigenvalues of their states $\rho^{\mathrm{E}'\lambda}(t)$ for $\lambda = \pm$ read

$$\Lambda^{\mathrm{E}'\lambda}_\eta(t) = \frac{1}{2}\left[1 + \eta\frac{\sqrt{[c(t) + \langle(-\mathbb{1})^n(0)\rangle g(t)]^2 - [1-g(t)^2][1-\langle(-\mathbb{1})^n(0)\rangle^2]} + \lambda[\langle(-\mathbb{1})^n(0)\rangle - g(t)]}{c(t)+1}\right], \tag{3.41}$$

where the shorthand-notation $c(t) := \coth(\Gamma t/2)$ has been used. These reveal the generic short- and long-time behavior discussed in Sec. 2.1.3: Initially $\Lambda^{\mathrm{E}'\lambda}_\eta(0) = \frac{1}{2}[1+\eta] = \delta_{\eta,+}$, i.e., each mode is pure as it should be by construction. In the stationary limit, the factorization (2.12) is recovered as one effective mode acquires the spectrum of $\rho(0)$ and the other that of

[3] Within the spin formulation (3.5), the lack of parity-superselection complicates the structure of both system and effective environment density matrices but leaves their positivity properties unaffected, cf. App. C.3.

[4] Since the effective environment has finite dimension 4, it can always be considered as consisting of two qubits [57]. However, because the joint state is block-diagonal by the superselection property of the dynamics, it is consistent to consider the environment as two fermions.

$\rho(\infty)$, see App. C.2 for details.

Information measures. Due to the factorization of the effective environment state, its entropy is a sum $S(\rho^{\mathrm{E}'}(t)) = \sum_\lambda S(\rho^{\mathrm{E}'\lambda}(t)) = -\sum_{\eta,\lambda} \Lambda_\eta^{\mathrm{E}'\lambda}(t) \log_2 \Lambda_\eta^{\mathrm{E}'\lambda}(t)$ of binary entropies of the two effective modes. This fact simplifies the coherent information I_c [Eq. (2.8)] in two interesting cases: For a pure *initial* system state $[\langle(-\mathbb{1})^n(0)\rangle = \pm 1]$, the spectra of the effective environment and the system generally coincide for *all* times, see Sec. 2.1.3. One of the modes $\Lambda_\eta^{\mathrm{E}'\lambda}(t)$ is then fixed to the pure initial system state $\rho(0)$ with zero entropy whereas the other has the spectrum of $\rho(t)$. Consequently, the entropies of the effective environment and the system match exactly, causing $I_\mathrm{c}(t) = 0$ as it should. This is different for the pure *stationary* system state $[g(\infty) = \sigma = \pm 1]$ obtained in the off-resonant semigroup limit (3.19) with $g(t) = \theta(t)\sigma$, where one mode instantly acquires the pure spectrum of $\rho(\infty)$. The coherent information does not vanish in this case but reduces to the difference $I_\mathrm{c}(t) = S(\rho(t)) - S(\rho^{\mathrm{E}'\sigma}(t))$ of just two binary entropies because the other mode evolves different from $\rho(t)$. Remarkably, this other mode starts in the *stationary* system state and converges to the *initial* system state $\rho(0)$ as $t \to \infty$ to reproduce the stationary factorization (2.12). Finally, we note that the positivity of the coherent information mismatch (2.9) cannot be understood by a cancellation of $S(\rho(t))$ with the entropy of one of these effective modes, see Eq. (C.7) and Fig. 3.6. Its correct long-time limit $2S(\rho(0))$ [Eq. (2.10)] is however evident.

3.6 Exact quantum master equations

The exact dynamics in the form of Eqs. (3.16), (3.36), or (3.38) is the solution of two different quantum master equations. These are more suitable for formulating approximations and discussing their impact [218].

3.6.1 Time-nonlocal QME (Nakajima-Zwanzig)

In the real-time approach of Sec. 3.4, it is natural to consider the time-nonlocal QME (1.7):

$$\frac{d}{dt}\Pi(t) = -iL\Pi(t) + \int_0^t dt' \Sigma(t-t')\Pi(t'). \tag{3.42a}$$

Here, the Liouvillian $L = [\varepsilon d^\dagger d, \bullet]_-$ accounts for the uncoupled system whereas the (Nakajima-Zwanzig) *memory-kernel* describes its interaction with the environment. This QME is obtained from the Dyson equation (2.16) similarly to Eq. (3.36) by considering irreducible contributions to the perturbation series, see App. A.2.2 for details. As before, the time-local infinite-temperature result is separated from the time-nonlocal corrections of the correlation function γ [Eq. (3.34)] in the memory-kernel

$$\Sigma(s) = \tfrac{\Gamma}{2} \sum_\eta \Big[\bar\delta(s) - \eta e^{-\frac{\Gamma}{2}s}\gamma(s)\Big]\mathcal{L}_\eta, \tag{3.42b}$$

which is time-translationally invariant since it depends on the relative time $s = t - t'$ only.

Although clear from its solution (3.36), it is difficult to analyze the CP property of this time-nonlocal QME because the GKSL theorem (3.2) only applies to the *time-local* form discussed later on. In fact, the explicit structure of the memory kernel $\Sigma(s)$ ensuring CP will be determined in Ch. 5. However, this structure is quite complicated and even here not easily identified due to the finite-temperature effects introduced by $\gamma(s)$. In contrast,

semigroup-divisibility is readily identified and corresponds to a time-local Keldysh correlation function $\gamma(s) \to \bar{\delta}(s)$, which is only the case for the on-resonant [Eq. (3.18)] and off-resonant [Eq. (3.19)] limits. A further distinction of CP-divisibility is not obvious outside these semigroup-limits ($0 < \epsilon < \infty$): The frequency-dependence of the Laplace-transform

$$\Sigma(z) = \int_0^\infty dt e^{izt} \Sigma(t) = \tfrac{\Gamma}{2} \sum_\eta \left[1 + i \frac{\eta}{\pi} \sum_{\chi=\pm} \chi \psi \left(\frac{1}{2} + \tfrac{\frac{\Gamma}{2} - i(z - \chi\epsilon)}{2\pi T} \right) \right] \mathcal{L}_\eta \tag{3.43}$$

computed in App. A.2.2 does not seem to suggest any further qualitative difference, in particular, concerning the CP-divisibility property [Eq. (3.24)]. Thus, the time-nonlocal QME is less suited for discussing the CP and CP-divisibility properties of the dynamics. Nevertheless, the frequency-representation is a crucial starting point for advanced approximations [23, 35, 158, 165] because the Laplace variable z represents the physical energy.

3.6.2 Time-local QME (TCL)

The evolution is equivalently described by an exact *time-local* or time-convolutionless (TCL) quantum master equation [110, 111, 206, 219, 220]

$$\frac{d}{dt} \Pi(t) = \left[-iL + \Sigma^{\mathrm{TCL}}(t) \right] \Pi(t). \tag{3.44a}$$

In our case, we can directly construct the generator either by taking the time-derivative of the exponential form (3.36b), by superfermion considerations [App. A.2.3], or by explicitly inverting the EOM result (3.16) to calculate $\left[\frac{d}{dt}\Pi(t)\right]\Pi(t)^{-1}$ [App. A.1.2]. Either way we find that the time-local generator

$$\Sigma^{\mathrm{TCL}}(t) = \tfrac{\Gamma}{2} \sum_\eta \left[1 - \eta h(t) \right] \mathcal{L}_\eta \tag{3.44b}$$

is composed of constant GKSL superoperators with time-dependent coefficients involving the function $h(t)$ discussed earlier [Eq. (3.11)]. Different from the time-nonlocal QME, the structure of (3.44) clearly distinguishes both types of Markovian evolution occurring in our model: In the semigroup-divisible limits where $h(t) = h(\infty)$ is constant, the GKSL version of Eq. (3.2) applies and we obtain the necessary and sufficient condition $|h(\infty)| = |g(\infty)| \leq 1$ for CP in agreement with the real-time approach [Eq. (3.36)] and the time-nonlocal QME discussed above. If $h(t)$ is time-dependent, the CP-divisibility version of Eq. (3.2) requires $|h(t)| \leq 1$ for all $t \geq 0$ for the evolution to be CP-divisible, recovering the result from the real-time approach [Sec. 3.4.2]. If $|h(t)| \geq 1$ for some t, the GKSL coefficients are temporarily negative and we conclude that the evolution is not CP-divisible. In contrast to the real-time solution (3.36), the latter does *not* make any general statement about CP.

Finally, we note that despite the simplicity of the model, solving the QME (3.44a) to obtain the solution [Eqs. (3.16), (3.36), or (3.38)] requires time-ordering since the time-local generator (3.44b) does not commute $[\Sigma^{\mathrm{TCL}}(t), \Sigma^{\mathrm{TCL}}(t')]_- \neq 0$ with itself at different times [169]. Nevertheless, the relation between the time-local generator and the time-nonlocal memory-kernel involves *no* time-ordering but due to Eq. (3.11) a simple integration,

$$\Sigma^{\mathrm{TCL}}(t) = \int_0^t ds\, \Sigma(s). \tag{3.45a}$$

This is remarkable in the light of the general relation

$$\Sigma^{\mathrm{TCL}}(t) := \int_0^t dt' \Sigma(t-t')\Pi(t')\Pi^{-1}(t). \tag{3.45b}$$

The reason that both relations are valid for this model is *not* that $\Sigma(s)$ is time-local – which it is not– or that we approximated $\Pi(t) \approx \Pi(t')$ –which we did not. That Eq. (3.45) indeed holds for this model, is easy to see in the real-time approach [App. A.2.3] and is also confirmed by an explicit calculation [App. A.1.3] revealing that the superoperator identity $\Sigma(t-t')\Pi(t')\Pi^{-1}(t) = \Sigma(t-t')$ holds for all t, t' even though $\Pi(t')\Pi^{-1}(t) \neq \mathcal{I}$.

3.6.3 (Born-)Markov approximate QMEs

We can now investigate the impact of some approximations formulated on the level of the QMEs [108]. Based on the semigroup-divisible limits discussed in Sec. 3.3.2, we first discuss an obvious approximation[5] obtained by setting $h(t) \approx h(\infty)$ [Eq. (3.21)] which amounts to replacing the generator in the time-local QME (3.44) by its *exact stationary value*:

$$\Sigma^{\mathrm{TCL}}(t) \approx \Sigma^{\mathrm{TCL}}(\infty) = \tfrac{\Gamma}{2} \sum_\eta [1 - \eta h(\infty)]\, \mathcal{L}_\eta = \Sigma(i0^+). \tag{3.46}$$

The resulting approximate dynamics is governed by a GKSL equation with constant operators and coefficients, the latter being automatically positive since $|h(\infty)| = |g(\infty)| \leq 1$ [Eq. (3.23)]. The approximation (3.46) thus strictly respects both CP and TP.

By construction, the approximation reproduces the *exact* stationary state [Sec. 3.7] which is possible because (3.46) is nonperturbative in the parameters Γ, T, and ϵ, in contrast to the Γ-linear Born-Markov approximation discussed below. Despite this, it does not capture the interesting reentrant behavior discussed in Sec. 3.7 since the nontrivial time-dependence of the functions $\gamma(s)$, $h(t)$ and $g(t)$ has been dropped. Only in the semigroup limits, close to resonance ($|\epsilon| \ll T$) and far off resonance ($|\epsilon| \gg T$), also the transient dynamics is exact. Whereas the first case forms the starting point for the renormalized perturbation theory [Sec. 3.4] around the infinite-temperature limit, the second case relates to infinite-bias approximations [223–229]. The approximation (3.46) may be called 'Markov-only' since we obtain the same approximation in the time-*nonlocal* QME from an 'exact coarse-graining' procedure $\Sigma(t-t') \approx \Sigma(i0^+)\, \bar{\delta}(t-t')$ where only the zero Laplace-frequency component $z \to i0^+$ of the *exact* memory kernel (3.43) is retained. Note carefully that the zero-frequency and long-time approximations relate to *different* objects which are not simply related by a time-energy uncertainty relation: $\Sigma(z)$ is *not* the Laplace transform of $\Sigma^{\mathrm{TCL}}(t)$, note the upper integration limit Eq. (3.45a). Also note that the approximation can as well be implemented on the level of individual Kraus operators by replacing $g(t) \to g(\infty)$. An interesting open question is how this can be effected in a direct microscopic calculation of Kraus operators [32–34] at finite T. Furthermore, the equivalence in Eq. (3.46) of the zero-frequency memory-kernel $\Sigma(i0^+)$ and the stationary TCL generator $\Sigma^{\mathrm{TCL}}(\infty)$ raises the question on which of these objects a Markov approximation should in general be imposed, and we will further comment on this issue in the final chapter 6.

[5] In the 'initial slip' approach [221, 222] one also replaces the time-local QME by another time-constant QME which has the same stationary state as the original equation. To further improve this approximation one additionally modifies the *initial condition*, see Ref. [108]. Importantly, a constant initial slip will never recover the interesting reentrant behavior discussed in Sec. 3.7 because the dynamical map remains a semigroup.

Finally, we note that the combined Born-Markov approximation recovers the well-known Golden-Rule result $\Sigma^{\mathrm{TCL}}(\infty) = \Sigma(i0^+) \approx \Gamma \sum_\eta f(\eta\epsilon/T)\mathcal{L}_\eta$ in GKSL form where $f(x) = [e^x+1]^{-1}$ is the Fermi function. For this, one additionally expands the time-local generator up to linear order in Γ (Born) which implies a zeroth-order approximation for $h(\infty)$ in Eq. (3.21):

$$h(\infty) \approx \tfrac{2}{\pi} \operatorname{Im} \psi \left(\tfrac{1}{2} + \tfrac{i\epsilon}{2\pi T}\right) = 1 - 2f(\epsilon/T). \tag{3.47}$$

This approximation still respects TP as well as CP since $|f(\epsilon/T)| \leq 1$ *independent* of Γ, i.e., *even* for Γ values where it is inapplicable. In this respect, Born-Markov GKSL equations may be deceptive as the CP-TP property does not indicate a good approximation. Including higher order corrections changes this. Then, too large values of Γ definitely lead to loss of CP signaling an inconsistency in the calculation, which is a good thing. The presented expressions can be used as a benchmark to study how systematic higher-order approximations [155, 156, 230, 231] in Γ improve upon the Born-Markov results with respect to the CP, semigroup- and CP-divisibility properties. We note that the real-time renormalization group [35, 158] already obtains the exact solution for this model in the one-loop approximation [36, 232] and is in fact equivalent [157] to our derivation in Sec. 3.4.

3.7 Impact on observable dynamics

We now combine the insights of all approaches to study the *observable* impact of the divisibility criteria. We analyze in detail the time-evolution of the level occupation through the parity $\langle(-\mathbb{1})^n(t)\rangle = 1 - 2\langle n(t)\rangle$ determining the system state and the information measures introduced in Sec. 2.1.3.

3.7.1 Spectral decomposition

It is useful to start from the spectral decomposition (3.16b) obtained in the EOM approach from a simple rearrangement of terms. In the parity-basis the dynamical map is diagonal,

$$\Pi(t) = \sum_{k=1}^{4} \Pi_k(t)\ |m_k(t))\,(a_k(t)|\,, \tag{3.48}$$

with the right eigenvectors $|m_k(t))$ (modes) and left eigenvectors $(a_k(t)|$ (amplitudes) to the common eigenvalue $\Pi_k(t)$ as listed in Table 3.1. Explicit calculation shows that these eigenvectors are indeed properly normalized with respect to the Hilbert-Schmidt scalar product $(A|B) = \mathrm{Tr}_{\mathrm{S}} A^\dagger B$, cf. Sec. 2.3.1. Similarly, the time-local generator (3.44b) is diagonalized [App. A.1.2] after converting to braket-form:

$$\Sigma^{\mathrm{TCL}}(t) = \sum_{k=1}^{4} \Sigma_k^{\mathrm{TCL}}\ \left|m_k^{\mathrm{TCL}}(t)\right)\left(a_k^{\mathrm{TCL}}(t)\right|. \tag{3.49}$$

Remarkably, the eigenvalues of the time-local generator are *time-constant* and related to the evolution eigenvalues as $\Pi_k(t) = e^{\Sigma_k^{\mathrm{TCL}} t}$, a form suggestive of a Markovian semigroup where time-ordering is not an issue, cf. Eq. (3.45a). Also, the evolution eigenvalues always *decay* in time, irrespective of the restrictions imposed by CP [Eq. (3.22)] or CP-divisibility [Eq. (3.24)]. These restrictions are thus entirely incorporated in the *eigenvectors* in Table 3.1. In particular, only the first mode vector ($k = 1$) and last amplitude covector ($k = 4$) feature a nontrivial time-dependence in terms of the functions $g(t)$ and $h(t)$, which prevents the

	$\Pi(t)$		
k	Amplitude	Eigenvalue	Mode
1	$(\mathbb{1}\|$	1	$\frac{1}{2}\big[\,\|\mathbb{1})+g(t)\,\|(-\mathbb{1})^n)\,\big]$
$\frac{2}{3}$	$\big(d_\eta^\dagger\big\|$	$e^{(i\eta\varepsilon-\frac{1}{2}\Gamma)t}$	$\big\|d_\eta^\dagger\big)$
4	$\frac{1}{2}\big[\,((-\mathbb{1})^n\|-g(t)\,(\mathbb{1}\|\,\big]$	$e^{-\Gamma t}$	$\|(-\mathbb{1})^n)$

	$\Sigma^{\mathrm{TCL}}(t)$		
k	Amplitude	Eigenvalue	Mode
1	$(\mathbb{1}\|$	0	$\frac{1}{2}\big[\,\|\mathbb{1})+h(t)\,\|(-\mathbb{1})^n)\,\big]$
$\frac{2}{3}$	$\big(d_\eta^\dagger\big\|$	$i\eta\varepsilon-\frac{1}{2}\Gamma$	$\big\|d_\eta^\dagger\big)$
4	$\frac{1}{2}\big[\,((-\mathbb{1})^n\|-h(t)\,(\mathbb{1}\|\,\big]$	$-\Gamma$	$\|(-\mathbb{1})^n)$

Table 3.1: Time-dependent eigenvectors and eigenvalues of the evolution $\Pi(t)$ and its time-local generator $\Sigma^{\mathrm{TCL}}(t)$. The mode-operators $m_1(t)$ and $m_1^{\mathrm{TCL}}(t)$ are trace-normalized and positive if and only if $|g(t)|\leq 1$ and $|h(t)|\leq 1$, respectively. The subsets $k=1,4$ and $k=2,3$ of the eigenvectors do *not* correspond to the subsets of Kraus operators in Eq. (3.38). Reprinted table (adapted) with permission from J. Chem. Phys. **151**, 044101 (2019), see Ref. [134]. Copyright 2019 by the American Institute of Physics.

generator $\Sigma^{\mathrm{TCL}}(t)$ from commuting with itself at different times. As noted in Sec. 3.6.2 the latter complicates the solution of the time-local QME and the corresponding summation of the perturbation expansion. For the following discussion, we therefore focus on the nontrivial dynamics of these modes.

3.7.2 Fixed point of $\Pi(t)$ – Reentrant states

The time-independent eigenvalue $\Pi_1(t)=1$ corresponds to a *fixed point* $\Pi(t)\,|m_1(t))=|m_1(t))$ at finite time t. Its existence is guaranteed by the trace preservation of the evolution [Sec. 2.3.1] and should be clearly distinguished from the *stationary state*

$$\rho(\infty)=\Pi(\infty)\rho(0)=m_1(\infty), \tag{3.50}$$

which is reached *independently* of the initial state $\rho(0)$. The fixed point $m_1(t)$ is guaranteed to be a physical state if the condition $|g(t)|\leq 1$ holds, which is in agreement with general fixed-point theorems, see Ch. 6. of Ref. [233]: These state first that any continuous PP-TP map from the set of finite-dimensional density operators into that set has at least one fixed point density operator. Second, this set of fixed points is linearly spanned by a finite set of fixed-point density operators. In our case, the left and right eigen-supervectors for eigenvalue $\Pi_1=1$, are positive operators if $|g(t)|\leq 1$ as mentioned in the caption of Table 3.1. Consequently, $|g(t)|>1$ excludes the map $\Pi(t)$ to be PP-TP and thereby also CP-TP due to their coincidental equivalence in this model, see the discussion at the end of Sec. 3.3.3.

As we show below, preparing the system in such a state, $\rho(0)=m_1(t^{\mathrm{r}})$ with some parameter t^{r}, will force the evolution $\Pi(t)$ to exactly recover it at least once at time $t=t^{\mathrm{r}}$. This distinct *reentrant* behavior cannot arise within semigroup limits or approximations and is therefore an indicator for the loss of semigroup-divisible dynamics. In terms of particle transport, it implies a *reversal* of the time-dependent *particle current* to the environment –a pronounced effect that can equivalently be seen in the parity of the fermionic level given by

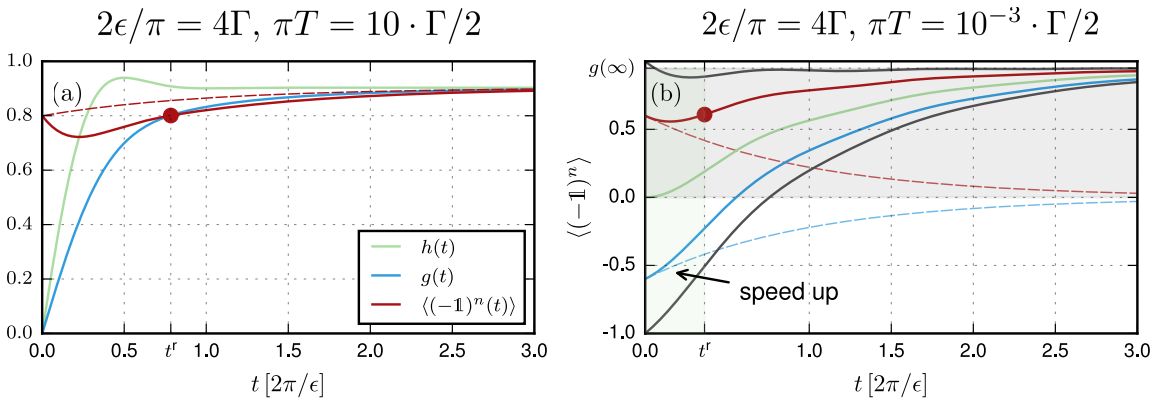

Figure 3.3: (a) Reentrance (dot) of the parity $\langle(-\mathbb{1})^n(t)\rangle$ (red) at time t^{r} for $2\epsilon/\pi = 4\Gamma$ and $\pi T = 10 \cdot \Gamma/2$. Asymptotically the parity approaches the function $g(t)$ (blue). Note that the minimum implied by the reentrance occurs precisely when the parity crosses the function $h(t)$ (green), cf. Eq. (3.54). The reentrant behavior is not captured by the non-perturbative 'Markov-only' approximation (3.46) to the parity (red dashed). (b) Parity evolution for different initial conditions and $2\epsilon/\pi = 4\Gamma$ and $\pi T = 10^{-3} \cdot \Gamma/2$. When initialized in the range $[0, g(\infty))$ (gray shade) the parity shows reentrant behavior (red curve, dot). For a fixed initial value, the reentrant time (green shade) scales as $t^{\mathrm{r}} \sim \pi/\epsilon$ with the level detuning $\epsilon = \varepsilon - \mu$. In this window, the deviation from the leading exponential behavior $e^{-\Gamma t}$ (dashed lines) sets in. For reentrant dynamics, this causes the parity to reverse while for non-reentrant dynamics it speeds up the approach to the stationary state from below. Neither effect is captured by the 'Markov-only' semigroup approximation (3.46) (not shown). Reprinted figure (adapted) with permission from J. Chem. Phys. **151**, 044101 (2019), see Ref. [134]. Copyright 2019 by the American Institute of Physics.

Eq. (3.27b) and repeated here for convenience:

$$\langle(-\mathbb{1})^n(t)\rangle = e^{-\Gamma t}\langle(-\mathbb{1})^n(0)\rangle + (1 - e^{-\Gamma t})g(t). \tag{3.51}$$

Fig. 3.3(a) illustrates that the parity (red curve) is dominated at short times $t \sim \Gamma^{-1}$ by the exponentially decaying first term. This decay is however soon counteracted with the nonlinear time-dependence introduced by $g(t)$ (blue curve) in the second term which sets in on an independent time-scale $t \sim \pi/\epsilon$ determined by the level detuning ϵ, cf. Eq. (3.20). As shown in Fig. 3.3(b) for $\epsilon \geq 0$, their competition causes the parity evolution to display two qualitatively different types of behavior depending on the initial parity value $\langle(-\mathbb{1})^n(0)\rangle$:

(i) If the initial parity lies within the range of $g(t)$, i.e., within $[0, g(\infty))$ for $\epsilon > 0$ and $(g(\infty), 0]$ for $\epsilon < 0$, see the discussion after Eq. (3.14), one can find a parameter t^{r} such that $\langle(-\mathbb{1})^n(0)\rangle = g(t^{\mathrm{r}})$. The evolution then revisits this parity value at $t = t^{\mathrm{r}}$ (red):

$$\langle(-\mathbb{1})^n(t^{\mathrm{r}})\rangle = \langle(-\mathbb{1})^n(0)\rangle = g(t^{\mathrm{r}}). \tag{3.52}$$

In cases where $g(t)$ is nonmonotonic, the parity may revisit the initial value several times whenever $g(t)$ revisits it (not shown). It is remarkable that the initial decay with $e^{-\Gamma t}$ (red dashed line in Fig. 3.3(b)) goes in the 'wrong' direction, *away* from the stationary value. Thus, if the level is initially prepared as being 'too empty' relative to

the stationary value, it first becomes significantly *more empty* before filling up again. This behavior can be controlled with the level detuning $\epsilon = \varepsilon - \mu$ and the effects are most pronounced in between the two Markovian semigroup limits: For $|\epsilon| \ll T$, the range of reentrant initial values (gray vertical range in Fig. 3.3(b)) shrinks because $g(t) \to 0$ [Eq. (3.18)]. For $|\epsilon| \gg T$, instead the time-scale for revisiting the initial value (green horizontal range) shrinks because $g(t) \to \theta(t)$ [Eq. (3.19)]. The reentrant behavior at low temperatures is most pronounced when $|\epsilon| \sim \Gamma \gg T$, i.e., when μ is positioned on the *flank* of the Γ-broadened resonance at ε. Note that even with all these parameters fixed, the time-scale t^{r} for reentrance still depends on the initial condition in the range of $g(t)$ and can thus be chosen independently.

(ii) No reentrance occurs if the initial value of $\langle(-\mathbb{1})^n(0)\rangle$ lies outside the range of $g(t)$. The parity then decays to its stationary value $g(\infty)$ either from above or below (gray curves in Fig. 3.3(b)). The approach from above may still be nonmonotonic, in particular for $|\epsilon| \gg T$ when the stationary state is nearly pure and $\langle(-\mathbb{1})^n(\infty)\rangle = |g(\infty)| \to 1$.

3.7.3 Fixed point of $\Sigma^{\mathrm{TCL}}(t)$ – Local stationary states

The reentrant behavior of the parity implies by continuity that it must have gone through an extremum (minimum) at some earlier time $t^{\mathrm{e}} \leq t^{\mathrm{r}}$. We thus turn to analyzing its time-*local* behavior reflected by the derivative

$$\tfrac{d}{dt}\langle(-\mathbb{1})^n(t)\rangle = -\Gamma\Big[\langle(-\mathbb{1})^n(t)\rangle - h(t)\Big], \tag{3.53}$$

and more generally by the eigenvectors of the time-local generator $\Sigma^{\mathrm{TCL}}(t)$ which differ from those of $\Pi(t)$ only by the replacement $g(t) \to h(t)$, see Table 3.1. The existence of a time-dependent zero-mode $\big|m_1^{\mathrm{TCL}}(t)\big)$ is implied by the trace-preservation. In contrast to $|m_1(t))$, this mode is *not* a physical state unless $|h(t)| \leq 1$ holds at a *fixed* time t. Therefore, the parity cannot have an extremum[6] at instants where $|h(t)| > 1$, irrespective of the initial parity.

We stress that the condition for an extremum at time t is weaker than the CP-divisibility criterion (3.24) demanding $|h(t)| \leq 1$ for *all* times $t > 0$ of the evolution. In this simple system, CP-divisibility can be studied by families of occupation evolutions with varying initial conditions: The evolution is CP-divisible, if this family reveals the existence of extrema in *any* time-interval as shown in Fig. 3.4(a) by the corresponding transport current. The loss of CP-divisibility is instead accompanied by the emergence of time-intervals *without* extrema as shown in Fig. 3.4(b) for a lower temperature. Within the time-intervals where extrema do occur, $|h(t')| \leq 1$, and the dynamical map factorizes as $\Pi(t) = \Pi(t,t')\Pi(t')$ into two CP-TP maps [Eq. (3.37)]. It thus makes sense to denote the dynamics as *locally* CP-divisible at time t'. Physically, this means the dynamics is still insensitive to reinitializing the environment but only in restricted time-intervals which are *observable* quantifiers of non-semigroup dynamics.

Nature of extrema. Let us now focus on the nature of extremal points t^{e} which occur when the physical zero-mode is visited, $\rho(t^{\mathrm{e}}) = m_1^{\mathrm{TCL}}(t^{\mathrm{e}})$ during some evolution. At such points, the evolution temporarily comes to a complete halt, $\frac{d}{dt}\rho(t^{\mathrm{e}}) = 0$, before speeding up again towards the stationary state. As noticed above, this halting is equivalent to an extremum of

[6] This argument fails for more complicated systems where a single scalar observable is not sufficient to describe the system density operator [Eq. (3.26)]: The physical zero-mode is only visited if all observables spanning an orthonormal operator-basis are extremal at the *same* time.

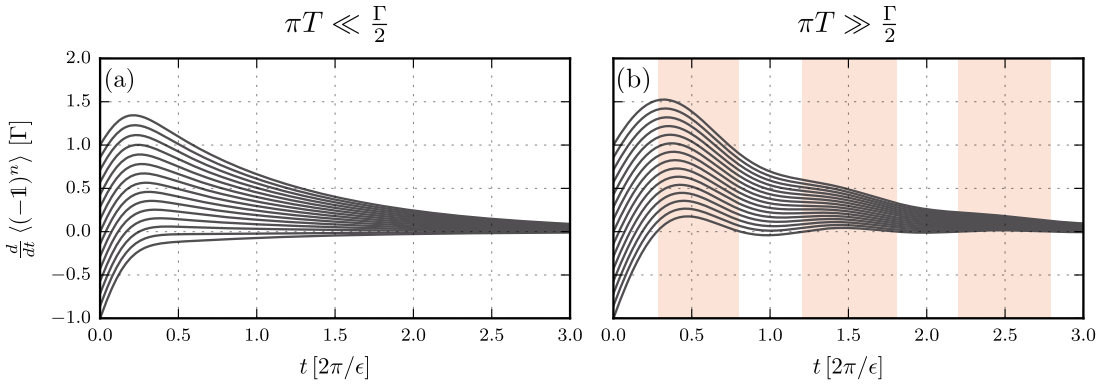

Figure 3.4: A family of parity evolutions is obtained by varying the initial conditions $\langle(-\mathbb{1})^n(0)\rangle \in [-1,1]$. Plotted are the corresponding transport currents for $2\epsilon/\pi = 4\Gamma$. (a) At high temperature $\pi T = 20 \cdot \Gamma/2$, we have CP-divisible evolution characterized by the occurrence of current-reversals at any time. (b) At low temperature $\pi T = 10^{-3} \cdot \Gamma/2$, we have non-CP-divisible evolution, as a current-reversal is prohibited in broad time-intervals (red shade), irrespective of the initial condition. In the complementary intervals, the dynamics is still *locally* CP-divisible, see discussion in the text. Reprinted figure (adapted) with permission from J. Chem. Phys. **151**, 044101 (2019), see Ref. [134]. Copyright 2019 by the American Institute of Physics.

the parity and by Eq. (3.53) requires

$$\langle(-\mathbb{1})^n(t^{\mathrm{e}})\rangle = h(t^{\mathrm{e}}). \tag{3.54}$$

In App. B.4, we show that for $\Gamma/2 \geq \pi T$, *any* fixed initial condition $\langle(-\mathbb{1})^n(0)\rangle \in [-1,1]$ satisfies Eq. (3.54) for infinitely many times t^{e}. This means that the parity keeps on oscillating although with ever decreasing amplitude. For $\Gamma/2 \leq \pi T$, there exist initial parity conditions which *never* satisfy the condition for any t^{e} and their evolutions show no extrema at all. However, there is always a range of initial parities that does satisfy it for some t^{e} and it is in this range that the reentrant behavior occurs.

The halting $\frac{d}{dt}\rho(t^{\mathrm{e}}) = 0$ does not imply that higher time-derivatives are zero at t^{e} as it does in the stationary limit. The curvature at an extremal point,

$$\tfrac{d^2}{dt^2}\rho(t^{\mathrm{e}}) = [\tfrac{d}{dt}\Sigma^{\mathrm{TCL}}(t^{\mathrm{e}})]\,\rho(t^{\mathrm{e}}) = \Sigma(t^{\mathrm{e}})\rho(t^{\mathrm{e}}), \tag{3.55}$$

is determined due to Eq. (3.45a) by the *memory-kernel* of the time-*non*local QME. Although $\rho(t^{\mathrm{e}}) = m_1^{\mathrm{TCL}}(t^{\mathrm{e}})$ is never a zero eigenvector of $\Sigma(t^{\mathrm{e}})$, the curvature may still vanish. This happens at times t^{p} where the memory-kernel (3.42b) itself vanishes

$$\gamma(t^{\mathrm{p}}) = 0 \quad \Leftrightarrow \quad t^{\mathrm{p}} = \frac{\pi}{\epsilon}\ell \quad \ell = 1,2,\ldots \tag{3.56}$$

and coincides with the zeros of the correlation function (3.12). Since $\frac{d}{dt}h(t) = e^{-\frac{\Gamma}{2}t}\gamma(t)$ [Eq. (3.11)], the function $h(t)$ equivalently becomes extremal at the time t^{p}. Thus, if the parity $\langle(-\mathbb{1})^n(t)\rangle$ crosses $h(t)$ at one of its extremal points t^{p}, its curvature

$$\tfrac{d^2}{dt^2}\langle(-\mathbb{1})^n(t)\rangle = -\Gamma\left[\tfrac{d}{dt}\langle(-\mathbb{1})^n(t)\rangle - \tfrac{d}{dt}h(t)\right] \tag{3.57}$$

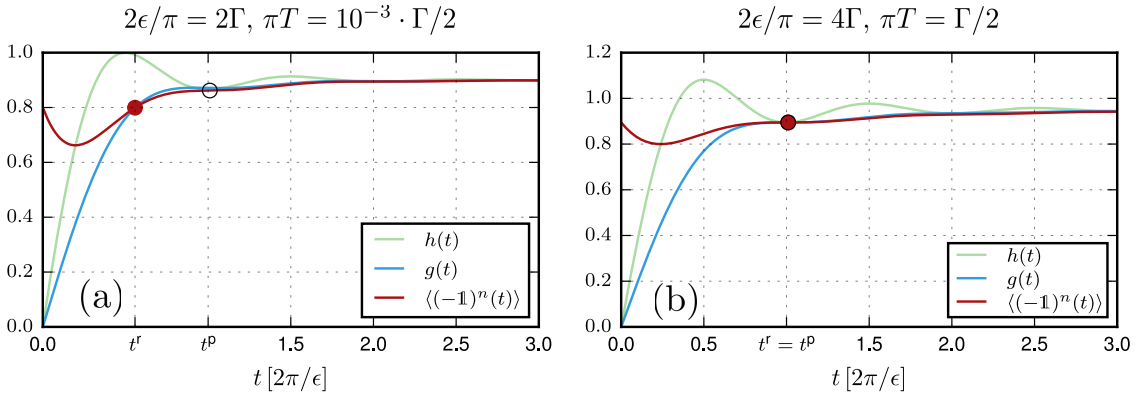

Figure 3.5: (a) Local stationary state: The level occupation parity (red) can develop a plateau (circle) when it crosses with $h(t)$ (green) at $t^{\mathrm{p}} = \ell\pi/\epsilon$ [Eq. (3.56)] for any $\ell = 1, 2, \ldots$. Here $\ell = 2$ and we have taken low temperature $\pi T = 10^{-3}\cdot\Gamma/2$ for which the curvature (3.57) is negligibly small. The time-width of the plateau scales as ϵ^{-1} with the level-detuning since $\epsilon = \varepsilon - \mu$ determines the inverse slope of $\gamma(t^{\mathrm{p}})$ [Eq. (3.12)], here $2\epsilon/\pi = 2\Gamma$. We note that the value (3.57) is only exactly zero for a specific, much higher temperature where the dynamics is very close to a featureless semigroup. (b) Local stationarity at reentrance: The reentrant point (dot) of the parity (red) can coincide with a plateau (circle) only at one of the *touching points* of $g(t)$ (blue) and $h(t)$ (green) located at the minima $t^{\mathrm{p}} = \ell\pi/\epsilon$ for $\ell = 0, 2, 4, \ldots$. These curves first touch exactly for $\Gamma/2 = \pi T$ and are generic also for lower temperatures: It requires very large level-detunings ϵ to significantly pull the green curve below the blue one. Here $2\epsilon/\pi = 4\Gamma$ and $\ell = 2$. Reprinted figure (adapted) with permission from J. Chem. Phys. **151**, 044101 (2019), see Ref. [134]. Copyright 2019 by the American Institute of Physics.

vanishes exactly. Moreover, around points where $t^e \approx t^p$, the parity can also develop a pronounced *approximate* plateau as illustrated in Fig. 3.5(a). The state may be called *locally stationary* close to such points.

Local stationarity at reentrance. As seen in Table 3.1, the eigenvectors of the evolution and its time-local generator are in general different. However, there are special cases where they coincide, namely at the crossing points t^{r} of the functions $g(t)$ and $h(t)$. The initial condition can thus be chosen as $\langle(-\mathbb{1})^n(0)\rangle = g(t^{\mathrm{r}}) = h(t^{\mathrm{r}}) = \langle(-\mathbb{1})^n(t^{\mathrm{r}})\rangle$ such that the reentrant point [Eq. (3.52)] is also an extremum ($t^{\mathrm{r}} = t^{\mathrm{e}}$). This is always possible for $\Gamma/2 > \pi T$, where the reentrant point is either a maximum or a minimum. For $\Gamma/2 = \pi T$ it is instead a saddle point [App. B.4] and the parity shows a plateau at the reentrant point ($t^{\mathrm{r}} = t^{\mathrm{p}}$). The system then not only recovers the initial state but even becomes *locally* stationary at reentrance as is illustrated in Fig. 3.5(b). For $\Gamma/2 < \pi T$ such a situation can never arise.

3.7.4 Information measures

Above we have distinguished the initial from the reentrant state by following the time-evolution between $t = 0$ and $t = t^{\mathrm{r}}$. If one instead measures the system only at these two times, one cannot distinguish these states. Information measures [Sec. 2.1.3] do allow for such a distinction and furthermore quantify the system's backaction on its environment.

In Fig. 3.6 we plot the respective entropies of the system and the effective environment for the three different initially mixed states of Fig. 3.3(b). For zero initial parity (green), the

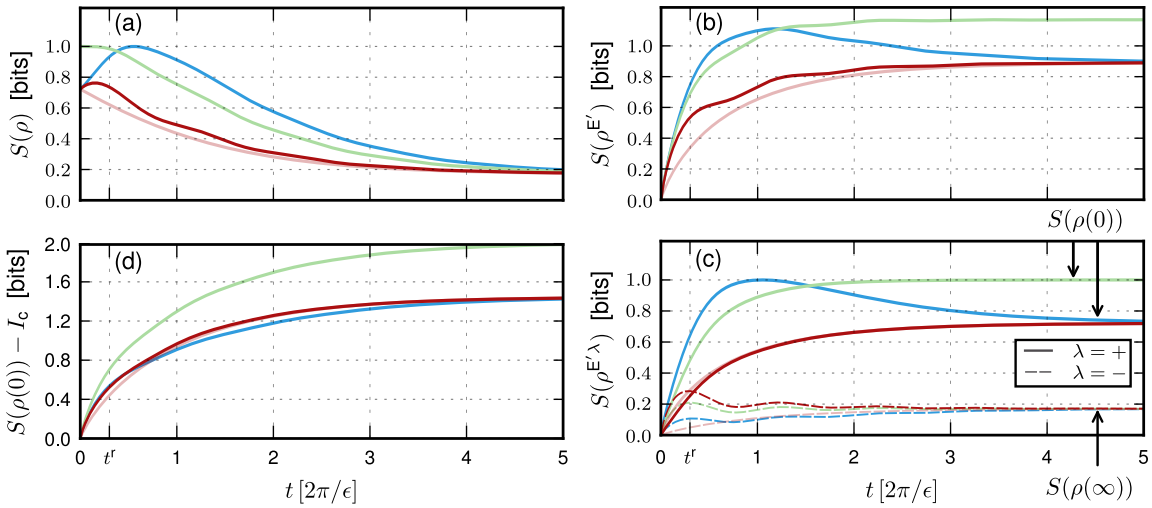

Figure 3.6: (a) System entropy for the middle three parity evolutions of Fig. 3.3(b) (same color coding). The system entropies may initially differ (mixture of preparation) but converge to the same stationary value. For the reentrant dynamics (red), we compare with the 'Markov-only' approximation (3.46) (light red). (b) The corresponding effective environment entropies are initially the same (by purification) but converge to different stationary values (backaction on the effective environment). (c) Decomposition of (b) into entropies of the effective environment modes, $S(\rho^{\mathrm{E}'}(t)) = \sum_\lambda S(\rho^{\mathrm{E}'\lambda}(t))$, see Eq. (3.41). One mode (solid, $\lambda = +$) captures the smooth large variations while the other (dashed, $\lambda = -$) adds smaller oscillatory behavior. Consistent with Eq. (2.12), the former mode converges to the spectrum of $\rho(\infty)$ and the latter to that of $\rho(0)$. (d) Coherent-information mismatch [Eq. (2.9)]. In this quantity the 'Markov-only' approximation deviates only very little. Reprinted figure (adapted) with permission from J. Chem. Phys. **151**, 044101 (2019), see Ref. [134]. Copyright 2019 by the American Institute of Physics.

system entropy in Fig. 3.6(a) decreases from its maximal value. For the evolution without reentrance (blue), the system entropy first increases until it reaches the maximal entropy state of one bit before decreasing again. In this case, the nonmonotonic behavior is solely due to the fact that the system entropy cannot distinguish the sign of the parity which has to pass through zero to reach the stationary value of opposite sign. Because of the fermionic superselection, this reversal can only be achieved via the maximal entropy state, i.e., the corresponding Bloch vector must shrink to zero in order to reverse, and is also captured by the 'Markov-only' semigroup approximation (not shown). This behavior should be clearly distinguished from the reentrant dynamics (red) where the system entropy also increases initially but never reaches the maximal value: The system initially evolves in the 'wrong' direction before turning around towards the stationary state –a behavior not present in the 'Markov-only' approximation (light red).

The effective environment entropy in Fig. 3.6(b) also depends on the initial system state. Unlike the system entropy this dependence remains in the stationary limit where it converges to $S(\rho(0))$ [Eq. (2.12), Sec. 2.1.3]. At large times it therefore does not distinguish between the reentrant and non-reentrant evolutions starting from opposite parity signs (blue and red curves merge at large times). However, at short times it distinguishes these particularly clearly: The reentrant and non-reentrant evolutions have a distinct backaction, the former

having a smaller –but still sizable– entropy footprint in the effective environment. This shows that the state of the environment is definitely different at the reentrant point t^{r} although the system state is recovered exactly. The splitting between the blue and red curves does not arise in the t-linear regime where both evolutions speed towards the maximally mixed state and their effective-environment entropies still coincide. They only split up when the nonlinearity caused by $g(t)$ kicks in which is precisely what distinguishes the two parity evolutions in Fig. 3.3(b): It is responsible for the reversal of the parity evolution in the reentrant case, and its speed-up in the non-reentrant one.

The contributions of the individual effective environment modes $\rho^{\mathrm{E}'\lambda}(t)$ discussed at the end of Sec. 3.5 are shown in Fig. 3.6(c). Remarkably, these modes separate the oscillatory behavior of the effective environment entropy ($\rho^{\mathrm{E}'-}$, dashed curves) from the dominant evolution ($\rho^{\mathrm{E}'+}$, solid curves). The 'Markov-only' approximation (light red) significantly deviates from the former but nearly perfectly reproduces the latter.

Finally, in Fig. 3.6(d) we show the corresponding coherent-information mismatch $S(\rho(0)) - I_{\mathrm{c}}(t)$. Its dominating increase underscores that the initial entanglement with the auxiliary system $\mathrm{P_S}$, involved in the preparation of the mixture $\rho(0)$ [Sec. 2.1.3], is continuously being converted into entanglement with the effective environment E' until all entanglement is broken in the stationary state, cf. Fig. 2.3. This happens irrespective of the reentrant behavior of the level occupation and the corresponding reversals of the particle current. The curves in Fig. 3.6(d) evolve in groups split according to whether the magnitude of the initial parity is small (green) or large (blue, red). The sign of the initial parity –decisive for the occurrance of reentrant behavior– causes only a small splitting (blue, red). One further notices that modulations on the timescale π/ϵ –clearly present in the individual entropies– are absent in the (mismatch of the) coherent information. This highlights a π-phase-shift between the modulations of the two entropies which may be easily overlooked in Fig. 3.6(a) and (b). In fact, only in the limit of large detuning $\epsilon \gg \Gamma/2 \geq \pi T$, one can find nonmonotonic behavior on time-scales where the stationary state is far from reached. Still, both $S(\rho(t))$ and $S(\rho^{\mathrm{E}'}(t))$ show oscillations in this case long after the oscillations in $I_{\mathrm{c}}(t)$ have died out.

3.8 Summary

We addressed a number of recent questions regarding open quantum systems by considering the exact analytic solution of a resonant level with arbitrary coupling Γ to a thermal reservoir at arbitrary temperature T. Our analysis relied on different approaches to the exact dynamics which provided complementary insights to overcome the fundamental CP-TP duality outlined in Sec. 2.3.1. In particular, the Kraus operator-sum enabled an exact analysis in terms of a strongly correlated system of one fermion coupled to an *effective* two-fermion *environment*. The presented exact expressions may also prove useful as benchmarks, in particular for general methods that aim at directly computing Kraus operators for open quantum systems in novel CP approximations [32–34, 85, 137]. This idea will be further pursued in Ch. 5.

To evaluate the impact of approximations, it proved useful to also discuss two exact quantum master equations for the same dynamics, one time-local and one time-nonlocal. Notably, we found an example of a 'Markov-only' semigroup approximation that is non-perturbative in all parameters, yet simultaneously completely positive (CP) and trace-preserving (TP). The fact that this approximation relies only on the exact value of *stationary occupation* $\langle n(\infty)\rangle = \frac{1}{2}[1 - g(\infty)]$ may be relevant for TD-DFT approaches to interacting open systems [234] based on a mapping to the *noninteracting* limit studied here.

Despite its simplicity, this model displays both semigroup- and CP-divisible behavior as well as dynamics that is neither of these, i.e., truly non-Markovian. Physical parameters allow one to tune between these three regimes, in particular the level-detuning ϵ and the competition between thermal (T) and quantum fluctuations (Γ). We explored how these distinctions are reflected in the transient dynamics of the level occupation when varying the initial condition. We found that the loss of semigroup-divisibility is the most pronounced distinction, see also the recent discussion in Ref. [96]. Counter to intuition, the system occupation may temporarily *increase* significantly in order to reach a stationary state with *smaller* occupation. This measurable behavior occurs for a wide range of parameters and a finite, sharp range of initial conditions. It derives from the *time-dependent* fixed point of the dynamical map: For semigroup dynamics, this continuous family of fixed points collapses onto the stationary state but is clearly distinct in the other two regimes.

We also found that the occupation dynamics can come to a halt at several extrema before continuing towards the unique global stationary state. For $\Gamma/2 > \pi T$, this generically happens irrespective of the initial state, whereas in the opposite case a definite window of initial states is required. Additionally, the extrema can turn into *locally stationary* states where even the *evolution curvature* is strongly suppressed. From this analysis, we found that CP-divisibility can be observed in this system by studying families of occupation measurements with varying initial conditions: Whereas the loss of semigroup-divisibility is accompanied by the *appearance* of extrema in such families, the loss of CP-divisibility is instead associated with the *loss* of extrema. The dynamics may however still be *locally* CP-divisible in definite time-windows –a distinction that allows for a more fine-grained characterization of non-Markovianity. Thus, CP-divisibility provides an interesting quantitative guide to the more subtle features of the dynamics beyond the semigroup limit.

4 Periodic driving within the Markovian limit

In this chapter the rationale of the previous investigation is inverted: Instead of considering the non-Markovian dynamics of an *exactly solvable* model, we now turn to the well-known *Markovian approximation* encountered in many quantum-optical setups and investigate the effect of periodic driving on the open system's dynamics. The periodic modulation of parameters causes the dynamics to lag behind the instantaneous, fixed-parameter evolution, and generates non-Markovian memory-effects in the sense that the dynamics becomes CP-divisible within this originally semigroup-divisible Markovian setting.

We focus on periodic modulation protocols for driven-dissipative systems coupled to a transmission line (and more generally, to a reservoir) where the dissipation rates $\gamma_i(t)$ of the explicitly time-dependent GKSL quantum master equation (1.6) are temporarily suppressed. As mentioned in the introduction, such a suppression of the so-called Liouvillian dissipation gap is a decisive feature of systems undergoing driven-dissipative phase transitions, e.g., in the open Rabi model [235], which give rise to interesting long-lived metastable [236] and periodic steady states. Later in Sec. 4.6, we will investigate the Kerr nonlinearity model, which has already been solved analytically in the time-independent stationary case by Drummond and Walls [237] and recently experienced a revival of interest in the driven setting in theoretical studies [30, 238–240] as well as experimentally. For example, the bistable behavior of Kerr nonlinearities has been experimentally exploited to confine the manifold of available states in superconducting qubits to coherent states under special two-photon driving schemes [43].

From a methodical point of view, numerically accessing such metastable and periodic steady states is notoriously unstable and time-consuming due to the fact that the differential equations governing the dynamics have to be integrated over long periods of time. To overcome this issue, we reformulate the *generic* time-local quantum master equation (QME) using Floquet's theorem such that integration over a *single* period of driving is sufficient for calculating the exact periodic steady state. On this basis we also provide a systematic expansion in both the adiabatic and high-frequency regime. Importantly, the method applies to *any* time-local QME with a periodic-in-time generator, not only to the GKSL equation considered in the applications of this chapter. Applied to our prolem, we show how memory-effects manifest themselves in a nonadiabatic behavior of system-observables even for relatively slow driving frequencies.

Publications and acknowledgments. This chapter and the accompanying App. D (including the adapted figures) have been published in V. Reimer, K. G. L. Pedersen, N. Tanger, M. Pletyukhov, and V. Gritsev, Physical Review A **97**, 043851 (2018) [Copyright 2018 by the American Physical Society], see Ref. [135]. The steady-state formalism has been developed by M. Pletyukhov and K. G. L. Pedersen while its numerical implementation was performed by V. Reimer. We acknowledge useful discussions with D. Krimer concerning this numerical implementation and with M. R. Wegewijs on issues surrounding the adiabatic expansion.

4.1 Introduction

Classical Floquet theory [241] gave long-standing inspiration for studies of a variety of time-periodic processes in nature and has found a huge domain of applicability in fields ranging from dynamical system's theory to technology. In quantum mechanics, Bloch's theorem for crystals [242] represents the momentum-space analog of Floquet's seminal work, while in the time domain the concept of quasienergy was introduced only in the 1960s by Zel'dovich [243]. Periodic time-dependent processes are natural in quantum optics where the input laser field provides a fast periodic driving of the system. To the best of our knowledge, it was Shirley [244] who first applied a Floquet formalism in quantum optics. He clarified the connection between a semiclassical external field drive and its strong, quantized, resonant single-mode field counterpart applied to an N-level atom based on general considerations using Floquet's theorem. Various extensions of this work, which focused on the semiclassical picture suggested by the strong-intensity nature of laser fields, have been reviewed in Refs. [245–247]. In the quantum regime, studies of periodically driven-dissipative (open) quantum systems have led to a whole new class of physics inaccessible in equilibrium systems. Most of the earlier developments are reviewed in Refs. [28, 248], including the paradigmatic two-level systems, tunneling problems and spin-boson models. More recent examples with the earlier mentioned potential for technological applications cover the emergence of topological phases –the so-called Floquet topological insulators [52]– nonthermal steady states exhibiting localization [249] and artificial gauge systems [250].

A particularly useful approach for studying driven-dissipative systems is the so-called Floquet-Liouville approach [251] which reduces to a GKSL master equation (1.5) under the Markov approximation [252]. We note that there is a subtlety concerning different procedures of performing the Markovian approximation. In general, the Markovian approximation for the eigenenergy spectrum performed on the level of the undriven Hamiltonian differs from performing it on the level of the driven Floquet quasienergy spectrum. Applications of such approaches, which have been shown to capture some interesting features of periodically driven-dissipative quantum systems, range from transport problems such as electronic pumping [50] to dynamical decoupling schemes for qubit control [253]; see also Ref. [29] for a review. However, due to the large separation of system and driving time scales –a regime where the Markovian approximation is very well valid– it has been most widely applied in the context of quantum optics; see, e.g., Refs. [254–261].

Analytical investigations employing the Floquet-Liouville approach are in practice restricted to either adiabatic or high-frequency limits, and only for few problems [262, 263] it is feasible to derive closed systems of equations. Whereas for closed systems the high-frequency Magnus expansion is typically –and successfully– used [264], the complex eigenenergies characteristic for open systems prohibit any truncation of the Magnus series because it typically yields exponentially increasing (i.e., unphysical) terms. On the other hand, an adiabatic approximation may be invalid even for slow driving frequencies if the effective dissipation rate is (temporarily) suppressed. This will be the case for models discussed in this chapter and we show that *nonadiabatic effects* become prominent even when the modulation is slow compared with bare dissipation rates. Here, we establish a general framework for studying the periodic steady state in the long-time regime of periodically driven-dissipative quantum systems that is capable of systematically addressing both slow and fast modulations. It extends the previously developed scattering formalism [265], allowing us to capture multiphoton processes via the equation of motion approach. The latter is designed in such a way that an integration

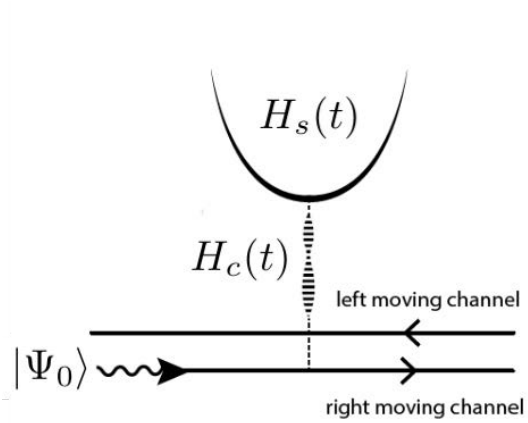

Figure 4.1: Driven-dissipative waveguide model: A local system is coupled to a transmission line supporting left- and right-propagating modes. Either the system's parameters or its coupling to the transmission line is periodically modulated. The input pulse into the transmission line is given by a coherent state $|\Psi_0\rangle$ in the right-propagating mode ω_0. The pulse's intensity is characterized by the photonic flux f. Reprinted figure with permission from Phys. Rev. A **97**, 043851 (2018), see Ref. [135]. Copyright 2018 by the American Physical Society.

is required over a single period of modulation only. The adiabatic and high-frequency limits can therefore be efficiently benchmarked against exact numerical results. We apply our framework to investigate nonadiabatic effects which in general arise due to a nearly vanishing Liouvillian gap and can appear useful for implementing adiabatic quantum computation with superconducting qubits [266], and various dynamical decoupling schemes [267].

The chapter is organized as follows. First, the generic quantum-optical setup of driven-dissipative systems is introduced in Sec. 4.2. In Sec. 4.3 we then develop the steady state formalism which is applied to three quantum optical systems exhibiting a critical suppression of the smallest dissipation rate. In Sec. 4.4, a two-level system with a periodically driven coupling to the transmission line is considered. This model exhibits the striking feature of alternating in time between bunching and antibunching statistical behavior of reflected photons. In Sec. 4.5 we show that similar nonadiabatic effects can be realized with a three-level Λ-system when the drive field intensity is periodically modulated. Finally, in section 4.6 we consider the Kerr-nonlinearity model where the system's response to changing parameters across the region of the dissipative phase transition is studied. There, the emergence of the hysteretic behavior recently predicted [240] and experimentally observed [30] is of interest.

4.2 Driven-dissipative waveguide models

The models considered within this chapter all share the notion of a quantum system described by the local Hamiltonian $H_s(t)$ which is driven via a coupled transmission line, or waveguide, by a coherent pulse $|\Psi_0\rangle$ characterized in terms of the photonic flux f, as shown in Fig. 4.1. The whole setup is described by the Hamiltonian

$$H(t) = H_s(t) + H_w + H_c(t), \tag{4.1}$$

with the waveguide contribution $H_w = \sum_\alpha \int d\omega(\omega_0+\omega) a^\dagger_{\alpha\omega} a_{\alpha\omega}$ written in terms of left- and a right-propagating fields labeled by mode (ω) and direction ($\alpha = L, R$) indices. We either assume a time-dependent coupling strength[1] $g(t)$ in the coupling Hamiltonian

$$H_c(t) = \sum_\alpha \int d\omega \left[\frac{g(t)}{\sqrt{2}} a^\dagger_{\alpha\omega} O + \text{h.c.} \right], \tag{4.2}$$

where O is some operator of the local system, or a periodic modulation of some parameters of the local quantum system Hamiltonian $H_s(t)$ itself.

The form of H_w implies the general assumption that the dispersion of the transmission line can be linearized around a working frequency ω_0, such that $\omega_k = \nu(k-k_0)+\omega_0$, where ν is the group velocity. For convenience, we employ units in which $\nu = \hbar = 1$ holds. Extending the linearized dispersion to the full spectrum is known as the wideband approximation and is valid if the working frequency ω_0 is large compared with all other energy scales, including the driving frequency, $\omega_0 \gg \Omega$, and nearly resonant with a transition in the local system described by the operator O. Note that this also falls in line with neglecting counter-rotating terms in the rotating wave approximation (RWA) leading to the coupling Hamiltonian (4.2) and effectively constitutes the Markovian limit which holds even in the case of time-periodic modulation as is shown in App. D. Time dynamics of the system's reduced density matrix is then governed by the GKSL master equation

$$\frac{d}{dt}\rho(t) = -i\left[H_{\text{eff}}(t), \rho(t)\right] + \gamma(t)\mathcal{D}\left[O\right]\rho(t), \tag{4.3a}$$

with a time-dependent dissipation rate $\gamma(t) \equiv \pi|g(t)|^2$, and

$$H_{\text{eff}}(t) = H_s(t) + \sqrt{\pi f} g(t) O + \sqrt{\pi f} g^*(t) O^\dagger, \tag{4.3b}$$

$$\mathcal{D}[O]\rho(t) = O\rho(t)O^\dagger - \frac{1}{2}O^\dagger O\rho(t) - \frac{1}{2}\rho(t)O^\dagger O. \tag{4.3c}$$

4.3 Periodic steady-state formalism

The aim of this section is to set up a formalism, which allows us to directly access the periodic steady-state solution of Eq. (4.3) in the long-time limit by using Floquet's theorem in the time representation. Traditionally (see, e.g., Ref. [236], for a recent application), Floquet's theorem is employed to get rid of an explicit time dependence of periodic Hamiltonians or Liouvillians by switching to the Fourier representation. The problem is thereby reduced to a static eigenvalue problem for the so-called Floquet quasienergies and modes in an enlarged Hilbert space. While this procedure is in principle always possible, it introduces certain difficulties for practical numerical calculations, since it necessitates a truncation of the infinite number of Floquet modes. This is especially perilous if an additional cut-off, e.g., in the Fock basis, is required, such as, for example, in the case of the Kerr nonlinearity model considered in Sec. 4.6. For this reason, we prefer a formulation in terms of differential equations for periodic steady states which can be solved on a single period of modulation.

[1] The coupling strength $g(t)$ used in this chapter should not be confused with the function $g(t)$ of Ch. 3.

The starting point of our consideration is the generic time-local QME,

$$\frac{d}{dt}\rho(t) = -iL(t)\rho(t), \tag{4.4}$$

for the reduced density operator $\rho(t)$ of the local system generated by some periodic-in-time Liouvillian superoperator $L(t)$, generalizing the one in Eq. (4.3). In spite of the time-dependence, it must have a zero eigenvalue, as dictated by the trace-preservation, cf. Sec. 2.3.1. It is convenient to explicitly split off the corresponding zero-eigenmode of $L(t)$. To do so, we fix some matrix representation of $\rho(t)$ and express the occupation probability of the ground state by $\rho_{00}(t) = 1 - \sum_{i=1}^{N-1} \rho_{ii}(t)$, where N is the number of states in the system. In the vectorized form, i.e., by restacking the columns of the matrix representation of $\rho(t)$ into an N^2-dimensional vector $(\rho_{00}, \vec{\rho})^T$, the master equation (4.4) turns into

$$\frac{d}{dt}\begin{bmatrix}\rho_{00}(t)\\ \vec{\rho}(t)\end{bmatrix} = \begin{bmatrix}-iL_{00}(t) & \vec{C}^T(t)\\ \vec{C}(t) & -i\bar{L}(t)\end{bmatrix} \cdot \begin{bmatrix}\rho_{00}(t)\\ \vec{\rho}(t)\end{bmatrix}. \tag{4.5}$$

As a result, all information has been encoded in the (N^2-1)-dimensional state vector $\vec{\rho}(t)$ governed by the differential equation

$$\frac{d}{dt}\vec{\rho}(t) = [-\vec{C}(t)\otimes\vec{E}^T - i\bar{L}(t)]\vec{\rho}(t) + \vec{C}(t) \equiv A(t)\vec{\rho}(t) + \vec{C}(t), \tag{4.6}$$

where $\vec{E}$ consists of ones (zeros) in the positions of the diagonal (off-diagonal) elements of $\vec{\rho}$.

For a time-independent Liouvillian, Eq. (4.6) allows for a direct calculation of the true stationary state $\vec{\rho}_{\mathrm{st}} = -A^{-1}\vec{C}$. In the case of a time-periodic driving, time translational invariance is lost even in the long-time limit and the time-periodic steady state $\vec{\rho}_{\mathrm{ps}}(t)$ will essentially follow the persistent external modulation after some transient time regime in which the influence of the initial state gradually decays. We are interested in this long-time limit and take the initial time $t_0 = -M_0 T \to -\infty$ to be in the far past, where we assume without loss of generality that it is back by a large integer multiple $M_0 \gg 1$ of the driving period T. The split structure of Eq. (4.6) is reflected in the ansatz

$$\vec{\rho}(t) = \lim_{t_0\to-\infty} O(t)\vec{\rho}(t_0) + \vec{\rho}_{\mathrm{ps}}(t) \tag{4.7}$$

which gives a clear physical interpretation of the appearing vectors and matrices.

The matrix $O(t)$ describes the gradual decay of the initial conditions in the far past and is solely governed by the periodic matrix $A(t)$,

$$\frac{d}{dt}O(t) = A(t)O(t), \qquad O(0) = \mathbb{1}. \tag{4.8}$$

Note that the reference time has been shifted from t_0 to zero which is possible here due to the periodic nature of $A(t)$. According to Floquet's theorem, the solution of this differential equation can be represented as

$$O(t) = P(t)e^{Bt}, \tag{4.9}$$

where $P(t) = P(t+T)$ is a periodic matrix function with the initial condition $P(0) = \mathbb{1}$. The constant matrix B, which is obtained from the monodromy matrix $O(T) = P(T)e^{BT} = e^{BT}$,

has eigenvalues with negative real parts such that $\lim_{t\to\infty} O(t) = 0$ holds, and all information about initial conditions in Eq. (4.7) is lost as required.

After the initial conditions have fully decayed, only the periodic steady-state vector $\vec{\rho}_{\mathrm{ps}}(t)$ remains. It is governed by the differential equation

$$\frac{d}{dt}\vec{\rho}_{\mathrm{ps}}(t) = A(t)\vec{\rho}_{\mathrm{ps}}(t) + \vec{C}(t), \qquad \lim_{t_0\to-\infty} \vec{\rho}_{\mathrm{ps}}(t_0) = 0, \tag{4.10}$$

where unlike in the case of $O(t)$ the reference time t_0 remains unaltered to account for the fact that we are interested in the long-time limit. The differential equation (4.10) can be formally integrated to

$$\vec{\rho}_{\mathrm{ps}}(t) = O(t)\int_{-\infty}^{t} dt' O^{-1}(t')\vec{C}(t'). \tag{4.11}$$

The periodicity of this solution is straightforwardly seen from Eq. (4.9) and the periodicity of $P(t)$ and $\vec{C}(t)$, and therefore it is sufficient to study its behavior on the finite interval $\tau_c \in [0, T]$. To further evaluate Eq. (4.11), we first split the integration range into two intervals $[-\infty, 0]$ and $[0, \tau_c]$,

$$\vec{\rho}_{\mathrm{ps}}(\tau_c) = O(\tau_c)\int_{-\infty}^{0} dt' O^{-1}(t')\vec{C}(t') + \vec{c}(\tau_c), \tag{4.12a}$$

where

$$\vec{c}(\tau_c) = O(\tau_c)\int_{0}^{\tau_c} dt' O^{-1}(t')\vec{C}(t') \tag{4.12b}$$

is defined in analogy with Eq. (4.11) with the reference time shifted to zero. We note that instead of inverting the large matrix $O(t)$ appearing in Eq. (4.12b), it is more favourable to instead numerically solve the differential equation

$$\frac{d}{dt}\vec{c}(t) = A(t)\vec{c}(t) + \vec{C}(t), \qquad \vec{c}(0) = 0. \tag{4.13}$$

Next, the interval $[-\infty, 0]$ is split into an infinite number of intervals $[-(n+1)T, -nT]$, $n \in \mathbb{N}_0$. Using the periodicity of $P(t)$, we represent the first term of Eq. (4.12a) by a geometric progression with the factor e^{BT}. Resumming it, we obtain

$$\vec{\rho}_{\mathrm{ps}}(\tau_c) = O(\tau_c)(1 - O(T))^{-1}\vec{c}(T) + \vec{c}(\tau_c). \tag{4.14}$$

Thus, to evaluate $\vec{\rho}_{\mathrm{ps}}(t)$, it is sufficient to solve the set of equations (4.8) and (4.13) on the finite interval $0 \le \tau_c \le T$. In fact, the solution (4.14) obeys the differential equation (4.10) with periodic boundary conditions rather than the initial condition therein.

4.3.1 Adiabatic expansion

In the adiabatic limit, the external driving of parameters is sufficiently slow such that the state can instantaneously adapt to its new environment, $\rho_{\mathrm{ps}}(t) \approx -A^{-1}(t)\vec{C}(t) \equiv \rho_{\mathrm{inst}}(t)$. To consistently compute adiabatic corrections to the instantaneous solution $\rho_{\mathrm{inst}}(t)$, we insert

the relation $O^{-1}(t) = -\frac{d}{dt}[O^{-1}(t)]A^{-1}(t)$ into Eq. (4.11). Integrating it by parts we obtain

$$\vec{\rho}_{\rm ps}(t) = \rho_{\rm inst}(t) - O(t)\int_{-\infty}^{t} dt' O^{-1}(t')\tfrac{d}{dt'}\rho_{\rm inst}(t'). \tag{4.15}$$

Iterating this procedure leads to a geometric series that can be resummed to

$$\vec{\rho}_{\rm ps}(t) = \frac{1}{1 - A^{-1}(t)\frac{d}{dt}}\vec{\rho}_{\rm inst}(t) \approx \vec{\rho}_{\rm inst}(t) + A^{-1}(t)\tfrac{d}{dt}\vec{\rho}_{\rm inst}(t). \tag{4.16}$$

We note that convergence of this series relies on some sort of an adiabaticity condition. If such a condition is violated or generally not provided, the expansion (4.16) breaks down.

4.3.2 High-frequency expansion

The Magnus expansion is frequently used for analyzing high-frequency processes in driven quantum optical systems. Note, however, that it is originally designed for applications in closed systems where the evolution is unitary. For driven-dissipative systems with Liouvillian dynamics, it often produces –according to our experience– exponentially growing, unphysical terms already in the first order of expansion. Instead of the Magnus expansion, we perform a straightforward high-frequency expansion of the master equation (4.6) in the following way: Since in the long-time limit $A(t)$, $\vec{C}(t)$, and $\vec{\rho}(t)$ are all periodic functions of time, let us explicitly split off the constant zero-frequency component for each of these objects:

$$X(t) = \overline{X} + \widetilde{X}(t), \quad \overline{X} = \frac{1}{T}\int_0^T dt' X(t'). \tag{4.17}$$

Here $\widetilde{X}(t)$ is a periodic function with zero time average. Then, omitting the vector notation in the following, we rewrite the master equation (4.6), which must also hold in the long-time limit with periodic boundary conditions, as

$$\frac{d}{dt}\widetilde{\rho}(t) = \left(\overline{A} + \widetilde{A}(t)\right)\bar{\rho} + \left(\overline{A} + \widetilde{A}(t)\right)\widetilde{\rho}(t) + \overline{C} + \widetilde{C}(t). \tag{4.18}$$

The constant average $\bar{\rho}$ can be expressed in terms of the periodic part $\widetilde{\rho}$ if one integrates Eq. (4.18) over one period,

$$\bar{\rho} = -\overline{A}^{-1}\left(\overline{C} + \frac{1}{T}\int_0^T dt' \widetilde{A}(t')\widetilde{\rho}(t')\right). \tag{4.19}$$

Now, we expand $\rho(t)$ in powers of the inverse modulation frequency $\Omega = 2\pi/T$:

$$\bar{\rho} = \sum_{n=0}^{\infty}\frac{1}{\Omega^n}\bar{\rho}^{(n)}, \qquad \widetilde{\rho}(t) = \sum_{n=1}^{\infty}\frac{1}{\Omega^n}\widetilde{\rho}^{(n)}(t). \tag{4.20}$$

The hierarchy of differential equations resulting from this ansatz,

$$\frac{d}{dt}\widetilde{\rho}^{(1)}(t) = \widetilde{A}(t)\bar{\rho}^{(0)} + \widetilde{C}(t), \tag{4.21a}$$

$$\frac{d}{dt}\widetilde{\rho}^{(n)}(t) = \widetilde{A}(t)\bar{\rho}^{(n-1)} + \overline{A}\widetilde{\rho}^{(n-1)}(t) + \widetilde{A}(t)\widetilde{\rho}^{(n-1)}(t) - \frac{1}{T}\int_0^T dt'\widetilde{A}(t')\widetilde{\rho}^{(n-1)}(t') \qquad , n \geq 2 \tag{4.21b}$$

can be iteratively solved as follows. First, we extract from Eq. (4.19) the leading order of the expansion for the constant average

$$\bar{\rho}^{(0)} = -\overline{A}^{-1}\overline{C}, \tag{4.22}$$

with which we can formally solve Eq. (4.21a):

$$\widetilde{\rho}^{(1)}(t) = -\left(\int_0^t dt'\widetilde{A}(t') - \frac{1}{T}\int_0^T dt\int_0^t dt'\widetilde{A}(t')\right)\overline{A}^{-1}\overline{C} + \int_0^t dt'\widetilde{C}(t') - \frac{1}{T}\int_0^T dt\int_0^t dt'\widetilde{C}(t'). \tag{4.23}$$

Knowing $\widetilde{\rho}^{(1)}(t)$, we can then also extract $\bar{\rho}^{(1)}$ from Eq. (4.19):

$$\bar{\rho}^{(1)} = -\overline{A}^{-1}\frac{1}{T}\int_0^T dt'\widetilde{A}(t')\widetilde{\rho}^{(1)}(t'). \tag{4.24}$$

The higher-order contributions are obtained by an analogous iterative procedure.

4.4 Driven two-level system

We first apply the Floquet formalism developed above to a setup in which the local quantum system has two levels (a qubit) and the coupling to the transmission line is periodically modulated. This setup has recently been discussed in the regime of weak intensities $f \ll \gamma$ of the coherent input pulse using Floquet scattering theory [265]. The present approach allows us to extend these results to larger input powers $f \geq \gamma$.

The Hamiltonian (4.1) of this system is specified by $H_s(t) = \omega_e\sigma_+\sigma_-$ and $O = \sigma_-$. Going to the co-rotating frame, we find that the master equation (4.6) for the reduced state-vector $\vec{\rho}(t) \to \vec{s}(t) = \langle\hat{\vec{s}}(t)\rangle \equiv [\langle\tilde{\sigma}_+(t)\rangle, \langle\tilde{\sigma}_-(t)\rangle, \langle 1+\sigma_z(t)\rangle]^T$ uses the matrix

$$A(t) = \begin{bmatrix} -i\delta - \gamma(t)/2 & 0 & -i\sqrt{\pi f}g(t) \\ 0 & i\delta - \gamma(t)/2 & i\sqrt{\pi f}g^*(t) \\ -2i\sqrt{\pi f}g^*(t) & 2i\sqrt{\pi f}g(t) & -\gamma(t) \end{bmatrix}, \tag{4.25a}$$

and the vector

$$\vec{C}(t) = \left[i\sqrt{\pi f}g(t), -i\sqrt{\pi f}g^*(t), 0\right]^T. \tag{4.25b}$$

Here we introduced the detuning parameter $\delta = \omega_0 - \omega_e$ as well as $\langle\tilde{\sigma}_\mp(t)\rangle = \langle\sigma_\mp(t)\rangle e^{\pm i\omega_0(t-t_0)}$. Importantly, in a broad range of f, the smallest dissipation rate is solely determined by the coupling strength $g(t)$, and temporarily quenching $g(t) \to 0$ will cause a critical slowing down of the system's Liouvillian dynamics. We exploit this property to design a modulation protocol aiming to achieve time-intervals where the modulation frequency $\Omega = 2\pi/T$ exceeds the scale set by the smallest dissipation rate, $\Omega > \gamma_{\min}(t)$. Within these time intervals, we expect the system's response to be nonadiabatic such that the expansion (4.16) breaks down.

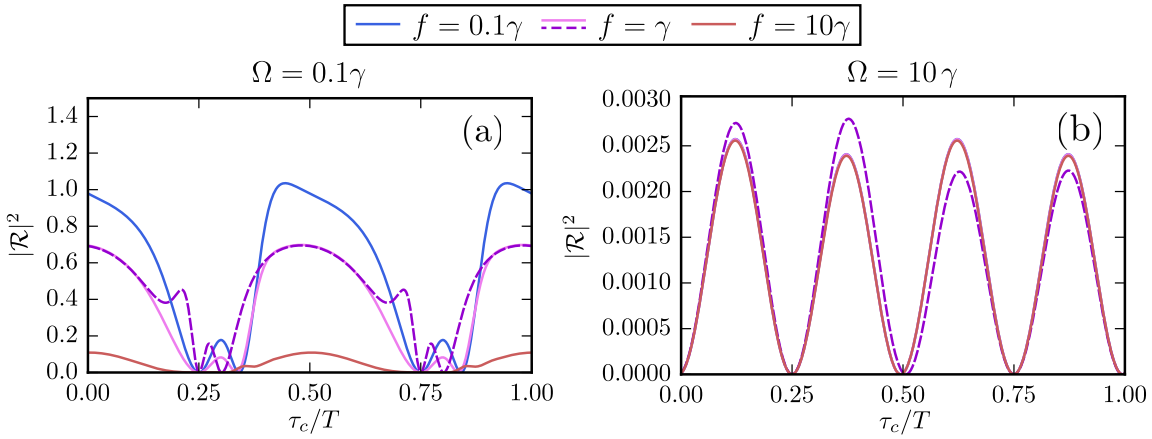

Figure 4.2: Reflection off the qubit on resonance, $\delta = 0$, for the time-modulated coupling $g(t) = g_0 \cos \Omega t$ with (a) slow $\Omega = 0.1\gamma$ and (b) fast $\Omega = 10\gamma$ modulation frequencies, in units of $\gamma = \pi g_0^2$. (a) The adiabatic approximation (dashed line) obtained from Eq. (4.16) deviates from the numerical solution in the vicinities of time instants when the coupling is quenched. For all values of f, the reflection is suppressed at these points. At large f, the reflection is completely suppressed because of the qubit's saturation. (b) The high-frequency modulation suppresses the reflection for any input power f. The numerical result (solid lines) is well approximated by the high-frequency result (dashed line) obtained from Eqs. (4.22)-(4.24). Reprinted figure (adapted) with permission from Phys. Rev. A **97**, 043851 (2018), see Ref. [135]. Copyright 2018 by the American Physical Society.

4.4.1 Reflection and transmission

Applying the standard input-output relations (cf. App. D), we find that the reflection and transmission amplitudes solely depend on the second component of the vector $\vec{s}(t)$:

$$\mathcal{R}(t) \equiv \frac{\langle a_{L,\mathrm{out}}(t)\rangle}{\langle a_{R,\mathrm{in}}(t)\rangle} = -i\sqrt{\frac{\pi}{f}}g(t)s_2(t) \tag{4.26a}$$

$$\mathcal{T}(t) \equiv \frac{\langle a_{R,\mathrm{out}}(t)\rangle}{\langle a_{R,\mathrm{in}}(t)\rangle} = 1 + \mathcal{R}(t). \tag{4.26b}$$

The numerically obtained reflection $|\mathcal{R}|^2(\tau_c)$ in the periodic steady state with a cosinusoidal modulation of $g(t)$ is shown in Fig. 4.2 for different input powers f on a single period T. The results for weak input powers are equivalent to those obtained by the Floquet scattering approach in Ref. [265]. This is confirmed analytically by perturbatively evaluating Eq. (4.11) in the weak power limit $f \ll |\bar{\gamma} - i\bar{\delta}|$. Doing so, we obtain

$$s_{\mathrm{ps},2}(t) \approx -i\sqrt{\pi f}e^{-F(t)}\int_{-\infty}^{t} dt' e^{F(t')}g^*(t'), \tag{4.27}$$

with $F(t) = \int_0^t dt'[\gamma(t') - i\delta(t')]$ and reproduce the reflection amplitude in Eq. (34) of Ref. [265].

We note that, for the modulation protocol $g(t) = g_0 \cos \Omega t$, where the coupling periodically switches its sign, the period of the steady-state reflection (shown in Fig. 4.2) is exactly half of the modulation period T. Moreover, reflection goes to zero not only at the quench times when $g(t) = 0$ but also at some intermediate times. While this feature has already been

noticed previously in Ref. [265] for weak input powers, we now see that this also persists with increasing f. These are first indications of a memory-effect in this Markovian setup which will become more pronounced later on in Sec. 4.4.3 when looking at the photon-statistics. Remarkably, the adiabaticity is violated around the quench points even at sufficiently slow modulation, as one can conclude in Fig. 4.2(a) from the comparison of the numerical solution (solid line) for $f = \gamma \equiv \pi g_0^2$ with the corresponding adiabatic approximation of Sec. 4.3.1 (dashed line). In the beginning ($\tau_c \approx 0$), in the middle ($\tau_c \approx T/2$), and in the end ($\tau_c \approx T$) of the modulation period, the instantaneous relaxation rate $\gamma(t)$ is larger than Ω, and the adiabatic approximation approaches the numerical result. The overall decrease of the reflection with increasing f is naturally associated with the qubit's saturation. In contrast to the adiabatic approximation, the high-frequency approximation at fast modulations, introduced in Sec. 4.3.2, is most accurate in the vicinities of the quench points, as follows from its comparison (dashed line) with the numerical solution (solid lines) in Fig. 4.2(b). In general, fast modulation tends to suppress the reflection for any value of the input power f.

4.4.2 Power spectrum

The power spectrum is related to the correlation function of outgoing photons

$$\begin{aligned} g_\alpha^{(1)}(\tau,\tau_c) = \langle a_{\alpha,\mathrm{out}}^\dagger(\tau_c+\tau)a_{\alpha,\mathrm{out}}(\tau_c)\rangle = \quad & \delta_{\alpha,L}e^{i\omega_0\tau}f\mathcal{R}^*(\tau_c+\tau)\mathcal{R}(\tau_c) && \text{(4.28a)}\\ + \; & \delta_{\alpha,R}e^{i\omega_0\tau}f\mathcal{T}^*(\tau_c+\tau)\mathcal{T}(\tau_c) && \text{(4.28b)}\\ + \quad & e^{i\omega_0\tau}\pi g^*(\tau_c+\tau)g(\tau_c)G_1(\tau,\tau_c), && \text{(4.28c)} \end{aligned}$$

where the terms (4.28a) and (4.28b) give rise to the elastic contribution to the power spectrum for reflected and transmitted photons, respectively, while the common term (4.28c) constitutes the inelastic contribution. A proper definition of the power spectrum requires time-translational invariance, which can be restored in the periodic steady state by averaging the variable $\tau_c \in [0,T]$ over a period of modulation. With the Fourier expansion $\mathcal{R}(\tau_c) = \sum_m \mathcal{R}^{(m)}e^{-im\Omega\tau_c}$ of the steady-state reflection (and, equivalently, transmission) amplitude, we hence obtain for the elastic contribution

$$S_{L,\mathrm{el}}(\omega) = \frac{1}{2\pi}\int_{-\infty}^{\infty}d\tau\left[\frac{1}{T}\int_0^T d\tau_c\, g_{L,\mathrm{el}}^{(1)}(\tau,\tau_c)\right]e^{-i\omega\tau} = f\sum_m |\mathcal{R}^{(m)}|^2\,\delta(\omega-\omega_0-m\Omega), \quad (4.29)$$

which peaks not only at the working frequency ω_0, but also at frequencies shifted from ω_0 by integer multiples of Ω. An analogous expression holds for $S_{R,\mathrm{el}}(\omega)$ of the transmitted photons with the replacement $\mathcal{R} \to \mathcal{T}$.

Evaluation of the inelastic contribution (4.28c) to the power spectrum requires knowledge of the vector $\vec{G}(\tau,\tau_c) = \langle \hat{\vec{s}}(\tau_c+\tau)\hat{s}_2(\tau_c)\rangle - \vec{s}_{\mathrm{ps}}(\tau_c+\tau)s_{\mathrm{ps},2}(\tau_c)$ in the long-time limit. We note that only its first component is required, which has the property $G_1(-|\tau|,\tau_c) = G_1(|\tau|,\tau_c)^*$. It is thus sufficient to find an equation for $\vec{G}(\tau,\tau_c)$ by means of the quantum regression theorem for $\tau > 0$ only. It reads

$$\frac{d}{d\tau}\vec{G}(\tau,\tau_c) = A(\tau_c+\tau)\vec{G}(\tau,\tau_c), \quad (4.30)$$

and its solution can be expressed in terms of $O(t)$ governed by the same periodic matrix $A(t)$:

$$\vec{G}(\tau,\tau_c) = O(\tau+\tau_c)O^{-1}(\tau_c)\vec{G}^{(0)}(\tau_c). \quad (4.31)$$

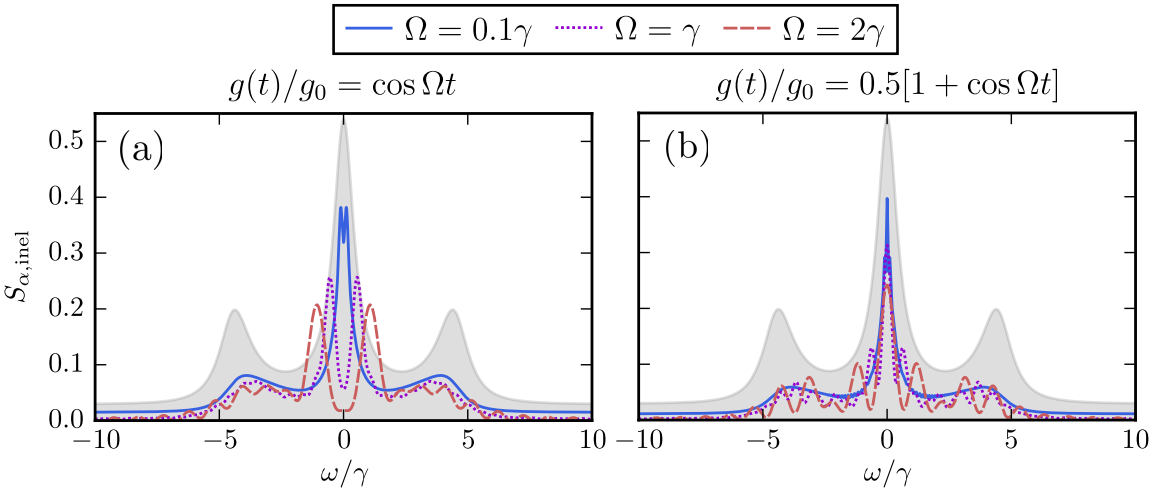

Figure 4.3: Inelastic power spectra of the qubit strongly driven ($f = 200\gamma$) on resonance ($\delta = 0$) for (a) the sign-change protocol $g = g_0 \cos\Omega t$ and (b) the on-off protocol $g(t) = \frac{g_0}{2}(1+\cos\Omega t)$ for various modulation frequencies Ω. The Mollow triplet for the corresponding stationary case at coupling $g = g_0$ is shown for comparison in gray. Additional broadened peaks consistent with the Floquet spectrum arise due to the periodic modulation and may destructively interfere as seen, for example, in the missing main peak in the case of the sign-change protocol (a). Similar features in the power spectrum have been reported in Ref. [268] for a qubit subject to a pulsed excitation. Reprinted figure (adapted) with permission from Phys. Rev. A **97**, 043851 (2018), see Ref. [135]. Copyright 2018 by the American Physical Society.

As the initial condition $\vec{G}(0,\tau_c) = \vec{G}^{(0)}(\tau_c)$, we use the periodic steady-state values of $\vec{s}_{\rm ps}(\tau_c)$:

$$\vec{G}^{(0)}(\tau_c) = \begin{bmatrix} \frac{1}{2}s_{\rm ps,3}(\tau_c) - |s_{\rm ps,2}(\tau_c)|^2 \\ -s_{\rm ps,2}^2(\tau_c) \\ -s_{\rm ps,3}(\tau_c)s_{\rm ps,2}(\tau_c) \end{bmatrix}. \tag{4.32}$$

From the representation $O(t) = P(t)e^{Bt}$ we find for the inelastic contribution

$$\begin{aligned} g^{(1)}_{\alpha,\rm inel}(\tau,\tau_c) = \;& \pi e^{i\omega_0\tau}\Theta(\tau)\vec{V}_+(\tau_c+\tau)\cdot e^{B\tau}\vec{V}_0(\tau_c) \\ & + \pi e^{i\omega_0\tau}\Theta(-\tau)\left[\vec{V}_+(\tau_c)e^{-B\tau}\cdot\vec{V}_0(\tau_c+\tau)\right]^* \end{aligned} \tag{4.33}$$

with the periodic vector functions

$$\vec{V}_+(\tau_c) = g^*(\tau_c)P(\tau_c)\vec{n}_1, \tag{4.34}$$

$$\vec{V}_0(\tau_c) = g(\tau_c)P^{-1}(\tau_c)\vec{G}^{(0)}(\tau_c), \tag{4.35}$$

and $\vec{n}_1 = (1,0,0)^T$. We insert the Fourier expansions $\vec{V}_{+,0}(\tau_c) = \sum_m \vec{V}^{(m)}_{+,0}e^{-im\Omega\tau_c}$ for the periodic vectors to evaluate the τ_c-average over a single period of modulation to restore time-translational invariance. Additionally, it is useful to express the matrix $B = \sum_{j=1}^3 b_j\,\vec{\chi}_r^{(j)}\otimes\vec{\chi}_l^{(j)}$ in terms of its eigenvalues b_j and the corresponding biorthonormal left and right eigenvectors obeying $\vec{\chi}_l^{(j)}\cdot\vec{\chi}_r^{(j')} = \delta_{jj'}$. This gives direct analytical access to resonance positions $\omega_{m,j} =$

$\omega_0 + m\Omega + \mathrm{Im}\, b_j$ and widths $\sigma_j = -\mathrm{Re}\, b_j$ in the inelastic power spectrum

$$\begin{aligned} S_{\alpha,\mathrm{inel}}(\omega) &= \frac{1}{2\pi}\int_{-\infty}^{\infty} d\tau \left[\frac{1}{T}\int_0^T d\tau_c\, g^{(1)}_{\alpha,\mathrm{inel}}(\tau,\tau_c)\right] e^{-i\omega\tau} \\ &= \sum_m \sum_{j=1}^{3} \mathrm{Re}\left[\frac{(\vec{V}_+^{(-m)}\cdot\vec{\chi}_r^{(j)})(\vec{\chi}_l^{(j)}\cdot\vec{V}_0^{(m)})}{i(\omega-\omega_0-m\Omega-\mathrm{Im}\, b_j)-\mathrm{Re}\, b_j}\right]. \end{aligned} \tag{4.36}$$

This result indicates equidistant additional resonances introduced by the periodic modulation which can be understood from a dressed state picture: The periodic modulation further splits the dressed states of the qubit driven through the transmission line into m equidistant Floquet modes. Numerical results shown in Fig. 4.3 confirm this behavior but also show that, for the modulation protocol $g(t) = g_0 \cos\Omega t$, some of the resonances are suppressed and the main peak splits into two side peaks. This behavior can in principle be used for frequency shifting and engineering correlated states of light.

As a final consistency check, we confirm the power conservation, i.e., that the output photon fluxes $f_\alpha(\tau_c) = g^{(1)}_\alpha(0,\tau_c)$ average over one period of modulation to give the input flux $f = \bar{f}_L + \bar{f}_R$. In the formal expression, we need to prove the identity

$$\begin{aligned} f &\stackrel{!}{=} \frac{1}{T}\int_0^T d\tau_c\, [f_L(\tau_c) + f_R(\tau_c)] \\ &= f - \frac{1}{2T}\int_0^T d\tau_c \left[\sum_{j=1}^{3} A_{3,j}(\tau_c) s_{\mathrm{ps},j}(\tau_c) + C_3(\tau_c)\right] \\ &= f - \frac{1}{2T}\int_0^T d\tau_c\, \dot{s}_{\mathrm{ps},3}(\tau_c), \end{aligned} \tag{4.37}$$

which is indeed fulfilled due to the periodicity of $s_{\mathrm{ps},3}(\tau_c)$.

4.4.3 Second-order coherence function

We finally turn to analyzing the statistical properties of the scattered photons with help of the second-order coherence function

$$g^{(2)}_{\alpha\alpha}(\tau,\tau_c) = \frac{\langle a^\dagger_{\alpha,\mathrm{out}}(\tau_c)\, n_{\alpha,\mathrm{out}}(\tau_c+\tau)\, a_{\alpha,\mathrm{out}}(\tau_c)\rangle}{f_\alpha(\tau+\tau_c) f_\alpha(\tau_c)}. \tag{4.38}$$

Here $n_{\alpha,\mathrm{out}} = a^\dagger_{\alpha,\mathrm{out}} a_{\alpha,\mathrm{out}}$ is the outgoing photon number in channel α. Also this function has been studied earlier in the context of Floquet scattering theory [265] for weak input powers f, but within this framework we can extend those results to larger values of f for which the scattering theory becomes impractical. Similar to the procedure for the power spectrum, the quantum regression theorem allows us to write the functions (4.38) in terms of the vector

$$\vec{J}(\tau,\tau_c) = \langle \hat{s}_1(\tau_c)\hat{\vec{s}}(\tau+\tau_c)\hat{s}_2(\tau_c)\rangle - \frac{1}{2} s_{\mathrm{ps},3}(\tau_c)\vec{s}_{\mathrm{ps}}(\tau+\tau_c), \tag{4.39}$$

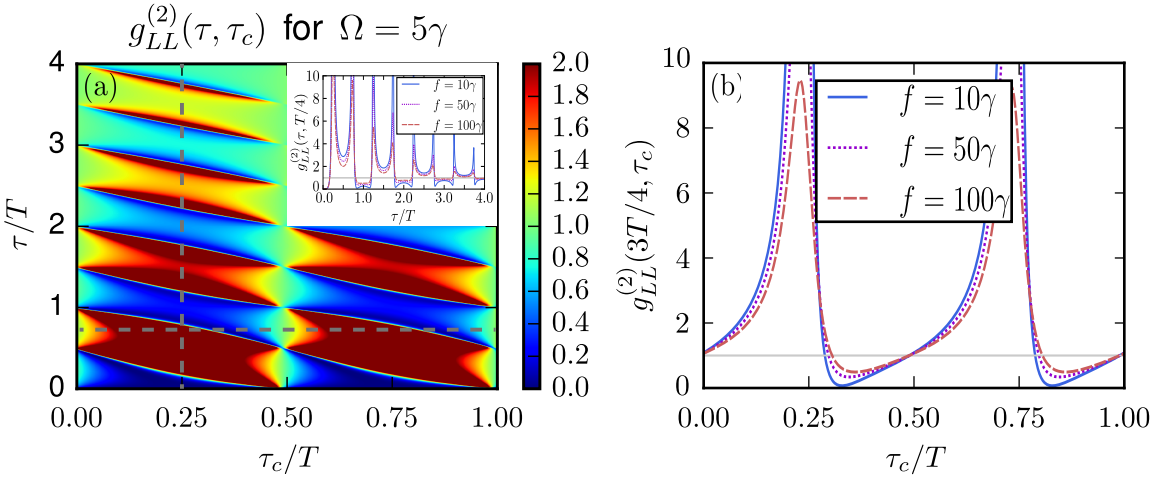

Figure 4.4: (a) Second-order coherence function $g^{(2)}_{LL}(\tau,\tau_c)$ for the sign-change protocol $g(t) = g_0\cos(\Omega t)$ of the moderately driven ($f = 10\gamma$) qubit on resonance ($\delta = 0$) at fast modulation frequency $\Omega = 5\gamma$. The oscillations decay with the delay time τ at the rate γ as can be seen, e.g., along the vertical cut at $\tau_c = T/4$ shown in the inset. Thus, this rapidly changing behavior takes place only for sufficiently fast modulations. (b) The strong oscillations in time τ_c between bunching and antibunching behavior reported in Ref. [265] become less pronounced with increasing input power f as the qubit becomes saturated. The delay time τ is fixed at the value $3T/4$, which corresponds to the horizontal cut in (a). Reprinted figure (adapted) with permission from Phys. Rev. A **97**, 043851 (2018), see Ref. [135]. Copyright 2018 by the American Physical Society.

obeying the same differential equation (4.30) in the variable τ as $\vec{G}(\tau,\tau_c)$ obeys, but with the initial conditions $\vec{J}^{(0)}(\tau_c) = -\frac{1}{2}s_{\mathrm{ps},3}(\tau_c)\vec{s}_{\mathrm{ps}}(\tau_c)$. We find

$$g^{(2)}_{LL}(\tau,\tau_c) = 1 + \frac{2\mathrm{Re}[\nu_3(\tau_c)\nu_3(\tau+\tau_c)J_3(\tau,\tau_c)]}{f_L(\tau+\tau_c)f_L(\tau_c)} \tag{4.40a}$$

$$g^{(2)}_{RR}(\tau,\tau_c) = 1 + \frac{2\mathrm{Re}[\nu_3(\tau_c)\vec{\nu}(\tau+\tau_c)\cdot\vec{J}(\tau,\tau_c)]}{f_R(\tau+\tau_c)f_R(\tau_c)} + \frac{2\mathrm{Re}[\nu_2(\tau_c)\vec{\nu}(\tau+\tau_c)\cdot\vec{G}(\tau,\tau_c)]}{f_R(\tau+\tau_c)f_R(\tau_c)}, \tag{4.40b}$$

where $\vec{\nu}(t) = (0,0,\frac{1}{4}\gamma(t))^T - \vec{C}^*(t)$ is a modification of the vector (4.25b).

As shown in Fig. 4.4, the oscillations between strong bunching and antibunching behavior observed in Ref. [265] become less pronounced as the input power f is increased, see panel (b) of this figure, corresponding to the horizontal (dashed gray) cut in panel (a). This behavior can again be attributed to the qubit's saturation. For sufficiently fast modulation frequencies ($\Omega \gtrsim \gamma$), the bunching peaks remain sizable on the range of several T in the delay time τ even for the moderate input power $f = 10\gamma$; see the inset of Fig. 4.4(a) corresponding to the vertical (dashed gray) cut of the contour plot. Thus, the rapid bunching-to-antibunching changes in behavior of the $g^{(2)}$ function, which result from the system's nonadiabatic response to an external modulation due to memory-effects and which have been predicted in Ref. [265] for weak input powers, appear to persist in a broad range of f. We observe that the positions of the bunching peaks remain insensitive to the input power, and only their heights gradually go down with increasing f.

4.5 Driven Λ-system

Next, we consider a three-level system in the Λ-scheme where a direct transition from the ground state $|g\rangle$ to an intermediate metastable state $|s\rangle$ is forbidden. Such systems are known to exhibit electromagnetically induced transparency (EIT), an effect which was first observed in atomic vapors [45, 46]. This phenomenon has also been demonstrated in superconducting circuits [269], paving the way for potential applications in quantum information processing. The drive field at frequency ω_d, which is nearly resonant with frequency $(\omega_e - \omega_s)$ of the transition $|s\rangle \to |e\rangle$ to the excited state, is conventionally treated classically. Our interest lies in a time modulation of the drive amplitude $F(t)$ causing a periodic switching between opaque and transparent behavior of this system upon irradiation of the coherent probe field $|\Psi_0\rangle$ at frequency ω_0, which is nearly resonant with frequency ω_e of the transition $|g\rangle \to |e\rangle$. This model is described by the Hamiltonian

$$H(t) = \omega_e|e\rangle\langle e| + \omega_s|s\rangle\langle s| + \left[F(t)e^{-i\omega_d t}|e\rangle\langle s| + \text{h.c.}\right] + H_w + \sum_\alpha \int d\omega \left[\frac{g}{\sqrt{2}} a^\dagger_{\alpha\omega}|g\rangle\langle e| + \text{h.c.}\right]. \tag{4.41}$$

In the following, we show that this system exhibits nonadibatic effects similar to those of the two-level system with a modulated coupling strength. Simultaneously, the Λ-scheme with a periodically modulated drive field is more feasible for an experimental realization. Dissipative dynamics of the Λ-system in the corotating frame is governed by the QME (4.6) with

$$A(t) = \begin{bmatrix} -\gamma & 0 & -i\sqrt{\gamma f/2} & i\sqrt{\gamma f/2} & -iF(t) & iF^*(t) & 0 & 0 \\ 0 & 0 & 0 & 0 & iF(t) & -iF^*(t) & 0 & 0 \\ -2i\sqrt{\gamma f/2} & -i\sqrt{\gamma f/2} & -i(\delta_1 - i\gamma/2) & 0 & 0 & 0 & iF^*(t) & 0 \\ 2i\sqrt{\gamma f/2} & i\sqrt{\gamma f/2} & 0 & i(\delta_1 + i\gamma/2) & 0 & 0 & 0 & -iF(t) \\ -iF^*(t) & iF^*(t) & 0 & 0 & -i(\delta_2 - i\gamma/2) & 0 & 0 & i\sqrt{\gamma f/2} \\ iF(t) & -iF(t) & 0 & 0 & 0 & i(\delta_2 + i\gamma/2) & -i\sqrt{\gamma f/2} & 0 \\ 0 & 0 & iF(t) & 0 & 0 & -i\sqrt{\gamma f/2} & -i(\delta_1 - \delta_2) & 0 \\ 0 & 0 & 0 & -iF^*(t) & i\sqrt{\gamma f/2} & 0 & 0 & i(\delta_1 - \delta_2) \end{bmatrix},$$

$$\vec{C} = \left[0, 0, i\sqrt{\gamma f/2}, -i\sqrt{\gamma f/2}, 0, 0, 0, 0\right]^T, \tag{4.42}$$

which are written in the basis

$$\vec{s}(t) = \langle\hat{\vec{s}}(t)\rangle = [\langle P_e(t)\rangle, \langle P_s(t)\rangle, \langle\tilde{\sigma}^{(g)}_+(t)\rangle, \langle\tilde{\sigma}^{(g)}_-(t)\rangle, \langle\tilde{\sigma}^{(s)}_+(t)\rangle, \langle\tilde{\sigma}^{(s)}_-(t)\rangle, \langle\tilde{\sigma}^{(r)}_+(t)\rangle, \langle\tilde{\sigma}^{(r)}_-(t)\rangle]^T.$$

Here, $P_e = |e\rangle\langle e|$, $P_s = |s\rangle\langle s|$, $\sigma^{(g)}_- = |g\rangle\langle e|$, $\sigma^{(s)}_- = |s\rangle\langle e|$, $\sigma^{(r)}_- = |g\rangle\langle s|$, $\sigma^{(g,s,r)}_+ = (\sigma^{(g,s,r)}_-)^\dagger$, and the tildes indicate expectation values to be evaluated in the corotating frame analogous to the two-level system. Additionally, we have defined the detunings $\delta_1 = \omega_0 - \omega_e$ and $\delta_2 = \omega_d - (\omega_e - \omega_s)$, and the bare dissipation rate $\gamma = \pi|g|^2$. Note that for a computation of the transmission amplitude $\mathcal{T}$ one can use Eqs. (4.26a) and (4.26b) with $\langle\tilde{\sigma}_-\rangle \to \langle\tilde{\sigma}^{(g)}_-\rangle$. Unlike in the two-level system, dissipation rates of the Λ-system depend on multiple parameters. At fixed γ, the smallest dissipation rate $\gamma_{\min}$ has a nearly quadratic parametric dependence on the drive amplitude F, as shown in Fig. 4.5. This indicates that we can push the system into the nonadiabatic regime with $\Omega > \gamma_{\min}$ by sweeping the values of F towards zero. Note that $\gamma_{\min}$ shows little sensitivity to the intensity f of the probe field.

In the EIT model with constant $F \neq 0$, the system is fully transparent on resonance $\delta_1 = \delta_2 = 0$ leading to $|\mathcal{T}|^2 = 1$. When F is momentarily quenched, the metastable state $|s\rangle$ is decoupled for a short while, and the remaining two-level system $\{|g\rangle, |e\rangle\}$ tends to

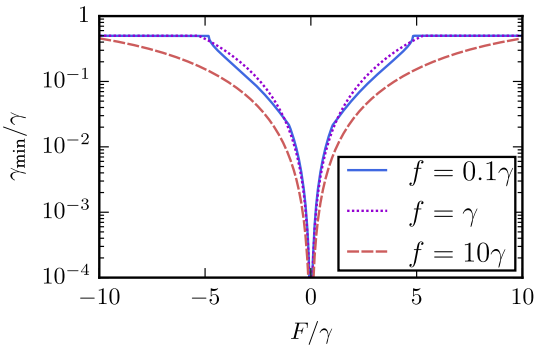

Figure 4.5: Smallest dissipation rate $\gamma_{\min}$ of the Λ-system as a function of the classical drive field amplitude F. Instead of directly modulating the coupling strength g, the three-level Λ-system allows tuning of $\gamma_{\min}$ by means of F. The input power f of the probe field has little effect on this behavior. Reprinted figure with permission from Phys. Rev. A **97**, 043851 (2018), see Ref. [135]. Copyright 2018 by the American Physical Society.

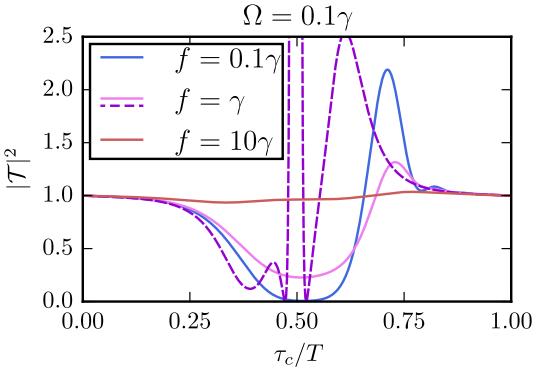

Figure 4.6: Transmission through the Λ-system driven on resonance ($\delta_1 = \delta_2 = 0$) by both probe and drive pulses. The drive field has a periodically modulated amplitude $F(t) = 10\gamma\,[1+\cos\Omega t]$ at $\Omega = 0.1\gamma$. The adiabatic approximation (dashed line) is only valid far from the critical region defined by $\Omega > \gamma_{\min}$ (cf. Fig. 4.5). In the time window where it breaks down, the system responds nonadiabatically as memory-effects kick in. At large powers f of the probe field, these effects are washed out because of the system's saturation. Reprinted figure with permission from Phys. Rev. A **97**, 043851 (2018), see Ref. [135]. Copyright 2018 by the American Physical Society.

develop full reflection (and, hence, zero transmission), provided that the probe field does not saturate the system. In the next time instant, the state $|s\rangle$ is recoupled again, which leads to nonadiabatic changes in transmission properties. Changing F periodically in time, e.g., by $F(t) = 10\gamma[1+\cos\Omega t]$ can thus result in a periodic steady-state behavior of the transmission with large deviations from unity on a single period of modulation. This is illustrated in Fig. 4.6. Switching between opaqueness and transparency closely resembles the behavior of the two-level system where the modulated coupling effectively performs the function similar to that of F, although with the reciprocal effect. As is seen from the comparison of the adiabatic approximation (dashed line) with the numerical solution (solid line) at $f = \gamma$, the system's response is nonadiabatic during a large part of the period for rather slow modulation frequency $\Omega = 0.1\gamma$. This behavior is due to the modulation protocol of F which deeply penetrates into the critical region defined by $\Omega > \gamma_{\min}$ (cf. Fig. 4.5). In the high-frequency regime of modulation (not shown), the regular EIT effect with unit transmission on resonance is again restored as long as the time average $\bar{F} \neq 0$. For $\bar{F} = 0$ we obtain an effective decoupling of the metastable state $|s\rangle$, reproducing the transmission of the unmodulated two-level system. These conclusions are also supported by the high-frequency expansion (4.20).

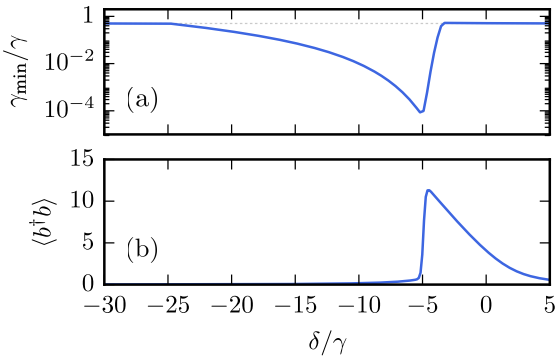

Figure 4.7: (a) Smallest dissipation rate $\gamma_{\min}$ of the undriven Kerr nonlinearity model as a function of detuning δ for $U = -\gamma/2$ and $f = 16\gamma$. Similar to the two- and three-level systems, the smallest dissipation rate is significantly suppressed within the critical region, although it remains finite. (b) One of the important signatures of the driven-dissipative phase transition this system undergoes is a prominent increase in the stationary occupation number $\langle b^\dagger b\rangle$ which peaks at the same parameter value for which the minimal dissipation rate is reached. In the following, the periodic modulation of δ is considered across the whole critical region with modulation frequency $\Omega \ll \gamma$. Reprinted figure with permission from Phys. Rev. A **97**, 043851 (2018), see Ref. [135]. Copyright 2018 by the American Physical Society.

4.6 Driven Kerr-nonlinearity system

In the third application of our formalism, we consider the driven Kerr-nonlinearity model. It consists of a single cavity mode b with an effective local photon-photon interaction U, which is coupled to the transmission line. Its dissipative dynamics in the co-rotating frame is again governed by the GKSL master equation (4.3a) with $O = b$ and

$$H_{\text{eff}}(t) = -\delta(t) b^\dagger b + \frac{U}{2} b^\dagger b^\dagger b b + \sqrt{\gamma f}(b + b^\dagger). \tag{4.43}$$

The modulation-parameter to be considered in the following is the detuning $\delta = \omega_0 - \omega_e$ of the driving field ω_0 with respect to the cavity frequency ω_e.

Before turning to the time-dependent case, let us revisit the results obtained by Drummond and Walls [237] and recently extended to include two-photon driving [240] in the time-independent stationary case. The dissipative phase transition that this system exhibits for large $f \gg \gamma$ and small $|U| \ll \gamma$ has numerous manifestations. Experimentally, the most feasible quantity is the stationary occupation $\langle b^\dagger b\rangle$. Sweeping the detuning δ over the bistability critical region, i.e., where the corresponding semiclassical solution has multiple solutions, one can observe a strong enhancement in the occupation number (shown in Fig. 4.7, bottom). Away from this region, $\langle b^\dagger b\rangle$ decays to small values. The peak value rapidly grows with increasing ratio f/U^2. This behavior goes hand in hand with the entropy of the cavity: Outside of the critical region, the state is a pure coherent state corresponding to zero entropy, but becomes a complicated mixed state within the critical region. This critical behavior can again be attributed to the smallest dissipation rate $\gamma_{\min}$ being significantly suppressed (shown in Fig. 4.7, top), a phenomenon which is also known as the critical slowing down. In fact, the Liouvillian gap does not completely close. The minimal value of the dissipation is reached at

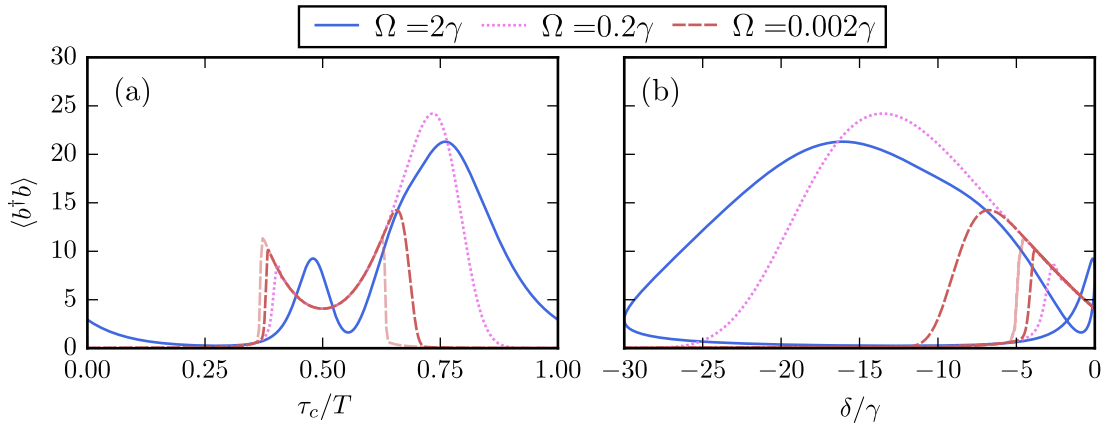

Figure 4.8: (a) Periodic steady-state occupation $\langle b^\dagger b\rangle(t)$ of the Kerr nonlinearity model under periodic modulation of detuning $\delta(t) = -15\gamma[1 + \cos\Omega t]$ for various modulation frequencies Ω. (b) The same dependence in the parametric representation. For moderate modulation frequencies, the occupation is strongly enhanced compared with the true stationary state shown in the lower panel of Fig. 4.7. The adiabatic approximation based on Eq. (4.16) is given by the light brown curve (note that in the parametric representation it lies very close to the stationary state result). The numerical results for rather small frequency $\Omega = 0.002\gamma$ (brown) still drastically deviate from the corresponding adiabatic approximation (light brown). As discussed by Casteels *et al.* [239], the dynamical hysteresis seen in the parametric plot is directly related to the breakdown of adiabaticity in the critical region, and the hysteresis area depends on the width of the parameter range where $\Omega > \gamma_{\min}$. Reprinted figure (adapted) with permission from Phys. Rev. A **97**, 043851 (2018), see Ref. [135]. Copyright 2018 by the American Physical Society.

δ where also the occupation number peaks.

Of particular interest is a periodic modulation of parameters which drives the system in and out of the critical region. Recently, it has been proposed [239] that in this way one can dynamically simulate a hysteretic behavior in the Kerr model, which has been experimentally observed [30] in the corresponding setup soon after. Interestingly, the hysteresis-like behavior follows the stable branches of the semiclassical mean-field solution rather than the exact stationary quantum solution. An explanation of this property has been provided in the context of the driven-dissipative Rabi model [236] where it has been shown that long-lived metastable states with a small effective decay rate prevent reaching the true stationary state. As pointed out in Ref. [239], this goes together with a breakdown of adiabaticity, which we have also seen in the previously discussed models. These studies give strong indications that such behavior seems to be common for all systems featuring dissipative phase transitions. In contrast to modulating f as discussed in Ref. [239], we choose to vary in time the parameter δ. This is advantageous since one can sweep *in* and *out* of the critical region in the positive and negative sweep directions, starting on both sides from noncritical regions characterized by zero values of entropy. In particular, we have found that it is hard to ensure this when sweeping f at fixed δ. Our modulation protocol is designed to cover the whole critical region; namely, $\delta(t) = -15\gamma[1 + \cos\Omega t]$ for the parameters $U = -\gamma/2$ and $f = 16\gamma$.

The periodic steady-state occupation over a single period and its parametric dependence on the parameter δ is shown in Fig. 4.8. The left panel of Fig. 4.8 reveals a clear rise in

occupation whenever δ is deep inside the critical region, which is followed by an exponential drop. Note that, in comparison with the time-independent stationary state, the occupation is significantly enhanced for intermediate modulation frequency $\Omega = 0.2\gamma$ (dotted line). A further increase of Ω up to the value 2γ does not further enhance the occupancy (solid line); moreover, hysteretic properties are no longer seen in the parametric representation of the right panel of Fig. 4.8. For slow modulation, the periodic steady-state solution does not converge to the adiabatic approximation based on Eq. (4.16) (light brown curve) even for $\Omega = 0.002\gamma$. This points towards the nonadiabatic system's response when its parameters are driven across the region of bistability.

4.7 Summary

Based on Floquet's theorem, we have derived a representation for the periodic steady state density operator of a periodically driven-dissipative open quantum system. We have established both adiabatic and high-frequency expansions in a systematic way. Importantly, the corresponding approximations can be efficiently benchmarked against numerical results which are achieved by integration over a single period of modulation. A breakdown of the adiabatic approximation signals the system's nonadiabatic response when it enters the regime of critical slowing down. These represent interesting memory-effects in this originally Markovian setup.

We applied the developed formalism to three different models with periodically time-dependent parameters, which all exhibit a temporary suppression of the smallest dissipation rate. For the two-level system, a modulation of the coupling strength to the transmission line causes significant changes in transmission properties, power spectra, and statistical properties of scattered photons. For the three-level Λ-system, a modulation of the classical driving of the metastable state can lead to considerable modifications of the phenomenon of electromagnetically induced transparency (EIT). In the driven Kerr-nonlinearity model, we have studied periodic sweeping of the detuning δ across the parameter region featuring the driven dissipative phase transition. We have found that, even for apparently slow modulation frequencies, nonadiabatic effects may still dominate, indicating that adiabatic expansions will generally fail in the critical parameter regimes of such systems.

5 Complete positivity beyond the Markovian limit

We now pursue the strategy outlined in Sec. 2.3.2 and combine the insights from quantum-information and statistical field theory to establish the explicit operational structure of the real-time diagrammatic series that ensures the complete positivity (CP) and trace-preservation (TP) of the dynamical map (2.1). Importantly, this operational approach can be implemented in the existing Keldysh real-time technique and allows approximations for *general time-nonlocal* quantum master equations beyond the Born-Markov limit to be systematically compared and developed while keeping the CP and TP structure explicit.

To find a diagrammatic expansion of the Kraus operators (2.6) themselves, we exploit a fundamental *two-stage* structure of the coupling expansion: Whereas the first stage naturally defines the dissipative timescales of the system –*before* having integrated out the environment completely– the second stage sums up elementary physical processes, each described by a CP superoperator. We illustrate the physically different roles of the two emerging coupling-expansion parameters for the infinite-temperature limit of the resonant level model discussed in Ch. 3. This two-stage structure allows us to establish the highly nontrivial functional relation between the (Nakajima-Zwanzig) memory-kernel *superoperator* $\Sigma(t,t')$ for the reduced density operator in Eq. (1.7) and novel memory-kernel *operators* $\sigma(t,t')$ that generate the Kraus operators of an operator-sum. Our considerations build on the result that a Kraus operator for a physical measurement process on the environment can be obtained by 'cutting' a group of Keldysh real-time diagrams 'in half'. This naturally leads to Kraus operators *lifted* to the system *plus environment* which have a diagrammatic expansion in terms of time-nonlocal memory-kernel operators. These lifted Kraus operators obey coupled time-evolution equations which constitute an unraveling of the original Schrödinger equation for system plus environment. Whereas both equations lead to the same reduced dynamics, only the former explicitly encodes the operator-sum structure of the coupling expansion.

Publications and acknowledgments. Sections 5.1–5.3 of this chapter have emerged from the author's Master thesis [136] where the general idea of a diagrammatic representation of conditional dynamical maps based on Kraus operators has already been formulated. Several significant refinements of that work were necessary to rigorously establish the explicit diagrammatic structure of the memory-kernel that enabled the results of Secs. 5.4 and 5.5. In particular, the notion of dynamics conditional on measurements on the effective environment, and the corresponding hierarchy equations that represent an unraveling of the full Schrödinger equation have been refined by V. Reimer. This work (including the adapted figures) has been published in V. Reimer, and M. R. Wegewijs, SciPost Physics **7**, 012 (2019) [CC BY 4.0 License], see Ref. [137]. We acknowledge useful discussions with B. Criger, D. P. DiVincenzo, M. Pletyukhov, R. Saptsov, H. Schoeller and N. Schuch as well as R. van Leeuwen for a discussion of the related Ref. [179] during a visit at the University of Jyväskylä.

5.1 Introduction

To motivate this most technical chapter, we briefly recall the strategy outlined in Sec. 2.3.2 for approximate treatments of open-system dynamics beyond the Born-Markov limit, and present a more in-depth discussion of the immediate consequences in the light of the CP-TP duality introduced earlier [Sec. 2.3.1]. The necessity of going beyond the well-known Born-Markov limit is clearly prompted by the experimental importance of effects due to strong coupling and non-Markovianity –both of which are tied together [101]– in particular in quantum transport situations. However, a key challenge is to ensure that such extensions do not uproot the CP and TP properties of the reduced dynamics while *simultaneously* maintaining a clear view on microscopic contributions to physical processes. In this chapter, we make a further [32, 85] step towards clarifying this challenging issue in a general setting by employing the Keldysh real-time diagrammatic series [Sec. 2.2.2] and complementing it with the operational picture of Kraus operator-sums [Sec. 2.1.2].

The latter express the reduced-state evolution as a sum of conditional evolutions

$$\rho(t) = \sum_e K^e(t)\rho(0)K^e(t)^\dagger, \tag{5.1}$$

that corresponds to an averaging over all outcomes e of *possible measurements* on the inaccessible environment. The quadratic form manifests the CP property whereas TP is enforced by the sum rule $\sum_e K^e(t)^\dagger K^e(t) = \mathbb{1}$. Although it is well-known how the Kraus operators $K^e(t)$ –acting only on the system– can be expressed in the joint unitary $U(t)$ and the initial environment state ρ^{E}, the direct evaluation of these quantities soon becomes intractable when dealing with microscopic models with a *continuous* environment and local interactions. To solve such models (approximately), statistical theories such as the Nakajima-Zwanzig projection technique [99, 100] or the equivalently derived [112, 156] Keldysh real-time approach [115], which we focus on here, have been developed. In these approaches one instead considers general Dyson equations (2.16) or equivalent time-nonlocal QMEs (1.7) also called kinetic equations of the form

$$\tfrac{d}{dt}\rho(t) = -i[H,\rho(t)] + \int_0^t dt'\Sigma(t,t')\rho(t') \equiv -i[H,\rho(t)] + [\Sigma * \rho](t). \tag{5.2}$$

The time-nonlocal nature of the self-energy or memory-kernel superoperator $\Sigma(t,t')$ and the time-convolution $*$ in Eq. (5.2) underscore the non-Markovian nature of the general dynamics. What makes the practical evaluation feasible is the exploitation of *Wick factorization* of environment correlations in the cases of practical interest where the environment is noninteracting and initially in a mixed thermal state. Noting that Wick's theorem can be generalized (cf. Sec. 2.2.1 and Ref. [151]), we stress that the kinetic method is in general on equal footing with the operator-sum approach.

It must thus be possible to express the dynamical map $\rho(t) = \Pi(t)\rho(0)$ which solves Eq. (5.2) in the form of an operator-sum (5.1). How to actually do this on the level of the microscopic coupling $V(t)$ has remained unclear until recently. In this chapter we will find the explicit nontrivial relation between the two fundamental equations (5.1) and (5.2), in particular between $\Sigma(t,t')$ and $K^e(t)$, at every step linking the two complementary approaches. Following up work in this direction [32, 85] we develop a transparent set of diagrammatic rules by which all of this can be achieved. This allows for a *microscopic* understanding of the CP-TP structure of the reduced evolution $\Pi(t)$ and its memory kernel $\Sigma(t,t')$ in terms

of quantities that are relevant in practical calculations for open systems with continuous environments. This is a crucial prerequisite for an improved understanding of approximations, particularly in light of the CP-TP duality pointed out in Sec. 2.3.

TP approximations. As it turns out, most approximations formulated in terms of the memory kernel $\Sigma(t,t')$ of the kinetic equation (5.2) have no problem with guaranteeing the trace-preservation but impose no restrictions at all to ensure complete positivity. For such TP approximations one cannot be sure that complete positivity is not lost, implying that negative density operators may come out depending on the input[1]. This may be fatal for a calculation: Actual loss of positivity of the state implies that the results cannot even be taken as a 'rough indication' of what is going on since negative probabilities are meaningless. Such loss of positivity is sometimes related to the quality of the approximation indicating that 'not enough processes were taken into account'. However, we will make explicit that this failure instead indicates that what one is actually summing up in such approximations are not *physical processes* but rather *partial mathematical contributions* to such processes. These issues tie in with the current interest from the side of statistical physics and quantum thermodynamics to formulate approximation schemes which guarantee meaningful results for *entropic* quantities, cf. Sec. 2.1.3. In this context the Keldysh approach has already proven useful by its extension to 'parallel-worlds' [163] to compute Renyi entropies. Our operator-sum formulation of the Keldysh approach identifies a variety of approximations that give meaningful entropic quantities, including also the exchange entropy [138, 146] associated with the environment [134] which requires the *evolution* $\Pi(t)$ to be *completely* positive.

CP approximations. Indeed, we will find it is not difficult *characterize* large families of approximations which strictly guarantee complete positivity independent of the details –and thus of the quality– of the approximation. Although they are harder to evaluate and have not been explored much, they also have the advantage of a bounded quantitative measure for the TP error related to probabilities of *physical* processes[2] unaccounted for. Importantly, the characterization of CP approximations also provides a guide for less ambitious strategies motivated by practical concerns. It indicates how in TP-approximations one can systematically 'improve towards complete positivity' by identifying which diagrams should be added to give a *better partial* account of a physical process without insisting on strict CP. It must be stressed that failure of CP approximations to guarantee TP can be fatal, too: Although perhaps less important for short-time dynamics, TP ensures that dissipative dynamics achieves a stationary state at large times, cf. Sec. 2.3.1. Such approximations guaranteeing complete positivity connect to the interests of quantum information theory where this property is essential to maintain the connection to several fundamental theorems as pointed out in Sec. 1.1. Our approach is therefore centered around the *time-evolution of* (operators underlying the) *Kraus operators* and provides a systematic way for going beyond the limited GKSL approach (1.5) *without* giving up CP. Importantly, we show how this can be done by exploiting known statistical physics techniques.

CP-TP duality. Thus, neither route is without challenges and the problems encountered in the two approximation strategies are in fact fundamentally tied together, cf. Sec. 2.3. Here, we will identify the *microscopic* origin of the noticed duality in terms of elementary

[1] As pointed out in the introduction, we focus here on complete positivity (CP) instead of positivity-preservation (PP) which may still produce positive outputs for any input but which has neither an intuitive operational understanding nor a simple mathematical characterization.

[2] Since such terms represent partial measurements of the system's environment, there is an interesting analogy to syndrome measurements in quantum-error correction.

diagrammatic contributions to the real-time expansion. We will show that in some approximation schemes based on selection of diagrams CP and TP cannot be achieved *simultaneously*. Approximations that are both CP *and* TP require more sophisticated schemes that additionally manipulate integration boundaries. The Born-Markov is a well-known example of this but extensions have also been recently explored in Refs. [32–34, 85, 181, 182]. We will also comment on this approach and indicate its relation to our formalism which focuses on the *prerequisites* for a clearer understanding of all the above mentioned approximation schemes. This is of common interest to both research fields: Although our encompassing formalism remains geared towards applications –by its formulation in terms of microscopic couplings and Keldysh diagrams of Eq. (5.2)– it is firmly rooted in the operator-sum (5.1) and defined operationally in terms of quantum circuits.

The chapter is organized as follows. Sec. 5.2 first extends the concept of purification to the *unitary evolution* $U(t)$ to identify its internal structure related to Wick normal-ordering. These physically motivated steps reveal clearly how measurements condition the time-evolution and connect the CP structure with Wick's theorem. In Sec. 5.3 we then connect the obtained operator-sum representation with Keldysh real-time diagrams which allows us to identify *groups* of diagrams associated with a physical process conditioned on a measurement outcome. Each such process also corresponds to a *Keldysh operator* acting on both system and environment which is obtained by 'cutting' the group of Keldysh diagrams 'in halves' and summing them. These are the central objects of interest from which the corresponding Kraus operators can be obtained as normal-ordered environment matrix-elements. Sec. 5.4 builds on this partial 'undoing' of the environment trace which is a convenient way to see the connection between microscopic Keldysh diagrams and Kraus operators. Focusing on the *generators* of infinitesimal evolution in either approach, we derive two equivalent hierarchies of time-nonlocal evolution equations. The hierarchy for the Keldysh operators presents a useful exact unraveling of the original Schrödinger equation for system plus environment. It explicitly encodes the operator-sum structure of the reduced dynamics *before* tracing out the environment. The result of this analysis is the explicit functional dependence of the memory kernel superoperator $\Sigma = \sum_m \Sigma_m[\sigma_0, \ldots, \sigma_m]$ in Eq. (5.2) on the self-energy operators $\sigma_0, \ldots, \sigma_m$ generating the Keldysh operators in Eq. (5.1). It expresses the *operator-sum theorem* for general *infinitesimal* reduced evolutions and reveals at the deepest level that CP and TP appear as incompatible constraints because of the difference between *time-ordering* of the microscopic *couplings* on one and on two branches of the Keldysh real-time contour. The formalism is finally illustrated in Sec. 5.5 for the infinite-temperature limit of the resonant level model discussed in Ch. 3. This Markovian example only serves to highlight the inner workings of the approach and physical principles involved, delegating the technically much more demanding applications to future work.

5.2 Quantum-information approach to reduced dynamics

Mimicking the discussion in Ch. 2, we again start with the quantum-information bird's-eye view and show how extensions of their techniques can guide calculations of Eq. (2.1) that address the challenging cases where the environment consists of reservoirs with a *continuum* of modes in *mixed thermal states* and where particles strongly *interact* on the system. Microscopic models of this type lead to interesting quantum many-body and transport phenomena which preclude direct evaluation of the dynamical map $\Pi(t)$ and require advanced methods to obtain good approximations. Starting point for the following considerations is the purified system-environment evolution depicted in Fig. 2.2. There, we already purified the environ-

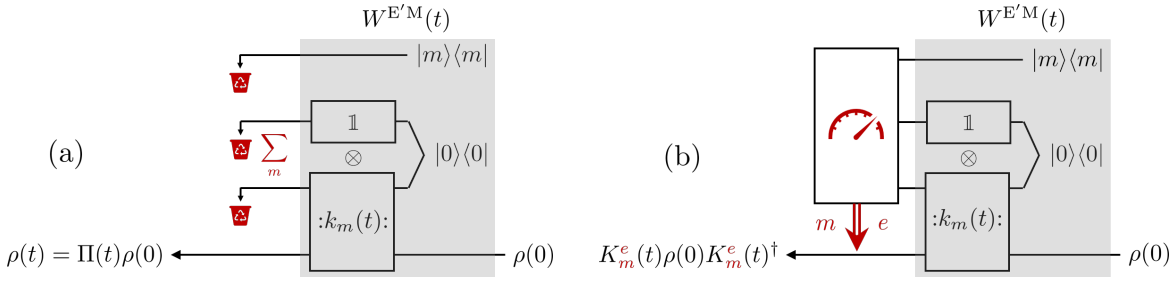

Figure 5.1: Quantum circuits corresponding to the refined operator-sum (5.6) and its terms. The auxiliary meter M keeps track of *which* modes m of the environment have interacted with the system. (a) Reduced evolution: neither the outcomes of *possible* measurements on the purified environment, e, nor those on the auxiliary meter, m, are communicated. (b) Conditioned evolution: the list of modes m that have interacted with the system *and* the measured states $|e\rangle$ are communicated. Reprinted figure (adapted) under CC BY 4.0 License from SciPost Phys. **7**, 012 (2019), see Ref. [137].

ment degrees of freedom and expressed the dynamical map in terms of an isometry $W^{\mathrm{E}'}(t)$, cf. Eq. (2.6). The central idea is to explicitly keep track of the dynamical correlations the coupling $V(t)$ generates between system and *effective* environment. A computational approach which makes this explicit at each step will manifestly guarantee the CP property as we work out in detail for the Keldysh diagrammatic approach in Sec. 5.3.

5.2.1 Purification of the evolution operator

To achieve this, the picture of the measurement-conditioned evolution needs to be further refined by additionally *purifying* the (interaction-picture) unitary $U(t) = T\exp\left[-i\int_0^t d\tau V(\tau)\right]$. In Eq. (2.6), the states $|e\rangle$ of the purified environment do not account for the internal structure of the *evolution* U relative to the environment state ρ^{E}. Only when expanding the unitary into normal-ordered components as discussed in App. E,

$$U(t) = k_0(t) + \sum_{m\neq 0} :k_m(t): \quad , \tag{5.3}$$

this structure becomes apparent. Here, m refers to *modes* of the environment in light of the later application to noninteracting environments, noting that it can similarly be applied to interacting ones as well. By construction, the operator $k_0(t)$ is exceptional in that it acts trivially on the environment as all modes have been fully contracted. The normal-ordering $::$ [cf. Sec. 2.2.1] of the remaining terms with uncontracted modes $m \neq 0$ needs not be evaluated in the end but continues to play a simplifying role: It ensures that the trace

$$\operatorname*{Tr}_{\mathrm{E}} :k_{m'}(t)^\dagger: :k_m(t): \rho^{\mathrm{E}} \propto \delta_{m'm} \tag{5.4}$$

gives a nonzero system operator only if the modes m and m' match.

We can exploit the structure (5.3) from the start by explicitly keeping track of the labels of the environment modes m using a superoperator $W^{\mathrm{E}'\mathrm{M}} : \mathrm{S} \to \mathrm{S}\otimes\mathrm{E}'\otimes\mathrm{M}$ which stores these in a register $|m\rangle$ in an auxiliary *meter* space M. This leaves the original evolution (2.1)

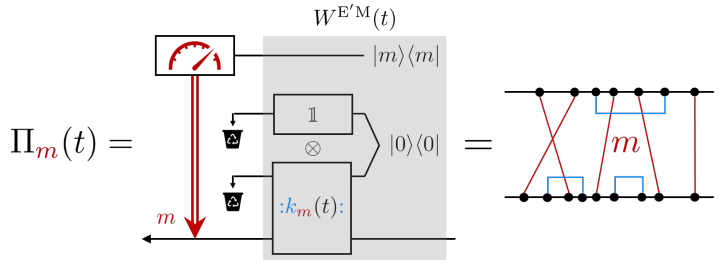

Figure 5.2: *Partially* conditioned evolution (5.8b): The list of modes m that interacted with the system is communicated (not the measurement outcomes). The key result Eq. (5.11b) demonstrates that this circuit corresponds to the indicated Keldysh diagrams with fixed modes on the red contractions summed over all possible blue contractions, cf. Fig. 5.3. Reprinted figure (adapted) under CC BY 4.0 License from SciPost Phys. **7**, 012 (2019), see Ref. [137].

unaltered if we additionally trace out the meter-space:

$$\Pi(t) = \operatorname*{Tr}_{\mathrm{E}'\mathrm{M}} W^{\mathrm{E}'\mathrm{M}}(t) \bullet W^{\mathrm{E}'\mathrm{M}}(t)^\dagger, \qquad W^{\mathrm{E}'\mathrm{M}}(t) := \sum_m \left(:k_m(t):\otimes \mathbb{1}^{\mathrm{P}_\mathrm{E}}\right)|0\rangle \otimes |m\rangle\,. \tag{5.5}$$

Due to the normal-ordering (5.4), the new map is also an isometry, $W^{\mathrm{E}'\mathrm{M}\dagger} W^{\mathrm{E}'\mathrm{M}} = \mathbb{1}^{\mathrm{S}}$, and can thus be regarded as an additional purification of the map (2.6) that extends the isometry $W^{\mathrm{E}'} \to W^{\mathrm{E}'\mathrm{M}}$. This amounts to altering Fig. 2.2 to Fig. 5.1 without changing the input-output relation of the circuit: Purifying the environment to an entangled state $|0\rangle$ (to eliminate thermal noise) and purifying the unitary $U(t)$ to an isometry $W^{\mathrm{E}'\mathrm{M}}(t)$ (using normal-ordering) thus results in the refined operator-sum

$$\Pi(t) = \sum_{m,e} K_m^e(t) \bullet K_m^e(t)^\dagger, \qquad K_m^e(t) := \langle e| \otimes \langle m|\, W^{\mathrm{E}'\mathrm{M}}(t) = \langle e|\, :k_m(t):\otimes \mathbb{1}^{\mathrm{P}_\mathrm{E}}\, |0\rangle\,, \tag{5.6}$$

where measuring the meter's register picks out the normal-ordered component $:k_m:(t)$ of the evolution. The trace over the purified environment M and the meter E' instead corresponds to discarding the measurement outcomes m (mode labels) and e (state of purified environment) by summing over them. Here, the *Keldysh*[3] *operators* $k_m(t)$ are still operators on system and environment, in contrast to the *Kraus operators* $K_m^e(t)$ which act on the system only. By construction, the Keldysh operator $k_0(t) = K_0^0(t) \otimes \mathbb{1}^{\mathrm{E}}$ factorizes and gives rise to the environment-average of the unitary $U(t)$,

$$K_0^e(t) = \langle e|0\rangle \operatorname*{Tr}_{\mathrm{E}} U(t)\rho^{\mathrm{E}} = \delta_{e,0}\langle U(t)\rangle^{\mathrm{E}} \tag{5.7}$$

as the only remaining Kraus operator for $m = 0$. Keeping explicit information about the environment E via the Keldysh operators $k_m(t)$ is at first a technical trick to avoid writing out matrix elements. Later on in Sec. 5.4.2 it will however allow for an interesting unraveling of the Schrödinger equation of system plus environment.

[3] This nomenclature will be motivated in Sec. 5.3.

Importantly, we can choose the level of refinement and write the time-evolution as

$$\Pi(t) = \operatorname*{Tr}_{\mathrm{E}} U(t)\Big[\,\bullet\otimes\rho^{\mathrm{E}}\Big]U(t)^\dagger = \sum_m \operatorname*{Tr}_{\mathrm{E}} :k_m(t):\,\Big[\,\bullet\otimes\rho^{\mathrm{E}}\Big]\,:k_m(t)^\dagger: \quad , \tag{5.8a}$$

by only resolving the trace over the meter-space M. This is the key relation of this chapter: In Sec. 5.3 we show that this exactly corresponds to calculations employing Keldysh real-time diagrams and Wick's theorem. There the *Keldysh* operators $k_m(t)$ (acting on the system and environment) are uniquely represented by groups of Keldysh diagrams for a *conditional* propagator (acting on the system only),

$$\Pi_m(t) = \operatorname*{Tr}_{\mathrm{E}} :k_m(t):\,\Big[\,\bullet\otimes\rho^{\mathrm{E}}\Big]\,:k_m(t)^\dagger: \quad , \tag{5.8b}$$

depending on the measurement outcome m. This corresponds precisely to the modified quantum circuit as shown in Fig. 5.2 and explicitly ensures that Π_m is a CP superoperator. It is these objects that one should calculate while formally keeping track of m in order to obtain a CP result for $\Pi = \sum_m \Pi_m$.

Finally, we remark that the above purification approach can be completely avoided by directly working in Hilbert-Schmidt or Liouville-space which is useful for, e.g., deriving projection-based approaches that guarantee CP evolution [85]. The above quantum-information approach, however, emphasizes the clear *operational* test: If a complicated mathematical expression can be expressed as a physically implementable quantum circuit without initial system-environment correlations, then it *must* be a CP superoperator.

5.2.2 Trace preservation (I): State-evolution correspondence

So far we have focused on the CP property which is almost trivialized in the quantum-information approach: When $\Pi(t)$ is written in the operator-sum form it can be verified term-by-term. We however noted earlier [Sec. 2.3.1] that this implies the opposite for the TP property of the evolution: It requires a nontrivial sum of quadratic operator expressions

$$\sum_{m,e} K_m^e(t)^\dagger K_m^e(t) = \mathbb{1}^{\mathrm{S}}, \tag{5.9a}$$

to match the system identity operator at all times t. This translates to the condition

$$\sum_m \operatorname*{Tr}_{\mathrm{E}} :k_m(t)^\dagger::k_m(t):\,\big(\mathbb{1}^{\mathrm{S}}\otimes\rho^{\mathrm{E}}\big) = \sum_m \Pi_m^\dagger(t)\mathbb{1}^{\mathrm{S}} = \mathbb{1}^{\mathrm{S}}. \tag{5.9b}$$

for the Keldysh operators and implies that the conditional propagators $\Pi_m(t)$ are trace-nonincreasing (TNI) superoperators, $\operatorname{Tr}\Pi_m \leq \operatorname{Tr}$. Keeping in mind applications with continuous environments these are highly nontrivial conditions to check or guarantee. In this respect, the relation of $k_m(t)$ to the Keldysh real-time expansion announced at Eq. (5.8) is an intriguing way to *microscopically* understand, and possibly overcome, the CP-TP duality explained on a general level in Sec. 2.3: The above relation may still be difficult to check and the conditional propagators Π_m in that regard are not more advantageous than Π itself. But on the level of diagrammatic contributions we have an explicit means to scrutinize the trace-preservation with the flipping-rule (2.17) and we will return to this issue in Sec. 5.3.3 after providing the diagrammatic rules that allow the construction of the maps Π_m.

5.3 Field-theory approach to reduced dynamics

The considerations of the previous section hold generally –noting the key assumption of an initially uncorrelated system and environment. In the following, we will focus on the Keldysh real-time diagrammatic technique introduced in Sec. 2.2.2 which is a powerful tool for calculating density-operator evolutions beyond the weak-coupling limit [154–156, 159] for noninteracting, continuous reservoirs of fermions or bosons in thermal states. We note, however, that most of our conclusions can be generalized. Our aim is to reorganize this well-established diagrammatic expansion such that one can easily identify the Keldysh- and Kraus operators in terms of practical Wick-averages. This makes our approach of immediate relevance for various approximation schemes [152, 161, 162, 231] in terms of such diagrams.

5.3.1 Reorganized Keldysh real-time expansion: Cutting and pasting rules

The diagrammatic series can be reorganized as guided by the quantum-information considerations of the previous Sec. 5.2 and allows us to identify which *groups* of diagrams rigorously correspond to *physical* measurement processes. To this end, we write the normal-ordering expansion (5.3) as

$$U(t) = k_0(t) + \sum_{q=1}^{\infty} \sum_{m_q \dots m_1} :k_{m_q \dots m_1}(t): \quad , \tag{5.10}$$

which is constructed in App. E in detail. Here, $k_{m_q \dots m_1}(t)$ is the evolution $U(t)$ partially contracted such that only the modes labeled by $m = m_q \dots m_1$ remain. We ignore the ordering of the modes, i.e., $k_{m_q \dots m_1}$ is invariant under mode permutations and the summation $m_q \dots m_1$ is restricted so as not to double count terms. As noted earlier [cf. Eq. (5.7)], the special case $k_0(t)$ denotes the part of $U(t)$ in which no environment operators are left, i.e., the *environment average* $k_0(t) := \langle U(t) \rangle^{\mathrm{E}}$. Our central formula (5.8) explicitly ensures that the CP-TP evolution of interest,

$$\Pi(t) = \sum_{q=0} \sum_{m_q \dots m_1} \Pi_{m_q \dots m_1}(t), \tag{5.11a}$$

decomposes into superoperators

$$\Pi_{m_q \dots m_1}(t) = \operatorname*{Tr}_{\mathrm{E}} :k_{m_q \dots m_1}(t): \Big[\bullet \otimes \rho^{\mathrm{E}} \Big] :k_{m_q \dots m_1}(t)^\dagger: \tag{5.11b}$$

which are CP-TNI because they are *conditional* evolutions depending on measurement outcomes $m_q \dots m_1$ indicating which environment modes the system has interacted with. In Fig. 5.3 we explain how each $\Pi_{m_1 \dots m_q}$ corresponds to a precise *group* of Keldysh diagrams. In (a)-(b) we first sketch how the standard Keldysh expansion is obtained using the now more pertinent left-right form of diagrams introduced in Fig. 2.4(a). In Fig. 5.3(c) we show how the diagrammatic elimination of the environment E (stage 1) and the meter M (stage 2) corresponds to Wick-contracting [Eq. (5.11b)] and summing over modes $m_q \dots m_1$ [Eq. (5.11a)], respectively. Thus, the *elementary physical processes* contained in the standard real-time expansion for the propagator $\Pi(t)$ when computed in terms of Wick contractions are the conditional propagators $\Pi_{m_q \dots m_1}(t)$. However, once the mode-sums for *these* contractions have been performed the CP property is hidden and approximations may inadvertently break up the CP structure. We now discuss the two computational stages that the above implies.

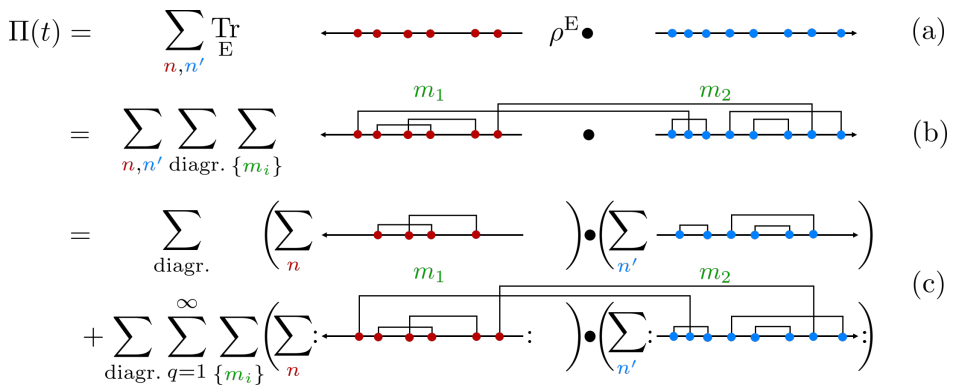

Figure 5.3: Reorganization of the standard real-time expansion in terms of left-right Keldysh diagrams [cf. Fig. 2.4]: (a) Expansion of the unitary U $[U^\dagger]$ into vertices $-iV$ in red $[+iV$ in blue]. (b) Evaluation of the trace gives both inter- and intra-branch contractions (c) Two-stage reorganization of (b). Stage 1: Sum up *all* intra-branch contractions separately (round brackets), but restrict the number of inter-branch contractions to $q = 0, 1, 2, \ldots$ fields and fix their modes $m_q \ldots m_1$. Stage 2: Sum up all contributions from modes $m_q \ldots m_1$ for all q. Reprinted figure under CC BY 4.0 License from SciPost Phys. **7**, 012 (2019), see Ref. [137].

Stage 1, Eq. (5.11b) First, the conditional propagator Π_m needs to be computed by eliminating E. This can be done in two equivalent ways:

(A) Compute $\Pi_{m_q \ldots m_1}$ directly. An advantage of our approach as compared to Refs. [32–34, 85] is that it does not necessarily require a fundamentally new formulation. The standard rules [see App. F.1] of the existing Keldysh approach merely have to be complemented with a diagrammatic CP-rule which instructs one to keep track of $m_q \ldots m_1$:

Rule for the conditional propagator $\Pi_{m_q \ldots m_1}$*: Sum* all *diagrams that have a* fixed *number* q *of contractions between the* different *branches of the Keldysh contour with a* fixed *set of mode indices* $m_q \ldots m_1$ *assigned to these lines in every possible order. This includes summing* all *possible intra-branch contractions separately and summing over the mode indices of these contractions. Perform all two-branch ordered time integrations.*

Note that this rule requires *both* reducible and irreducible diagrams in the two-branch sense to be summed. In Fig. 5.4(a) we illustrate why this is technically important and make explicit the intricate difficulty of relating time-ordering on one and two branches of the Keldysh contour. To obtain Π_m, we sum up terms on the right which are single functions of the final time t obtained by two-branch time-ordered integrations. If the CP-rule is obeyed, this sum is able to produce a single term that factorizes[4] into two separate functions of time, $\mathrm{Tr}_\mathrm{E} :k_m(t):(\bullet \otimes \rho^\mathrm{E}) :k_m(t)^\dagger:$. Here, the time-integrations are performed independently *inside* k_m on each branch separately. Note that this 'completing of the square' of ordered time-integrations is not possible when summing two-branch irreducible diagrams only, and the latter can therefore never correspond to physical processes [Eq. (5.17)].

(B1) Compute $\Pi_{m_q \ldots m_1}$ from $k_{m_q \ldots m_1}$. Alternatively, one can evaluate the right-hand side of Eq. (5.11b). The required Keldysh operators can be obtained from the value of a Keldysh diagram that is cut in half, i.e., from a single time-branch.

[4] Such factorization brings computational speed up in higher-order perturbative calculations [156] and is also necessary to simplify the noninteracting limit, see also page 19 of Ref. [157].

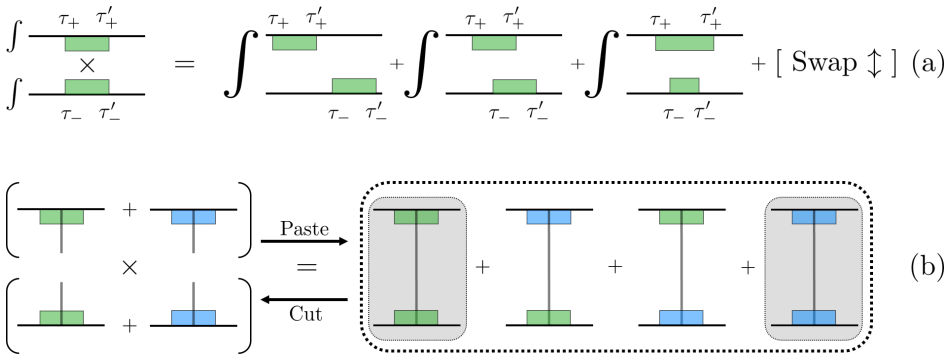

Figure 5.4: Cutting and pasting rules for Keldysh diagrams to test and guarantee CP, respectively. (a) *Time-ordering*: Factorization into separate one-branch time-ordered expressions (left) –dictated by the operator-sum form– requires both two-branch reducible and irreducible Keldysh diagrams to be summed (right). (b) *Cutting*: Given a selection of diagrams on the *right*-hand side, one can verify it has an operator-sum form by first cutting *horizontally* and summing up the halves. *Pasting*: Subsequently pasting the halves back together should recover the selection. Leaving out, for example, the center two diagrams on the right-hand side, this test of 'completing the square' will fail. When directly selecting *half*-diagrams on the *left*-hand side, every possible approximation (select only green, only blue or select both) by construction produces one of the three groups indicated by dashed lines and shading on the right, each of which is a CP superoperator. Reprinted figure under CC BY 4.0 License from SciPost Phys. **7**, 012 (2019), see Ref. [137].

> *Cutting rule for* $k_{m_q \dots m_1}$*: Sum* all half-*diagrams that have* q external *fields acting on a* fixed *set of environment modes* $m_q \dots m_1$ *over which we symmetrize. This includes summing over* all *possible intra-branch contractions and their mode indices. Perform all one-branch time-ordered integrations, including the times of the* external *vertices.*

(B2) The full diagrammatic rules for calculating the Keldysh are summarized in App. F.2 and are conveniently similar to the standard Keldysh rules [App. F.1]. The required value for $\Pi_{m_q \dots m_1}$ is then obtained by pasting two halves together as follows:

> *Pasting rule for* $\Pi_{m_q \dots m_1}$*: Fully contract the* external *vertices appearing on both sides of* $\mathrm{Tr}_{\mathrm{E}} :k_{m_q \dots m_1}(t):(\bullet \otimes \rho^{\mathrm{E}}) :k_{m_q \dots m_1}(t)^\dagger:$ *in all possible ways.*

We note that the normal-ordering in Eq. (5.11b) is only an instruction to simplify the evaluation by discarding all internal Wick contractions of k_m and $k_m^\dagger$. This is in contrast to the Kraus operators $K_m^e(t) = \langle e| \left(:k_m(t): \otimes \mathbb{1}^{\mathrm{P_E}}\right) |0\rangle$ for which the normal-ordering has to be explicitly evaluated[5]. It should also be noted that when using Wick contractions, the most elementary physical process Π_m is *never* described by a single or even a finite number of Keldysh real-time diagrams. Typically, guaranteeing CP in approximate dynamics calls for methods that are nonperturbative in the system-environment coupling.

Stage 2, Eq. (5.11a) It remains to sum the computed Π_m over the modes[6] $m_q \dots m_1$ and their number $q = 0, 1, \dots$ in order to eliminate the meter-space M. Our example in Sec. 5.5

[5] In Refs. [32–34] Kraus operators are considered which depend on the internal times of the coupling vertices. In our Kraus operators K_m^e we instead perform all internal time-integrations and directly work with the underlying Keldysh operators k_m which are not yet restricted by normal-ordering.

[6] This list may include repetitions, e.g., for an environment with three modes, $m = (112333)$ is included.

will illustrate that truncating q, the number of modes, in stage 2 correlates with the time to reach the stationary state relative to the time-scale that is set by the time-dependence of $\Pi_{m_q \ldots m_1}(t)$ obtained in stage 1 [Eq. (5.39)]. Because the expansion index $m_q \ldots m_1$ is physically motivated, the truncation of stage 2 never jeopardizes CP.

5.3.2 CP approximations

The above transparent rules translate the operator-sum theorem to the framework of the standard real-time expansions on one and two branches of the Keldysh time-contour. Above all, this provides explicit means for translating problems and solutions between the very different formulations employed in quantum information theory and statistical physics on the microscopic level of the system-environment coupling V.

As expected, evaluating the objects obtained by these simple rules is by no means easy. The importance of our general framework is that at least the large variety of existing approximations can be formulated, compared and systematically improved. In Sec. 5.4 we make a further step towards practical applications by deriving useful self-consistent and infinitesimal evolution equations. The reorganized expansion [Eq. (5.11), Fig. 5.3] already shows how *CP approximations* can be constructed generically. Fig. 5.4(b) illustrates this for approximations based on selecting *complete* Keldysh diagrams[7]. In order to guarantee CP, such a selection must pass the test of *horizontally cutting* the Keldysh diagrams using their standard representation [Fig. 2.4(b)] and summing up their halves to obtain k_m [left hand side in Fig. 5.4(b)]. By the pasting rule, one can check that k_m reproduces the groups of two-branch diagrams originally selected [right-hand side in Fig. 5.4(b)]. This amounts to checking that one can diagrammatically 'complete the square' to the operator-sum (5.11b).

Clearly, directly selecting groups of *two-branch* diagrams, each group corresponding to one conditional propagator Π_m, passes this test. This amounts to selecting *physical* processes, i.e., possible measurements performed on the meter M, and *therefore* preserves CP. This is illustrated by the example later on [Eq. (5.41)]. The approximate propagator is a TNI superoperator [Eq. (5.9)] expressing that probability was lost by omitting physical processes. A more advanced scheme is to select complete *one-branch* diagrams for the Keldysh operators k_m directly [left-hand side in Fig. 5.4(b)]. One can then infer which distinct two-branch diagrams they generate and equivalently select only these in the standard Keldysh expansion. This amounts to a modification of the propagator Π_m by selecting a subset of diagrams from that group. Because this is done without breaking the CP operator-sum structure, the modified contribution still corresponds to a physical process occurring with a positive probability, cf. Sec. 5.3.4, *provided* the superoperators are TNI which is not automatic[8].

5.3.3 Trace-preservation (II): Microscopic state-evolution correspondence

We now address the constraints imposed by TP to continue the discussion initiated in Sec. 5.2.2. There we pointed out that the decomposition into CP-TNI superoperators by itself does not mitigate the CP-TP duality issue. Within the reorganized Keldysh expansion, the diagrammatic cutting and pasting rules of the previous section however allow one to explicitly track both CP and TP properties on the microscopic level of the coupling V: the former by the two-stage decomposition (5.11), the latter by the diagrammatic rule (2.17). This

[7] We note that this is not the only way to construct CP approximations: The pasting rule can be modified as to ensure both CP and TP. This is effectively what is done in Ref. [33, 34], see discussion in Sec. 5.3.4.

[8] For $S_A\rho := \mathrm{Tr}_\mathrm{E} A(\rho \otimes \rho^\mathrm{E})A^\dagger$ we have $\mathrm{Tr}S_A\rho \leq \mathrm{Tr}(S_A + S_B)\rho$ but $\mathrm{Tr}S_A\rho$ can exceed $\mathrm{Tr}S_{A+B}\rho$ for $B = -A$.

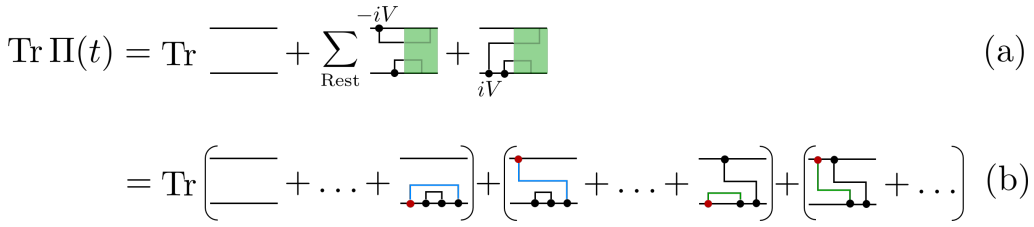

Figure 5.5: (a) Standard real-time expansion: Trace-preservation is guaranteed by the vertex flipping rule (2.17). (b) Reorganized expansion: Brackets indicate groups of diagrams that belong to the same physical process generated by one Keldysh operator k_m. Applying the simple rule of (a) reveals a nontrivial network of cancellations between diagrams in different brackets corresponding to different Keldysh operators. This shows that CP and TP cannot be ensured simultaneously by selection of complete Π_m-groups of diagrams. Reprinted figure under CC BY 4.0 License from SciPost Phys. **7**, 012 (2019), see Ref. [137].

vertex-flipping [Fig. 5.5(a)] reveals the nontrivial interrelation of the Keldysh (and Kraus) operators that is implied by the nonlinear constraint (5.9b) involving *all* Keldysh operators:

$$\mathbb{1}^{\mathrm{S}} = \sum_{q=0}^{\infty} \sum_{m_q \ldots m_1} \operatorname*{Tr}_{\mathrm{E}} :k_{m_q \ldots m_1}(t)^\dagger: \, :k_{m_q \ldots m_1}(t): \left(\mathbb{1}^{\mathrm{S}} \otimes \rho^{\mathrm{E}}\right). \tag{5.12}$$

In Fig. 5.5(b) we sketch a group of two-branch diagrams for some process $\Pi_{m_q \ldots m_1}$ (indicated by the middle bracket). Consider the two possible situations for the latest (leftmost) vertex indicated in red. This vertex is either already contracted within the same branch (green); then, the TP rule (2.17) demands that we also take into account a corresponding diagram whose latest vertex lies on the opposite branch and thus contributes to a process $\Pi_{m_{q+1} \ldots m_1}$ with one additional external vertex (right bracket). Otherwise, the vertex is contracted with the opposite branch (blue); then, the TP rule (2.17) requires a term in the process $\Pi_{m_{q-1} \ldots m_1}$ with one less external vertex (left bracket). This implies that the TP condition for the Keldysh operators making up each process is guaranteed by the pairwise contribution of coupling vertices to 'adjacent' operators, schematically

$$k_{m_{q-1} \ldots m_1} \longleftrightarrow k_{m_q \ldots m_1} \longleftrightarrow k_{m_{q+1} \ldots m_1}. \tag{5.13}$$

Thus, the TP condition on the Keldysh and Kraus operators that appears nontrivial [Eq. (5.9)] is *microscopically* clear. These pair cancellations do not form a simple chain but rather a network correlating[9] all terms in the operator-sum $\Pi = \sum_m \operatorname{Tr}_{\mathrm{E}} :k_m:(\bullet \otimes \rho^{\mathrm{E}}) :k_m^\dagger:$.

The CP structure requires one to include all possible two-branch time-orderings of the individual vertices [cf. Fig. 5.4(a)]. In particular, we must include both terms in the middle bracket in Fig. 5.5(b) which then rigidly connects two independent TP constraints (2.17). Because this applies to *every* pair of diagrams in the middle bracket, all groups of diagrams connected to it by a TP constraint must be included as well. Continuing this argument to these other groups one finds that eventually *all* diagrams have to be included. This is the ultimate microscopic ground for the CP-TP duality as it appears in practical approximations, complementing the general considerations of Sec. 2.3. We stress that this does *not* rule out the possibility of CP-TP approximations by diagram selection as we discuss below.

[9] In terms of the state-evolution correspondence this network realizes the correlations within the Choi-state choi[Π] which ensure that its partial state is maximally mixed, see the requirement (2.20) in Sec. 2.3.

5.3.4 CP versus TP approximations

Having understood the conflicting demands of CP and TP microscopically, consider again the first *CP approximation* scheme discussed in Sec. 5.3.2. Let the approximated propagator $\Pi_{q_{\max}} = \sum_{q=0}^{q_{\max}} \sum_{m_q \ldots m_1} \Pi_{m_q \ldots m_1}$ be obtained by discarding terms with more than $q_{\max}$ inter-branch contractions. The TP error for such a truncation is quantified by the trace distance

$$\left| \mathbb{1}^{\mathrm{S}} - \Pi^{\dagger}_{q_{\max}}(\mathbb{1}^{\mathrm{S}}) \right| \tag{5.14}$$

of the operator-constraint (5.9b) computed from the adjoint of the approximated evolution. This error will be monotonically reduced by increasing $q_{\max}$ since the added terms are CP-TNI operators. Physically, this means we account for more modes that have interacted with the system up to the considered time t. One expects that more modes are required when the system interacts longer with the environment. We stress that this truncation is *not* a naive short-time expansion[10] of $\Pi(t)$: The time-dependence of $\Pi_m(t)$, obtained in stage 1, defines a cutoff on the number of modes to be kept in the stage 2 expansion depending on the evolution time t. This will be illustrated for a simple example in Sec. 5.5.

This should be compared with the situation encountered in the frequently used TP approximations. Under the TP constraint, discarding diagrams without further precautions will uproot the operator-sum structure of the expansion, and thus violate CP. If one has computed the evolution map $\Pi(t)$ (not the evolution of a specific initial state or only the stationary state) one can check this by explicitly calculating the associated Choi-operator (2.18) as we did for the exact dynamical map in Ch. 3. A CP-violation is then detected by negative eigenvalues of this operator but this is hardly ever discussed for TP approximations. Also, checking the evolved state $\rho(t)$ for *all* possible inputs $\rho(0)$ only establishes positivity-preservation which we noted in the introduction and in Sec. 2.1 lacks a clear operational understanding. Additionally, there seems to be no way of systematically 'improving towards CP' in TP approximations –see however Eq. (5.26) below– other than numerically approximating the exact result better. It is now clear that this breakdown of CP in TP approximations is not due to 'missing physics' but instead indicates that one has uprooted the statistical structure: One is not summing up physical processes but mathematical contributions.

The above indicates that approximations which *simultaneously* guarantee TP and CP require schemes more sophisticated than the diagram selections considered so far. The difficulty of ensuring TP in CP-approximations was noted in Refs. [85, 169]. Building on Refs. [32, 181, 182], very recent work constructed systematic CP-TP approximations for a broad class of systems [33, 34]. There it is noted that the CP constraint is trivially satisfied, but the TP constraint requires an ingenious truncation of environment correlation functions and the detailed proof of TP is nontrivial. It can be shown that this truncation on the level of the Kraus operators used in Refs. [33, 34] corresponds to a selection of Keldysh real-time diagrams for $\Pi(t)$ which allow TP to be verified more easily using the rule (2.17), illustrating its usefulness. The novel feature of this diagram selection is that it entails a modification of the *pasting rule* (5.11b) which we kept fixed in our above considerations.

[10] This should be contrasted with Refs. [32–34] which introduces an expansion around the long-time limit: Whereas the leading order is exact in this limit, next-to-leading order corrections are only required to access times $t < \infty$ where non-Markovian effects are important.

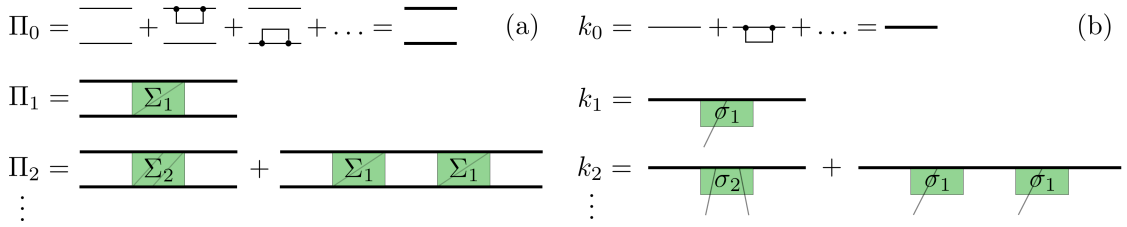

Figure 5.6: Hierarchies for propagators (a) on the double-branch and (b) on a single branch of the Keldysh contour. Each tier of the hierarchy corresponds to a *physical* process. The tier index (5.16) indicates the modes of the contracted lines in (a) and external uncontracted lines in (b). Horizontally cutting the Π_m diagrams in (a) produces the corresponding k_m diagrams in (b) and the converse is given by Eq. (5.11b). Cutting the *self-energy* diagrams Σ_m in (a) produces the diagrams σ_m in (b) when discarding one-branch reducible fragments. The nontrivial converse construction of $\Sigma_m[\sigma_0 \dots \Sigma_m]$ is described in Sec. 5.4.3. This figure shows examples for bilinear coupling, but all considerations also hold for multilinear coupling. Reprinted figure under CC BY 4.0 License from SciPost Phys. **7**, 012 (2019), see Ref. [137].

5.4 Hierarchies of self-consistent and kinetic equations

With so much room for approximations, it is of practical interest to have equivalent self-consistent and infinitesimal formulations of the measurement-conditioned evolution. In Sec. 5.4.1 we show how to compute Π_m directly from *memory-kernels* Σ_m. This approach is closely related to well-developed techniques in statistical physics and is therefore discussed first. It avoids all use of the Keldysh operators k_m (and Kraus operators) and instead implements stage 1 through the task of computing the self-energy *super*operators Σ_m. In Sec. 5.4.2 we address the calculation of the Keldysh operators k_m and by analogy introduce their *memory-kernels* σ_m which is possible since the k_m are closely related to the Π_m due to the cutting rule. This instead implements stage 1 through the task of computing the self-energies σ_m –operators on system and environment.

The two approaches are graphically summarized in Fig. 5.6 and are equivalent, being related by $\Pi_m = \mathrm{Tr}_\mathrm{E} :k_m:(\bullet \otimes \rho^\mathrm{E}) :k_m^\dagger:$. In both approaches it remains to perform stage 2, the sum over modes m, collecting all CP contributions $\Pi = \sum_m \Pi_m$. The equations also share the same forward-feeding hierarchical structure which makes them of practical importance in view of the success of numerical methods [119] based on similar hierarchical formulations. However, the approaches are dual in that the relative difficulty of guaranteeing CP and TP are opposite. These two hierarchies allow us in Sec. 5.4.3 to derive an *infinitesimal* form of the operator-sum theorem by explicitly determining the functional relation between the families of memory-kernels Σ_m and σ_m.

5.4.1 Hierarchy for conditional evolutions Π_m

We start from the unraveling (5.11a) where each CP-TNI conditional evolution superoperator Π_m is represented by the sum of all diagrams with q fixed contractions involving modes $m = m_q \dots m_1$ between opposite branches. Their irreducible counterparts Σ_m can be correspondingly introduced by restricting *all* contractions to be two-contour irreducible [Fig. 2.4(b)]. The full self-energy Σ in the standard Dyson equation (2.16) –the sum over all two-branch irreducible diagrams– is then obtained by summing over all modes m of these

conditional self-energy superoperators Σ_m:

$$\Pi(t) = \sum_m \Pi_m(t), \qquad \Sigma(t,t') = \sum_m \Sigma_m(t,t'). \tag{5.15}$$

In the following we use simplified notation for the labels of the environment modes:

$$0 = (\text{no modes}), \quad 1 = m_1, \quad 2 = m_2 m_1, \quad \ldots. \tag{5.16}$$

As sketched in Fig. 5.6, the expansion (5.15) unravels the Dyson equation (2.16) into a hierarchy of equations that is physically motivated: Each tier is labeled by the measurement outcome m, listing the environment modes that interacted with the system in the process Π_m. In the lowest tier of the hierarchy, $q = 0$, no modes interacted with system. We obtain an independent self-consistent equation

$$\Pi_0 = \pi + \pi * \Sigma_0 * \Pi_0, \tag{5.17a}$$

where π denotes the free system propagator which reduces to $\pi = \mathcal{I}$ in the interaction picture and we omit the explicit time-arguments of the convolutions $*$ in the following. Importantly, this is the only self-consistent step in the hierarchy. Its solution $\Pi_0 = \pi + \pi \sum_{l=1}^{\infty} (*\Sigma_0 * \pi)^l$ amounts to a renormalization of the free system propagator π, giving a CP-TNI superoperator, see Eq. (5.21) below. This should be contrasted with the standard Dyson equation (2.16) which produces a solution Π based on π, both of which are CP-TP, see Sec. 2.3. Although Σ_0 involves all orders of the microscopic coupling V, it does not contain all diagrams of the standard Σ in Eq. (2.16). The solution of the zeroth tier (5.17a) enters the following tiers with a simpler, forward-feeding structure:

$$\Pi_1 = \Pi_0 * \Sigma_1 * \Pi_0 \tag{5.17b}$$

$$\Pi_2 = \Pi_0 * \Sigma_2 * \Pi_0 + \Pi_0 * \Sigma_1 * \Pi_0 * \Sigma_1 * \Pi_0 \tag{5.17c}$$

$$\Pi_3 = \Pi_0 * \Sigma_3 * \Pi_0 + \Pi_0 * \Sigma_2 * \Pi_0 * \Sigma_1 * \Pi_0 + \Pi_0 * \Sigma_1 * \Pi_0 * \Sigma_1 * \Pi_0 * \Sigma_1 * \Pi_0 + \Pi_0 * \Sigma_1 * \Pi_0 * \Sigma_2 * \Pi_0 \tag{5.17d}$$

$$\vdots$$

This enables an iterative solution of Π_0, Π_1, Π_2, ..., given the conditional self-energies Σ_0, Σ_1, Σ_2, ... and allows one to systematically implement approximation strategies discussed in Sec. 5.3.1. One checks that summing Eqs.(5.17) gives back the self-consistent equation (2.16). In the hierarchy (5.17) it is implicitly understood that one symmetrizes the mode indices appearing on the right-hand side, i.e., in equation (5.17c) the indices on the two Σ_1's occurring in the second term on the right hand side of $\Pi_2 = \Pi_{m_1 m_2} = \Pi_{m_2 m_1}$ should be considered as independent variables: $\Sigma_1 * \Pi_0 * \Sigma_1 = \Sigma_{m_1} * \Pi_0 * \Sigma_{m_2} + (m_1 \leftrightarrow m_2)$. Also note that on the right-hand side individual contributions –or partial sums of them– do *not* correspond to a physical process: Only their full sum makes up Π_m which is CP-TNI due to its operator-sum form (5.11b). Moreover, these terms consist of sequences of irreducible blocks Σ_m and Π_0 and are thus *reducible*. This goes against the widespread intuition that contributions to irreducible kernels such as Σ (and its components Σ_m) correspond to physical processes.

To further highlight how the physical processes Π_m influence each other in *time*, we cast the self-consistent hierarchy (5.17) into an equivalent hierarchy of time-nonlocal kinetic

equations for infinitesimal conditional evolutions. These read in the interaction picture,

$$\frac{d}{dt}\begin{bmatrix}\Pi_0\\ \Pi_1\\ \Pi_2\\ \Pi_3\\ \vdots\end{bmatrix} = \begin{bmatrix}\Sigma_0 & 0 & 0 & 0 & 0 & \cdots\\ \Sigma_1 & \Sigma_0 & 0 & 0 & 0 & \cdots\\ \Sigma_2 & \Sigma_1 & \Sigma_0 & 0 & 0 & \cdots\\ \Sigma_3 & \Sigma_2 & \Sigma_1 & \Sigma_0 & 0 & \cdots\\ \vdots & & & & & \vdots\end{bmatrix} * \begin{bmatrix}\Pi_0\\ \Pi_1\\ \Pi_2\\ \Pi_3\\ \vdots\end{bmatrix}, \tag{5.18}$$

with initial conditions $\Pi_0(0) = \mathcal{I}$ and $\Pi_m(0) = 0$ for $m \neq 0$. Each column of the matrix of self-energy superoperators sums to the standard self-energy $\Sigma = \sum_m \Sigma_m$, and by summing the column-entries of Eq. (5.18) to obtain $\Pi = \sum_m \Pi_m$, we reproduce the standard kinetic equation (5.2), $\frac{d}{dt}\Pi = \Sigma * \Pi$, in the interaction picture. Thus, the hierarchy presents an unraveling of the time-nonlocal kinetic equation (5.2). The lower-triangular form of the matrix ensures that the coupled kinetic equations feed forward and can be iteratively solved for Π_0, Π_1, ..., the formal solution being given by Eq. (5.17).

An advantage of the hierarchies over the standard (kinetic) equation Eq. (2.16) [Eq. (5.2)] is that both TP and CP have become explicit, even though the duality of their constraints persists [Sec. 5.2.2, 5.3.3]. The individual conditional self-energies do not preserve the trace, i.e., $\mathrm{Tr}\,\Sigma_m \neq 0$ because the Π_m are TNI, but we can still see that Π is TP: Summing the elements in each column of the matrix appearing in Eq. (5.18) and taking the trace gives $\mathrm{Tr}\,\Sigma = \sum_m \mathrm{Tr}\,\Sigma_m = 0$ because contributions from subsequent Σ_m cancel pairwise by our earlier arguments[11]. As we know, CP is guaranteed for each Π_m separately by Eq. (5.11a). In both hierarchies this is expressed by the forward-feeding structure which ensures that neglecting *complete higher tiers* (corresponding to larger number of modes $m_q \ldots m_1$) does not affect the lower tiers: If the latter are solved using the required finite set of *exact* Σ_m, the solutions are guaranteed to be CP. Thus, although there are no Kraus operators to be seen in Eq. (5.17)-(5.18), we can fully exploit the implications of the operator-sum theorem by unraveling the standard approach of statistical physics based on Eq. (5.2). At the same time, we can take advantage of the diagrammatic technique to compute the required (sub)set of conditional self-energies Σ_m using rules which are very similar to the standard ones [App. F.1].

5.4.2 Hierarchy for Keldysh operators k_m

To set up more refined CP approximations one may consider additionally modifying the Σ_m but doing so without uprooting CP is more complicated. In Sec. 5.3.2 we discussed a second approximation scheme which achieves this more easily by selecting one-branch diagrams for the Keldysh operators k_m. Because the Keldysh operators k_m are constructed from the Π_m by the cutting rule [Sec. 5.3] they obey an analogous hierarchy of equations (5.19) illustrated in Fig. 5.6(b). We start from the unraveling (5.10) of the unitary evolution $U = k_0 + \sum_{m\neq 0} :k_m:$ into its average k_0 and operators which are explicitly normal-ordered. By analogy with the decomposition (5.15), we introduce σ_m as the sum of all *one-branch* irreducible Keldysh half-diagrams representing k_m, i.e., irreducibility is understood with respect to the time-ordering on the upper branch of the Keldysh time-contour only. The Keldysh operators k_m are then

[11] TP is preserved through cancellation of pairs of diagrams appearing in different conditional evolutions: Eq. (5.13) implies that terms in $\Pi_{m_q \ldots m_1}$ cancel with those in 'adjacent' $\Pi_{m_q \pm 1 \ldots m_1}$. Since the argument leading to Eq. (5.13) also holds when removing Π_0 at the latest time, we find that contributions to the irreducible block $\Sigma_{m_q \ldots m_1}$ cancel with those in other blocks $\Sigma_{m_q \pm 1 \ldots m_1}$.

generated by the self-energy operators σ_m through the hierarchy

$$k_0 = u + u * \sigma_0 * k_0 \tag{5.19a}$$
$$k_1 = k_0 * \sigma_1 * k_0 \tag{5.19b}$$
$$k_2 = k_0 * \sigma_2 * k_0 + k_0 * \sigma_1 * k_0 * \sigma_1 * k_0 \tag{5.19c}$$
$$k_3 = k_0 * \sigma_3 * k_0 + \cdots \tag{5.19d}$$
$$\vdots$$

that inherits its structure from Eq. (5.17). Here u is the free evolution of system *and* environment[12] which reduces to $u = \mathbb{1}^{\mathrm{S}} \otimes \mathbb{1}^{\mathrm{E}}$ in the interaction picture. As before, we symmetrize over the mode indices on the right-hand side [Eq. (5.17)]. We note that the sum of Eqs. (5.19) results in the self-consistent equation

$$k = u + u * \sigma * k \tag{5.20}$$

for the operator $k(t) := \sum_m k_m(t)$ with $\sigma(t,t') := \sum_m \sigma_m(t,t')$. Importantly, this is *not* the self-consistent form of the Schrödinger equation due to the lack of normal-ordering relative to Eq. (5.10). Only *after explicitly normal-ordering* the hierarchy equations, the Schrödinger-Dyson equation, $U = u + u*(-iV)U$, with a *time-local* coupling V is recovered, as it should. This nontrivial consistency check is worked out in App. E.2.

The zeroth tier Eq. (5.19a) is again an independent self-consistent equation. In this case, the self-energy σ_0 sums up all one-branch irreducible contractions without external fields and therefore acts trivially on the environment just as k_0. The solution $k_0 = u + u\sum_{l=1}^{\infty}(*\sigma_0 * u)^l$ of Eq. (5.19a) can then be related to the solution of Eq. (5.17a),

$$\Pi_0(t) = K_0^0(t) \bullet K_0^0(t)^\dagger, \tag{5.21}$$

noting that the zeroth operator [Eq. (5.7)] factorizes, $k_0 = K_0^0 \otimes \mathbb{1}^{\mathrm{E}} = \langle U \rangle^{\mathrm{E}} \otimes \mathbb{1}^{\mathrm{E}}$, and that the free system evolution is $\pi = \mathrm{Tr}_{\mathrm{E}}\, u(\bullet \otimes \rho^{\mathrm{E}})u^\dagger$. Although this separates the evolution into operators on the left and right, in general $K_0^0(t)$ is *not* generated by an effective nonhermitian Hamiltonian because $\sigma_0(t,t')$ is in general a time-nonlocal operator [cf. Eq. (5.31)]. Higher tiers determine the k_m which act nontrivially on several modes m of the environment. When one has solved the hierarchy for these operators one obtains the conditional propagators Π_m by the pasting formula (5.11b). The Kraus operators $K_m^e(t) = \langle e| :k_m(t): \otimes \mathbb{1}^{\mathrm{P_E}} |0\rangle$ are determined by the solutions for $k_m(t)$ obtained from Eq. (5.19).

Taking the time-derivative of (5.19) we obtain a hierarchy of time-nonlocal kinetic equations for the Keldysh operators in the interaction picture,

$$\frac{d}{dt}\begin{bmatrix} k_0 \\ k_1 \\ k_2 \\ k_3 \\ \vdots \end{bmatrix} = \begin{bmatrix} \sigma_0 & 0 & 0 & 0 & 0 & \dots \\ \sigma_1 & \sigma_0 & 0 & 0 & 0 & \dots \\ \sigma_2 & \sigma_1 & \sigma_0 & 0 & 0 & \dots \\ \sigma_3 & \sigma_2 & \sigma_1 & \sigma_0 & 0 & \dots \\ \vdots & & & & & \vdots \end{bmatrix} * \begin{bmatrix} k_0 \\ k_1 \\ k_2 \\ k_3 \\ \vdots \end{bmatrix}, \tag{5.22}$$

[12] Refs. [32–34] derive a hierarchy for *Kraus* operators acting only on the system. Here we instead have a hierarchy of Keldysh operators which still act on the environment. Moreover, the hierarchy is expressed in terms of *self-energy* generators σ_m which provides some advantages.

with initial conditions $k_0(0) = \mathbb{1}$ and $k_m(0) = 0$ for $m \neq 0$. As before, these equations enable an iterative solution of the Keldysh operators k_0, k_1, k_2, ..., given the conditional self-energy operators σ_0, σ_1, σ_2, ... Importantly, this allows one to implement the second kind of approximation strategy discussed in Sec. 5.3.2. We note that summing the column-entries of Eq. (5.22) gives a single *time-nonlocal* evolution equation,

$$\frac{d}{dt}k = \sigma * k, \tag{5.23}$$

which is the differential formulation of Eq. (5.20), but *not* the Schrödinger equation due to the lack of normal-ordering in the quantity k. Accounting for the normal-ordering, Eq. (5.22) [Eq. (5.19)] constitutes a time-nonlocal unraveling of the (Dyson) Schrödinger equation for system plus environment which has the advantage that it can be solved step-by-step. An advantage relative to Eq. (5.18) [Eq. (5.17)] is that the difficulty of guaranteeing CP and TP has been reversed. Indeed, in Eq. (5.19)-(5.22) we are free to formulate *any* approximation in terms of the *generators* σ_m without *ever* compromising CP because they feed into the Keldysh operators k_m constituting the CP operator-sum. Importantly, such k_m-approximations will not only *select* conditional evolutions Π_m but also *modify* them [cf. Sec. 5.3.2]. Such a one-branch diagrammatic selection does however not guarantee TP because the network of pairwise cancellations between different Keldysh operators [Eq. (5.13), Fig. 5.5] implies constraints that tie all σ_m together. This makes TP harder to implement than in the two-branch propagator hierarchy (5.18).

5.4.3 Operator-sum theorem for the time-nonlocal memory-kernel

The formal solutions of the hierarchies in Sec. 5.4.1 and Sec. 5.4.2 are related by our key relation (5.11b), $\Pi_m = \mathrm{Tr}_\mathrm{E} :k_m:(\bullet \otimes \rho^\mathrm{E}) :k_m^\dagger:$. The operator equations (5.22) [(5.19)] thus constitute an *exact* purification of the hierarchy of *super*operator equations (5.18) [(5.17)]. This implements the state-evolution correspondence [Sec. 2.3] while explicitly separating out the normal-ordering procedure. The nontrivial reversal of the difficulty of imposing the constraints of CP and TP –despite the structural similarities of the two types of hierarchies– results from this duality and will now be traced *microscopically* to the difference in irreducibility and time-ordering on one and two time-branches: Whereas the self-energy superoperators Σ_m were constructed from *two-branch* irreducible diagrams, the self-energy operators σ_m are irreducible on a *single branch*, ignorant of time variables on the opposite branch[13].

To clarify this, we explicitly construct Σ_m from the σ_m by working out the nontrivial time-ordering constraints in the Kraus *operator-sum theorem* (for finite time-evolution) in order to transpose it to the level of the Nakajima-Zwanzig *memory-kernel* (for infinitesimal evolution). Note that this time-ordering issue goes unnoticed in semigroup limits where one can easily apply the operator-sum theorem directly to $\Pi(t + dt) = \Pi(dt)\Pi(t)$ leading to the GKSL form of the quantum master equation [233]. Here we go beyond such simple limits where our diagrammatic approach shows its advantage: The functional form of the self-energies $\Sigma_m[\sigma_0 \dots \sigma_m]$ can be precisely determined starting from the prescription provided by the irreducible version of the pasting –or purification– equation (5.11b):

$$\Sigma_m[\sigma_0 \dots \sigma_m] = \underset{\mathrm{E}}{\mathrm{Tr}} :k_m[\sigma_m \dots \sigma_0]: \left[\, \bullet \otimes \rho^\mathrm{E} \right] :k_m^\dagger[\sigma_m^\dagger \dots \sigma_0^\dagger]: \Big|_{\mathrm{irred}}. \tag{5.24}$$

[13] This is a fundamental difference between the Liouville-von Neumann and Schrödinger equation which by our considerations ties in with the state-evolution correspondence.

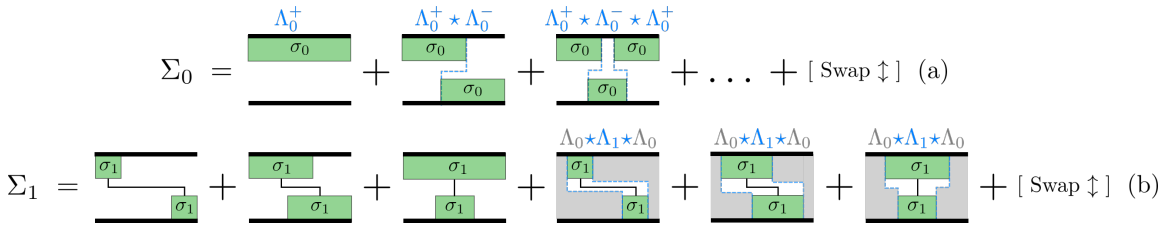

Figure 5.7: Conditional components Σ_m of the memory-kernel Σ as explicit functional (5.26) of the Keldysh- and Kraus operator memory-kernels σ_m. The bold black lines indicate the full conditional propagator k_0 with no external vertex. (a) For Σ_0, two-branch irreducibility can only be ensured by alternating sequences of σ_0 $[\sigma_0^\dagger]$ on opposite branches, cf. Eq. (5.25). (b) For the remaining Σ_m, a dressed expansion can be set up in terms of the generators σ_m following the rules (i)-(v) in the main text. This includes summation over all *two-branch time-orderings* of the self-energies $\sigma_m(\tau, \tau')$ [cf. Fig. 5.4(a)]. A construction of Σ_2 is provided in App. F.3. The irreducible fragments Λ_m obtained in step (iii) can be complemented by the generalization $\Lambda_0(t_+, t_-, t'_+, t'_-)$ of Eq. (5.26a) to a four-time object, see rule (iv). Reprinted figure under CC BY 4.0 License from SciPost Phys. **7**, 012 (2019), see Ref. [137].

Inserting $k_m[\sigma_0 \dots \sigma_m]$ in terms of its generators, it remains to work out the *two-branch irreducibility* constraints on the one-branch time-integrations hidden inside k_m and $k_m^\dagger$. We now show that this amounts to a 'dressed' real-time expansion on the Keldysh contour in terms of effective vertices $\sigma_0, \sigma_1, \dots$ with an intricate internal time-ordering structure.

In Fig. 5.7(a) we sketch the case for Σ_0 where the two-branch irreducibility can be achieved in only two ways using one-branch irreducible building blocks. Either a generator σ_0 (green) spans over a whole branch (first diagram); then the time-integrations on the other branch remain unrestricted and the full one-branch propagator k_0 appears (bold line). Otherwise, the two-branch irreducibility can only be maintained by an alternating sequence of generators σ_0 on the upper and $\sigma_0^\dagger$ on the lower branch with temporal overlaps, filled up with $k_0^\dagger$ resp. k_0 propagations in between (further diagrams). We see that the basic blocks of the memory-kernel on two branches are *four-time* superoperators[14] describing irreducible time-evolution from time t'_+ to t_+ on the upper and reducible evolution from t'_- to t_- on the lower branch,

$$\Lambda_0^+(t_+, t_-, t'_+, t'_-) = \sigma_0(t_+, t'_+) \bullet k_0^\dagger(t_-, t'_-), \tag{5.25a}$$

with $t_+ \geq t_- \geq t'_- \geq t'_+$ and conversely

$$\Lambda_0^-(t_+, t_-, t'_+, t'_-) = k_0(t_+, t'_+) \bullet \sigma_0^\dagger(t_-, t'_-), \tag{5.25b}$$

with $t_- \geq t_+ > t'_+ \geq t'_-$. Two-branch irreducibility is enforced by letting the one-branch irreducible generator σ_0 $(\sigma_0^\dagger)$ start earlier and end later than their reducible counterparts $k_0^\dagger$ (k_0) on the opposite branch. In terms of these auxiliary objects the functional form of Σ_0 can be written down explicitly:

$$\Sigma_0(t, t') = \sum_{n=1}^{\infty} \sum_{p=\pm} \left[\Lambda_0^p \star \Lambda_0^{-p} \star \dots \star \Lambda_0^{(-p)^{n-1}} \right](t, t, t', t'). \tag{5.26a}$$

[14] Similar objects are considered in Refs. [32–34].

Here, the two-branch convolution

$$\Big[\Lambda_0^+ \star \Lambda_0^-\Big](t_+,t_-,t'_+,t'_-) := \int_{t'_+}^{t_+} d\tau_+ \int_{t'_-}^{t_-} d\tau_-\, \Lambda_0^+(t_+,t_-,\tau_+,\tau_-)\, \Lambda_0^-(\tau_+,\tau_-,t'_+,t'_-)$$

accounts for independent one-branch convolutions imposing the two-branch time-ordering.

Once Σ_0 has been constructed in this way, the remaining tiers of the self-energy Σ_m can be obtained from a dressed expansion governed by the following diagrammatic rules illustrated in Fig. 5.7(b). We start from a Keldysh contour where each branch, running from the external times t' to t, is dressed to the Keldysh operator k_0 $[k_0^\dagger]$. To obtain $\Sigma_{m_q\ldots m_1}(t,t')$ for fixed modes $m_q\ldots m_1$ perform the following steps:

(i) Distribute in all possible ways the q external vertices acting on the fixed set of modes $m_q\ldots m_1$ among self-energy blocks σ_μ $[\sigma_\mu^\dagger]$ with $\mu\neq 0$ on the upper [lower] branch.

(ii) Integrate over all internal time-arguments of these blocks, but *restrict* them to *definite two-branch time-orderings*, see the first three contributions in Fig. 5.7(b). Let the earliest (latest) self-energy block start (end) at t' (t). Note that a single block may extend over a whole branch. Sum over the *finite* number of possibilities of such orderings.

(iii) Contract the external vertices in all possible ways to obtain *two-branch irreducible fragments* $\Lambda_\mu(t_+,t_-,t'_+,t'_-)$ as shown for the first three contributions in Fig. 5.7(b). Analogous to Eq. (5.25), the four time-arguments indicate propagation times on the upper and lower contour respectively .

(iv) Insert the four-time generalization of Eq. (5.26a), $\Lambda_0(t_+,t_-,t'_+,t'_-)$, at all positions where the two-branch irreducibility is not yet ensured. Such cases only occur for tiers with more than one mode ($q\geq 2$), see App. F.3. This enforces two-branch irreducibility.

(v) Add all irreducible extensions of the constructed diagrams by attaching Λ_0 on the left or on the right or on both sides as shown in the last contributions of Fig. 5.7(b).

Due to this generic structure, the two-branch irreducible fragments $\Lambda_\mu[\sigma_0\ldots\sigma_m]$ form yet another hierarchy for the conditional self-energy superoperators,

$$\Sigma_1(t,t') = \big[(\Delta+\Lambda_0)\star\Lambda_1\star(\Delta+\Lambda_0)\big](t,t,t',t') \tag{5.26b}$$

$$\Sigma_2(t,t') = \big[(\Delta+\Lambda_0)\star\Lambda_2\star(\Delta+\Lambda_0)\big](t,t,t',t') + \big[(\Delta+\Lambda_0)\star\Lambda_1\star\Lambda_0\star\Lambda_1\star(\Delta+\Lambda_0)\big](t,t,t',t'), \tag{5.26c}$$

$$\vdots$$

where the two-branch convolution takes care of the intricate time-ordering required for CP. Here $\Delta(t_+,t_-,t'_+,t'_-) = \delta(t_+-t'_+)\,\delta(t_--t'_-)$ is a shorthand for 'no insertion'. Except for the Δ's, Σ_m inherits a structure similar to that of the hierarchy (5.17) for Π_m. Also here symmetrization over the mode labels is understood implicitly.

The above diagrammatic rules allow different terms of the functional to be explicitly written down as illustrated in App. F.3 for a nontrivial example in second order of the dressed expansion. Importantly, it is again *only* the zeroth tier Σ_0 that requires summation over an *infinite* set of diagram contributions via the relation (5.26a). The remaining contributions

–dressed up by the so obtained Σ_0– represent a *finite* number of terms to evaluate. As of course expected for this general problem, evaluating these terms is challenging. In the limits where the GKSL form (1.5) applies the arising complications disappear and the jump operators J_i automatically emerge from the conditional self-energies $\sigma_m(t,t')$ of the Keldysh operators with external fields ($m \neq 0$) as the example in the following Sec. 5.5 illustrates.

The functional form (5.26) precisely encodes the nontrivial structure of the memory-kernel of the Nakajima-Zwanzig quantum master equation imposed by the Kraus operator-sum theorem. This means that *whatever* (approximated) σ_m one uses, a memory kernel Σ_m (or $\Sigma = \sum_m \Sigma_m$) with the functional form (5.26) will generate a CP evolution Π_m (Π) through the kinetic equation (5.18) [Eq. (5.2)]. It is *this* structure of the kernel –enforced by Eq. (5.24)– that guarantees that the solution can be expressed as $\Pi_m = \mathrm{Tr}_\mathrm{E} :k_m:(\bullet \otimes \rho^\mathrm{E}) :k_m^\dagger:$. The general importance of the nontrivial functional (5.26) is that it establishes a microscopic framework for approximations that go beyond the restrictive limits of the GKSL approach without giving up CP. This is by no means easy, but non-Markovian examples for which the time-independent GKSL form does *not* apply, e.g. the resonant level model of Ch. 3 or the examples presented in Refs. [33, 85] should nevertheless be solvable with our approach. Knowing the explicit structure (5.26) of the self-energy is also a prerequisite for setting up functional renormalization-group (RG) approaches. It may thus provide a starting point for connecting the *exact* hierarchies of RG equations formulated on one [270] and two [35, 158] branches of the Keldysh contour while explicitly preserving the CP structure of the density-operator evolution. This would allow one to assess the implications for CP of truncation schemes for such RG hierarchies. Interestingly, some RG approaches [35, 36, 158] also entail a two-stage approach similar in spirit to ours but based on an RG flow starting from the Markovian infinite-temperature limit [36, 157] that we study next in Sec. 5.5. We stress that the functional (5.26) is also relevant for less ambitious efforts. Consider, for example, a TP-approximation based on a selection of complete diagrams [152, 161, 162, 228, 229, 271] such that it breaks CP [Sec. 5.3.4]. Then the functional (5.26) allows one to systematically identify which groups of diagrams are missing, what their time-ordering structure is, and provides a guide for adding *some* –but not all– terms to *improve* towards[15] a complete operator-sum form. This amounts to partially 'completing the square' of the *solution* $\Pi(t)$, while working directly on the level of the self-energy of the *kinetic equation*.

5.5 Simple example: Resonant level at infinite temperature

In this final section, we illustrate the developed ideas on a simple example for which all calculations can be explicitly followed, both on the level of the Keldysh operators k_m and the conditional propagators Π_m. The aim is to illustrate *how* CP is guaranteed explicitly by the dual hierarchies when systematically constructing the self-energies and then solving each of their tiers. For this we return to the wideband resonant level model thoroughly analyzed in Ch. 3, but restrict ourselves to its Markovian infinite-temperature $T \to \infty$ limit which is already sufficient to highlight the intricate difficulties of the formalism.

Recall the total Hamiltonian (3.3) of this model

$$H^\mathrm{tot} = H^0 + V = \varepsilon\, d^\dagger d + \int_\omega \omega\, b_\omega^\dagger b_\omega + \sqrt{\frac{\Gamma}{2\pi}} \int_\omega \Big(d^\dagger b_\omega + b_\omega^\dagger d \Big), \tag{5.27}$$

[15] The improvement can be monitored via the Choi-operator (2.18) associated with $\Pi(t)$ [Sec. 5.3.4, Sec. 2.3].

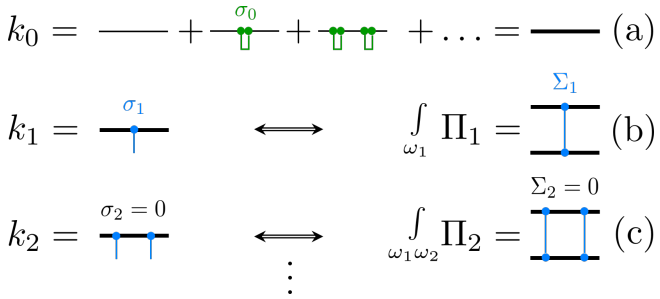

Figure 5.8: Hierarchy of the Keldysh-operators (left) and conditional propagators (right) for the model (5.27). The combined infinite-temperature and wideband limit forces all contractions to be instantaneous in time (drawn as vertical) suppressing all vertex correction diagrams. In combination with the bilinearity of the coupling V this causes all self-energies σ_m and Σ_m of tier $m \geq 2$ to vanish identically, but only after integrating over the environment mode energies ω_i, thereby partially performing stage 2. Reprinted figure under CC BY 4.0 License from SciPost Phys. **7**, 012 (2019), see Ref. [137].

where the system (field d) is bilinearly coupled to the modes of the environment (field b_ω) by tunnel rates Γ that are independent of their energy ω (wideband limit) denoting $\int_\omega := \int_{-\infty}^{\infty} d\omega$. The particle-hole index η indicates a creation ($\eta = +$) or annihilation ($\eta = -$) operator where the convention of *anticommuting* system and reservoir fields requires the inclusion of a fermion sign η_1 in the coupling term $V = -\sum_{\eta_1} \int_{\omega_1} \sqrt{\frac{\Gamma}{2\pi}} \eta_1 d^\dagger_{\eta_1} b_{\eta_1\omega_1}$. In this example, the modes of the environment are thus labeled by particle-hole indices and continuous energies:

$$(m_q \ldots m_1) = (\eta_q \omega_q \ldots \eta_1 \omega_1). \tag{5.28}$$

The combined infinite-temperature and wideband limit leads to simplifications whenever we contract[16] environment modes *and* sum the mode energy, cf. Eq. (3.9):

$$\int_\omega \frac{\Gamma}{2\pi} \langle b_{\eta'\omega'} e^{-i\eta\omega(\tau-\tau')} b_{\eta\omega} \rangle^{\mathrm{E}} = \frac{\Gamma}{4} \bar{\delta}(\tau - \tau') \delta_{\eta',-\eta}. \tag{5.29}$$

This limit therefore causes strictly Markovian semi-group dynamics and renders the model easily solvable. We note upfront that the $T \to \infty$ and wideband limit needs to be taken *twice*: Once, when we compute the conditional propagator Π_m in stage 1 by summing one-branch-diagrams to obtain k_m which is then pasted together with $k_m^\dagger$ using Eq. (5.11b); we take the limit a second time in stage 2 where we integrate over the environment energy ω contained in the mode index $m = \eta\omega$. Importantly, the pasting result (5.11b) of stage 1 *cannot* be simplified without this stage 2 energy-integration. As a result, the stage 1-2 distinction is easily blurred when simplifying expressions. We will first illustrate this for k_m in Sec. 5.5.1. This becomes a more prominent issue when computing Π_m directly –without the use of Keldysh operators– which we illustrate in Sec. 5.5.2.

5.5.1 One-branch hierarchy for k_m

Starting with the lowest tier of the hierarchy Eq. (5.19), we first have to compute the generators for the Keldysh operators. Only the single bubble-diagram depicted in Fig. 5.8(a)

[16] Note that $\int_0^\tau d\tau' \bar{\delta}(\tau - \tau') = 1$ is adapted to working with time-convolutions, cf Eq. (3.19a).

contributes which in the Schrödinger picture translates to

$$\begin{aligned}\sigma_0(\tau,\tau') &= \left\langle e^{iH^0\tau}\,(-iV)\,e^{-iH^0(\tau-\tau')}\,(-iV)\,e^{-iH^0\tau'}\right\rangle^{\mathrm{E}}\otimes e^{-iH^{\mathrm{E}}(\tau-\tau')}\\ &= -\frac{\Gamma}{4}\bar{\delta}(\tau-\tau')\sum_{\eta} d_\eta d_{-\eta}\otimes e^{-iH^{\mathrm{E}}(\tau-\tau')} \;=\; -\frac{\Gamma}{4}\bar{\delta}(\tau-\tau')\mathbb{1}^{\mathrm{S}}\otimes\mathbb{1}^{\mathrm{E}}. \end{aligned} \tag{5.30}$$

In contrast to the general case [Eq. (5.21) ff.], the time-locality of this generator gives rise to a simple power series in the iteration of the zeroth tier self-consistent equation (5.19a) that can be resummed into an exponential with a nonhermitian Hamiltonian $H^0_\infty := H^0 - i\frac{\Gamma}{4}\mathbb{1}^{\mathrm{S}}\otimes\mathbb{1}^{\mathrm{E}}$ for system and environment:

$$\begin{aligned}k_0(t) &= e^{-iH^0t} + \int_0^t d\tau\int_0^\tau d\tau' e^{-iH^0(t-\tau)}\sigma_0(\tau,\tau')k_0(\tau')\\ &= e^{-iH^0t} + \int_0^t d\tau\, e^{-iH^0(t-\tau)}\left[-\frac{\Gamma}{4}\mathbb{1}^{\mathrm{S}}\otimes\mathbb{1}^{\mathrm{E}}\right]k_0(\tau) \;=\; e^{-iH^0_\infty t}. \end{aligned} \tag{5.31}$$

For the next tier of self-energy operators we explicitly write the mode index $1 = (\eta_1\omega_1)$ and see in Fig. 5.8(b) that it is basically the bare vertex:

$$\sigma_{\eta_1\omega_1}(\tau,\tau') = i\bar{\delta}(\tau-\tau')\sqrt{\frac{\Gamma}{2\pi}}\eta_1 d^\dagger_{\eta_1} b_{\eta_1\omega_1}. \tag{5.32}$$

We can then evaluate Eq. (5.19b) for the Keldysh operator without the need for iteration:

$$\begin{aligned}k_{\eta_1\omega_1}(t) &= \int_0^t d\tau\int_0^\tau d\tau'\, k_0(t-\tau)\sigma_{\eta_1\omega_1}(\tau,\tau')k_0(\tau')\\ &= i\eta_1\sqrt{\frac{\Gamma}{2\pi}}\int_0^t d\tau e^{i\eta_1(\omega_1-\varepsilon)\tau}\,e^{-iH^0_\infty t}\,d^\dagger_{\eta_1}b_{\eta_1\omega_1}. \end{aligned} \tag{5.33}$$

For higher tiers $q \geq 2$, the self-energies vanish $\sigma_{m_q\ldots m_1} = 0$ because the $T\to\infty$ and wide-band limit suppresses all *one-branch* vertex corrections. Thus, only repeated convolutions of k_1 remain for the q-th tier equation and we obtain

$$k_{\eta_q\omega_q\ldots\eta_1\omega_1}(t) = \frac{1}{q!}\prod_{j=1}^{q}\left(i\eta_j\sqrt{\frac{\Gamma}{2\pi}}\int_0^t d\tau_j e^{i\eta_j(\omega_j-\varepsilon)\tau_j}\right)e^{-iH^0_\infty t}\,d^\dagger_{\eta_q}b_{\eta_q\omega_q}\ldots d^\dagger_{\eta_1}b_{\eta_1\omega_1}, \tag{5.34}$$

with implicit symmetrization over the mode-indices. The time-ordering on the integrals has been lifted with the prefactor $1/q!$ accounting for the corresponding double-counting. We see that the decay rate Γ inside the *exponential* (5.31) appearing in Eq. (5.34) is generated initially when solving the lowest hierarchy-tier for $k_0(t)$. Through the hierarchy it sets the timescale for all higher $k_m(t)$ *before* we have integrated out the meter M by performing the sum over m. We stress that to further simplify the results for Π_m in stage 1 we *must* partially perform stage 2, $\sum_m \Pi_m$, in order to exploit the $T\to\infty$ and wideband limit for a *second* time: Only when integrating $\Pi_m = \mathrm{Tr}_{\mathrm{E}}:k_m:(\bullet\otimes\rho^{\mathrm{E}}):k_m^\dagger:$ over the mode-energies ω_i (leaving the η_i untouched), can the time-integrations in Eq. (5.34) be further reduced to $\bar{\delta}$-functions.

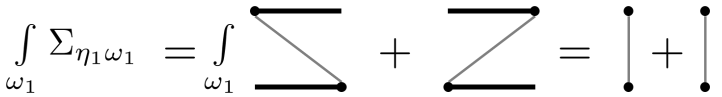

Figure 5.9: Energy-integrated functional $\Sigma_1[\sigma_0, \sigma_1]$, cf. Fig. 5.7(b). Due to the energy integration, the two-branch convolution reduces to a $\bar{\delta}$-function in time. Reprinted figure under CC BY 4.0 License from SciPost Phys. **7**, 012 (2019), see Ref. [137].

5.5.2 Two-branch hierarchy for Π_m

First, the zeroth tier conditional propagator is obtained directly from the pasting rule,

$$\Pi_0(t) = \operatorname*{Tr}_{\mathrm{E}} k_0(t)[\bullet \otimes \rho^{\mathrm{E}}]k_0(t)^\dagger = e^{-iH_\infty t} \bullet e^{-iH_\infty^\dagger t} := K_0(t) \bullet K_0(t)^\dagger, \tag{5.35}$$

inheriting the effective Hamiltonian $H_\infty := \varepsilon d^\dagger d - i\frac{\Gamma}{4}\mathbb{1}^{\mathrm{S}}$ from the Keldysh operator (5.31). Alternatively, one computes Σ_0 from (5.26a),

$$\Sigma_0(\tau, \tau') := \sigma_0(\tau, \tau') \bullet + \bullet\, \sigma_0^\dagger(\tau, \tau') = -\frac{\Gamma}{2}\bar{\delta}(\tau - \tau')\mathbb{1}^{\mathrm{S}} \otimes \mathbb{1}^{\mathrm{E}}, \tag{5.36}$$

where due to the time-locality only the first type of diagram in Fig. 5.7(a) contributes.

For the next tier, we can again proceed in two equivalent ways. The direct approach inserts Eq. (5.33) into the pasting formula $\Pi_1 = \mathrm{Tr}_{\mathrm{E}} :k_1:(\bullet \otimes \rho^{\mathrm{E}}) :k_1^\dagger:$ to obtain Eq. (5.38) below. Alternatively, one can bypass computing k_1 altogether by computing Σ_1 and then generating Π_1 through the two-branch hierarchy. Using our general functional (5.26b) to compute $\Sigma_1[\sigma_0, \sigma_1]$, only the single pair of diagrams shown in Fig. 5.9 contributes. Its construction from k_0 [Eq. (5.31)] and σ_1 [Eq. (5.32)] is straightforward with the two-branch convolution:

$$\begin{aligned}\int_{\omega_1} \Sigma_{\eta_1\omega_1}(t, t') &= \int_{\omega_1} \Big[(\sigma_{\eta_1\omega_1} \bullet k_0^\dagger) \star (k_0 \bullet \sigma_{\eta_1\omega_1}^\dagger) + (k_0 \bullet \sigma_{\eta_1\omega_1}^\dagger) \star (\sigma_{\eta_1\omega_1} \bullet k_0^\dagger)\Big](t, t, t', t') \\ &= \frac{\Gamma}{2}\bar{\delta}(t - t') d_{\eta_1}^\dagger \bullet d_{\eta_1}.\end{aligned} \tag{5.37}$$

As pointed out above, we are now forced to integrate over the mode energies to exploit the $T \to \infty$ and wideband limit a *second* time. This causes the general functional (5.26) to vastly simplify due to the time-locality of the contractions between the *opposite* time-branches. Equivalent manipulations are also required in the evaluation of the direct approach. Analogous to Eq. (5.33), we can then evaluate the first tier equation (5.17b) without iteration for the conditional propagator:

$$\int_{\omega_1} \Pi_{\eta_1\omega_1}(t) = \Pi_0 * \int_{\omega_1} \Sigma_{\eta_1\omega_1} * \Pi_0(t) = \tfrac{\Gamma}{2} t e^{-iH_\infty t} d_{\eta_1}^\dagger \bullet d_{\eta_1} e^{iH_\infty t}. \tag{5.38}$$

Importantly, the time-convolution produced the linear factor t with a time-scale $\frac{\Gamma}{2} \sim \Sigma_1$.

All higher self-energies identically vanish only when *integrated* over mode energies $\int_{\omega_q \ldots \omega_1} \Sigma_{m_q \ldots m_1} \equiv 0$ for $q \geq 2$ because the $T \to \infty$ and wideband limits suppress vertex corrections generated by contractions between *two branches*. For the q-th tier equation inte-

grated over the energies, only repeated convolutions of Σ_1 remain,

$$\begin{aligned}\Pi_{\eta_q\ldots\eta_1}(t) &:= \int\limits_{\omega_q\ldots\omega_1} \Pi_{\eta_q\omega_q\ldots\eta_1\omega_1}(t) = \Pi_0 * \int\limits_{\omega_q} \Sigma_{\eta_q\omega_q} * \Pi_0 * \ldots * \int\limits_{\omega_1} \Sigma_{\eta_1\omega_1} * \Pi_0(t) \\ &= \int\limits_{\omega_q} \Pi_{\eta_q\omega_q} * \ldots * \int\limits_{\omega_1} \Pi_{\eta_1\omega_1}(t) = K_{\eta_q\ldots\eta_1}(t) \bullet K^\dagger_{\eta_q\ldots\eta_1}(t), \end{aligned} \tag{5.39}$$

where we used $\Pi_0 * \Sigma_1 * \Pi_0 = \Pi_1$ and inserted Eq. (5.38). This agrees with the direct approach which pastes k_m [Eq. (5.34)] to obtain Π_m. For each set of modes *integrated* over their frequencies, we get a *single* Kraus operator:

$$K_{\eta_q\ldots\eta_1}(t) = \sqrt{\frac{(\frac{\Gamma}{2}t)^q}{q!}} e^{(-i\varepsilon d^\dagger d - \frac{\Gamma}{4})t}\, d^\dagger_{\eta_q}\ldots d^\dagger_{\eta_1}. \tag{5.40}$$

Note that the conditional propagator (5.39) is symmetric in the mode-indices as required, whereas the Kraus operators (5.40) themselves are not: Possible signs from permuting the fermionic fields d_{η_i} in the Kraus operators exactly cancel when plugged into the propagator. The *prefactor* $(\frac{\Gamma}{2}t)^q/q!$ is generated *only* in Eq. (5.39) where we integrate over the mode-energies of the inter-branch contractions, i.e., we partially evaluated stage 2. Doing so results in the $\bar{\delta}$-functions (second wideband limit), and the time-ordered integral reduces to $t^q/q!$. As we noted at Eq. (5.34), this *cannot* be seen in k_m or Π_m obtained in stage 1.

Different from the exact study of this model in Ch. 3, we end up with an *infinite* set of Kraus operators (5.40) which in this specific case can be reduced to the finite set (3.38). For this one needs to complete stage 2 by summing over the particle-hole indices η_i:

$$\sum_{q=0}^{\infty}\sum_{\eta_q\ldots\eta_1}\Pi_{\eta_q\ldots\eta_1} = \sum_{q=0}^{\infty}\sum_{\eta_q\ldots\eta_1}\frac{(\frac{\Gamma}{2}t)^q}{q!}e^{-\frac{\Gamma}{2}t}e^{-i\varepsilon t d^\dagger d}\, d^\dagger_{\eta_q}\ldots d^\dagger_{\eta_1}\bullet d_{\eta_1}\ldots d_{\eta_q}e^{+i\varepsilon t d^\dagger d} = e^{\mathcal{L}t}. \tag{5.41}$$

The Kraus operators can then be read of by splitting the strings of field operators d_{η_i} into even and odd contributions in q and employing the Pauli principle. In the present infinite-temperature limit, the series can be explicitly resummed into an exponential with the GKSL generator $\mathcal{L} = -i[\varepsilon d^\dagger d, \bullet] + \frac{\Gamma}{2}\sum_\eta \big(-\frac{1}{2}[d_\eta d^\dagger_\eta, \bullet] + \sum_\eta d^\dagger_\eta \bullet d_\eta\big)$. Although we could have derived this GKSL master equation $\partial_t\rho(t) = \mathcal{L}\rho(t)$ –which is exact for this model, cf. Eq. (3.35)– to more easily obtain the result (5.41), all steps and physical arguments that we discussed can also be applied for *general* evolutions –for which *no* GKSL equation can be derived. Clearly, in the latter case the evaluation steps will be technically more difficult.

Discussion. The two distinct occurrences of the coupling constant Γ in the simple results for the *time-dependence* of the Keldysh operator (5.34) and the Kraus operator (5.40) illustrate the two fundamental stages of the real-time expansion. As we anticipated in Sec. 5.3.2, the physically motivated hierarchy index $m = \eta\omega$ (measurement outcomes) 'counts the powers' in stage 2 of the expansion. This yields the series in powers q of *the prefactor* $\frac{\Gamma}{2}$ in Eq. (5.41) which is CP order-by-order.

The $\frac{\Gamma}{2}$ in the exponential is instead generated in stage 1 and controls how many terms in stage 2 should be kept for a good approximate result. Truncating terms beyond $q = q_{\max}$

introduces a bounded TP error [cf. Sec. 5.3.4],

$$0 \leq 1 - \sum_{q=0}^{q_{\max}} \frac{(\frac{\Gamma}{2}t)^q}{q!} e^{-\frac{\Gamma}{2}t} \leq 1, \tag{5.42}$$

which quantifies the neglected process in which more than $q_{\max}$ interactions with the reservoir took place. The contribution of the q-th order process is maximal for times $\frac{\Gamma}{2}t = q$. Due to the complete positivity of this approximation, the error (5.42) monotonically decreases as $q_{\max}$ is increased. The required value of $q_{\max}$ for the TP error to be negligible depends on the time scale of interest: For $\Gamma t \ll 1$ a small $q_{\max}$ suffices, while for $\Gamma t \gg 1$ a large $q_{\max}$ is required. This is expected since TP guarantees that the $\Pi(t)$ has a stationary state. In contrast, CP tends to be more critical at short times, see the discussion in Sec. 5.1.

Finally, we note that the above illustrates how easily limiting procedures –even in an exactly solvable problem– can hide the CP structure (5.11) of the real-time expansion. We stress that even though the energy integrations –partially accomplishing stage 2– were necessary to analytically solve the problem, they were *never* needed to reveal CP: In our formulation, the conditional propagators have the operator-sum form at each step. Note that Eq. (5.39) written *without* energy integrations requires the higher self energies Σ_m to recover the explicit operator sum $\Pi_m = \mathrm{Tr}_{\mathrm{E}} :k_m:(\bullet \otimes \rho^{\mathrm{E}}) :k_m^\dagger:$. Then, even in this simple model, vertex corrections are relevant and the Σ_m are *not* zero for $m \neq 0, 1$.

5.6 Summary

Measurement-conditioned evolution. In this chapter we studied the dynamics of the reduced density operator $\rho(t) = \Pi(t)\rho(0)$ by combing the operator-sum representation – ubiquitous in quantum-information theory – with the Keldysh real-time expansion of the statistical field theory. We decomposed the reduced evolution Π into elementary conditional evolutions Π_m which are completely positive *because* they correspond to possible measurement outcomes m in a quantum circuit [Fig. 5.1]. This way we recovered the standard real-time expansion in a crucially reorganized two-stage form, revealing it actually consists of two intertwined expansions [Eq. (5.11)]. Based only on fundamental operational principles of measurements, this extends the idea of an expansion in alternating 'life-time broadened evolution' and 'quantum-jumps' to general CP-TP dynamics (2.1), in particular to dynamics that *cannot* be described by GKSL quantum master equations or its generalizations.

Cutting diagrams – unraveling the Schrödinger equation. By cutting the Π_m superoperator diagrams on the Keldysh double-time contour into halves we obtained what we called *Keldysh operators* k_m on a single time branch. These 'lift' the *Kraus operators* $K_m^e(t) = \langle e| :k_m(t): \otimes \mathbb{1}^{\mathrm{P_E}} |0\rangle$ to act on both system *and* environment, encoding their *time-evolution* [Eq. (5.6)] *and* the Wick normal-ordering. From the obtained diagrammatic expansion we inferred memory-kernels for these quantities and derived a hierarchy of self-consistent evolution equations for the Keldysh operators [Eq. (5.19)] . This hierarchy generates time-nonlocal, non-Hamiltonian dynamics on one time branch. The corresponding hierarchy of *kinetic* equations for the Keldysh operators [Eq. (5.22)] constitutes a time-nonlocal unraveling of the Schrödinger equation conditioned on the measurements m. The advantage over the original Schrödinger equation is that these one-branch kinetic equations already explicitly encode the operator-sum decomposition that guarantees CP *before* having integrated out the environment completely.

Pasting diagrams – unraveling the quantum master equation. By pasting the obtained Keldysh / Kraus operator diagrams back together –reconnecting the time branches– we obtained an equivalent self-consistent hierarchy [Eq. (5.17)]. This expresses the operator-sum theorem on the Keldysh real-time contour of statistical field theory. The corresponding hierarchy of *kinetic* equations [Eq. (5.18)] unravels the general (Nakajima-Zwanzig) quantum master equation. We expressed its two-time-branch memory-kernel superoperator explicitly in terms of the one-time-branch memory-kernels of the Keldysh operators that also determine the Kraus operators [Eq. (5.26)]. Irrespective of which approximations to the latter are inserted, a Nakajima-Zwanzig memory-kernel with this functional form generates solutions which are guaranteed to be CP. This puts the celebrated GKSL characterization of time-evolution generators on a more general footing. The tiers of our hierarchies are labeled by a physical quantity, the modes which have interacted with the system as determined by a *possible measurement* on the environment, and *this* guarantees CP order-by-order. We have illustrated how this hierarchy can be truncated based on the dissipative time-scale generated at an earlier stage [Eq. (5.40)]. It is no surprise that our simple rules in general lead to quantities that are difficult to calculate. However, the merit of the approach is that it indicates new routes to systematically address the open problems of devising and comparing CP approximations, improving positivity in existing TP approximations, and further exploring the most challenging issue of CP-TP approximations [32–34, 85]. The very recent advances reported in Ref. [33, 34] indicate that there is still room for further progress.

The role of time. A recurring theme has been the complementarity between the approaches from quantum-information and statistical field theory that we combined. This was not entirely unexpected given the celebrated correspondence between reduced quantum evolutions and bipartite quantum states [170–172]. However, we showed how this entails a duality in approximating reduced time-evolutions –strictly fixing CP tends to uproot TP and *vice versa*– and our two types of self-consistent and kinetic equations explicitly encode this. By descending to the level of the microscopic coupling $V(t)$ –instead of staying on the formal level of the joint unitary $U(t) = Te^{-i\int_0^t d\tau V(\tau)}$– we exposed the crucial role of *time* as the common thread parametrizing both evolution operators and superoperators. The corresponding difference between time-ordering on one and two branches of the Keldysh contour led to two notable mutual insights: On the one hand, the operational (input-output) approach of quantum information theory ignores time and hides the one-branch time-ordering inherited from the unitary U *inside* the Kraus operators. This trivializes the CP structure through the operator-sum theorem, but makes TP seem a nontrivial 'global' constraint in practice. In contrast, the statistical physics approach, formulated on the two branches of the Keldysh contour, trivializes the TP structure because the trace connects the two branches, but thereby makes CP seem a nontrivial 'global' constraint. On the *microscopic* level of the coupling V we found that these two approaches resolve each other's enigmas: The nontrivial TP constraint for Kraus / Keldysh operators living on one time branch is achieved by pairwise cancellations [Eq. (5.13), Fig. 5.5] when considering the double time-branch. Likewise, the nontrivial CP constraint on Keldysh diagrams is achieved by grouping their two-branch diagrams according to one-branch time-ordering [Eq. (5.11), Fig. 5.4(b)].

6 Conclusions and perspectives

The central theme of this work has been the extensive analysis of open-system *dynamics* as derived from microscopic impurity models and guided by crucial insights from the *operational* blackbox understanding of quantum information theory. To conclude the thesis we focus on highlighting the important synergies between quantum information and statistical field theory that have enabled our advances, referring the reader to the summaries in Secs. 3.8, 4.7 and 5.6 for more specific aspects.

6.1 Quantum information concepts in statistical field theory

Throughout the thesis **quantum master equations** have reappeared in various forms as the most common practical tool to describe the effective evolution of an open quantum system's reduced density operator within a field-theoretical treatment. One of the main objectives set out in the introduction has been a deepening of the understanding of quantum master equations beyond the paradigmatic Born-Markov regime governed by the semigroup-divisible GKSL form (1.5). Our efforts in this regard have been threefold:

- **Ch. 3**: To get a clear idea of the issues involved, we studied the noninteracting resonant level model as an instance of an exactly solvable model that features semigroup- and CP-divisible as well as 'truly' non-Markovian dynamics. This allowed us to gain detailed insights into how typical Born-Markov approximations affect the divisibility properties. A surprisingly simple integral relation between the time-nonlocal (Nakajima-Zwanzig) quantum master equation and its time-local (TCL) counterpart was identified. Since the divisibility properties are best analyzed using the latter equation while approximation schemes are more conveniently formulated in the former, this poses an interesting problem for future work: Do similar relations hold in more complicated settings, for example, when multiple reservoirs or local interactions are included? If so, these may be useful for extending the scope of the Born-Markov approximation while preserving complete positivity and trace. Follow-up work by K. Nestmann has very recently confirmed this and we will further comment on this below.

- **Ch. 4**: Going beyond the semigroup-divisible GKSL form can even be relevant in situations where the Born-Markov approximation is generally applicable. For example, an explicit time-dependence due to a modulation of system parameters may also render the dynamics CP-divisible instead of semigroup-divisible. We encountered this situation for periodically driven-dissipative quantum optical systems and developed a formalism that allows for an efficient calculation of the time-periodic steady state. Although we focused on time-local GKSL master equations, the formalism can also be applied to arbitrary time-local master equations with a periodic-in-time generator. Here, an interesting avenue to pursue in future research is the limit of static or ultra-slow modulation beyond GKSL-type time-local master equations. The developed formalism may then serve as a starting point to devise approximation schemes that expand around the steady state.

- **Ch. 5**: To investigate the role of complete positivity in time-nonlocal master equations, we reorganized the real-time diagrammatic perturbation series into a hierarchy of self-consistent Dyson equations that enabled a perturbative diagrammatic calculation of Kraus operators. This inherently enforces the complete positivity of the dynamical

map. Even more, we established the very intricate CP structure of the time-nonlocal memory-kernel in terms of time-nonlocal generators of the Kraus operators. This work provides a novel paradigm for developing CP approximation schemes and allows one to improve or compare with existing ones , see further below in Sec. 6.2.

In these diverse analyses, two fundamental concepts of quantum information theory provided crucial guidance which we believe can also be beneficial for future research along these lines:

The concept of **purification** in the broad sense [Sec. 2.1.1] and Stinespring's dilation theorem [80] as a particular instance [Sec. 2.1.2] have proven to be invaluable tools. It underscores the importance of accounting for how states are *physically* prepared, namely by local unitary operations on parts of globally pure states in larger Hilbert spaces. However, within the information-theoretic formulation, it is not immediately clear how these concepts can be of any use in the computational setting of statistical physics. The previously mentioned DMRG extensions to finite temperatures [81] show that purification ideas can indeed facilitate the numerical analysis of microscopic impurity models. Our work shows that such concepts may also provide crucial analytical insights. One example of this is the case-study of the noninteracting resonant level model in Ch. 3 where the purification of the system and its environment proved to be useful for gaining an intuitive understanding of quantum Markovianity in terms of the divisibility properties of the dynamical map: A *physical* division is only possible if the effective environment can be reinitialized to a pure reference state without disturbing the entanglement between the system and its auxiliary preparation system. This is in close correspondence with being able to recover the initial state of the preparation system by post-processing only the reduced system state [71, 146] –the central problem of quantum communication and error correction schemes where rapid progress is being made. Also the two-stage reorganization of the real-time diagrammatic series in Ch. 5 required a purification not only of the mixed-state environment but also of the dynamical map. The former is achieved by disentangling thermal correlations initially present in the environment from those correlations that develop over time as a consequence of the system-environment coupling. Keeping track of the latter correlations turned out to be a crucial step in the purification of the dynamics and automatically identified groups of real-time diagrams as *physical* processes that are conditional on measurements performed in the effective environment.

Such **conditional system dynamics** forms the second recurring quantum-information concept of this thesis and provides an intuitive understanding of completely positive dynamical maps: Each Kraus operator corresponds exactly to the effective evolution of the open system given the initial and final state of its environment. The converse point is much less appreciated: Knowledge of individual Kraus operators reveals information also about the environment even though it has been traced out. The ignorance of the environment state is reflected in the statistical average of these processes in the Kraus operator-*sum*. The new real-time diagrammatic formulation of Ch. 5 explicitly keeps track of this conditional evolution at each step of the field theoretical calculation. As a result, we not only find diagrammatic representations of Kraus operators as Keldysh real-time diagrams cut in half horizontally. We also derive diagrammatic rules to construct them from a hierarchy of time-nonlocal elementary building blocks that specify their time-dependence. By considering the conditional dynamics as a function of *time* we have thus uncovered a deeper structure of the Kraus operators that is not prominently featured in quantum information theory.

6.2 Consistent approximations beyond Born-Markov

The general formalism developed in Ch. 5 has established a new foundation for devising approximations beyond Born-Markov that are consistent with the complete positivity property. Preserving this property is central to quantum information theory and allows one to apply its techniques to open-system dynamics which our case study in Ch. 3 demonstrated to lead to interesting new insights. To achieve this also for the models of primary interest in statistical physics that are not exactly solvable, numerous further questions need to be addressed. Here, we collect these issues, some of which have already been mentioned earlier:

(a) For instance, we have only considered the case of initially factorizing system-environment states that guarantee the complete positivity of the dynamical map, cf. the discussion in Sec. 1.1. Other methods exist that also take into account correlated initial states while maintaining this important property. In this regard, the superchannel formalism [66, 168] is an interesting avenue which similarly focuses on the operational understanding of the dynamics by taking into account the preparation, control, and measurement apparatus in experimental realizations of open systems. It is however not yet clear how field-theoretical methods similar to those of Ch. 5 can be used within this formalism or how it relates to Refs. [32–34, 85].

(b) A detailed case study of more realistic impurity models that either involve interacting levels or multiple reservoirs could further elucidate the impact of approximations on divisibility properties. For instance, how do nonequilibrium stationary states supporting finite transport currents influence the divisibility? The investigation of local interactions can be accomplished with real-time renormalization group (RT-RG) techniques that take the noninteracting limit as a reference solution. An intriguing question is how the exact RT-RG hierarchy encodes the complete positivity of the dynamics. Unraveling this requires a nontrivial translation of double-branch Keldysh diagrams to single-branch Liouville-space diagrams.

(c) In our applications, we employed the wideband-limit which leads to drastic simplifications especially for fermionic systems. It is known that in this limit there exists a fermionic duality [197] which relates the left and right eigenvectors of the dynamical map by parity-conjugation and an inversion of energy-parameters. Very recent results by V. Bruch for the resonant level model of Ch. 3 indicate that this 'symmetry' can also be identified on the level of the time-local generators and the Kraus operators. Yet, an interesting open question is how the duality is reflected in the real-time Kraus operator formalism we developed in Ch. 5. To see this, the wideband-limit needs to be explicitly evaluated in this new formulation. If this can be achieved, it will also make this formalism more effective in applications since many diagrammatic contributions can then be discarded from scratch as known from the double-branch formulation.

(d) Although Ch. 5 pinned down the issue of preserving complete positivity in approximations, it did not yet address the divisibility criteria we have been concerned with in Ch. 3. This requires a conversion of the insights about the CP structure of the time-nonlocal memory-kernel to general properties of the time-local generator in order to make use of the semigroup- and CP-divisibility results. Establishing a relation to *time-dependent* GKSL quantum master equations would also be of great practical interest. For example, the 'Markov-only' approximation that we identified strictly

produces a completely positive and trace-preserving dynamical map, despite its non-perturbative nature in the coupling. An expansion around this approximation could be attempted to incorporate non-Markovian effects, but it is unclear whether such an expansion is most easily formulated on the level of the time-local TCL generator or the time-nonlocal Nakajima-Zwanzig memory-kernel. This is because the equivalence of the stationary-state time-local kernel and the zero-frequency time-nonlocal kernel noticed in the resonant level model of Ch. 3 does not hold in general. Despite their generally nontrivial relation [272], it has very recently been shown by K. Nestmann that their zero right-eigenvectors always coincide and that one can devise an expansion of the much more complicated time-local kernel in terms of the time-nonlocal one which explicitly preserves the correct stationary state. If this can be translated into a Keldysh diagrammatic expansion, then the insights of Ch. 3 can also be applied to this problem.

(e) For the above efforts, a better understanding of the CP-TP duality encountered in Sec. 2.3.1 and that repeatedly appeared in Ch. 5 will be helpful: Within our framework, fixing the complete positivity of the dynamical map seems incompatible with simultaneously fixing trace-preservation. That this is in general *not* a dead end, is already clear from the Born-Markov approximation that manages to preserve both properties. Here, the key observation is that the Born-Markov approximation involves more than a first-order expansion in the system-environment coupling: The Markov approximation requires one to also modify integration boundaries in the time-nonlocal master equations. Instead, our considerations of approximation schemes were so far solely based on real-time diagram selection without such modifications. If this fact is overlooked, one would conclude that our results are inconsistent with the recent, closely related formalism that actually rigorously fixes both CP and TP within a perturbative treatment [32–34]. There, an equivalent hierarchy of CP dynamical maps is presented but the proposed approximation scheme involves an ingenious new type of 'factorization' of the dynamical map. An immediate question to follow up on is how this factorization scheme can be employed *diagrammatically* to rigorously fix not only complete positivity but also trace-preservation. For this one must allow for both a diagrammatic selection as well as a modification of the functional form of the perturbation series by relaxing the diagram rules.

A final remark should be made about a common misconception about formulating such advanced approximation schemes that arises from the different priorities in quantum information and statistical field theory: The former is interested in *consistent* approximations and has accordingly developed many techniques that focus on the fundamental physical *properties* of the dynamical map such as time-local quantum master equations of GKSL form and the Kraus operator-sum. In doing so, the details of a microscopic model are often neglected or oversimplified for the sake of making general statements. In contrast, the latter is first and foremost interested in *accurate* approximations that correctly reproduce certain *observables*, and their methods are geared towards achieving this in a systematic way, for instance in terms of time-nonlocal Nakajima-Zwanzig quantum master equations. The accuracy however often depends on the specific observable in mind and might lead to inconsistent results for others. In this sense, quantum information and statistical field theory employ complementary approximation paradigms, each with its own challenges. The CP-TP duality is a manifestation of the fact that the ideal scenario of consistent *and* accurate approximations where both views coincide is generically difficult to formulate but has been constructively proven possible [32–34]. The key virtue of combining the complementary views is that well-defined

physical quantities of quantum information theory become accurately accessible in a field-theoretical analysis without sacrificing model details as we practically demonstrated in Ch. 3 for a simple case study.

A Derivations of the resonant-level solution

In this appendix, we collect the explicit derivations of the dynamical map $\Pi(t)$ for the resonant level model of Ch. 3, where we employ three different approaches –Heisenberg equations of motion [Sec. 3.3], real-time superfermions [Sec. 3.4] and the Kraus operator-sum [Sec. 3.5]– each highlighting a different aspect of the open system's dynamics.

Publications and acknowledgments. This appendix collects substantial parts of the Apps. B [A.1], D [A.2], and E [A.3] published in V. Reimer, M. R. Wegewijs, K. Nestmann, and M. Pletyukhov, The Journal of Chemical Physics **151**, 044101 (2019) [Copyright 2019 by the American Institute of Physics], see Ref. [134], while other parts have been absorbed into the main Ch. 3 to better adapt to the thesis.

A.1 Equations of motion approach

A.1.1 Derivation

We first discuss the steps leading to the exact EOMs (3.10) for the environment-averaged system-observables constituting the dynamical map $\Pi(t)$, highlighting the correspondence to the real-time superfermion approach of Sec. 3.4. In particular, the specific superoperator structure of the latter approach clearly separates the steps in the derivation that need to be applied repeatedly in the EOM calculation.

Field evolution. The equation of motion for Heisenberg operators (distinguished only by the time-argument) for the reservoir fields,

$$\frac{d}{dt}b_{\eta\omega}(t) = i\eta\omega b_{\eta\omega}(t) + i\eta\sqrt{\frac{\Gamma}{2\pi}}d_\eta(t), \tag{A.1}$$

couples to the system fields via the second inhomogeneous term. The exact solvability follows from the linearity of this coupling, in contrast to the real-time approach where this is seen only *at the end* in form of the superfermion property (3.31). Integration of Eq. (A.1) expresses the field dynamics as free, time-local evolution in the system superposed with time-nonlocal dynamics resulting from tunneling at time τ and subsequent free evolution in the reservoir:

$$b_{\eta\omega}(t) = e^{i\eta\omega t}b_{\eta\omega} + i\eta\sqrt{\frac{\Gamma}{2\pi}}\int_0^t d\tau e^{i\eta\omega(t-\tau)}d_\eta(\tau). \tag{A.2}$$

However, inserting this into the EOM for the *system* fields gives a *time-local* equation,

$$\begin{aligned}\frac{d}{dt}d_\eta(t) &= i\eta\varepsilon d_\eta(t) + i\eta\sqrt{\frac{\Gamma}{2\pi}}\int d\omega b_{\eta\omega}(t) \\ &= i\eta\left(\varepsilon + i\eta\frac{\Gamma}{2}\right)d_\eta(t) + i\eta\sqrt{\frac{\Gamma}{2\pi}}\int d\omega e^{i\eta\omega t}b_{\eta\omega},\end{aligned} \tag{A.3}$$

since the energy-integration in the last term yielded a factor $\frac{1}{2}\times 2\pi\delta(t-\tau)$ due to the wide-band limit, noting that the time integrations run over the real *half*-axis, cf. the discussion

after Eq. (3.19a). As before, we can integrate this differential equation to

$$d_\eta(t) = e^{(i\eta\varepsilon-\frac{\Gamma}{2})t}d_\eta + i\eta\sqrt{\frac{\Gamma}{2\pi}}\int d\omega\int_0^t d\tau e^{(i\eta\varepsilon-\frac{\Gamma}{2})(t-\tau)}e^{i\eta\omega t}b_{\eta\omega}. \tag{A.4}$$

Relative to the free case, the system fields have acquired a dissipative renormalization $\frac{\Gamma}{2}$ in the exponent which corresponds to the solution of the infinite-temperature limit in the first stage of the real-time approach. Partial averaging over the initial reservoir state, we get rid of the reservoir part and obtain the *time-local* EOM (3.10a) for the field:

$$\frac{d}{dt}\langle d_\eta(t)\rangle^{\mathrm{E}} = \left(i\eta\varepsilon - \tfrac{1}{2}\Gamma\right)\langle d_\eta(t)\rangle^{\mathrm{E}}. \tag{A.5}$$

Note that no temperature-dependence has arisen yet even though we averaged over the equilibrium reservoir. Furthermore, the initial superselection, $\langle d_\eta(0)\rangle = 0$, is preserved by the dynamics. This does however *not* mean that the field amplitudes can be eliminated from the beginning: They are crucial for obtaining the dissipative renormalization factors $e^{-\frac{\Gamma}{2}t}$.

Occupations, parity and identity. To complete the operator-basis in the decomposition (3.6), we need two additional *system* operators. Their EOMs (3.10b) however do not require new equations because they follow by applying the product rule to the EOMs (A.3) and partially averaging only *afterwards*. A common choice –when using Green's functions– is to take the orthogonal system particle- and hole-occupation operators:

$$\begin{aligned}\frac{d}{dt}\left[d_\eta(t)d_{\bar\eta}(t)\right] &= \frac{d}{dt}\left[d_\eta(t)\right]d_{\bar\eta}(t) + d_\eta(t)\frac{d}{dt}\left[d_{\bar\eta}(t)\right] \\ &= -\Gamma d_\eta(t)d_{\bar\eta}(t) + \sqrt{\frac{\Gamma}{2\pi}}\int d\omega\left(i\eta e^{i\eta(\omega-\varepsilon+i\eta\frac{\Gamma}{2})t}b_{\eta\omega}d_{\bar\eta} + \mathrm{h.c.}\right) \\ &\quad + \frac{\Gamma}{2\pi}\int d\omega\int d\omega'\int_0^t dt'\left(e^{i\eta(\omega-\varepsilon+i\frac{\Gamma}{2})(t-t')}e^{i\eta(\omega t-\omega' t')}b_{\eta\omega}b_{\bar\eta\omega'} + \mathrm{h.c.}\right)\mathbb{1}.\end{aligned} \tag{A.6}$$

Partial-averaging causes all terms with a single reservoir field to vanish identically and due to Eq. (3.9) only a single energy-integral over $\omega = \omega'$ remains:

$$\begin{aligned}\frac{d}{dt}\langle d_\eta(t)d_{\bar\eta}(t)\rangle^{\mathrm{E}} &= -\Gamma\langle d_\eta(t)d_{\bar\eta}(t)\rangle^{\mathrm{E}} + \frac{\Gamma}{\pi}\int d\omega\int_0^t dt' e^{-\frac{\Gamma}{2}(t-t')}f(\eta\omega)\cos\left[(\omega+\mu-\varepsilon)(t-t')\right]\mathbb{1} \\ &= -\Gamma\langle d_\eta(t)d_{\bar\eta}(t)\rangle^{\mathrm{E}} - \tfrac{\Gamma}{2}[1-\eta\int_0^t d\tau e^{-\frac{\Gamma}{2}(t-t')}\gamma(t-t')]\mathbb{1}.\end{aligned} \tag{A.7}$$

Only at this step finite temperature effects have been accounted for through the second term containing the reservoir distribution function $f(\eta\omega) = (e^{\eta\omega/T}+1)^{-1} = \frac{1}{2} - \frac{\eta}{2}\tanh\left(\frac{\omega}{2T}\right)$ which we decomposed as in Eq. (3.9). This is similar to the second stage of summing the renormalized perturbation series in the real-time approach in Sec. 3.4. Finally, by taking the difference of Eq. (A.7) for $\eta = \mp$, one obtains the EOM (3.10b) given in the main text for the parity $(-\mathbb{1})^n = -\sum_\eta \eta d_\eta d_{\bar\eta}$. Summing Eq. (A.7) over $\eta = \pm$ verifies that the dynamics is trace-preserving $\langle\mathbb{1}(t)\rangle^{\mathrm{E}} = \mathbb{1}$.

A.1.2 Time-local quantum master equation

We noted that for our model the EOM approach naturally leads to *time-local* equations. In the above derivation, Eq. (A.5) and (A.7) are already time-local, in particular because

in Eq. (A.6) and Eq. (A.7) the operator $\mathbb{1}$ is t'-independent. To derive a corresponding time-local QME (3.44) for $\rho(t)$ we need compute the inverse appearing in the generator $-iL + \Sigma^{\mathrm{TCL}}(t) = [\frac{d}{dt}\Pi(t)]\Pi(t)^{-1}$. Both the derivative and the inverse are easily constructed from the spectral decomposition (3.16b) of the EOM solution:

$$-iL + \Sigma^{\mathrm{TCL}}(t) = \sum_{\eta} (i\eta\varepsilon - \tfrac{\Gamma}{2}) \left|d_\eta^\dagger\right) \left(d_\eta^\dagger\right| - \tfrac{\Gamma}{2} \left|(-\mathbb{1})^n\right) \Big[\left((-\mathbb{1})^n\right| - h(t) \left(\mathbb{1}\right| \Big]. \tag{A.8}$$

This is equivalent to the spectral decomposition (3.49) given in the main text, while the representation (3.44b) of the generator, $\Sigma^{\mathrm{TCL}}(t) = \frac{\Gamma}{2} \sum_\eta [1 - \eta h(t)]\, \mathcal{L}_\eta$, is obtained from

$$\mathcal{L}_\eta = d_\eta \bullet d_{\bar\eta} - \tfrac{1}{2}[d_{\bar\eta} d_\eta, \bullet]_+ = -\tfrac{1}{2} \left\{ \sum_{\eta'} \left|d_{\eta'}^\dagger\right) \left(d_{\eta'}^\dagger\right| + \left|(-\mathbb{1})^n\right) \Big[\left((-\mathbb{1})^n\right| + \eta \left(\mathbb{1}\right| \Big] \right\}. \tag{A.9}$$

A.1.3 Relation to the time-nonlocal quantum master equation

Finally, we show how the general expression (3.45b) for the time-local generator $\Sigma^{\mathrm{TCL}}(t)$ in terms of the time-nonlocal memory-kernel $\Sigma(t-t')$ is consistent with the relation (3.45a):

$$\Sigma^{\mathrm{TCL}}(t) = \int_0^t dt' \Sigma(t-t') \Pi(t') \Pi^{-1}(t) \stackrel{?}{=} \int_0^t ds \Sigma(s).$$

This relation surprisingly holds for our model despite $\Pi(t')\Pi^{-1}(t) \neq \mathcal{I}$. Using the spectral decomposition (3.16b) one finds

$$\begin{aligned} \Pi(t')\Pi^{-1}(t) &= \sum_{k=1}^{4} \frac{\Pi_{k'}(t')}{\Pi_k(t)} \left|m_{k'}(t')\right) \left(a_{k'}(t')|m_k(t)\right) \left(a_k(t)\right| \\ &= \sum_{k=1}^{4} \left|m_k(t')\right) \left(a_k(t)\right| + e^{-\Gamma t} \tfrac{1}{2}[g(t) - g(t')] \left|m_4(t')\right) \left(a_1(t)\right|. \end{aligned} \tag{A.10}$$

This superoperator would map the right eigenvectors at time t to those at time t' if the second term of Eq. (A.10) were not present. However, when the memory kernel (3.42b), rewritten in supervector form using Eq. (A.9),

$$\Sigma(s) = -\frac{\Gamma}{2} \left\{ \Big[\sum_\eta \left|d_\eta^\dagger\right) \left(d_\eta^\dagger\right| + \left|(-\mathbb{1})^n\right) \left((-\mathbb{1})^n\right| \Big] \bar\delta(s) - e^{-\frac{\Gamma}{2}s} \gamma(s) \left|(-\mathbb{1})^n\right) \left(\mathbb{1}\right| \right\}, \tag{A.11}$$

acts on this term from the left, it has no effect: The first term in $\Sigma(t-t')$ nullifies it due to $\bar\delta(t-t')$ and so does the second term because of $(a_1|m_k) = \delta_{1,k}$, see Table 3.1. For the same reasons, we can set $t = t'$ also in the first term of Eq. (A.10), reducing it to the identity since $\sum_{k=1}^4 \left|m_k(t)\right) \left(a_k(t)\right| = \mathcal{I}$. We thus find $\Sigma(t-t')\Pi(t')\Pi^{-1}(t) = \Sigma(t-t')$ for all t, t' as claimed in the main text, see also App. A.2.3.

A.2 Real-time superfermion approach

A.2.1 Derivation

We now discuss the direct summation of the perturbation series in two stages using the superfermion formalism employed in Sec. 3.4.1. This Liouville-space formulation is in principle equivalent to the Keldysh real-time diagrammatic series of Sec. 2.2.2 but differs in so far as that $\Pi(t) = \mathrm{Tr}_{\mathrm{E}}\{e^{-iL^{\mathrm{tot}}t}(\bullet \otimes \rho^{\mathrm{E}})\}$ is exppressed in terms of the Liouvillian superoperator $L^{\mathrm{tot}} := [H^{\mathrm{tot}}, \bullet]_-$ given by Eq. (3.29). Its expansion in the system-environment coupling,

$$\Pi(t) = \left\langle \hat{T} e^{-i\int_0^t L^V(s)} \right\rangle^{\mathrm{E}} = \sum_{k=0}^{\infty} \left\langle \left[(\mathcal{I} * (-iL^V) *)^k \, \mathcal{I} \right](t) \right\rangle^{\mathrm{E}}, \tag{A.12}$$

thus collapses the two branches of the Keldysh contour, each representing the separate expansion [Eq. (2.15a)] of the unitary $U(t) = e^{-iH^{\mathrm{tot}}t}$ and its adjoint $U(t)^\dagger$, onto a single branch. As usual, time-convolutions are denoted by $[A*B](t) \equiv \int_0^t d\tau A(t-\tau)B(\tau)$ and $\langle\circ\rangle^{\mathrm{E}} = \mathrm{Tr}_{\mathrm{E}} \circ \rho^{\mathrm{E}}$ is evaluated by Wick contractions. The free uncoupled evolution $\pi(t) = \mathcal{I}$ reduces to the identity superoperator in the interaction picture $L^V(\tau) := e^{iL^0\tau} L^V e^{-iL^0\tau}$ which we only indicate by time-arguments throughout this appendix. For this noninteracting model, the coupling Liouvillian $L^V = \sum_{q=\pm} L^{Vq}$ acquires a mere phase factor from the interaction picture,

$$L^{Vq}(\tau) = \sum_{\eta} \sqrt{\frac{\Gamma}{2\pi}} \int d\omega e^{i\eta(\omega-\varepsilon)\tau} J^q_{\eta\omega} G^{\bar{q}}_{\bar{\eta}}, \tag{A.13}$$

and the Wick contractions (3.34) can be written as:

$$\langle L^{V+}(\tau) L^{Vq}(\tau')\rangle^{\mathrm{E}} = \tfrac{\Gamma}{2} \sum_{\eta} \left[\bar{\delta}(\tau-\tau')\delta_{q,-} + \eta\gamma(\tau-\tau')\delta_{q,+}\right] G^+_\eta G^q_{\bar{\eta}}. \tag{A.14}$$

Stage one. For $\Pi_\infty(t) := \lim_{T\to\infty} \Pi(t)$ only contractions between pairs of *different* coupling components $L^{V+} \propto G^+$ and $L^{V-} \propto G^-$ –in this order– are nonzero in Eq. (A.12). Since these are time-local, all convolutions trivialize to products, leaving an ordinary power series

$$\Pi_\infty(t) = \mathcal{I} - \int\limits_{t\geq t_2\geq t_1\geq 0} dt_2 dt_1 \langle L^{V+}(\tau) L^{V-}(\tau')\rangle^{\mathrm{E}} + \ldots = \mathcal{I} + \hat{\Sigma}_\infty t + \ldots = e^{\hat{\Sigma}_\infty t} \tag{A.15}$$

with the *equal-time* correlator $\hat{\Sigma}_\infty := -\frac{\Gamma}{2}\sum_\eta G^+_\eta G^-_{\bar{\eta}}$ as the basic building block. It useful to note that $\mathcal{N} = \sum_\eta G^+_\eta G^-_{\bar{\eta}}$ counts the number of superfermions of its argument and with $G^+_\eta G^+_{\bar{\eta}} \Pi_\infty(t) = G^+_\eta G^+_{\bar{\eta}}$ due to the Pauli principle (3.31) gives rise to the relations

$$G^+_\eta \Pi_\infty(t) G^+_{\bar{\eta}} = e^{-\frac{\Gamma}{2}t} G^+_\eta G^+_{\bar{\eta}} \Pi_\infty(t) = e^{-\frac{\Gamma}{2}t} G^+_\eta G^+_{\bar{\eta}} \tag{A.16a}$$

$$\Pi_\infty(t) G^+_\eta G^+_{\bar{\eta}} = e^{-\Gamma t} G^+_\eta G^+_{\bar{\eta}} \Pi_\infty(t) = e^{-\Gamma t} G^+_\eta G^+_{\bar{\eta}}. \tag{A.16b}$$

Stage two. For finite temperatures T the expansion (A.12) contains additional *time-nonlocal* contractions between pairs of couplings of the same type $L^{V+} \propto G^+$. In between these pairs, the time-local infinite-temperature contributions already summed up in $\Pi_\infty(t)$

may still appear but these produce a simple decaying term due to the relations (A.16). More importantly, the Pauli principle (3.31) causes all contributions beyond first order in the time-nonlocal contraction to vanish identically:

$$\Pi(t) = \Pi_\infty(t) - \int\limits_{t\geq t_2\geq t_1\geq 0} dt_2 dt_1 \Pi_\infty(t-t_2)\,\langle L^{V+}(t_2)\Pi_\infty(t_2-t_1)L^{V+}(t_1)\rangle^{\mathrm{E}}\,\Pi_\infty(t_1) + \ldots \quad \text{(A.17a)}$$

$$= \Pi_\infty(t) - \int\limits_{t\geq t_2\geq t_1\geq 0} dt_2 dt_1 e^{-\Gamma(t-t_2)}\langle L^{V+}(t_2)e^{-\frac{\Gamma}{2}(t_2-t_1)}L^{V+}(t_1)\rangle^{\mathrm{E}} \quad \text{(A.17b)}$$

$$= \Pi_\infty(t) - \int\limits_{t\geq t_2\geq t_1\geq 0} dt_2 dt_1 e^{-\Gamma(t-t_2)}e^{-\frac{\Gamma}{2}(t_2-t_1)}\tfrac{\Gamma}{2}\gamma(t_2-t_1)\sum_\eta \eta G_\eta^+ G_{\bar\eta}^+ \quad \text{(A.17c)}$$

$$= \Pi_\infty(t) - \tfrac{1}{2}(1-e^{-\Gamma t})g(t)\sum_\eta \eta G_\eta^+ G_{\bar\eta}^+. \quad \text{(A.17d)}$$

In the final step we identified the function $g(t)$ from Eqs. (3.14) and (3.11). The renormalized series thus *terminates* as claimed in the main text. Reverting to the Schrödinger picture we obtain Eq. (3.36a). The exponential form (3.36b) then follows from employing Eq. (A.16) to write the finite-temperature term in Eq. (A.17d) as a *factor*:

$$\Pi(t) = \Big[\mathcal{I} - \tfrac{1}{2}(1-e^{-\Gamma t})g(t)\sum_\eta \eta G_\eta^+ G_{\bar\eta}^+\Big]\Pi_\infty(t) = e^{-\frac{1}{2}(1-e^{-\Gamma t})g(t)\sum_\eta \eta\mathcal{L}_\eta}\, e^{\hat\Sigma_\infty t} \quad \text{(A.18a)}$$

$$= e^{\frac{\Gamma}{2}t\sum_\eta[1-\eta g(t)]\mathcal{L}_\eta}. \quad \text{(A.18b)}$$

Written as an exponential it can be merged with $\Pi_\infty(t) = e^{\hat\Sigma_\infty t}$ using the Baker-Campbell-Hausdorff identity $e^X e^Y = e^{Y+\phi/(1-e^{-\phi})X}$ for operators obeying $[X,Y]_- = \phi X$ which results in Eq. (A.18b). Transformation to Schrödinger picture $\Pi(t) \to e^{-iLt}\Pi(t)$ gives Eq. (3.36b) of the main text due the identity $[L, G_\eta^+ G_{\bar\eta}^\pm]_- = 0$.

We finally show how the divisor $\Pi(t,t')$ follows from this approach. To this end, we determine a function $\alpha(t,t')$ such that the divisor retains the same form as $\Pi(t)$:

$$\Pi(t,t') = \Pi_\infty(t-t') + \alpha(t,t')\sum_\eta \eta G_\eta^+ G_{\bar\eta}^+. \quad \text{(A.19)}$$

Inserting this ansatz into the divisor equation $\Pi(t) = \Pi(t,t')\Pi(t')$ and using the Pauli principle (3.31) as well as Eq. (A.16), one finds a unique solution by comparing coefficients:

$$\begin{aligned}\alpha(t,t') &= \tfrac{1}{2}(1-e^{-\Gamma t})g(t) - \tfrac{1}{2}(1-e^{-\Gamma t'})g(t')e^{-\Gamma(t-t')} \\ &= \int_{t'}^{t} ds\, e^{-\Gamma(t-s)}h(s) \equiv (1-e^{-\Gamma(t-t')})g(t,t'). \end{aligned} \quad \text{(A.20)}$$

Here, the integral relation (3.14) allows one to merge the two terms to recover the EOM result (3.17) for $g(t,t')$. This justifies the explicit construction (3.37) of the divisor within the real-time approach.

A.2.2 Time-nonlocal quantum master equation

To derive the time-nonlocal QME (3.42a) within the real-time approach, we note that both stages can be written as self-consistent Dyson equations of the type (2.16). First, the infinite-

temperature limit (A.15) can be expressed in terms of a Dyson equation with a time-local memory-kernel,

$$\Pi_\infty(t) = \mathcal{I} + [\mathcal{I} * \Sigma_\infty * \Pi_\infty](t) \tag{A.21}$$
$$\Sigma_\infty(t-t') := -\langle L^{V+}(t) L^{V-}(t')\rangle^{\mathrm{E}} = -\tfrac{\Gamma}{2}\bar{\delta}(t-t')\sum_\eta G^+_\eta G^-_{\bar{\eta}},$$

which features the equal-time correlator $\hat{\Sigma}_\infty = -\frac{\Gamma}{2}\sum_\eta G^+_\eta G^-_{\bar{\eta}}$ introduced earlier. The infinite-temperature limit then feeds into the self-consistent form of Eq. (A.17a) where the memory-kernel is time-nonlocal:

$$\Pi(t) = \Pi_\infty(t) + [\Pi_\infty * \Delta\Sigma * \Pi](t) \tag{A.22}$$
$$\Delta\Sigma(t-t') := -\langle L^{V+}(t)\Pi_\infty(t-t')L^{V+}(t')\rangle^{\mathrm{E}} = -e^{-\frac{\Gamma}{2}(t-t')}\tfrac{\Gamma}{2}\gamma(t-t')\sum_\eta \eta G^+_\eta G^+_{\bar{\eta}}.$$

To get to Eq. (A.22) we used that higher orders $[\Delta\Sigma * \Pi_\infty *]^k = 0$ for $k = 2, 3, \ldots$ are zero in our model by the Pauli principle (3.31) and may thus be added on the right hand side to complete $\Pi_\infty(t)$ to $\Pi(t)$. This argument may be repeated to simplify the two coupled QMEs obtained as the time-derivatives of the above Dyson equations and combine them into the single time-nonlocal QME

$$\tfrac{d}{dt}\Pi(t) = \Sigma * \Pi(t), \qquad \Sigma(t) = \Sigma_\infty(t) + \Delta\Sigma(t). \tag{A.23}$$

The memory-kernel $\Sigma(t)$ is thus given by the sum of the time-local infinite-temperature kernel of (A.21) and the time-nonlocal finite-temperature kernel of (A.22). Converted to the Schrödinger picture, this is Eq. (3.42) of the main text. The Laplace transform $\Sigma(z) = \int_0^\infty dt e^{izt}\Sigma(t)$ discussed in Eq. (3.43) of the main text

$$\begin{aligned}\Sigma(z) &= \tfrac{\Gamma}{2}\sum_\eta \int_0^\infty ds e^{izs}\Big[\bar{\delta}(s) - \eta e^{-\frac{\Gamma}{2}s}\gamma(s)\Big]\mathcal{L}_\eta \\ &= \tfrac{\Gamma}{2}\sum_\eta \left[1 + i\frac{\eta}{\pi}\sum_{\chi=\pm}\chi\psi\left(\frac{1}{2} + \frac{\frac{\Gamma}{2} - i(z-\chi\epsilon)}{2\pi T}\right)\right]\mathcal{L}_\eta,\end{aligned} \tag{A.24}$$

is obtained by an integration analogous to the one performed in the derivation (B.10) of the closed form of the function $g(t)$:

$$\begin{aligned}\int_0^\infty ds e^{izs}e^{-\frac{\Gamma}{2}s}\gamma(s) &= i\,2T\sum_{\chi=\pm}\sum_{n=0}^\infty \chi\int_0^\infty ds e^{-[\pi T(2n+1)+\frac{\Gamma}{2}+i(\chi\epsilon-z)]s} \\ &= -\frac{i}{\pi}\sum_{\chi=\pm}\sum_{n=0}^\infty \frac{\chi}{n+\frac{1}{2}+\frac{\frac{\Gamma}{2}+i(\chi\epsilon-z)}{2\pi T}}.\end{aligned} \tag{A.25}$$

A.2.3 Relation to the time-local quantum master equation

We conclude with the conversion of the time-nonlocal QME (A.23) to the time-*local* QME (3.44) in the main text, avoiding an explicit calculation of the inverse $\Pi(t)^{-1}$ that is required

in the EOM approach [App. A.1.2]:

$$\tfrac{d}{dt}\Pi(t) = \int_0^t dt\Sigma(t-t')\Pi(t') \stackrel{!}{=} \left[\int_0^t dt'\Sigma(t-t')\right]\Pi(t) = \Sigma^{\mathrm{TCL}}(t)\Pi(t). \tag{A.26}$$

As stressed in the main text [Eq. (3.45a) ff.] this is an *exact* relation for our model as $\Sigma(t-t')\Pi(t') = \Sigma(t-t')\Pi(t)$. We can directly see this by splitting off the corrections Δ to the infinite-temperature limit in both the propagator $\Pi(t) = \Pi_\infty(t) + \Delta\Pi(t)$ and the memory-kernel $\Sigma(t) = \Sigma_\infty(t) + \Delta\Sigma(t)$. These are proportional to $\sum_\eta \eta G_\eta^+ G_\eta^+$ which causes the t'-dependence of $\Pi(t')$ to completely drop out: In the infinite-temperature terms, the time-argument is irrelevant due to the time-locality,

$$\Sigma_\infty(t-t')\Pi(t') = \Sigma_\infty(t-t')\Pi(t), \tag{A.27a}$$

whereas for the finite-temperature corrections, the relations (A.16) together with the Pauli principle (3.31) cause the time-dependence to drop out:

$$\Delta\Sigma(t-t')\Pi_\infty(t') = \Delta\Sigma(t-t'), \quad \Delta\Sigma(t-t')\Delta\Pi(t') = 0. \tag{A.27b}$$

A.3 Kraus operator-sum representation

To derive the Kraus operator sum (3.38) of the main text it is instructive to start from the spectral decomposition (3.16b) in super-braket notation repeated here for clarity:

$$\Pi(t) = \sum_\eta e^{(i\eta\varepsilon - \frac{1}{2}\Gamma)t} \left|d_\eta^\dagger\right) \left(d_\eta^\dagger\right| \tag{A.28a}$$

$$+ e^{-\Gamma t}\tfrac{1}{2} \left|(-\mathbb{1})^n\right) \Big[\left((-\mathbb{1})^n\right| - g(t) \left(\mathbb{1}\right| \Big] \tag{A.28b}$$

$$+ \tfrac{1}{2}\Big[\left|\mathbb{1}\right) + g(t) \left|(-\mathbb{1})^n\right) \Big] \left(\mathbb{1}\right|. \tag{A.28c}$$

As noted in Sec. 2.3.1, the Choi-operator (2.18) mixes up the elements of this spectral decomposition. Already the preparatory conversion of these three terms into a left-right action,

$$\Pi(t) = e^{-\frac{1}{2}\Gamma t} \sum_\eta \Big[e^{-i\eta\varepsilon t} \left|\eta\right\rangle \left\langle\eta\right| \bullet \left|\bar\eta\right\rangle \left\langle\bar\eta\right| \tag{A.29a}$$

$$+ \left(\cosh\tfrac{\Gamma t}{2} - \eta g(t) \sinh\tfrac{\Gamma t}{2}\right) \left|\eta\right\rangle \left\langle\eta\right| \bullet \left|\eta\right\rangle \left\langle\eta\right| \tag{A.29b}$$

$$+ \left(1 - \eta g(t) \sinh\tfrac{\Gamma t}{2}\right) \left|\eta\right\rangle \left\langle\bar\eta\right| \bullet \left|\bar\eta\right\rangle \left\langle\eta\right| \Big], \tag{A.29c}$$

by representing the fields $d_\eta = \left|\eta\right\rangle \left\langle\bar\eta\right|$ and $d_\eta d_{\bar\eta} = \left|\eta\right\rangle \left\langle\eta\right|$ in terms of ordinary brakets, mixes the different spectral components of $\Pi(t)$. In particular, Eq. (A.28b)-(A.28c) together produce the third term (A.29c). The Choi-operator is constructed from this form by replacing basis superoperators with corresponding basis operators, $\mathrm{choi}[\left|\eta\right\rangle \left\langle\eta'\right| \bullet \left|\chi\right\rangle \left\langle\chi'\right|] = \left|\eta\eta'\right\rangle \left\langle\chi'\chi\right|$, which

$\sum_{\eta=\pm}\Big[K^0_\eta(t)^\dagger K^0_\eta(t)+K^1_\eta(t)^\dagger K^1_\eta(t)\Big]=\mathbb{1}$	$\sum_{\eta=\pm}K^0_\eta(t)^\dagger d^\dagger_{\eta'}K^0_\eta(t)=e^{(i\eta\varepsilon-\Gamma/2)t}d^\dagger_{\eta'}$
$\sum_{\eta=\pm}\Big[K^0_\eta(t)K^0_\eta(t)^\dagger+K^1_\eta(t)K^1_\eta(t)^\dagger\Big]=\mathbb{1}+(1-e^{-\Gamma t})g(t)(-\mathbb{1})^n$	$\sum_{\eta=\pm}K^0_\eta(t)d^\dagger_{\eta'}K^0_\eta(t)^\dagger=e^{(-i\eta\varepsilon-\Gamma/2)t}d^\dagger_{\eta'}$
$\sum_{\eta=\pm}\Big[K^0_\eta(t)K^0_\eta(t)^\dagger-K^0_\eta(t)^\dagger K^0_\eta(t)\Big]=0$	$\sum_{\eta=\pm}K^1_\eta(t)d^\dagger_{\eta'}K^1_\eta(t)^\dagger=0$
$\sum_{\eta=\pm}\Big[K^1_\eta(t)K^1_\eta(t)^\dagger+K^1_\eta(t)^\dagger K^1_\eta(t)\Big]=(1-e^{-\Gamma t})\mathbb{1}$	$\sum_{\eta=\pm}K^1_\eta(t)^\dagger d^\dagger_{\eta'}K^1_\eta(t)=0$

Table A.1: Sum-rules satisfied by the Kraus operators (3.38). Reprinted table (adapted) with permission from J. Chem. Phys. **151**, 044101 (2019), see Ref. [134]. Copyright 2019 by the American Institute of Physics.

act on states $|\eta\eta'\rangle = |\eta\rangle \otimes |\eta'\rangle$ of a doubled Hilbert space:

$$\begin{aligned}\mathrm{choi}[\Pi(t)] = e^{-\frac{1}{2}\Gamma t}\Big\{ &\cosh\tfrac{\Gamma t}{2}\mathbb{1}\otimes\mathbb{1} && \text{(A.30a)}\\ &+\sum_\eta\Big[e^{-i\eta\varepsilon t}\,|\eta\eta\rangle\langle\bar\eta\bar\eta| - \eta g(t)\sinh\tfrac{\Gamma t}{2}\,|\eta\eta\rangle\langle\eta\eta|\Big] && \text{(A.30b)}\\ &+\sum_\eta\Big[1-\eta g(t)\sinh\tfrac{\Gamma t}{2}\Big]\,|\eta\bar\eta\rangle\langle\eta\bar\eta|\Big\}. && \text{(A.30c)}\end{aligned}$$

The term (A.30c) coming from Eq. (A.29c) requires no diagonalization and gives rise to the eigenvalues (3.38f) given in the main text. In contrast, the diagonalization of terms (A.30a) and (A.30b) results in the eigenvalues (3.38c) and further mixes all spectral components (A.28). The Kraus operators (3.38b) and (3.38e) themselves follow from the Choi eigenvectors

$$|K^0_\eta(t)\rangle\rangle = \sqrt{\lambda^0_\eta(t)}\,\frac{\eta\sqrt{r(t)}^\eta\,|--\rangle + \frac{1}{\sqrt{r(t)}^\eta}e^{-i\varepsilon t}\,|++\rangle}{\sqrt{r(t)+\frac{1}{r(t)}}} \qquad \text{(A.31a)}$$

$$|K^1_\eta(t)\rangle\rangle = \sqrt{\lambda^1_\eta(t)}\;|\eta\bar\eta\rangle \qquad \text{(A.31b)}$$

by using the identities $|\eta\eta\rangle = d_\eta d_{\bar\eta}\otimes\mathbb{1}\,|\mathbb{1}\rangle$, $|\eta\bar\eta\rangle = d_\eta\otimes\mathbb{1}\,|\mathbb{1}\rangle$ and $\mathrm{choi}[K_m\bullet K_m^\dagger] = |K_m\rangle\rangle\langle\langle K_m|$. The mixing of spectral components is now nontrivially encoded in all of these Kraus operators. More specifically, the eigenvectors of $\Pi(t)$ for our model follow from the quadratic sum-rules listed in Table A.1 together with the fact that the Kraus operators have a definite fermion-parity $(-\mathbb{1})^n K^k_\eta(t)(-\mathbb{1})^n = (-1)^k K^k_\eta(t)$.

B Properties of the time-dependent functions

The dynamics of the resonant level model in Ch. 3 is fully determined by the three functions whose key properties we derive in this appendix.

Publications and acknowledgments. This appendix is presented in App. B of the publication V. Reimer, M. R. Wegewijs, K. Nestmann, and M. Pletyukhov, The Journal of Chemical Physics **151**, 044101 (2019) [Copyright 2019 by the American Institute of Physics], see Ref. [134].

B.1 $\gamma(t)$ – Time-nonlocal memory-kernel

The time-dependent Keldysh correlation function $\gamma(s)$ [Eq. (3.12)] with the relative time-argument $s = t - t' > 0$ forms the basis of all three functions and appears explicitly in the time-nonlocal QME (3.42). It involves an energy integration which can be explicitly carried out by inserting $\tanh(z) = \sum_{n=-\infty}^{\infty}[z + i\pi(n+1/2)]^{-1}$ and closing the integration contour in the upper (lower) complex plane to pick up half of its poles in the residue theorem for the $\eta = +$ ($\eta = -$) summand:

$$\begin{aligned}\gamma(s) &= \sum_{n=-\infty}^{\infty}\sum_{\eta=\pm}\frac{1}{2\pi}\int d\omega \frac{e^{i\eta(\omega-\epsilon)s}}{\omega/(2T) + i\pi(n+1/2)} \\ &= i\,2T\sum_{n=0}^{\infty} e^{-\pi T(2n+1)s}\sum_{\eta}\eta e^{-i\eta\epsilon s} = 2T\frac{\sin(\epsilon s)}{\sinh(\pi T s)}.\end{aligned} \tag{B.1}$$

From this representation we can read of its zeros $\gamma(t^{\mathrm{e}}) = 0$ at times $t^{\mathrm{e}} = \ell\pi/\epsilon$ for $\ell = 1, 2, \ldots$ that lead to observable effects [Eq. (3.56) ff.]. The sign of this correlation function in the first interval, $\operatorname{sgn}\gamma(s) = \operatorname{sgn}\epsilon$ for all $s \in (0, \pi/\epsilon]$, determines the sign of $h(t)$ and $g(t)$ for *all* $t > 0$. We will restrict attention to the case $\epsilon \geq 0$ unless stated otherwise.

B.2 $h(t)$ – Time-local generator

The function $h(t) := \int_0^t ds e^{-\frac{\Gamma}{2}s}\gamma(s)$ [Eq. (3.11)] appears in the EOM (3.10b) for the parity-evolution as well as in the time-local QME (3.44) of the main text. By integrating the decaying oscillations of the correlation function $\gamma(s)$ with a nonnegative, decaying envelope, $h(t)$ has a finite stationary limit $h(\infty) = g(\infty)$ [Eq. (3.21)] which coincides with that of $g(t)$ and is explicitly derived below, cf. Eqs. (B.5a) and (B.7). It inherits the correlation function's nonmonotonic behavior and has extrema at every of its zeros since $dh(t)/dt = e^{-\frac{\Gamma}{2}t}\gamma(t)$. These are either local maxima at $t = (2\ell-1)\pi/\epsilon$ or local minima at $t = 2\ell\pi/\epsilon$ for $\ell = 1, 2, \ldots$. The global maximum always exceeds the stationary value $h(\infty)$ since in the sum $h(\pi/\epsilon) - h(\infty) = \sum_{\ell=1}^{\infty}\int_{(2\ell-1)\pi/\epsilon}^{(2\ell+1)\pi/\epsilon} ds\, e^{-\Gamma s/2}\gamma(s) > 0$ each integral is positive. Moreover, the value $h(\pi/\epsilon) = \int_0^{\pi/\epsilon} ds\, e^{-\Gamma s/2}\gamma(s)$ can significantly exceed 1 for $\epsilon \neq 0$ and reaches its maximal value in the limit

$$\lim_{T,\Gamma\to 0} h\big(\tfrac{\pi}{\epsilon}\big) = \tfrac{2}{\pi}\,\mathrm{Si}(\pi) \approx 1.179 > 1 = \lim_{T,\Gamma\to 0} h(\infty), \tag{B.2}$$

which can be seen from the final representation in Eq. (B.1) and the fact that the sign of $\gamma(s)$ does not change in the first interval. Depending on parameters, several subsequent local maxima may also exceed 1 as seen in Fig. 3.2. This leads to loss of CP-divisibility and the physically observable effects discussed in Sec. 3.7.

B.3 $g(t)$ – Dynamical map

The function $g(t)$ directly determines the parity evolution (3.13b), the exponent of the dynamical map (3.36) and the Kraus operators (3.38). By convoluting $h(t)$ with a nonnegative decaying envelope, the oscillations from the correlation function $\gamma(s)$ are further smoothed out which causes $g(t)$ to be monotonous for a wide range of parameters as we show below. The key steps to understanding the properties of $g(t)$ are first the conversion to a *single* time-integral over $\gamma(s)$,

$$g(t) = \int_0^t ds' \frac{\sinh\left[\frac{\Gamma}{2}(t-s')\right]}{\sinh\left[\frac{\Gamma}{2}t\right]} \gamma(s'), \tag{B.3}$$

by factorizing the double-integral obtained when inserting $h(\tau)$ into the definition (3.14): This is achieved by changing to relative $s' = \tau - s$ and cumulative time-variables $\theta = \tau + s$ the latter of which can be directly evaluated. Then performing the relative-time integration (s') after interchanging it with the energy-integration (ω) *inside* γ [Eq. (3.12)] results in a sum of contributions from all reservoir modes:

$$g(t) = \frac{1}{\pi}\int d\omega \tanh\left(\frac{\omega+\epsilon}{2T}\right) \frac{\Gamma/2}{(\Gamma/2)^2+\omega^2} \frac{\cosh(\Gamma t/2)-\cos(\omega t)}{\sinh(\Gamma t/2)} \tag{B.4a}$$

$$= g(\infty)\left(1 - \frac{1}{e^{\Gamma t/2}+1}\right) + \frac{\Gamma t/2}{\sinh(\Gamma t/2)} \frac{1}{\pi}\int d\omega \tanh\left(\frac{\omega+\epsilon}{2T}\right) \frac{\omega^2}{(\Gamma/2)^2+\omega^2} \frac{t}{2}\left(\frac{\sin(\omega t/2)}{\omega t/2}\right)^2. \tag{B.4b}$$

In the second line, we explicitly split off the stationary value,

$$g(\infty) = \frac{1}{\pi}\int d\omega \tanh\left(\frac{\omega+\epsilon}{2T}\right) \frac{\Gamma/2}{(\Gamma/2)^2+\omega^2} \tag{B.5a}$$

$$\leq \lim_{\epsilon\to\infty} g(\infty) = \frac{1}{\pi}\int d\omega \frac{\Gamma/2}{(\Gamma/2)^2+\omega^2} = 1, \tag{B.5b}$$

which is upper bounded by the off-resonant limit where $g(t)$ instantaneously reaches its stationary value of 1 [Eq. (3.19)]. Inspection of Eq. (B.4b) shows that this is in fact the upper bound of $g(t)$: There the prefactor of $g(\infty)$ is upper bounded by 1 and the second term is always negative by symmetry of the integrand. Including the signs, we obtain the bound (3.22) given in the main text:

$$|g(t)| \leq |g(\infty)| \leq \lim_{|\epsilon|\to\infty} |g(\infty)| \leq 1. \tag{B.6}$$

Evaluating the integral (B.5a) analogous to the calculation (A.25) yields the representation

$$g(\infty) = \tfrac{2}{\pi}\operatorname{Im}\psi\left(\frac{1}{2} + \frac{\Gamma/2 + i\epsilon}{2\pi T}\right) \tag{B.7}$$

given in the main text [Eq. (3.21)] in terms of the Digamma function ψ which reduces to the odd part $\tanh[\epsilon/(2T)]$ of the Fermi-distribution function (3.9) in the weak-coupling limit

$\Gamma \to 0$. Finite Γ broadens this step around $\epsilon = 0$ as reflected by the linearization

$$g(\infty) \approx \frac{\epsilon\, \psi_1\left(\frac{1}{2} + \frac{\Gamma/2}{2\pi T}\right)}{\pi^2 T} = \begin{cases} \frac{4}{\pi}\frac{\epsilon}{\Gamma} & |\epsilon| \ll T \ll \Gamma \\ \frac{1}{2}\frac{\epsilon}{T} & |\epsilon| \ll \Gamma \ll T \end{cases}, \tag{B.8}$$

using $\psi_1(z) := d\psi(z)/dz$ and $\psi_1(1/2) = \pi^2/2$. The representation (B.7) furthermore shows that the stationary value approaches the upperbound (B.5b) as function of ϵ with a powerlaw due to the asymptotic behavior $\psi(z) \sim \ln z$:

$$|g(\infty)| \approx 1 - \frac{\Gamma}{|\epsilon|} \qquad |\epsilon| \gg \Gamma, T. \tag{B.9}$$

Finally, we express $g(t)$ in terms of special functions by inserting the series-representation of sinh in the denominator of Eq. (B.1) and express the numerator in terms of exponentials:

$$\begin{aligned} g(t) &= \sum_{\eta,\chi=\pm} \eta\chi \frac{iTe^{\eta\frac{\Gamma}{2}t}}{\sinh\left[\frac{\Gamma}{2}t\right]} \sum_{n=0}^{\infty} \int_0^t ds\, e^{-[\pi T(2n+1)+\eta\frac{\Gamma}{2}+i\chi\epsilon]s} \\ &= -\sum_{\eta,\chi=\pm} \eta\chi \frac{iTe^{\eta\frac{\Gamma}{2}t}}{\sinh\left[\frac{\Gamma}{2}t\right]} \sum_{n=0}^{\infty} \frac{e^{-[\pi T(2n+1)+\eta\frac{\Gamma}{2}+i\chi\epsilon]t} - 1}{\pi T(2n+1) + \eta\frac{\Gamma}{2} + i\chi\epsilon} \\ &= \sum_{\eta=\pm} \frac{\eta}{\pi \sinh\left[\frac{\Gamma}{2}t\right]} \mathrm{Im} \sum_{n=0}^{\infty} \frac{e^{-[\pi T+i\epsilon]t} e^{-2n\pi Tt} - e^{\eta\frac{\Gamma}{2}t}}{n + \alpha_{\eta\Gamma}(T,\epsilon)} \\ &= \sum_{\eta=\pm} \eta\, \mathrm{Im} \frac{e^{-[\pi T+i\epsilon]t}\Phi\left(e^{-2\pi Tt}; 1; \alpha_{\eta\Gamma}\right) + e^{\eta\frac{\Gamma}{2}t}\psi\left(\alpha_{\eta\Gamma}\right)}{\pi\, \sinh\left[\frac{\Gamma}{2}t\right]}. \end{aligned} \tag{B.10}$$

In the final result we identified the imaginary parts of the Lerch transcendent function $\mathrm{Im}\,\Phi(z;s;\alpha) := \mathrm{Im}\sum_{n=0}^{\infty}\frac{z^n}{(n+\alpha)^s}$ and the Digamma function $\mathrm{Im}\,\psi(\alpha) := -\mathrm{Im}\sum_{n=0}^{\infty}\frac{1}{n+\alpha}$ of the complex variable $\alpha_{\eta\Gamma} = \frac{1}{2} + \frac{\eta\Gamma/2+i\epsilon}{2\pi T}$. Note that the poles of the Lerch and Digamma functions for $\alpha_{-\Gamma}$ cancel exactly in Eq. (B.10), as has also been noted in Ref. [157].

B.4 $dg(t)/dt$ – Extremal points

Using Eq. (3.14) one finds a useful expression for the time-derivative of $g(t)$ in terms of the correlation function that is similar to Eq. (B.3):

$$\frac{d}{dt}g(t) = \frac{\Gamma}{2}\int_0^t ds \frac{\sinh\frac{\Gamma}{2}s}{\left(\sinh\frac{\Gamma}{2}t\right)^2}\gamma(s) = \frac{\Gamma T}{\left(\sinh\frac{\Gamma}{2}t\right)^2}\int_0^t ds \frac{\sinh\frac{\Gamma}{2}s}{\sinh\pi Ts}\sin\epsilon s \tag{B.11a}$$

$$= \frac{\Gamma}{1-e^{-\Gamma t}}\left[h(t) - g(t)\right]. \tag{B.11b}$$

The form (B.11b) gives a simple proof that $g(t)$ and $h(t)$ have the same stationary limit $g(\infty) = h(\infty) = \int_0^\infty ds e^{-\frac{\Gamma}{2}s}\gamma(s)$ as claimed in Eq. (3.21). The latter integral agrees with result (B.5a) but is simpler to evaluate than the $t \to \infty$ limit of Eq. (B.3). It also shows that $g(t)$ is nonmonotonous if and only if $h(t)$ and $g(t)$ cross, a fact used in Sec. 3.7.3. Instead, Eq. (B.11a) gives direct access to the short-time behavior (3.20) of both functions determined by the Keldysh correlation function, $h(t) = 2g(t) \approx \gamma(0^+)t = 2\epsilon/\pi t$. Furthermore, it enables the investigation of parameter regimes in which crossings of $h(t)$ and $g(t)$ appear:

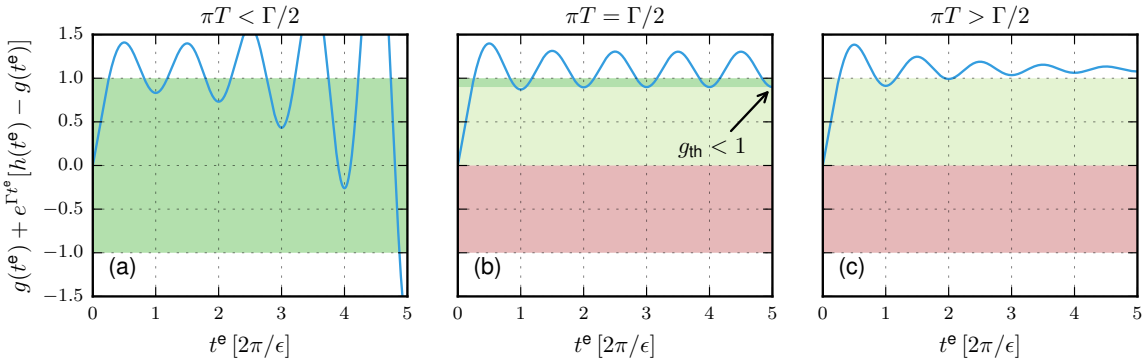

Figure B.1: Right hand side of condition (B.13) for $\epsilon = \pi\Gamma$ and (a) $\pi T = 0.01 \cdot \Gamma/2$, (b) $\pi T = \Gamma/2$ and (c) $\pi T = 1.5 \cdot \Gamma/2$. Reprinted figure (adapted) with permission from J. Chem. Phys. **151**, 044101 (2019), see Ref. [134]. Copyright 2019 by the American Institute of Physics.

- If $\Gamma/2 = \pi T$, the remaining s-integration is simple and results in

$$\tfrac{d}{dt} g(t) = \frac{\Gamma T}{\epsilon} \frac{1 - \cos(\epsilon t)}{[\sinh(\Gamma t/2)]^2}, \tag{B.12}$$

  showing that crossings of $g(t)$ and $h(t)$ occur at times $t^{\mathrm{c}} = 2\ell \frac{\pi}{\epsilon}$ for $\ell = 0, 1, 2, \ldots$ which coincide with the minima of $h(t)$. Consequently, $h(t) \geq g(t)$ and $g(t)$ develops a plateau at times t^{c} where it touches $h(t)$ at its minimum before continuing towards its stationary value that is in this case asymptotically reached as $dg(t)/dt \propto e^{-\Gamma t}$.

- For $\Gamma/2 < \pi T$, the monotonously decreasing exponential envelope in the integrand Eq. (B.11a) ensures the integral is strictly positive and thus $h(t) > g(t)$ for all times. Here, the derivative $dg(t)/dt$ decays faster than $e^{-\Gamma t}$.

- For $\Gamma/2 > \pi T$ the envelope is monotonously increasing, allowing positive contributions to the integral (B.11a) to be overcompensated by later negative ones. As a consequence, $h(t) < g(t)$ is possible and crossings occur in the vicinity of the minima of $h(t)$. Here, the derivative $dg(t)/dt$ decays slower than $e^{-\Gamma t}$.

Finally, also the condition $\langle(-\mathbb{1})^n(t^{\mathrm{e}})\rangle = h(t^{\mathrm{e}})$ for the appearance of a parity extremum at time t^{e} [Eq. (3.54)] can be analyzed using Eq. (B.11). Inserting the parity-evolution (3.51) into this condition leads to a requirement for the initial parity:

$$\langle(-\mathbb{1})^n(0)\rangle = g(t^{\mathrm{e}}) + e^{\Gamma t^{\mathrm{e}}}[h(t^{\mathrm{e}}) - g(t^{\mathrm{e}})] = g(t^{\mathrm{e}}) + \frac{4T}{1 - e^{-\Gamma t^{\mathrm{e}}}} \int_0^{t^{\mathrm{e}}} ds \frac{\sinh \frac{\Gamma}{2} s}{\sinh \pi T s} \sin \epsilon s. \tag{B.13}$$

The right-hand side is plotted in Fig. B.1 and –just as the monotonicity of $g(t)$– qualitatively changes with the temperature / coupling ratio:

(a) For $\pi T < \Gamma/2$, the second term in Eq. (B.13) is an oscillating function of t^{e} whose envelope exponentially diverges after an initial decay. Consequently, *any* fixed initial condition $\langle(-\mathbb{1})^n(0)\rangle \in [-1, 1]$ satisfies Eq. (B.13) for infinitely many times t^{e} indicated by dark green in Fig. B.1. The converging parity thus keeps on oscillating.

(b) For $\pi T = \Gamma/2$, this is possible only when the initial parity exceeds a threshold g_{th} just below 1 as indicated in Fig. B.1. Below this threshold there are either a few t^{e} solutions for $[0, g_{\mathrm{th}})$ (at least one due to parity reentrance) as indicated in light green, or the condition is *never* satisfied for $[-1, 0]$ (no parity extrema at all) as indicated in red.

(c) For $\pi T > \Gamma/2$, the right-hand side of Eq. (B.13) converges to a value exceeding 1 in an oscillating fashion: The condition is satisfied only a finite number of times for an initial parity in $[0, 1]$ and never for $[-1, 0)$.

C | Effective-environment state

We present the explicit construction of the effective-environment state (3.40) in the resonant level model and its factorization (3.41) into independent fermion.

Publications and acknowledgments. This appendix is presented in App. E of the publication V. Reimer, M. R. Wegewijs, K. Nestmann, and M. Pletyukhov, The Journal of Chemical Physics **151**, 044101 (2019) [Copyright 2019 by the American Institute of Physics], see Ref. [134].

C.1 Effective environment density matrix

First, we construct the density matrix $\rho^{\mathrm{E}'}(t)^{kk'}_{\eta\eta'} := \mathrm{Tr}_{\mathrm{S}} K^k_\eta(t)\rho(0)K^{k'}_{\eta'}(t)^\dagger$ of the effective environment and for now focus on the odd- and even-parity diagonal blocks $k = k'$ that remain when the initial system state $\rho(0)$ obeys superselection. The odd block ($k = 1$),

$$\rho^{\mathrm{E}'}(t)^{11}_{\eta\eta'} = \delta_{\eta\eta'}\Lambda^{\mathrm{E}'1}_\eta \tag{C.1a}$$

$$\Lambda^{\mathrm{E}'1}_\eta = \tfrac{1}{2}\lambda^1_\eta(t)\Big[1 + \eta\langle(-\mathbb{1})^n(0)\rangle\Big], \tag{C.1b}$$

is already diagonal in this basis with the Choi eigenvalues (3.38f). The even block ($k = 0$) is however nondiagonal and has to be explicitly diagonalized. Using Eqs. (3.38c) and (3.38d) we obtain for the matrix elements and eigenvalues:

$$\rho^{\mathrm{E}'}(t)^{00}_{\eta\eta'} = \tfrac{1}{2}\left[\lambda^0_\eta(t)\left[1 + \eta P(t;0)\right]\delta_{\eta\eta'} - \langle(-\mathbb{1})^n(0)\rangle\,\frac{2\sqrt{\lambda^0_+(t)\lambda^0_-(t)}}{r(t) + \frac{1}{r(t)}}\delta_{\bar\eta,\eta'}\right] \tag{C.2a}$$

$$\Lambda^{\mathrm{E}'0}_\eta(t) = \tfrac{1}{2}\left[\sum_{\eta''}\lambda^0_{\eta''}(t)\left[1 + \eta'' P(t;0)\right]\right] \times \tfrac{1}{2}\left[1 + \eta\sqrt{1 - \frac{\lambda^0_+(t)\lambda^0_-(t)\left[1 - \langle(-\mathbb{1})^n(0)\rangle^2\right]}{\left(\frac{1}{2}\sum_{\eta'}\lambda^0_{\eta'}(t)\left[1 + \eta' P(t;0)\right]\right)^2}}\right]. \tag{C.2b}$$

Here, the notation $P(t;0) := \langle(-\mathbb{1})^n(0)\rangle \cdot [r(t) - \frac{1}{r(t)}]/[r(t) + \frac{1}{r(t)}]$ is used as a shorthand. This result shows that the effective environment density matrix depends on both the Choi eigenvalues $\lambda^0_\eta(t)$ *and* the Choi eigen*vectors* through $r(t)$, in addition to the initial state $\rho(0)$ through $\langle(-\mathbb{1})^n(0)\rangle$. In particular, each eigenvalue is positive if and only if the initial state is positive, $|\langle(-\mathbb{1})^n(0)\rangle| \leq 1$, and the evolution $\Pi(t)$ is CP, $|g(t)| \leq 1$.

C.2 Factorization into independent fermion modes

The eigenvalues (C.1b) and (C.2b) are already products of positive factors but the dynamics of the effective environment is easier analyzed in terms of the factorization

$$\Lambda^{\mathrm{E}'0}_\eta(t) = \Lambda^{\mathrm{E}'+}_\eta(t) \cdot \Lambda^{\mathrm{E}'-}_\eta(t) \tag{C.3a}$$

$$\Lambda^{\mathrm{E}'1}_\eta(t) = \Lambda^{\mathrm{E}'+}_\eta(t) \cdot \Lambda^{\mathrm{E}'-}_{\bar\eta}(t) \tag{C.3b}$$

used in the main text [Eq. (3.41)]. These factors $\Lambda^{\mathrm{E}'\lambda}_\eta \geq 0$ are additionally normalized as $\sum_\eta \Lambda^{\mathrm{E}'\lambda}_\eta(t) = 1$ and therefore represent probabilities. By taking different sums of Eq. (C.3)

we find from this ansatz that the expression

$$\Lambda_\eta^{\mathrm{E}'\lambda}(t) = \Lambda_\eta^{\mathrm{E}'0}(t) + \Lambda_{\lambda\cdot\eta}^{\mathrm{E}'1}(t) \quad \text{with} \quad \eta,\lambda = \pm \tag{C.4}$$

holds. Substituting back into Eq. (C.3) and using the normalization $\sum_{k=0,1}\Lambda_\eta^{\mathrm{E}'k} = 1$ leads to a nontrivial condition on the eigenvalues of the two diagonal blocks in Eq. (3.40): $\Lambda_+^{\mathrm{E}'0}\Lambda_-^{\mathrm{E}'0} = \Lambda_+^{\mathrm{E}'1}\Lambda_-^{\mathrm{E}'1}$. One verifies using Eqs. (C.1b) and (C.2b) that this indeed holds true independent of the physical parameters. Thus, the eigenvalues of the parity-blocks $k = 0$ and $k = 1$ in Eq. (3.40) are not independent: Even though the effective two-fermion environment is coupled to the system, its state (3.40) *always* factorizes into two *uncorrelated* fermion modes. To obtain the representation Eq. (3.41) given in the main text, we insert Eqs. (C.1b) and (C.2b) into Eq. (C.4) and use the shorthand notation $c(t) := \coth(\Gamma t/2)$:

$$\Lambda_\eta^{\mathrm{E}'\lambda} = \frac{1}{2}\Big[1 + \eta\frac{\sqrt{[c(t) + \langle(-\mathbb{1})^n(0)\rangle g(t)]^2 - [1-g(t)^2][1-\langle(-\mathbb{1})^n(0)\rangle^2]} + \lambda[\langle(-\mathbb{1})^n(0)\rangle - g(t)]}{c(t)+1}\Big] \tag{C.5a}$$

$$= \frac{1}{2}\Big[1 + \eta\frac{\sqrt{[c(t)\langle(-\mathbb{1})^n(0)\rangle + g(t)]^2 + [1-c(t)^2][1-\langle(-\mathbb{1})^n(0)\rangle^2]} + \lambda[\langle(-\mathbb{1})^n(0)\rangle - g(t)]}{c(t)+1}\Big]. \tag{C.5b}$$

The η-index corresponds to the ordering $0 \leq \Lambda_-^{\mathrm{E}'\lambda}(t) \leq \Lambda_+^{\mathrm{E}'\lambda}(t) \leq 1$ and the second line shows that system-state eigenvalues, written as

$$\Lambda_\eta(t) = \tfrac{1}{2}\left[1 + \eta\frac{[c(t)-1]\langle(-\mathbb{1})^n(0)\rangle + 2g(t)}{c(t)+1}\right], \tag{C.6}$$

are *not* bounded by only one of the effective mode's eigenvalues but by *both* in a crossed way:

$$\Lambda_-^{\mathrm{E}'\lambda}(t) \leq \Lambda_\lambda \leq \Lambda_+^{\mathrm{E}'\bar{\lambda}}. \tag{C.7}$$

Based on the representations (C.5), one can identify the two simple special cases discussed in Sec. 3.5: For pure initial system states with $\langle(-\mathbb{1})^n(0)\rangle = \sigma = \pm$, the eigenvalues of the effective environment modes reduce to

$$\begin{aligned}\Lambda_\eta^{\mathrm{E}'\sigma}(t) &= \tfrac{1}{2}[1 + \sigma\cdot\eta] = \Lambda_{\sigma\cdot\eta}(0) \\ \Lambda_\eta^{\mathrm{E}'\bar{\sigma}}(t) &= \tfrac{1}{2}\Big[1 + \sigma\cdot\eta\frac{[c(t)-1]\sigma + 2g(t)}{c(t)+1}\Big] = \Lambda_{\sigma\cdot\eta}(t).\end{aligned} \tag{C.8}$$

Comparing with Eq. (C.6), one sees that in this case one of the effective modes is locked to the spectrum of the pure initial system state $\rho(0)$ whereas the other mode has exactly the same spectrum as the system state. Consequently, the factorization (2.12) is trivially recovered in the stationary limit as $\rho(t) \to \rho(\infty)$. Pure stationary system states are only reached in the off-resonant semigroup limit (3.19) where $g(t) = \theta(t)g(\infty)$ instantly jumps to its stationary value $g(\infty) = \sigma = \pm$ while $\rho(t)$ still evolves in time. In this case, the modes then reduce to

$$\begin{aligned}\Lambda_\eta^{\mathrm{E}'\bar{\sigma}}(t) &= \tfrac{1}{2}[1 + \sigma\cdot\eta] = \Lambda_{\sigma\cdot\eta}(\infty) \\ \Lambda_\eta^{\mathrm{E}'\sigma}(t) &= \tfrac{1}{2}\Big[1 + \eta\frac{[c(t)-1] + 2\sigma\langle(-\mathbb{1})^n(0)\rangle}{c(t)+1}\Big] \neq \Lambda_{\sigma\cdot\eta}(t).\end{aligned} \tag{C.9}$$

Correspondingly, one of the effective environment modes instantly attains the *stationary* sys-

tem spectrum of $\rho(\infty)$ while the spectrum of the other mode evolves *different* from $\rho(t)$, converging to the *initial* system spectrum: $\Lambda_\eta^{\mathrm{E}'\sigma}(\infty) = \frac{1}{2}[1 + \sigma \cdot \eta\langle(-\mathbb{1})^n(0)\rangle] = \Lambda_{\sigma\cdot\eta}(0)$. Finally, we note that the stationary limit (2.12) of the effective environment is reached *irrespective* of these special cases, as it should. Which mode takes on the role of the initial, respectively stationary system spectrum depends on both the initial $\langle(-\mathbb{1})^n(0)\rangle$ and stationary state $\langle(-\mathbb{1})^n(\infty)\rangle = g(\infty)$ through the sign $\sigma = \mathrm{sgn}[\langle(-\mathbb{1})^n(0)\rangle + \langle(-\mathbb{1})^n(\infty)\rangle]$:

$$\begin{aligned}\Lambda_\eta^{\mathrm{E}'\sigma}(\infty) &= \tfrac{1}{2}\big[1 + \sigma \cdot \eta\langle(-\mathbb{1})^n(0)\rangle\big] = \Lambda_{\sigma\cdot\eta}(0)\\ \Lambda_\eta^{\mathrm{E}'\bar{\sigma}}(\infty) &= \tfrac{1}{2}\big[1 + \sigma \cdot \eta\langle(-\mathbb{1})^n(\infty)\rangle\big] = \Lambda_{\sigma\cdot\eta}(\infty).\end{aligned} \tag{C.10}$$

C.3 Pseudo-spin model without superselection

Above and in the main text [Eq. (3.40)] we claimed that the off-diagonal blocks of $\rho^{\mathrm{E}'}(t)$ are zero for all $t \geq 0$ if $\rho(0)$ obeys superselection, i.e., $\langle d(0)\rangle = 0$. Indeed, the off-diagonal blocks

$$\rho^{\mathrm{E}'}(t)^{01}_{\eta\eta'} = \langle d_\eta\rangle(0)\sqrt{\lambda^1_\eta\lambda^0_{\eta'}}\frac{[\sqrt{r(t)}]^{-\eta\eta'}}{r(t) + 1/r(t)}[\eta' e^{-i\varepsilon t}]^{\frac{1+\eta}{2}} \tag{C.11}$$

do not couple to the diagonal blocks which explicitly confirms that the dynamics preserves superselection. As mentioned in Sec. 3.2, the model may however also be considered as an unconventional but valid spin problem, cf. Eq. (3.5). In this case there is no superselection constraint such that the effective environment state has no special block structure:

$$\rho^{\mathrm{E}'}(t) = \begin{bmatrix}\rho^{\mathrm{E}'}(t)^{00} & \rho^{\mathrm{E}'}(t)^{01}\\ \rho^{\mathrm{E}'}(t)^{10} & \rho^{\mathrm{E}'}(t)^{11}\end{bmatrix}. \tag{C.12}$$

Consequently, it *cannot* be considered as two fermions but only as two pseudo-spins. Allowing for transverse initial pseudo-spin, $\langle d(0)\rangle \neq 0$, the nonzero parity-off-diagonal blocks make it harder to explicitly see the positivity of the state (3.26). It is equivalent to the positivity of any one of its diagonal blocks, say $\rho^{\mathrm{E}'}_{11}(t) \geq 0$, and its Schur complement [273],

$$\rho^{\mathrm{E}'}(t)^{00} - \rho^{\mathrm{E}'}(t)^{01}\frac{1}{\rho^{\mathrm{E}'}(t)^{11}}\rho^{\mathrm{E}'}(t)^{01} \geq 0. \tag{C.13}$$

Thus, without superselection it is *not* sufficient that the other block $\rho^{\mathrm{E}'}(t)^{00} \geq 0$ is positive. Explicitly verifying this and the other general facts discussed above from Eqs. (C.1), (C.2) and (C.11) is possible but cumbersome.

D GKSL master equation within the RWA

In this appendix, we show how the Lindblad master equation (4.3a) can be derived from the microscopic model defined by the total Hamiltonian (4.1) and the coupling to the reservoir (4.2) within the rotating-wave approximation (RWA) even in the presence of time-dependent modulation.

Publications and acknowledgments. This appendix has been published in V. Reimer, K. G. L. Pedersen, N. Tanger, M. Pletyukhov, and V. Gritsev, Physical Review A **97**, 043851 (2018) [Copyright 2018 by the American Physical Society], see Ref. [135].

The derivation requires similar steps as those performed for the derivation of the resonant level model solution in App A.1.1: Consider first the Heisenberg equation of motion for the reservoir field operators

$$\tfrac{d}{dt}a_{\alpha\omega}(t) = -i(\omega_0+\omega)a_{\alpha\omega}(t) - \frac{i}{\sqrt{2}}g(t)O(t) \tag{D.1}$$

and formally integrate them to obtain

$$a_{\alpha\omega}(t) = e^{-i(\omega_0+\omega)(t-t_0)}a_{\alpha\omega}(t_0) - \frac{i}{\sqrt{2}}\int_{t_0}^{t} dt' e^{i(\omega_0+\omega)(t'-t)}g(t')O(t'). \tag{D.2}$$

The reservoir degrees of freedom can now be eliminated by inserting it into the Heisenberg equations of motion for the system operators $e_{lm} = |l\rangle\langle m|$ and averaging over the initial state of the reservoir. In fact, the energy integration appearing in

$$\begin{aligned}\tfrac{d}{dt}e_{lm}(t) = -i\left[e_{lm}, H_s(t)\right](t) - i\frac{g(t)}{\sqrt{2}}\left(\sum_\alpha \int d\omega a^\dagger_{\alpha\omega}(t)\left[e_{lm}, O\right](t)\right) \\ - i\frac{g^*(t)}{\sqrt{2}}\left(\left[e_{lm}, O^\dagger\right](t)\sum_\alpha\int d\omega a_{\alpha\omega}(t)\right)\end{aligned} \tag{D.3}$$

can also be performed within the RWA to give a δ-function in time,

$$\begin{aligned}\int d\omega a_{\alpha\omega}(t) &= \int d\omega\, e^{-i(\omega_0+\omega)(t-t_0)}a_{\alpha\omega}(t_0) - \frac{i}{\sqrt{2}}\int d\omega\int_{t_0}^{t} dt' e^{i(\omega_0+\omega)(t'-t)}g(t')O(t') \\ &= \sqrt{2\pi}a_{\alpha,\mathrm{in}}(t) - \frac{i\pi}{\sqrt{2}}g(t)O(t),\end{aligned} \tag{D.4}$$

making explicit the Markovianity of this approximation even in the presence of periodic driving. In the last step, we defined the input field as the Fourier-transform of the bare reservoir field in the far past. Analogously, we can also define the output field corresponding to the reservoir field in the far future,

$$a_{\alpha,\mathrm{out}}(t) = \lim_{t_1\to\infty}\frac{1}{\sqrt{2\pi}}\int d\omega e^{-i(\omega_0+\omega)(t-t_1)}a_{\alpha\omega}(t_1) = a_{\alpha,\mathrm{in}}(t) - i\sqrt{\pi}g(t)O(t), \tag{D.5}$$

which is needed for the calculation of reflection and transmission observables.

The reservoir-average can be calculated from the action of the input field (D.4) on the initial reservoir state. This state is considered to be a right-moving coherent wavepacket of width d with a mean number of photons $\bar{N}$ corresponding to a photonic flux $f = \bar{N}/d$. It can be defined as $|\Psi_0\rangle = e^{-\bar{N}/2} e^{\sqrt{\bar{N}} b_R^\dagger} |0\rangle$ in terms of the action on the reservoir vacuum state $|0\rangle$ of normalizable wave-packet operators

$$b_\alpha = \frac{1}{\sqrt{d}} \int_{-d/2}^{d/2} dx\, a_\alpha(x, t_0) e^{-i\omega_0 x} \tag{D.6}$$

obtained from the Heisenberg coordinate representation $a_\alpha(x,t) = \int d\omega a_{\alpha\omega}(t) e^{i\omega x}/\sqrt{2\pi}$. The commutation relations with the wave-packet operator,

$$\left[a_{\alpha\omega}, b_R^\dagger\right] = \delta_{\alpha,R} \int_{-d/2}^{d/2} e^{i(\omega_0-\omega)x}/\sqrt{2\pi d}, \tag{D.7}$$

imply the action of the input field on the initial state $|\Psi_0\rangle$ to be

$$a_{\alpha,\mathrm{in}}(t)|\Psi_0\rangle = \delta_{\alpha,R}\sqrt{f}\,\Theta\left(d/2 - |t-t_0|\right)|\Psi_0\rangle. \tag{D.8}$$

With this, the Heisenberg equations of motion (D.3), when averaged over the initially factorizing state $\rho_{\mathrm{tot}}(t_0) = \rho(t_0) \otimes |\Psi_0\rangle\langle\Psi_0|$, become

$$\tfrac{d}{dt}\langle e_{lm}(t)\rangle = \mathrm{Tr}\left[\tfrac{d}{dt} e_{lm}(t)\, \rho_{\mathrm{tot}}(t_0)\right] = \langle m| - i[H_{\mathrm{eff}}(t), \rho(t)] + \gamma(t)\mathcal{D}[O]\rho(t)|l\rangle, \tag{D.9}$$

where the effective Hamiltonian $H_{\mathrm{eff}}(t)$ and the Lindblad dissipator $\mathcal{D}[O]$ are specified by Eqs. (4.3b) and (4.3c), respectively, and follow from switching back to the Schrödinger picture. The GKSL master equation (4.3a) can be directly identified by the matrix elements $\rho_{ml} = \langle e_{lm}\rangle$ of the reduced density operator.

E Derivation of the Keldysh operators

The key idea that enables the reorganization of the Keldysh real-time diagrammatic series in Ch. 5 is the *purification* of the unitary evolution operator $U(t,t')$ in addition to that of the initial environment [Sec. 2.1.1]. This gives rise to the Keldysh operators $k_m(t)$ in Eq. (5.10) that we derive in some detail in this appendix.

Publications and acknowledgments. This appendix is presented in App. B of the publication V. Reimer, and M. R. Wegewijs, SciPost Physics **7**, 012 (2019) [CC BY 4.0 License], see Ref. [137].

E.1 Decomposition into average plus fluctuations

The unitary evolution operator $U(t,t') = T\exp[-i\int_{t'}^{t} d\tau H^{\rm tot}(\tau)]$ is governed by the total (possibly time-dependent) Hamiltonian $H^{\rm tot}(t) = H^0(t) + V(t)$ where the uncoupled system plus environment Hamiltonian H^0 generates the free evolution $u(t,t') = T\exp[-i\int_{t'}^{t} d\tau H^0(\tau)]$. The coupling is assumed to be normal-ordered, $V = :V:$, [cf. Sec. 2.2.1] and can be expanded as $V(t) = \sum_{m\neq 0} V_m(t)$ into normal-ordered terms $V_m = :V_m:$ acting only on environment modes m since $V_m^l = 0$ and $V_0 = \langle V\rangle = 0$ in Eq. (2.14). Omitting the explicit time-argument in the following, we first expand the unitary in powers of the couplings V and then expand each coupling into its mode contributions,

$$\begin{aligned} U &= u + u*(-iV)u + u*(-iV)u*(-iV)u + \dots \\ &= u + \sum_{\mu\neq 0} u*(-iV_\mu)u + \sum_{\mu'\mu\neq 0} u*(-iV_{\mu'})u*(-iV_\mu)u + \dots \\ &= U_0 + \sum_{m_1} U_{m_1} + \sum_{m_2 m_1} U_{m_2 m_1} + \dots = \sum_m U_m, \end{aligned} \tag{E.1}$$

where $u*Vu = \int_{t'}^{t} d\tau u(t,\tau)V(\tau)u(\tau,t')$ is a partially factorized convolution. In the last line we collected into $U_m(t,t')$ all strings of repeated couplings which together act on the definite set[1] of environment modes $m = m_q\dots m_1$. We do not distinguish the order of modes, i.e., $U_{m_q\dots m_1}$ is symmmetric. Next, we *decompose*[2] U by expanding each component

$$U_m = \langle U_m\rangle + :\Big(U_m + \sum_{m'\subset m} U_m^{m'}\Big): \tag{E.2}$$

into its average plus fluctuations [Eq. (2.14)]. Inserting into Eq. (E.1), we collect all terms with the fixed set of modes m originating from supersets $m' \supset m$ in the expansion (E.2) and

[1] The discussion applies to any normal-ordered coupling V. Only for the special case of bilinear coupling, does the number of modes count the coupling power, $U_{m_1} = u*V_{m_1}u$, $U_{m_2m_1} = u*V_{m_2}u*V_{m_1}u$, and so on. If V is instead biquadratic as, for example, in Appelbaum-Schrieffer-Wolf Hamiltonians describing Kondo physics, then $U_{m_2m_1}$ may be of first order in the coupling V.

[2] We are *not* normal-ordering U, i.e., *altering* $U \to :U:$. In Eq. (E.3) we merely add and subtract canceling partial contractions in the real-time expansion of U to separate out different kinds of fluctuations.

obtain the decomposition (5.10) into Keldysh operators k_m given in the main text:

$$U = \sum_m U_m \equiv k_0 + \sum_{m\neq 0} :k_m: \quad . \tag{E.3}$$

The special case denoted by $m = 0$ is the part of U in which no environment operators are left. It collects the full contraction of U, i.e., its *environment average*. Instead the Keldysh operator k_m is defined for $m \neq 0$ as the partially contracted evolution operator U such that only environment modes $m \subset m'$ remain:

$$k_0 \equiv \sum_m \langle U_m \rangle = \langle U \rangle, \quad k_m \equiv U_m + \sum_{m'\supset m} U^m_{m'} \quad . \tag{E.4}$$

We note that the Keldysh operators are themselves not normal-ordered: $k_m \neq :k_m:$, i.e., k_m has nonzero partial contractions for $m \neq 0$ while $k_0 = \langle k_0 \rangle \otimes \mathbb{1}_{\mathrm{E}}$ and $:k_0: = 0$. Yet, partial contractions of these objects never appear in the theory because the pasting rule (5.11b) explicitly normal-orders the Keldysh operators.

E.2 Consistency with the Schrödinger equation

The main text noted that summing the hierarchy (5.19) results in a self-consistent equation,

$$k \equiv k_0 + k_1 + k_2 + \ldots = k_0 + k_0 \sum_{l=1}^{\infty} [*(\sigma_1 + \sigma_2 + \ldots) * k_0]^l \tag{E.5a}$$

$$= u + u \sum_{l=0}^{\infty} [*(\sigma_0 + \sigma_1 + \sigma_2 + \ldots) * u]^l = u + u * \sigma * k \tag{E.5b}$$

with the sum of all self-energies $\sigma \equiv \sum_m \sigma_m$. Importantly, this is *not* the self-consistent form of Schrödinger equation because of the lack of explicit normal-ordering, $k(t) \neq U(t)$ and also $\sigma(t,t') \neq -iV(t)\delta(t-t')$. To check that the hierarchy (5.19), when properly normal-ordered, indeed unravels the Schrödinger equation, we must decompose $k = k_0 + (k - k_0)$ and separately consider the operator $k - k_0$ acting nontrivially on the environment. From Eq. (E.5a) we find that k also obeys the self-consistent equation

$$k = k_0 + k_0 * (\sigma - \sigma_0) * k. \tag{E.6}$$

Subtracting k_0, we rewrite the right-hand side by inserting the zeroth hierarchy equation (5.19a), $k_0 = u + u * \sigma_0 * k_0$, and again substitute Eq. (E.6) in the resulting term:

$$\begin{aligned} k - k_0 &= k_0 * (\sigma - \sigma_0) * k \\ &= u * (\sigma - \sigma_0) * k + u * \sigma_0 * k_0 * (\sigma - \sigma_0) * k \\ &= u * (\sigma - \sigma_0) * k + u * \sigma_0 * (k - k_0) \;=\; u * (\sigma * k - \sigma_0 * k_0). \end{aligned} \tag{E.7}$$

From this one can reproduce the self-consistent form of Schrödinger equation as follows. Starting from its right-hand side, insert $U = k_0 + :k - k_0:$ [cf. Eq. (E.3)]. Next, decompose

the result into its average plus normal-ordered expressions:

$$\begin{aligned} u + u * (-iV)U &= u + u * (-iV)\,(k_0 + :k - k_0:) \\ &= u + u * \sigma_0 * k_0 + u * :\sigma * k: \qquad \text{(E.8a)} \\ &= k_0 + :k - k_0: = k_0 + \sum_{m\neq 0} :k_m: = U. \qquad \text{(E.8b)} \end{aligned}$$

As a result of the hierarchy equations this is consistent with the decomposition (E.3): to obtain Eq. (E.8b) we used $k_0 = u + u * \sigma_0 * k_0$ again and inserted the *normal-ordering* of Eq. (E.7), noting that $:\sigma_0 * k_0: = 0$. Thus, k_0 together with the normal-ordering of $\sum_{m\neq 0} k_m$ as determined by the hierarchy (5.19) are equivalent to the self-consistent form of the Schrödinger equation.

The step leading to Eq. (E.8a) involves a nontrivial reorganization of terms,

$$\begin{aligned} (-iV)\,(k_0 + :k - k_0:) &= \sum_{n\neq 0}(-iV_n)\Big(k_0 + \sum_{m\neq 0} :k_m:\Big) \qquad \text{(E.9a)} \\ &= \sum_{n\neq 0}\langle -iV_n :k_n:\rangle + :\Big[\sum_m \sum_{l\subseteq nm} (-iV_n :k_m:)^l\Big]: \qquad \text{(E.9b)} \\ &= \sigma_0 * k_0 + :\Big[\sum_{n'm'} \sigma_{n'm'} * \sum_{m''} k_{m''}\Big]: = \sigma_0 * k_0 + :\sigma * k:, \qquad \text{(E.9c)} \end{aligned}$$

which involves the following detailed diagrammatic observations:

- First, the expansion (2.14) is applied to Eq. (E.9a). The first term in Eq. (E.9b) is the average which sums up all full contractions of fields in $V_n = :V_n:$ with those in $:k_n:$. The corresponding diagrams can be factorized into two parts. One factor is irreducibly contracted in some time interval $[t, t']$ such that summing all contributions to it gives the self-energy component $\sigma_0(t, t')$. The remaining factor for the time interval $[t', 0]$ contains all possible contributions without external modes and therefore sums up to $k_0(t')$. Since in $k_n(t)$ we integrate over all internal times, we also integrate over t' and obtain the convolution in the first term in Eq. (E.9c).

- The second term in Eq. (E.9b) involves[3] $(-iV_n :k_m:)^l$ where a subset $l \subseteq nm$ of modes in V_n and $:k_m:$ remains uncontracted. Denote by c the –possibly empty[4] – subset $c \subseteq n$ of modes in V_n that are contracted with a corresponding subset $c \subseteq m$ of modes in k_m. Again the diagrams factorize. One factor contains all diagrams *irreducibly* connected to V_n in some time-interval $[t, t']$ leaving modes n' from V_n and modes m' from k_m uncontracted. Summing over all modes c, we get by definition $\sigma_{n'm'}(t, t')$ representing all such irreducible contributions. The factor at earlier times $[t', 0]$ contains all possible contributions with further uncontracted modes m'' from k_m and therefore sums up to $k_{m''}(t')$. Thus, we have decomposed the modes in V_n as $n = n'c$ and in k_m as $m = cm'm''$ such that the uncontracted modes $n'm'$ and m'' are attributed to the irreducible and reducible factors of each diagram, respectively. In total, the modes $l = n'm'm''$ thereby remain uncontracted. Independently summing over the modes

[3]The first term $(-iV)k_0$ in Eq. (E.9a) is included through the term $m = 0$ of Eq. (E.9b).

[4]For $c = 0$ (no contractions) we have $n' = n$ and $m'' = m$ and $m' = 0$ and obtain $-iV_n\delta$ as a contribution to the self-energy $\sigma_{n'm'} = \sigma_n$, convoluted with the reducible part $k_{m''} = k_m$.

$n'm'$ and m'' –including the empty sets– we obtain $\sigma * k$ [Eq. (E.5)] for the second term in Eq. (E.9c), completing the derivation.

F | Real-time diagrammatic rules

This appendix collects the modifications to the standard Keldysh real-time diagrammatic rules [Sec. 2.2.2]. These allow for a diagrammatic representation of conditional dynamical maps Π_m and Keldysh operators k_m in Eq. (5.11), as well as of the CP structure of the memory-kernels Σ_m in terms of the single-branch self-energies σ_m in Sec. 5.4.3.

Publications and acknowledgments. This appendix collects the Apps. D [F.1], E [F.2], and F [F.3] published in V. Reimer, and M. R. Wegewijs, SciPost Physics **7**, 012 (2019) [CC BY 4.0 License], see Ref. [137].

F.1 Rules for conditional propagators Π_m

In the main text we focused on the reorganization Eq. (5.11) of the standard Keldysh expansion (2.15b) in the interaction-picture, repeated below for clarity:

$$\Pi(t) = \operatorname*{Tr}_{\mathrm{E}} \sum_n \int_{\tau_n \geq \ldots \geq \tau_1} [-iV(\tau_n)] \ldots [-iV(\tau_1)] \bullet \otimes \rho^{\mathrm{E}} \sum_{n'} \int_{\tau'_{n'} \geq \ldots \geq \tau'_1} [iV(\tau'_1)] \ldots [iV(\tau'_{n'})] \tag{F.1a}$$

$$= \sum_k \sum_{\text{diagrams}} \int_{t_k \geq \ldots \geq t_1} \operatorname*{Tr}_{\mathrm{E}} \ldots [-iV(t_i)] \ldots \bullet \otimes \rho^{\mathrm{E}} \ldots [iV(t_j)] \ldots . \tag{F.1b}$$

Here, we provide explicit diagrammatic rules for these contributions and how they should be adapted to obtain the conditional maps Π_m and their generators Σ_m:

(a) Distribute n $[n']$ vertices on the left (right) in all possible ways over the $k = n + n'$ ordered times $t_k \geq \ldots \geq t_1$ and sum over these diagrams.

(b) Pairwise contract all fields appearing in the vertices V and sum over all possible contractions. The sum over all modes is included in the vertices themselves, $V = \sum_{m \neq 0} V_m$. For fermions, the sign of each term is given by the parity $(-1)^{n_{\mathrm{c}}}$ of the number n_{c} of crossing contraction lines.

(c) Perform the ordered time integrations.

(d) To obtain the conditional propagator $\Pi_{m_q \ldots m_1}$, restrict in (b) the q inter-branch contractions to a definite set of modes $m_q \ldots m_1$ while summing over all modes of intra-branch contractions. For $\Sigma_{m_q \ldots m_1}$ restrict this to two-contour irreducible diagrams.

In practice, to compute the superoperators represented by the diagrams one needs to exploit the known energy eigenbases of H and H^{E}, the system and environment Hamiltonians, respectively. It is then convenient to revert to the Schrödinger picture which only changes the translation rules for the diagrams by inserting the free evolution

$$\pi(t, t') = T e^{-i \int_{t'}^{t} d\tau H(\tau)} \bullet T' e^{+i \int_{t'}^{t} d\tau H(\tau)} \tag{F.2}$$

with formal (anti)time-ordering T (T') between every two consecutive occurences of vertices at times $t \geq t'$ –irrespective of the branch they occur on.

We remark a few peculiarities concerning the above rules to avoid confusion:

- The times t_i label vertices on *either* contour: In the Keldysh technique each *two-branch time-ordered* integral is explicitly represented by a separate diagram which has several useful implications noted in Sec. 2.2.2.

- In the density-*operator* technique, the Keldysh contour is not drawn closed at latest time [cf. Fig. 2.4(b)], in contrast to the Keldysh contour for Green's functions [179] where this closure indicates an additional system-trace to obtain correlation *functions*.

- For the environments of interest here, the modes are labeled by discrete indices (particle type, electron spin, etc.) and a continuous orbital index or equivalent energy [35, 158], see Eq. (5.28). Thus in the above rules, the CP structure requires *suspending integrations* over the continuous environment energies for the inter-branch contractions but performing them for intra-branch contractions, see the application in Sec. 5.5.

F.2 Rules for Keldysh operators k_m

A key result of Sec. 5.3.1 is that the conditional propagator $\Pi_{m_q\ldots m_1}$, determined by the rules in App. F.1, can be 'cut into two halves', representing the *Keldysh operator* $k_{m_q\ldots m_1}$ and its adjoint, respectively. The Keldysh operators can therefore be obtained directly from a diagrammatic 'cutting and pasting' based on similar rules.

F.2.1 Cutting rules

The contributions to the Keldysh operator $k_{m_q\ldots m_1}(t)$ are obtained from the formal expansion

$$\sum_n \operatorname*{Tr}_{\mathrm{E}} \int_{\tau_n\geq\ldots\geq\tau_1} d\tau_n \ldots d\tau_1 [-iV(\tau_n)] \ldots [-iV(\tau_1)] \rho^{\mathrm{E}} \tag{F.3}$$

of a 'cut' single-branch auxiliary operator using the following rules:

(a) Pairwise contract all fields appearing in the vertices V and sum over all possible contractions, leaving q fields with a definite set of mode indices $m_q \ldots m_1$ *uncontracted*. For fermions, the number of crossing contraction lines $n_{\mathrm{c,intra}}$ introduces a sign $(-1)^{n_{\mathrm{c,intra}}}$, where the crossings with the external contraction lines must be *included*.

(b) Assign ordered times $\tau_q \geq \ldots \geq \tau_1$ to the uncontracted vertices and integrate over them.

(c) Independently sum over all orderings of the mode indices $m_q \ldots m_1$ to symmetrize the indices of the the Keldysh operator $k_{m_q\ldots m_1}(t)$. The self-energies $\sigma_{m_q\ldots m_1}$ are then obtained by restricting to *one-branch irreducible* diagrams.

These Keldysh operators k_m and their self-energies σ_m are the central objects of the developed formalism. Actual Kraus operators are subsequently derived from them:

$$K^e_{m_q\ldots m_1} = \langle e| :k_{m_q\ldots m_1}: \otimes \mathbb{1}_{\mathrm{E}'} |0\rangle = \operatorname*{Tr}_{E} \hat{e} :k_{m_q\ldots m_1}: \sqrt{\rho^{\mathrm{E}}}.$$

Here, $|e\rangle = \sum_{ij} e_{ij} |i\rangle \otimes |j\rangle$ denotes any desired basis of bipartite vectors for the purified environment E' and $\hat{e} = \sum_{ij} e_{ij} |i\rangle \langle j|$ is a corresponding basis of operators acting on E.

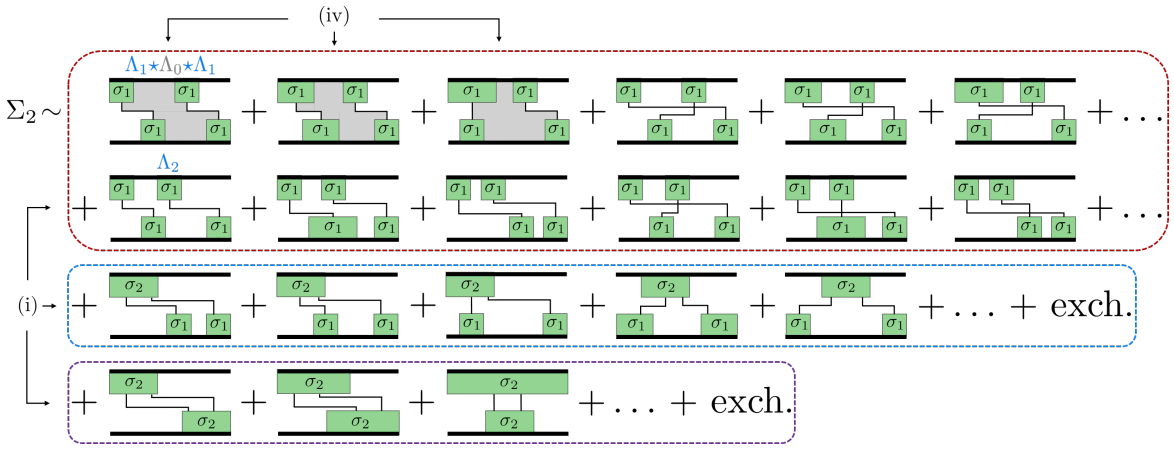

Figure F.1: Contributions to Σ_2 based on the diagrammatic rules (i)-(v) in Sec. 5.4.3. The bold lines indicate a renormalized propagation k_0 $[k_0^\dagger]$ on the upper (lower) branch. Each diagram represents a *definite* two-branch time-ordering, i.e., the time-integrations over the internal times τ_+, τ'_+ $[\tau_-, \tau'_-]$ on the upper [lower] branch are restricted as to not overtake each other. The colored boxes group the different distributions of the external vertices over generators σ_μ by rule (i). The first three diagrams are build up from reducible diagrams which are forced to be irreducible by inserting fragments Λ_0 (gray) by rule (iv). Reprinted figure under CC BY 4.0 License from SciPost Phys. **7**, 012 (2019), see Ref. [137].

F.2.2 Pasting rules

The Keldysh real-time diagrams for $\Pi_{m_q \dots m_1}$ are constructed from the above Keldysh operators $k_{m_q \dots m_1}$ by 'pasting' them together with the vertically flipped diagrams corresponding to $k^\dagger_{m_q \dots m_1}$. This diagrammatic pasting entails the following rules:

(a) Contract in all possible ways the external vertices of $k_{m_q \dots m_1}$ with those of $k^\dagger_{m_q \dots m_1}$ having the same mode index, remembering that $m_q \dots m_1$ may contain repetitions of the same mode index. For fermions, the number of crossing inter-branch contraction lines $n_{\mathrm{c,inter}}$ introduces an additional sign $(-1)^{n_{\mathrm{c,inter}}}$. Consequently, the correct fermionic sign in App. F.1 is recovered since $n_{\mathrm{c}} = n_{\mathrm{c,intra}} + n_{\mathrm{c,inter}}$.

(b) Assign ordered times $\tau_{2q} \geq \dots \geq \tau_1$ to the $2q$ consecutive external vertices –irrespective of the branch they occur on– and integrate over them. This produces the two-branch time-ordering in App. F.1 and yields $\Pi_{m_q \dots m_1}$.

(c) Sum over all modes $m_q \dots m_1$ of the inter-branch contractions to obtain Π.

F.3 Rules for self-energies Σ_m and σ_m

The general rules (i)-(v) of Sec. 5.4.3 for constructing the conditional self-energies Σ_m from the memory-kernels σ_m are illustrated using Fig. F.1. As pointed out in the main text, the functional form (5.26a) for Σ_0 is the only contribution requiring an *infinite* set of diagrams to be summed up. All following tiers require only a *finite* set of dressed diagrams constructed from Σ_0. Here we explicitly discuss the next-to-leading order Σ_2 which covers all difficulties to be encountered when applying the rules to these higher orders.

(i) We first distribute in all possible ways the external vertices among generators σ_μ with $\mu \neq 0$ on each branch. In Fig. F.1, the colored boxes group the three possible distributions for Σ_2: The first group (red) has two σ_1 blocks on each branch. The second group (blue) has two σ_1 blocks on one branch but a single σ_2 on the opposite branch. The final possibility (violet) has a single σ_2 on each branch.

(ii) Within each of these groups, we sum over diagrams with *definite two-branch time-ordering* and integrate over all internal time-arguments. We stress that the number of such orderings is *finite*, although we refrain from providing all contributions for Σ_2.

(iii) We contract the individual generators σ_μ in all possible ways between the branches, including 'exchange' diagrams that are explicitly shown only in the first (red) group.

(iv) To proceed, we have to distinguish two types of diagrams that we have constructed so far. Two-branch *reducible* contributions [first three diagrams in Fig. F.1] are constructed from multiple *two-branch irreducible fragments* $\Lambda_\mu(t_+, t_-, t'_+, t'_-)$ 'glued' together to enforce the two-branch irreducibility. This is achieved using the four-time generalization, $\Lambda_0(t_+, t_-, t'_+, t'_-)$, of the self-energy $\Sigma_0(t, t')$ [cf. Eq. (5.26a)] indicated in gray. Together with the two-branch convolution $\star$, we obtain terms of the form

$$\Sigma_2(t, t') \sim [\Lambda_1 \star \Lambda_0 \star \Lambda_1]\,(t, t, t', t') \tag{F.4}$$

for these contributions. The remaining *irreducible* contributions shown in Fig. F.1 are made up of already irreducible fragments and require no such 'fixing':

$$\Sigma_2(t, t') \sim \Lambda_2(t, t, t', t'). \tag{F.5}$$

(v) Finally, all constructed diagrams have to be complemented by their possible extensions with Λ_0 blocks on either side or both, as discussed in the main text [Eq. (5.26)]. These are not shown in Fig. F.1.

Bibliography

[1] W. H. Zurek, ed., *Complexity, entropy, and the physics of information* (Addison-Wesley, Redwood City, California, 1990).

[2] R. Landauer, Phys. Today **44**, 23 (1991).

[3] R. Clausius, *Abhandlungen über die mechanische Wärmetheorie* (Vieweg, Braunschweig, 1864).

[4] J. von Neumann, *Mathematische Grundlagen der Quantenmechanik* (Springer-Verlag, Berlin, 1932).

[5] C. E. Shannon, Bell Syst. Tech. J. **27**, 379 (1948).

[6] M. Saffman, J. Phys. B: At. Mol. Opt. Phys. **49**, 202001 (2016).

[7] G. Wendin, Rep. Prog. Phys. **80**, 106001 (2017).

[8] J. M. Gambetta, J. M. Chow and M. Steffen, npj Quantum Inf. **3**, 2 (2017).

[9] L. M. K. Vandersypen *et al.*, npj Quantum Inf. **3**, 34 (2017).

[10] P. Michler, ed., *Quantum Dots for Quantum Information Technologies* (Springer International Publishing, 2017).

[11] T. Albash and D. A. Lidar, Rev. Mod. Phys. **90**, 015002 (2018).

[12] S. E. Venegas-Andraca, Quantum Inf. Process. **11**, 1015 (2012).

[13] J. Preskill, Quantum **2**, 79 (2018).

[14] P. W. Shor, Phys. Rev. A **52**, R2493 (1995).

[15] A. M. Steane, Proc. R. Soc. Lond. A **452**, 2551 (1996).

[16] W. K. Wooters and W. H. Zurek, Nature **299**, 802 (1982).

[17] J. Goold *et al.*, J. Phys. A: Math. Theor. **49**, 143001 (2016).

[18] J. Eisert, M. Cramer and M. B. Plenio, Rev. Mod. Phys. **82**, 277 (2010).

[19] S.-J. Ran *et al.*, *Review of Tensor Network Contraction Approaches* (2017), arXiv: 1708.09213.

[20] F. Verstraete and J. I. Cirac, Phys. Rev. Lett. **104**, 190405 (2010).

[21] F. A. Buot, *Nonequilibrium Quantum Transport Physics in Nanosystems* (World Scientific, 2009).

[22] J. Vanherck *et al.*, Phys. Status Solidi B **254**, 1600614 (2017).

[23] S. Andergassen *et al.*, Nanotechnology **21**, 272001 (2010).

[24] R. Gaudenzi *et al.*, J. Comp. Phys. **146**, 092330 (2017).

[25] Y.-C. Cheng and G. R. Fleming, Annu. Rev. Phys. Chem. **60**, 241 (2009).

[26] J. Strümpfer and K. Schulten, J. Chem. Phys. **134**, 095102 (2011).

[27] H.-B. Chen *et al.*, Sci. Rep. **5**, 12753 (2015).

[28] M. Grifoni and P. Hänggi, Phys. Rep. **304**, 229 (1998).

[29] S. Kohler, J. Lehmann and P. Hänggi, Phys. Rep. **406**, 379 (2005).

[30] S. Rodriguez *et al.*, Phys. Rev. Lett. **118**, 247402 (2017).

[31] A. G. Redfield, Adv. Magn. Opt. Reson. **1**, 1 (1965).

[32] A. J. van Wonderen and L. G. Suttorp, EPL **102**, 60001 (2013).

[33] A. J. van Wonderen and L. G. Suttorp, J. Phys. A: Math. Gen. **51**, 175304 (2018).

[34] A. J. van Wonderen and L. G. Suttorp, *Exact density matrix of a discrete quantum system immersed in a thermal reservoir* (2018), arXiv: 1808.04198.

[35] H. Schoeller, Eur. Phys. Journ. Special Topics **168**, 179 (2009).

[36] R. B. Saptsov and M. R. Wegewijs, Phys. Rev. B **86**, 235432 (2012).

[37] O. Kashuba *et al.*, Phys. Rev. B **88**, 165133 (2013).

[38] C.-E. Bardyn *et al.*, New J. Phys. **15**, 085001 (2013).

[39] A. W. Chin, S. F. Huelga and M. B. Plenio, Phys. Rev. Lett. **109**, 233601 (2012).

[40] S. F. Huelga, Á. Rivas and M. B. Plenio, Phys. Rev. Lett. **108**, 160402 (2012).

[41] D. A. Lidar, Adv. Chem. Phys. **154**, 295 (2014).

[42] E. Khosravi *et al.*, Phys. Rev. B **85**, 075103 (2012).

[43] Z. Leghtas *et al.*, Science **347**, 6224 (2015).

[44] P. L. Kapitza, Sov. Phys. JETP **21**, 588 (1951).

[45] O. A. Kocharovskaya and Y. I. Khanin, Sov. Phys. JETP **63**, 945 (1986).

[46] K.-J. Boller, A. Imamoglu and S. E. Harris, Phys. Rev. Lett. **66**, 2593 (1991).

[47] H. Pothier *et al.*, EPL **17**, 249 (1992).

[48] G. Fève *et al.*, Science **316**, 1169 (2007).

[49] D. Bimberg *et al.*, IEEE Photon. J. **1**, 68 (2009).

[50] B. Roche *et al.*, Nat. Commun. **4**, 1581 (2013).

[51] D. Suter and G. A. Àlvarez, Rev. Mod. Phys. **88**, 041001 (2016).

[52] J. Cayssol, B. Dóra, F. Simon and R. Moessner, Phys. Status Solidi RRL **7**, 101 (2013).

[53] K. L. Hur *et al.*, C. R. Physique **19**, 451 (2018).

[54] D. Schmid, K. Ried and R. W. Spekkens, *Why initial system-environment correlations do not imply the failure of complete positivity: a causal perspective* (2018), arXiv: 1806.02381.

[55] P. Pechukas, Phys. Rev. Lett. **73**, 1060 (1994).

[56] J. Yin *et al.*, Science **256**, 1140 (2017).

[57] M. A. Nielsen and I. L. Chuang, *Quantum Computation and Quantum Information* (Cambridge University Press, Cambridge, 2010).

[58] R. Alicki, Phys. Rev. Lett. **75**, 3020 (1995).

[59] P. Pechukas, Phys. Rev. Lett. **75**, 3021 (1995).

[60] A. Brodutch *et al.*, Phys. Rev. A **87**, 042301 (2013).

[61] M. Ringbauer *et al.*, Phys. Rev. Lett. **114**, 090402 (2015).

[62] B. Vacchini and G. Amato, Sci. Rep. **6**, 37328 (2016).

[63] A. Shabani and D. A. Lidar, Phys. Rev. Lett. **102**, 100402 (2009).

[64] A. Shabani and D. A. Lidar, Phys. Rev. Lett. **116**, 049901 (2016).

[65] J. M. Dominy, A. Shabani and D. A. Lidar, Q. Info. Proc. **15**, 465 (2016).

[66] K. Modi, Sci. Rep. **2**, 581 (2012).

[67] B. M. Terhal, Rev. Mod. Phys. **87**, 307 (2015).

[68] A. Shabani and D. A. Lidar, Phys. Rev. A **80**, 012309 (2009).

[69] F. Masillo, G. Scolarici and L. Solombrino, J. Math. Phys. **52**, 012101 (2011).

[70] F. Buscemi, Phys. Rev. Lett. **113**, 140502 (2014).

[71] J. Preskill, *Quantum information and computation (lecture notes for physics 229)* (1998), URL http://www.theory.caltech.edu/people/preskill/ph229/.

[72] O. Gühne and G. Toth, Phys. Rep. **474**, 1 (2009).

[73] D. Chruściński and G. Sarbicki, J. Phys. A: Math. Theor. **47**, 483001 (2014).

[74] R. Horodecki, P. Horodecki, M. Horodecki and K. Horodecki, Rev. Mod. Phys. **81**, 865 (2009).

[75] J. M. McCracken, *Negative Quantum Channels: An Introduction to Quantum Maps that are Not Completely Positive* (Morgan & Claypool, San Rafael, California, 2014).

[76] J. Pearl, *Causality: Models, Reasoning, and Inference* (Cambridge University Press, Cambridge, 2009).

[77] J. Pearl and D. Mackenzie, *The Book of Why: The New Science of Cause and Effect* (Basic Books, New York, 2018).

[78] K. Ried *et al.*, Nat. Phys. **11**, 414 (2015).

[79] J. Biamonte *et al.*, Nature **549**, 195 (2017).

[80] W. F. Stinespring, Proc. Amer. Math. Soc. **6**, 211 (1955).

[81] C. Karrasch, J. H. Bardarson and J. E. Moore, New J. Phys. **15**, 083031 (2013).

[82] E. C. G. Sudarshan, P. M. Mathews and J. Rau, Phys. Rev. **121**, 920 (1961).

[83] K. E. Hellwig and K. Kraus, Commun. Math. Phys. **11**, 214 (1969).

[84] D. Chruściński, C. Macchiavello and S. Maniscalco, Phys. Rev. Lett. **118**, 080404 (2017).

[85] D. Chruściński and A. Kossakowski, Phys. Rev. Lett. **111**, 050402 (2013).

[86] Á. Rivas, S. F. Huelga and M. B. Plenio, Rep. Prog. Phys. **77**, 094001 (2014).

[87] H.-P. Breuer, E.-M. Laine, J. Piilo and B. Vacchini, Rev. Mod. Phys. **88**, 021002 (2016).

[88] I. de Vega and D. Alonso, Rev. Mod. Phys. **89**, 015001 (2017).

[89] V. Gorini, A. Kossakowski and E. C. G. Sudarshan, J. Math. Phys. **17**, 821 (1976).

[90] G. Lindblad, Commun. Math. Phys. **48**, 119 (1976).

[91] M. M. Wolf and J. I. Cirac, Commun. Math. Phys. **279**, 147 (2008).

[92] Á. Rivas, S. F. Huelga and M. B. Plenio, Phys. Rev. Lett. **105**, 050403 (2010).

[93] Á. Rivas and S. F. Huelga, *Open Quantum Systems. An Introduction* (Springer, Berlin, Heidelberg, 2012).

[94] B.-H. Lio *et al.*, Nature Phys. **7**, 931 (2011).

[95] M. Gessner *et al.*, Nature Phys. **10**, 105 (2014).

[96] S. Milz, M. S. Kim, F. A. Pollock and K. Modi, *CP divisibility does not mean Markovianity* (2019), arXiv: 1901.05223.

[97] H.-P. Breuer and F. Petruccione, *The Theory of Open Quantum Systems* (Oxford University Press, Cambridge, 2002).

[98] F. Benatti, D. Chruściński and S. Filippov, Phys. Rev. A **95**, 012112 (2017).

[99] S. Nakajima, Prog. Theor. Phys. **20**, 948 (1958).

[100] R. Zwanzig, J. Chem. Phys. **33**, 1338 (1960).

[101] C. Karlewski and M. Marthaler, Phys. Rev. B **90**, 104302 (2014).

[102] A. Wallraff *et al.*, Nature **431**, 162 (2004).

[103] T. Niemczyk *et al.*, Nat. Phys. **6**, 772 (2010).

[104] A. A. Houck, H. E. Türeci and J. Koch, Nat. Phys. **8**, 292 (2012).

[105] C. R. Kagan and C. B. Murray, Nat. Nanotechnol. **10**, 1013 (2015).

[106] A. Osada *et al.*, Phys. Rev. Applied **11**, 024071 (2019).

[107] M. Hell, M. R. Wegewijs and D. P. DiVincenzo, Phys. Rev. B **89**, 195405 (2014).

[108] R. S. Whitney, J. Phys. A: Math. Theor. **41**, 175304 (2008).

[109] G. Schaller, P. Zedler and T. Brandes, Phys. Rev. A **79**, 032110 (2009).

[110] F. Shibata, Y. Takahashi and N. Hashitsume, J. Stat. Phys. **17**, 171 (1977).

[111] S. Chaturvedi and F. Shibata, Z. Phys. B **35**, 297 (1979).

[112] C. Timm, Phys. Rev. B **83**, 115416 (2011).

[113] G. Gasbarri and L. Ferialdi, Phys. Rev. A **97**, 022114 (2018).

[114] M. J. W. Hall, J. D. Cresser, L. Li and E. Andersson, Phys. Rev. A **89**, 042120 (2014).

[115] H. Schoeller and G. Schön, Phys. Rev. B **50**, 18436 (1994).

[116] Y. Tanimura and R. Kubo, J. Phys. Soc. Jpn. **58**, 101 (1989).

[117] J. Jin, X. Zheng and Y. Yan, J. Chem. Phys. **128**, 234703 (2008).

[118] R. Härtle, G. Cohen, D. R. Reichman and A. J. Millis, Phys. Rev. B **88**, 235426 (2013).

[119] R. Härtle, G. Cohen, D. R. Reichman and A. J. Millis, Phys. Rev. B **92**, 085430 (2015).

[120] C. Schinabeck, R. Härtle and M. Thoss, Phys. Rev. B **97**, 235429 (2018).

[121] J. Cerrillo and J. Cao, Phys. Rev. Lett. **112**, 110401 (2014).

[122] A. A. Kananenka, C.-Y. Hsieh, J. Cao and E. Geva, J. Phys. Chem. Lett. **7**, 4809 (2016).

[123] R. Rosenbach *et al.*, New J. Phys. **18**, 023035 (2016).

[124] G. Cohen and E. Rabani, Phys. Rev. B **84**, 075150 (2011).

[125] G. Cohen *et al.*, Phys. Rev. B **87**, 195108 (2013).

[126] G. C. Knee, E. Bolduc, J. Leach and E. M. Gauger, Phys. Rev. A **98**, 062336 (2018).

[127] A. Gelzinis, E. Rybakovas and L. Valkunas, J. Chem. Phys. **147**, 234108 (2017).

[128] A. J. Daley, Adv. Phys. **63**, 77 (2014).

[129] S. Gleyzes *et al.*, Nature **446**, 297 (2007).

[130] Q. Ficheux, S. Jezouin, Z. Leghtas and B. Huard, Nat. Commun. **9**, 1926 (2018).

[131] X. Zhao, W. Shi, L.-A. Wu and T. Yu, Phys. Rev. A **86**, 032116 (2012).

[132] M. R. Dowling, M. J. Davis, P. D. Drummond and J. F.Corney, J. Comput. Phys. **220**, 549 (2007).

[133] G. Cohen, E. Gull, D. R. Reichman and A. J. Millis, Phys. Rev. Lett. **115**, 266802 (2015).

[134] V. Reimer, M. R. Wegewijs, K. Nestmann and M. Pletyukhov, J. Chem. Phys. **151**, 044101 (2019).

[135] V. Reimer *et al.*, Phys. Rev. A **97**, 043851 (2018).

[136] V. Reimer, Master's thesis, RWTH Aachen University (2016).

[137] V. Reimer and M. R. Wegewijs, SciPost Phys. **7**, 012 (2019).

[138] B. Schumacher, Phys. Rev. A **54**, 2614 (1996).

[139] C. Caves, *Quantum information theory (lecture notes)*, URL http://info.phys.unm.edu/~caves.

[140] J. Watrous, *The Theory of Quantum Information* (Cambridge University Press, Cambridge, 2018).

[141] M. M. Wilde, *Quantum Information Theory* (Cambridge University Press, 2013).

[142] A. S. Holevo and V. Giovannetti, Rep. Prog. Phys. **75**, 046001 (2012).

[143] C. Addis, B. Bylicka, D. Chruściński and S. Maniscalco, Phys. Rev. A **90**, 052103 (2014).

[144] D. Chruściński, A. Kossakowski and A. Rivas, Phys. Rev. A **83**, 052128 (2011).

[145] Y. Utsumi, Phys. Rev. B **92**, 165312 (2015).

[146] B. Schumacher and M. A. Nielsen, Phys. Rev. A **54**, 2629 (1996).

[147] M. Horodecki, J. Oppenheim and A. Winter, Nature **436**, 673 (2005).

[148] M. Horodecki, J. Oppenheim and A. Winter, Commun. Math. Phys. **269**, 107 (2007).

[149] H. Araki and E. H. Lieb, Commun. Math. Phys. **18**, 160 (1970).

[150] A. G. Hall, J. Phys. A: Math. Gen. **8**, 214 (1975).

[151] H. Schoeller, Annals of Physics **229**, 273 (1994).

[152] J. König, J. Schmid, H. Schoeller and G. Schön, Phys. Rev. B **54**, 16820 (1996).

[153] H. Schoeller, *Transport theory of interacting quantum dots* (Springer Netherlands, Dordrecht, 1997), pp. 291–330.

[154] B. Kubala and J. König, Phys. Rev. B **73**, 195316 (2006).

[155] M. Leijnse and M. R. Wegewijs, Phys. Rev. B **78**, 235424 (2008).

[156] S. Koller, M. Grifoni, M. Leijnse and M. R. Wegewijs, Phys. Rev. B **82**, 235307 (2010).

[157] R. B. Saptsov and M. R. Wegewijs, Phys. Rev. B **90**, 045407 (2014).

[158] H. Schoeller, *Dynamics of open quantum systems* (2018), arXiv: 1802.10014.

[159] J. König, H. Schoeller and G. Schön, Phys. Rev. Lett. **76**, 1715 (1996).

[160] J. König, H. Schoeller and G. Schön, Phys. Rev. Lett. **78**, 4482 (1997).

[161] Y. Utsumi *et al.*, Phys. Rev. B **71**, 245116 (2005).

[162] J. Kern and M. Grifoni, Eur. Phys. J. B **86**, 384 (2013).

[163] M. H. Ansari and Y. V. Nazarov, Phys. Rev. B **91**, 174307 (2015).

[164] S. Andergassen *et al.*, Phys. Rev. B **83**, 205103 (2011).

[165] M. Pletyukhov and H. Schoeller, Phys. Rev. Lett. **108**, 260601 (2012).

[166] F. Reininghaus, M. Pletyukhov and H. Schoeller, Phys. Rev. B **90**, 085121 (2014).

[167] C. J. Lindner and H. Schoeller, Phys. Rev. B **98**, 115425 (2018).

[168] S. Milz, F. A. Pollock and K. Modi, Open Sys. Info. Dyn. **24**, 1740013 (2017).

[169] D. Chruściński and A. Kossakowski, Phys. Rev. A **94**, 020103 (2016).

[170] J. E. de Pillis, Pacific J. Math. **23**, 129 (1967).

[171] A. Jamiołkowski, Rep. Math. Phys. **3**, 275 (1972).

[172] M.-D. Choi, Lin. Alg. Appl. **10**, 285 (1975).

[173] S. R. White, Phys. Rev. Lett. **69**, 2863 (1992).

[174] S. R. White, Phys. Rev. B **48**, 10345 (1993).

[175] U. Schollwöck, Rev. Mod. Phys. **77**, 259 (2005).

[176] D. Perez-Garcia, F. Verstraete, M. M. Wolf and J. I. Cirac, Quantum Inf. Comput. **7**, 401 (2007).

[177] U. Schollwöck, Ann. Phys. **326**, 96 (2011).

[178] R. Orús, Ann. Phys. **349**, 117 (2014).

[179] A.-M. Uimonen, G. Stefanucci, Y. Pavlyukh and R. van Leeuwen, Phys. Rev. B **91**, 115104 (2015).

[180] R. E. Cutkosky, J. Math. Phys. **1**, 429 (1960).

[181] A. J. van Wonderen and K. Lendi, EPL **71**, 737 (2005).

[182] A. J. van Wonderen and K. Lendi, J. Phys. A **39**, 14511 (2006).

[183] B. Vacchini and H.-P. Breuer, Phys. Rev. A **81**, 042103 (2010).

[184] L. Ferialdi, Phys. Rev. Lett. **116**, 120402 (2016).

[185] S. Bhattacharya, A. Misra, C. Mukhopadhyay and A. K. Pati, Phys. Rev. A **95**, 012122 (2017).

[186] E. Andersson, J. D. Cresser and M. J. W. Hall, J. Mod. Opt. **54**, 1695 (2007).

[187] T. Prosen, New J. Phys. **10**, 043026 (2008).

[188] T. Prosen, J. Stat. Mech. Theory Exp. **2010**, P07020 (2010).

[189] A. J. Leggett *et al.*, Rev. Mod. Phys. **59**, 1 (1987).

[190] M. Scala *et al.*, Phys. Rev. A **75**, 013811 (2007).

[191] L. Ferialdi, Phys. Rev. A **95**, 020101 (2017).

[192] L. Ferialdi, Phys. Rev. A **95**, 069908 (2017).

[193] E. Y. Wilner, H. Wang, M. Thoss and E. Rabani, Phys. Rev. B **89**, 205129 (2014).

[194] C. Caroli *et al.*, J. Phys. C: Solid State Phys. **4**, 2598 (1971).

[195] R. H. Lehmberg, Phys. Rev. A **2**, 883 (1970).

[196] K. Lalumière *et al.*, Phys. Rev. A **99**, 043806 (2013).

[197] J. Schulenborg *et al.*, Phys. Rev. B **93**, 081411 (2016).

[198] K. Roszak and T. Novotný, Phys. Scr. **T151**, 014053 (2012).

[199] N. Ubbelohde *et al.*, Sci. Rep. (2012).

[200] G. C. Wick, A. S. Wightman and E. P. Wigner, Phys. Rev. **88**, 101 (1952).

[201] Y. Aharonov and L. Susskind, Phys. Rev. **155**, 1428 (1967).

[202] V. Weisskopf and E. Wigner, **63**, 54 (1930).

[203] E. T. Jaynes and F. W. Cummings, Proc. IEEE **51**, 89 (1963).

[204] Y. Meir and N. S. Wingreen, Phys. Rev. Lett. **68**, 2512 (1992).

[205] J. Rammer, *Quantum Field Theory of Non-equilibrium States* (Cambridge University Press, Cambridge, 2007).

[206] L. Kidon, E. Y. Wilner and E. Rabani, J. Chem. Phys. **143**, 234110 (2015).

[207] G. Stefanucci and R. van Leeuwen, *Nonequilibrium Many-Body Theory of Quantum Systems: A Modern Introduction* (Cambridge University Press, Cambridge, 2013).

[208] C. W. Gardiner and P. Zoller, *Quantum Noise: A Handbook of Markovian and Non-Markovian Quantum Stochastic Methods with Applications to Quantum Optics* (Springer, Berlin Heidelberg, 2004).

[209] A. A. Clerk *et al.*, Rev. Mod. Phys. **82**, 1155 (2010).

[210] J. Schulenborg, J. Splettstoesser, M. Governale and D. Contreras-Pulido, Phys. Rev. B **89**, 195305 (2014).

[211] J. Schulenborg, J. Splettstoesser and M. R. Wegewijs, Phys. Rev. B **98**, 235405 (2018).

[212] M. J. W. Hall, J. Phys. A: Math. Theor. **41**, 205302 (2008).

[213] M. Schmutz, Z. Phys. B **30**, 97 (1978).

[214] D. Kosov, J. Chem. Phys. **131**, 171102 (2009).

[215] U. Harbola and S. Mukamel, Phys. Rep. **465**, 191 (2008).

[216] A. A. Dzhioev and D. S. Kosov, J. Chem. Phys. **134**, 044121 (2011).

[217] A. A. Dzhioev and D. S. Kosov, J. Phys.: Cond. Mat. **24**, 225304 (2012).

[218] L. Kidon, H. Wang, M. Thoss and E. Rabani, J. Chem. Phys. **149**, 104105 (2018).

[219] N. Hashitsume, F. Shibata and M. Shingu, J. Stat. Phys. **17**, 155 (1977).

[220] F. Shibata and T. Arimitsu, J. Phys. Soc. Jap. **49**, 891 (1980).

[221] U. Geigenmüller, U. M. Titulaer and B. U. Felderhof, Physica A **119**, 41 (1983).

[222] S. Gnutzmann and F. Haake, Z. Phys. b **101**, 263 (1996).

[223] Yu. V. Nazarov, JETP Lett. **49**, 105 (1989).

[224] S. A. Gurvitz and Y. S. Prager, Phys. Rev. B **53**, 15932 (1996).

[225] S. A. Gurvitz, Phys. Rev. B **56**, 15215 (1997).

[226] A. Oguri, J. Phys. Soc. Jpn. **71**, 2969 (2002).

[227] B. Wunsch, M. Braun, J. König and D. Pfannkuche, Phys. Rev. B **72**, 205319 (2005).

[228] J. N. Pedersen and A. Wacker, Phys. Rev. B **72**, 195330 (2005).

[229] J. N. Pedersen, B. Lassen, A. Wacker and M. H. Hettler, Phys. Rev. B **75**, 235314 (2007).

[230] J. König, H. Schoeller and G. Schön, EPL **31**, 31 (1995).

[231] C. Timm, Phys. Rev. B **77**, 195416 (2008).

[232] H. Schoeller, Lect. Notes Phys. **544**, 137 (2000).

[233] M. M. Wolf, *Quantum channels and operations - guided tour (lecture notes)* (2002), URL http://www-m5.ma.tum.de/foswiki/pub/M5/Allgemeines/MichaelWolf/QChannelLecture.pdf.

[234] N. Dittmann, J. Splettstoesser and N. Helbig, Phys. Rev. Lett. **120**, 157701 (2018).

[235] M.-J. Hwang, P. Rabl and M. B. Plenio, Phys. Rev. A **97**, 013825 (2018).

[236] A. L. Boité, M.-J. Hwang and M. B. Plenio, Phys. Rev. A **95**, 023829 (2017).

[237] P. D. Drummond and D. F. Walls, J. Phys. A: Math. Gen. **13**, 725 (1980).

[238] W. Casteels, R. Fazio and C. Ciuti, Phys. Rev. A **95**, 012128 (2017).

[239] W. Casteels, F. Storme, A. L. Boité and C. Ciuti, Phys. Rev. A **93**, 033824 (2016).

[240] N. Bartolo, F. Minganti, W. Casteels and C. Ciuti, Phys. Rev. A **94**, 033841 (2016).

[241] M. G. Floquet, Ann. École Norm. Sup. **12**, 47 (1883).

[242] F. Bloch, Z. Phys. **52**, 555 (1929).

[243] Y. B. Zel'dovich, Sov. Phys. JETP **24**, 1006 (1967).

[244] J. H. Shirley, Phys. Rev. **138**, B979 (1965).

[245] S.-I. Chu, Adv. At. Mol. Phys. **2**, 197 (1985).

[246] N. L. Manakov, M. V. Frolov, A. F. Starace and I. I. Fabrikant, J. Phys. B: At., Mol. Opt. Phys. **33**, R141 (2000).

[247] S.-I. Chu and D. A. Telnov, Phys. Rep. **390**, 1 (2004).

[248] Y. B. Zel'dovich, A. M. Perelomov and V. S. Popov, Sov. Phys. JETP **30**, 111 (1970).

[249] R. M. V. Khemani, A. Lazarides and S. L. Sondhi, Phys. Rev. Lett. **116**, 250401 (2016).

[250] M. Aidelsburger, S. Nascimbene and N. Goldman, C. R. Phys. **19**, 394 (2018).

[251] T.-S. Ho, K. Wang and S. I. Chu, Phys. Rev. A **33**, 1798 (1986).

[252] S. Kohler, T. Dittrich and P. Hänggi, Phys. Rev. E **55**, 300 (1997).

[253] K. Szczygielski and R. Alicki, Phys. Rev. A **92**, 022349 (2015).

[254] E. B. Davies and H. Spohn, J. Stat. Phys. **19**, 511 (1978).

[255] H. P. Breuer and F. Petruccione, Phys. Rev. A **55**, 3101 (1997).

[256] K. Szczygielski, D. Gelbwaser-Klimovsky and R. Alicki, Phys. Rev. E **87**, 012120 (2013).

[257] K. Szczygielski, J. Math. Phys. **55**, 083506 (2014).

[258] C. M. Dai, Z. C. Shi and X. X. Yi, Phys. Rev. A **93**, 032121 (2016).

[259] K. Brandner and U. Seifert, Phys. Rev. E **93**, 062134 (2016).

[260] R. Kosloff, Entropy **15**, 2100 (2013).

[261] M. P. Silveri, J. A. Tuorila, E. V. Thuneberg and G. S. Paraoanu, Rep. Prog. Phys. **80**, 056002 (2017).

[262] D. R. Dion and J. O. Hirschfelder, Adv. Chem. Phys. **35**, 265 (1976).

[263] H.-I. Yoo and J. Eberly, Phys. Rep. **118**, 239 (1985).

[264] M. Bukov, L. D'Alessio and A. Polkovnikov, Adv. Phys. **64**, 139 (2015).

[265] M. Pletyukhov, K. G. L. Pedersen and V. Gritsev, Phys. Rev. A **95**, 043814 (2017).

[266] R. Barends *et al.*, Nature **534**, 222 (2016).

[267] L. Viola, E. Knill and S. Lloyd, Phys. Rev. Lett. **82**, 2417 (1999).

[268] C. Gustin, R. Manson and S. Hughes, Opt. Lett. **43**, 779 (2018).

[269] J. A. A. Abdumalikov *et al.*, Phys. Rev. Lett. **104**, 193601 (2010).

[270] J. Paaske, A. Rosch and P. Wölfle, Phys. Rev. B **69**, 155330 (2004).

[271] O. Karlström *et al.*, J. Phys. A: Math. Theor. **46**, 065301 (2013).

[272] K. Nestmann and C. Timm, *Time-convolutionless master equation: Perturbative expansions to arbitrary order and application to quantum dots* (2019), arXiv: 1903.05132.

[273] F. Zhang, *The Schur Complement and Its Applications* (Springer, 2005).

Acknowledgments

I am deeply grateful for the many people supporting me during my doctoral studies not only on a professional but also on a personal level. This work wouldn't have been possible without your constant reassurance and guidance in difficult times, just as much as without the fun moments I was happy to share with you. Thank y'all!

Special thanks go to my supervisor Maarten Wegewijs for the wild ride these past four years have been. It has been an honor and a great deal of fun to play diagram-LEGO with you, Maarten. I am especially grateful that your eye for the seemingly trivial details has rubbed off on me –a blessing I will always keep in mind.

I thank my co-supervisor Mikhail Pletyukhov for sharing his expertise in quantum optics and periodic driving in many extensive discussions. Performing numerical calculations can be a tough fight but I am grateful for learning that lesson with you and our colleagues Kim Pedersen, Dmitry Krimer and Timo Hillmann. Also, the school and workshop in Bariloche, Argentina that you encouraged me to visit are certainly a highlight of my studies.

Thanks go also to Herbert Schoeller, not only for co-refereeing this thesis but especially for introducing me to Keldysh diagrammatics during my Bachelor's project in the first place. You spurred my interest in open quantum systems that would stay for the rest of my studies.

Furthermore, I would like to acknowledge the stimulating environment provided by the Deutsche Forschungsgemeinschaft in form of the Research Training Group *Quantum Many-Body Methods in Condensed Matter Systems* (RTG 1995). I very much appreciated the many opportunities offered within this framework, in particular the workshops and the Friday seminars that helped keeping up to date with my fellow doctoral researchers. Thanks to all members and everyone involved in the organization of the RTG, especially Volker Meden and Gillian Hewitt for the continued efforts to make this a success.

This work benefited from so many discussions I want to express my gratitude for, including David DiVincenzo, Barbara Terhal, Ben Criger, Norbert Schuch, Robert van Leeuwen, Rainer Härtle, Sabrina Maniscalco, Roman Saptsov, Thilo Plücker, Konstantin Nestmann, and Valentin Bruch. I also thank my colleagues and friends that have accompanied me over the years providing the much needed distraction. Thank you, *coole Menschen*, *Surrey House 35*, Johannes, Niklas, Benedikt, Martin, Indra, Stephan, Jonas, and everyone else not on this representative list.

Last but not least, my family has always been there when needed. I owe you everything and I am sincerely grateful for your support. Thank you, Elisabeth, Alexander, Jakob, Eduard, Andreas and Waldemar! It's finally done.

Curriculum vitae

Personal Data

Name	Viktor Reimer
Date of birth	September 5th, 1990
Place of birth	Dshetysaj, Kazakhstan
Nationality	German

Education

08/2003 – 07/2010	Gymnasium Leoninum Handrup Abitur
10/2010 – 09/2013	RWTH Aachen University Bachelor degree
10/2013 – 01/2014	University of Surrey (UK) Erasmus semester
10/2013 – 03/2016	RWTH Aachen University Master degree
since 08/2016	RWTH Aachen University PhD

Work Experience

04/2012 – 03/2016	RWTH Aachen University and Jülich Research Centre Teaching assistant
04/2016 – 06/2016	Allianz Lebensversicherungs-AG Stuttgart Intern
since 08/2016	RWTH Aachen University Doctoral researcher

Declaration of authorship

Eidesstattliche Erklärung

I hereby declare in lieu of an oath:
Ich erkläre hiermit an Eides statt:

1. This work was done wholly or mainly while in candidature for the doctoral degree at this faculty and university;
   Diese Arbeit wurde vollständig oder größtenteils in der Phase als Doktorand dieser Fakultät und Universität angefertigt;

2. Where any part of this thesis has previously been submitted for a degree or any other qualification at this university or any other institution, this has been clearly stated;
   Sofern irgendein Bestandteil dieser Dissertation zuvor für einen akademischen Abschluss oder eine andere Qualifikation an dieser oder einer anderen Institution verwendet wurde, wurde dies klar angezeigt;

3. Where I have consulted the published work of others or myself, this is always clearly attributed;
   Wenn immer andere eigene oder Veröffentlichungen Dritter herangezogen wurden, wurden diese klar benannt;

4. Where I have quoted from the work of others or myself, the source is always given. This thesis is entirely my own work, with the exception of such quotations;
   Wenn aus anderen eigenen oder Veröffentlichungen Dritter zitiert wurde, wurde stets die Quelle hierfür angegeben. Diese Dissertation ist vollständig meine eigene Arbeit, mit der Ausnahme solcher Zitate;

5. I have acknowledged all major sources of assistance;
   Alle wesentlichen Quellen von Unterstützung wurden benannt;

6. Where the thesis is based on work done by myself jointly with others, I have made clear exactly what was done by others and what I have contributed myself;
   Wenn immer ein Teil dieser Dissertation auf der Zusammenarbeit mit anderen basiert, wurde von mir klar gekennzeichnet, was von anderen und was von mir selbst erarbeitet wurde;

7. Parts of this work have been published before, see the list of publications.
   Ein Teil oder Teile dieser Arbeit wurden zuvor veröffentlicht, siehe die Publikationsliste.

City, Date / Ort, Datum

Viktor Reimer

List of publications

1. V. Reimer, M. R. Wegewijs, K. Nestmann and M. Pletyukhov
   Five approaches to exact open-system dynamics:
   Complete positivity, divisibility, and time-dependent observables
   The Journal of Chemical Physics **151**, 044101 (2019), see Ref. [134].

2. V. Reimer and M. R. Wegewijs
   Density-operator evolution:
   Complete positivity and the Keldysh real-time expansion
   SciPost Physics **7**, 012 (2019), see Ref. [137].

3. V. Reimer, K. G. L. Pedersen, N. Tanger, M. Pletyukhov and V. Gritsev
   Non-adiabatic effects in periodically driven-dissipative open quantum systems
   Physical Review A **97**, 043851 (2018), see Ref. [135].

4. V. Reimer
   Complete Positivity in Approximations to Open-system Dynamics:
   Kraus' Theorem on the Keldysh Contour
   Master thesis, RWTH Aachen University (2016), see Ref. [136].